Analysis of local hemodynamics in central and peripheral arteries

A thesis submitted to Brunel University

For the degree of

Doctor of Philosophy

By

Alessandra Borlotti

Institute for Bioengineering, Brunel University, London

April 2013

Declaration of Authenticity

I hereby declare that the work presented in this thesis is my own.

Alessandra Borlotti

Acknowledgements

I would like to thank those people who supported and helped me during the course of my PhD.

First and foremost, I would like to thank my first supervisor Doctor Ashraf Khir who has contributed with his advice, experience and patience to the work of this thesis and my second supervisor Doctor Quan Long for his support.

Many thanks to all the academics that I had the opportunity and pleasure to meet during my PhD, including Professor Kim Parker of Imperial College for the precious advice and pleasant discussions about arterial hemodynamics, Professor Patrick Segers, Doctor Sebastian Vermeersch and Doctor Ernst Rietzschel for sharing the Asklepios data that makes up the bulk of this thesis and Professor Colin Clark for the invaluable suggestions.

My warmest thanks also to the research fellow and friends of my group; Gianpaolo and Francesco for their friendship and incredible support in some of the most important steps of my life, Ye who has been my guide in the lab when I started my PhD and John, Karnal, Marcel, Olimpia and Irene.

I would like to thank also all my friends in BIB, Shav, Yi, Masoud, Niko, Luca, Xiao, Philippe, Sam, Lukasz for all the moments spent together. Special thanks to my friend Ning who was very helpful and supportive during the writing up of this thesis.

My thanks also go to everyone in BIB, for being so welcoming and friendly.

I am profoundly grateful to my mum, dad and sister who have always encouraged and supported me during my studies.

Last but certainly not least, I would like to thank and dedicate this thesis to my beloved husband Dario who is a constant source of inspiration and to our beautiful daughter Emma.

Abstract

To understand the function of the cardiovascular system, the propagation of waves in arteries has to be investigated, since they carry information which can be used for the prevention and diagnosis of cardiovascular diseases.

The main goal of this thesis is to improve the understanding of wave propagation in central and peripheral arteries studying the local hemodynamics of the ascending aorta, the carotid artery and the femoral artery by analysing human, animal and *in vitro* data. Also, another aim is to introduce a technique for non-invasive determination of the local arterial distensibility, the wave speed, and wave intensities.

Arterial hemodynamics is here studied using wave intensity analysis, a time domain technique based on pressure and velocity measurements that is derived from the 1D theory of wave propagation in elastic tubes. Also, variations of this technique were used, such as (i) the non-invasive wave intensity analysis that relies on diameter and velocity measurements and (ii) the reservoir-wave approach in which pressure is considered the sum of a pressure due to the elastic properties of the arteries and a pressure due to the travelling wave.

To identify the correct analysis to describe the wave propagation in the ascending aorta using pressure and velocity measurements, the hemodynamics of the canine ascending aorta was studied invasively using the traditional wave intensity (or wave-only) analysis and the reservoir-wave approach in both control condition and during total aorta occlusions in order to provide clear reflection sites. The models produced a remarkably similar wave intensity curves, although the intensity magnitudes were different. The reservoir-wave model always yielded lower values for all hemodynamic parameters studied. Both models led to the conclusion that distal occlusions have little or no effect on hemodynamics in the ascending aorta.

Since the ascending aorta is not an accessible vessel its examination in clinical routine is challenging. More superficial arteries, such as carotid, radial, brachial and femoral arteries, might be easier to examine, in particular using ultrasound equipment that is normally available in the clinic. These considerations led to the second study of this thesis that is the introduction of a new technique for the non-invasive determination

of arterial distensibility, local wave speed and wave intensities to study arterial hemodynamics in humans. The technique relies only on diameter and velocity measurements that can be obtained using ultrasound. In particular, the technique was used for the first time to study the hemodynamic of the carotid and femoral arteries in a large population of healthy humans to investigate the changes with age and gender. The carotid artery was more affected by the aging process than the femoral artery, even in healthy subjects. Local wave speed, distensibility and hemodynamic wave intensity parameters (except the reflection index) had strong correlations with age at the carotid artery. The mechanical properties and hemodynamic parameters of the femoral artery were not significantly age-dependent, but local wave speed, distensibility and forward wave intensity were significantly gender-dependent.

The findings of the first and second studies contributed to the design of the third study. The carotid artery is an elastic artery relatively close to the heart and thus the hemodynamics of this vessel is related to left ventricular function. For this reason, the carotid hemodynamics of the same healthy population was investigated for the first time using the reservoir-wave approach. Pressure and velocity measurements were separated into their reservoir and excess components and the effects of age and gender on these parameters were studied. It was found that in the carotid artery reservoir and excess components are strongly affected by the ageing process.

From the above studies some questions about the hemodynamics of central arteries remained unsolved. For this reason it was decided to carry out *in vitro* experiments in a mock circulatory system to investigate the effects of variation of compliance and stroke volume on the reservoir and excess pressure components of the ascending aorta. This allows for the study of different physiological and pathological conditions, such as age, hypertension, atherosclerosis and ventricular dysfunction in relation to vascular compliance and stroke volume. The reservoir and excess components of the measured pressure wave were both significantly related to aortic compliance and stroke volume, but the reservoir pressure had a stronger relationship with aortic compliance compared with the excess pressure and its magnitude increased more significantly when the aorta became stiffer. Wave speeds, calculated using measured and excess pressures, followed the same pattern, but the one calculated using excess pressure was smaller than the other. Wave speed was strongly related to aortic compliance, but not to the change of stroke volume.

In conclusion, the use of the wave-only and the reservoir-wave models led to different values of wave speed and intensities that can be explained considering the anatomy of the arterial system. Notably, elastic and muscular arteries are differently affected by age and gender. The hemodynamics of the carotid artery are strongly related to age also in healthy subjects. Pressure and flow velocity in the carotid artery can be separated into their reservoir and excess components. The new non-invasive technique based on diameter and velocity measurements could be relevant in clinical practice as a screening tool.

Table of Content

List of Tables

List of Figures

Glossary

A	Cross-sectional area
ba	Brachial artery
c	Wave speed
c_e	Wave speed calculated using Excess Pressure
c_{ee}	Wave speed calculated using Excess Pressure and Excess Velocity
C	Compliance
Cp	Dynamic compliance calculated using measured pressure
Cp_r	Dynamic compliance calculated using reservoir pressure
Cs	Static compliance
D	Diameter
DD_c	Diastolic carotid diameter
DD_f	Diastolic femoral diameter
$_nDs$	Non-invasive distensibility
D_s	Distensibility
dA	First derivative of Area
DBP	Diastolic blood pressure
dD	First derivative of Diameter
dI	Wave Intensity
dI_+	Forward Wave Intensity
dI_-	Backward Wave Intensity
dI_e	Wave Intensity calculated using Excess Pressure
dI_{e+}	Forward Wave Intensity calculated using Excess Pressure
dI_{e-}	Backward Wave Intensity calculated using Excess Pressure
dI_{FCW}	Peak Intensity of the Forward Compression Wave
dI_{eFCW}	Peak Intensity of the Forward Compression Wave calculating using Excess Pressure
dI_{BCW}	Peak Intensity of the Backward Compression Wave
dI_{eBCW}	Peak Intensity of the Backward Compression Wave calculating using Excess

	Pressure
dI_{FEW}	Peak Intensity of the Forward Expansion Wave
dI_{eFEW}	Peak Intensity of the Forward Expansion Wave calculating using Excess Pressure
${}_{n}dI$	Non-invasive Wave Intensity
${}_{n}dI_{+}$	Non-invasive Forward Wave Intensity
${}_{n}dI_{-}$	Non-invasive Backward Wave Intensity
${}_{n}dI_{+max}$	Non-invasive Peak Intensity of Forward Compression Wave
${}_{n}dI_{-min}$	Non-invasive Peak Intensity of Backward Compression Wave
dP	First derivative of Pressure
dU	First derivative of Velocity
E	Young's Modulus
h	Wall thickness
HR	Heart Rate
I	Wave Energy
lnDU-loop	Diameter-Velocity Loop
MAP	Mean Arterial Pressure
MD_c	Mean carotid diameter
MD_f	Mean femoral diameter
P	Pressure
P_r	Reservoir Pressure
P_e	Excess Pressure
P_∞	Asymptotic Pressure
P_d	Diastolic Pressure
PP	Pulse Pressure
PP_r	Pulse Reservoir Pressure
Ppeak	Systolic Pressure
$P_r$peak	Peak of Reservoir Pressure
$P_e$peak	Peak of Excess Pressure
PEI	Integral of Reservoir Pressure
PRI	Integral of Excess Pressure

PU-loop	Pressure-Velocity Loop
P_eU-loop	Excess Pressure-Velocity Loop
P_eU_e-loop	Excess Pressure-Excess Velocity Loop
PWV	Pulse Wave Velocity
p	p value
Q	Flow
R	Resistance
R_+	Forward Reflection Coefficient
R_-	Backward Reflection Coefficient
RI	Reflection Index
${}_nRI$	Non-invasive Reflection Index
RI_e	Reflection Index calculating using Excess Pressure
ρ	Density of the Fluid
SBP	Systolic blood pressure
SEM	Standard Error of the Mean
SD	Standard Deviation
SD_c	Systolic carotid diameter
SD_f	Systolic femoral diameter
T	Duration of the Cardiac Cycle
T_N	Dicrotic Notch Time
t	Time
t_{FCW}	Time of Forward Compression Wave Peak
t_{eFCW}	Time of Forward Compression Wave Peak calculating using Excess Pressure
t_{BCW}	Time of Backward Compression Wave Peak
t_{eBCW}	Time of Backward Compression Wave Peak calculating using Excess Pressure
t_{FEW}	Time of Forward Expansion Wave Peak
t_{eFEW}	Time of Forward Expansion Wave Peak calculating using Excess Pressure
$t_{BCWonset}$	Time of Backward Compression Wave Onset
$t_{eBCWonset}$	Time of Backward Compression Wave Onset calculating using Excess Pressure

$t_{FEWonset}$	Time of Forward Expansion Wave Onset
$t_{eFEWonset}$	Time of Forward Expansion Wave Onset calculating using Excess Pressure
τ	Time constant of the pressure exponential decay
U	Velocity
U_r	Reservoir Velocity
U_e	Excess Velocity
Upeak	Peak of Velocity
$U_r$peak	Peak of Reservoir Velocity
$U_e$peak	Peak of Excess Velocity
V	Stroke Volume set on the LVAD
V_{in}	Stroke Volume
WIA	Wave Intensity Analysis
Y	Admittance
Z	Characteristic Impedance

Chapter 1 : Background information

1.1 Introduction

The World Health Organisation (WHO) report states that cardiovascular diseases (CVDs) are the leading causes of death and disability in the world (World Health Organisation, 2012). CVDs are a group of disorders of the heart and blood vessels and include: coronary heart disease, cerebrovascular disease, peripheral arterial disease, heart disease, deep vein thrombosis and pulmonary embolism. The WHO reported that as recent as 2008 17.3 million of people died from CVDs and of these deaths, about 7.3 million were due to coronary heart disease and 6.2 million were due to stroke. In the UK it has been estimated that in 2009 around one third of all deaths were due to CVD (British Heart Foundation, 2012). Of these deaths, 82,000 were due to coronary heart disease, and about 49,000 were caused by stroke. For successful prevention, diagnosis and treatment of CVDs a deep understanding of the hemodynamics of the cardiovascular system both in normal and in disease conditions is needed.

1.2 The cardiovascular system

The cardiovascular system carries blood to the body tissues through the blood vessels. The blood is the vehicle for oxygen, nutrients and waste products. The circulatory system comprises the heart and a complex network of vessels that carries the blood from the heart to all the organs and the periphery (systemic circulation and microcirculation). The blood returns to the heart through the veins in order to be pumped to the lungs where it is oxygenated and it releases carbon dioxide (pulmonary circulation) as shown in **Figure 1.1**.

1.2.1 The heart and the cardiac cycle

The heart consists of four chambers, two superior called the right and left atrium and two inferior termed the right and left ventricle. The left side of the heart pumps blood into the systemic circulation, while the right side pumps blood into the pulmonary

circulation. The right atrium collects deoxygenated blood that then flows in to the right ventricle which pumps into the pulmonary circulation.

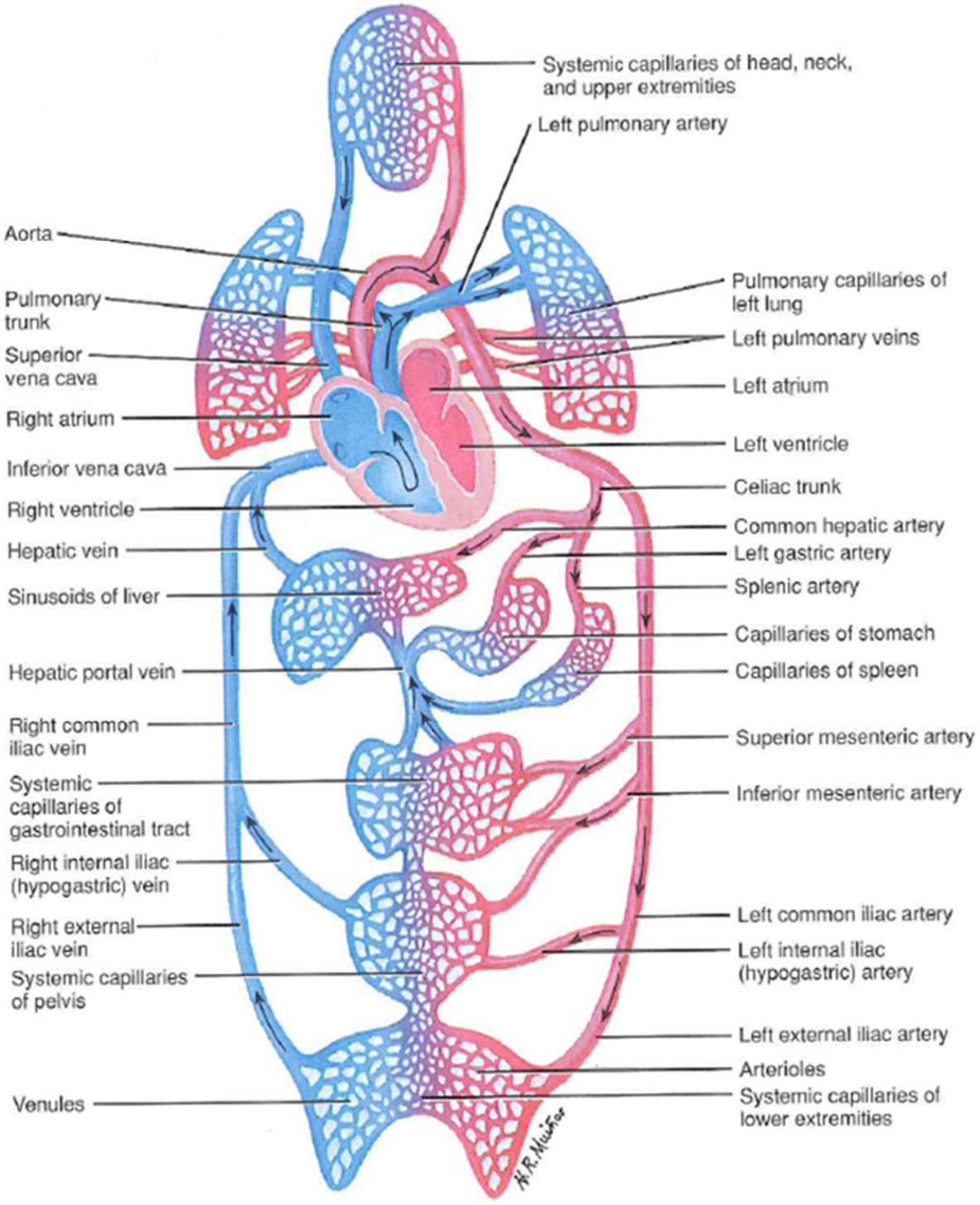

Figure 1.1: Circulatory system (Taken from Tortora, Grabowski 1993).

Blood is oxygenated in the lungs and returns to the heart, in the left atrium and then it passes into the left ventricle which pumps blood in the systemic circulation. The path of the blood through the left and right heart is shown in **Figure 1.2**. To avoid back flow, the four chambers are separated by four valves that open and close based on pressure changes as the heart contracts and relaxes. The valve between right atrium and right ventricle is called tricuspid valve, and the one that separates the left atrium from the left ventricle is termed mitral valve. The valves that lie in the opening of the ventricles are called pulmonary and aortic valves for the right and left side, respectively. During the cardiac cycle, atrial and ventricular contraction or relaxation cause pressure changes resulting in blood flowing from regions of higher pressure to regions of lower pressure.

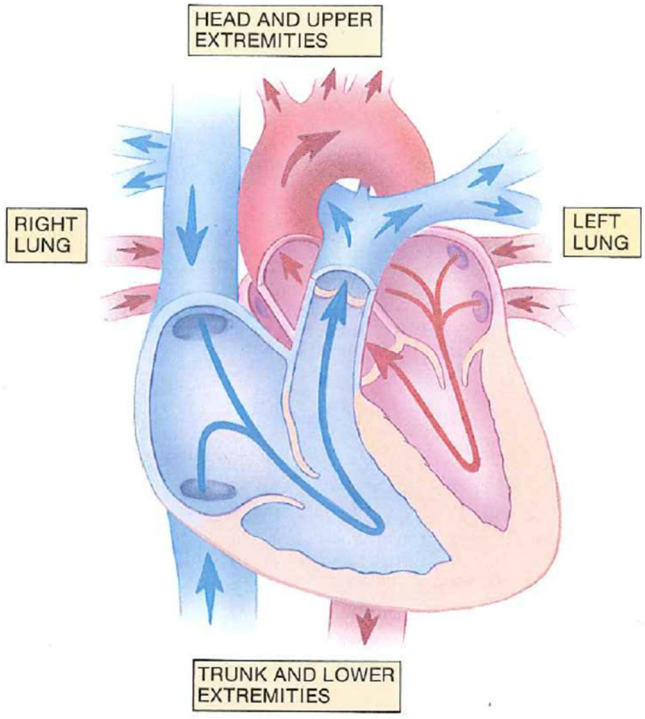

Figure 1.2: Path of blood through the heart (Taken from Tortora, Grabowski 1993).

During the cardiac cycle we can identify a phase called systole that refers to the contraction and a phase termed diastole that refers to the relaxation. From pressure waveforms measured in the left atrium, left ventricle and aorta the mechanics of the cardiac cycle can be easily described following **Figure 1.3**. It is possible to identify a first phase, "early diastole", when the pulmonary and aortic valves close, the atrio-ventricular (AV) valves are open, and the whole heart is relaxed. Then a second phase, called "atrial systole", characterized by atrial contraction and by the flow of blood from

the atrium to the ventricle. The third, "isovolumic ventricular contraction", is when the ventricles begin to contract, the AV and semilunar valves close, and volume is constant. The fourth, "ventricular ejection", is when the ventricles are empty and contracting, and the semilunar valves are open. During the fifth stage, "isovolumic ventricular relaxation", pressure decreases, blood does not enter the ventricles, they begin to relax, and the semilunar valves close due to the pressure of blood in the aorta.

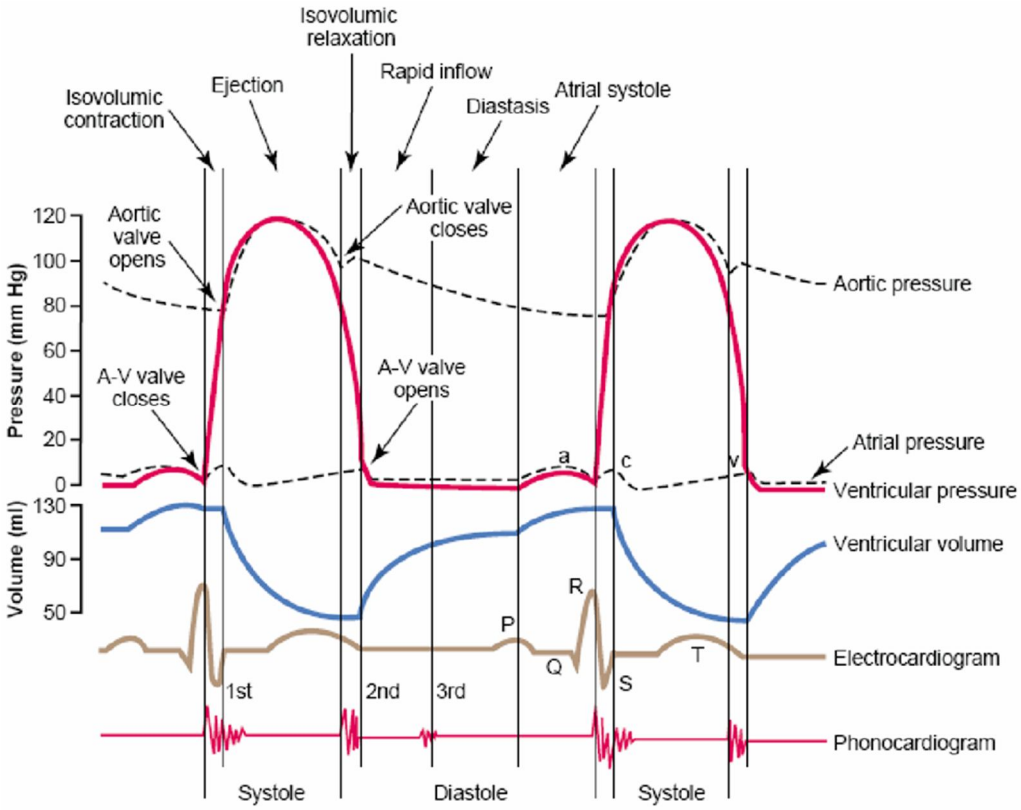

Figure 1.3: Cardiac events occurring in the cardiac cycle (Taken from Guyton, Hall 2006).

1.2.2 Systemic circulation

The systemic circulation starts from the aorta. The portion of the aorta that passes upward behind the pulmonary artery trunk as it emerges from the left ventricle is the ascending aorta. Then it turns to the left, forming the aortic arch that then runs down to the level of the fourth thoracic vertebra where the descending aorta starts. It splits into two common iliac arteries at the level of the fourth lumbar vertebra. The descending aorta between the aortic arch and the diaphragm is the thoracic aorta and the section between the diaphragm and the iliac arteries is the abdominal aorta. Each section of the aorta produces generations of other arteries that finally split into arterioles and

capillaries that supply blood to the tissues. Blood then returns to the right atrium through the systemic veins.

1.2.3 Arterial structure

The arterial wall is composed of three layers, as shown in **Figure 1.4**. The inner coat, termed tunica intima, is made of a lining of endothelium that is in contact with the blood, a basement membrane and a layer of elastic tissue called the internal elastic lamina. The central layer, or tunica media, consists of elastic fibers and muscle fibers. The third layer, tunica adventitia, is composed mainly of elastic and collagen fibers. This structure gives the vessels two important functional properties: elasticity and contractility.

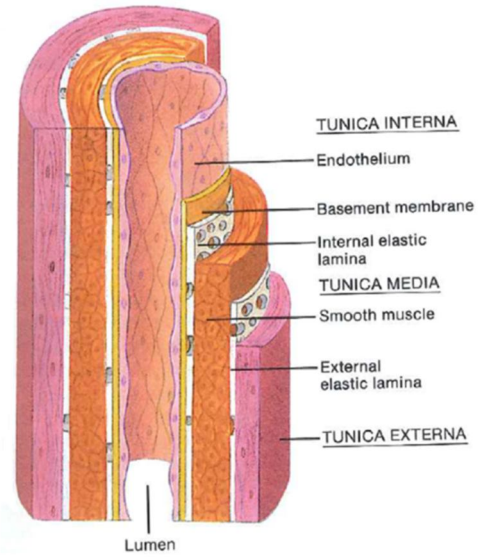

Figure 1.4: Anatomy of the arterial wall (Taken from Tortora, Grabowski 1993).

As blood is ejected into the arterial system, the large arteries distend and accommodate a fraction of the stroke volume and during the diastolic phase the elastic recoil of the vessels pushes the blood onward. The distensibility is largely determined by passive elastic structures. The contractility of the smaller vessel is determined by its smooth muscle that is arranged in both longitudinal and circumferential ways around the lumen.

1.2.3.1 Elastic arteries

Elastic arteries include the aorta and the brachiocephalic, common carotid, subclavian, vertebral, common iliac and pulmonary arteries. The wall of these vessels is thin compared to their diameters and another important feature of the elastic arteries is

that the tunica media layer contains more elastic fibers and less smooth muscle. During the ejection phase, the walls of the elastic arteries stretch in response to increased pressure. They accommodate blood and the elastic fibers store some of the energy. For this reason, the elastic arteries can be regarded as a pressure reservoir. When they recoil (during ventricular relaxation), the elastic energy stored drives blood towards the periphery.

1.2.3.2 Muscular arteries

Muscular arteries include the axillary, brachial, radial, intercostal, splenic, mesenteric, femoral, popliteal, and tibial arteries. They are medium-sized arteries containing more smooth muscle than elastic fibers in their tunica media. For this reason, they are capable of greater vasoconstriction and vasodilation that allow them to adjust the rate of blood flow that supplies the other structures. The wall of these arteries is quite thick because of the large amount of smooth muscle.

1.3 Role of arterial stiffness in hypertension

Arteries are not passive conduits of blood, but they have an active role in cardiovascular function, including in abnormalities of blood pressure. Distensibility of large arteries is an important and fundamental element in the relationship between pulsatile pressure and flow. Stiffening of these arteries can cause hypertension and can also be a consequence of this condition. An increase of arterial pressure causes acute and reversible stiffening of the large arteries without a change in the wall structure of the vessel. Arterial stiffness increases momentarily as blood pressure rises. Arterial stiffening increases also because the structure of the arterial wall changes. Persistently elevated blood pressure accelerates atherosclerosis, arterial smooth muscle hyperplasia and hypertrophy, and collagen synthesis, thus increasing arterial stiffness. Both of these mechanisms of stiffening of the large arteries are likely to be present in hypertension (Arnett et al. 2000, Franklin 2005). An initial increase in arterial blood pressure may generate a positive response in which hypertension biomechanically increases arterial stiffness without any structural change of the arterial wall, but later the pressure increase can lead to additional vascular hypertrophy and hyperplasia, collagen deposition, and atherosclerosis (Benetos 1997).

Arteries have an important role in converting pulsatile blood flow to steady flow. During systole, the aorta accommodates some of the stroke volume and the pressure increases. During diastole the aorta recoils to promote forward flow and pressure is partially maintained by the recovering of the expanded arterial walls. If the artery is stiffer, this cushioning function is compromised, resulting in a higher systolic and lower diastolic blood pressure. Elastin fibers work at low and normal pressures while collagen fibers work at higher pressures (systolic blood pressure greater than 200 mmHg). Differences in the ratio of elastin to collagen affect arterial stiffness. The lower the ratio of elastin to collagen, the stiffer is the artery. Elevated smooth muscle tone or smooth muscle cell hypertrophy also increases arterial stiffness. The loss of elasticity of the artery wall with age is particularly relevant after the 5th decade of life (Franklin et al. 2001), leading to the development of isolated systolic hypertension in the elderly and to an increased cardiovascular risk.

1.4 Blood flow in the arterial system

Interest in the cardiovascular system began many centuries ago, but the "modern" conception started with William Harvey (1578-1675) who published his discovery about the circulation of the blood in 1628 (Harvey 1628). In 1733 Hales (1677-1746) reported the first measurements of in vivo blood pressure and he also concluded that the change from pulsatile flow in arteries to the steady flow in veins was caused by the distensibility of the large arteries (Hales 1733). Hales was also the first to introduce the concept of peripheral resistance. The theoretical approach to the circulation began with Leonhard Euler (1707–1783). In 1755 he proposed the one-dimensional equations of conservation of mass and momentum in a distensible tube (Euler 1775). In 1808 Thomas Young (1773-1829) found the relationship between elastic properties and the velocity of propagation of the arterial pulse (Young 1809). An important milestone in cardiovascular mechanics was the development of the law of viscous flow in tubes by Jean Luis Poiseuille (1799-1869) in which the volume flow rate is proportional to the pressure drop (Poiseuille 1846). An important study on the field of wave propagation was carried out by the brothers Weber. In 1825 they published their monograph which established many of the fundamental properties of wave propagation and reflection (Weber, Weber 1825). This work was followed in 1877–1878 by the experimental work on wave speed of Moens (1846–1891)) and the

theoretical study of the wave speed of Korteweg (1848–1941) ((Moens 1879, Korteweg 1878). Korteweg's theoretical formulation showed that the wave speed was determined both, by the elasticity of the tube wall and the compressibility of the fluid. Otto Frank (1865-1944) dominated the scene in the early twentieth century. He expressed mathematically the qualitative concepts of Hales and he analyzed the cardiovascular system as a model in which the heart pumps blood into a central elastic reservoir (the Windkessel) from which the blood is drained to the periphery through non-elastic vessels (Frank 1905). Frank later introduced the theory of waves in arteries. In 1920 he derived the wave speed in terms of the elasticity and in 1926 he also included the effect of viscosity, the resulting motion of the wall and the energy of the pulse wave. The two theories proposed by Frank (Windkessel and pulse wave model) have an internal conflict since the Windkessel model is based on the assumption that the whole arterial system acts like a single compartment while the wave model predicts that information propagates through the vessels in the form of waves. In the work that McDonald published in 1955 (McDonald 1955), he assumed that the entire arterial system was in a steady-state oscillation produced by the regularly repeated beat of the heart and defined the pressure pulse as an assembly of sinusoidal waves of frequencies determined by Fourier series. McDonald and Womersley (Womersley 1955, McDonald 1955) developed together the concept of Impedance Analysis through the Fourier technique in the frequency domain. This approach is still the most common in arterial mechanics and has been further developed by Taylor (Taylor 1966), O'Rourke (O'Rourke & Taylor 1967; O'Rourke 1982) and Westerhof (Westerhof et al. 1969; Westerhof et al. 1971; Westerhof et al. 1972). In particular the latter developed the impedance approach to allow the separation of the pressure and flow waveforms into forward and backward components. An alternative approach to the analysis of blood flow in arteries in the frequency domain was based on the solution of the method of characteristics by Riemann (Riemann 1860). The first attempt of using this method to describe the wave propagation in the arteries was made by Anliker (Anliker et al. 1971). This work inspired Parker and Jones (Parker & Jones 1990) in the development of the wave intensity analysis. This technique has the advantage of obtaining an analysis in the time domain.

1.5 Wave propagation

Waves are disturbances that propagate in space and time and their travel implicates exchange of energy from one form to another. Waves propagate in arteries due to the balance between the inertial force of the blood and the restoring force of the walls (in arterial wave analysis fluid compressibility is usually neglected because blood is relatively incompressible). The contraction of the heart produces a forward travelling wave (or series of wavefronts) that propagates from the aorta to the peripheral circulation. A wave such as the one generated by the ventricle will propagate unaltered if it is travelling in a uniform tube containing an inviscid fluid, but non-uniformities in terms of the cross sectional area or elasticity of the tube will create wave reflections. Wave propagation in arteries has been mainly analysed by two approaches, one in the frequency domain using the impedance (or Fourier) analysis and one in the time domain through the wave intensity analysis.

1.5.1 Wave propagation in frequency domain: Impedance analysis

As discussed above the majority of studies on wave propagation were mostly done in the frequency domain, using impedance analysis. Arterial impedance (Z) (also called arterial input impedance) is another concept which counterparts the synonymous electrical term and is termed as the ratio between pressure (P) and flow (Q). Unlike resistance which is calculated from mean pressure and mean flow, impedance is a complex, time (or frequency)-dependent quantity that defines the dynamic relationship between pressure and flow. Usually, the impedance modulus decreases from its highest value at zero frequency to a minimum. The analysis of the complex relationship between pressure and flow in the frequency domain using Fourier analysis is possible only if the cardiovascular system is assumed to be in steady state. Using this analysis, the arterial pressure and flow waveforms can be decomposed into sinusoidal components (harmonics) with the appropriate frequencies, magnitudes and phase shifts. Although the impedance analysis has allowed for a better understanding of the wave propagation in arteries, as has been recently reported by Mitchell (Mitchell 2009), it has several limitations. First of all it implies the linearity of the system, i.e. that waves interact additively and also, even though Fourier transform recognizes the amplitude and phases of the various frequencies that contribute to a time series it cannot give information on their location within a time series. That means that Fourier analysis

cannot be used in case of non-periodic or transient flow. Linearity and periodicity are two debatable assumptions in the arterial system.

1.5.1.1 From the two to the four-element Windkessel model

As discussed in section 1.2.4, Frank quantitatively formulated the two-element Windkessel model. This model was inspired by the pumps in ancient fire engines that converted intermittent pumping into relatively steady flow by means of an air chamber (**Figure 1.5**).

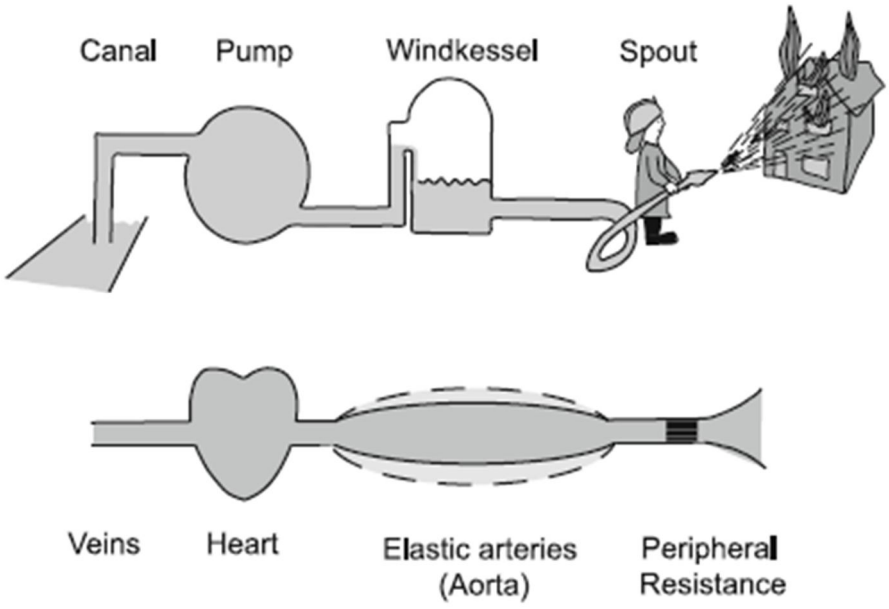

Figure 1.5: Sketch of the concept of the aortic two-element Windkessel. The model can be paralleled to an old fire engine pump and it can be described in terms of arterial compliance and peripheral resistance (Taken from Westerhof et al. 2009).

The Windkessel model includes a resistance and a compliance element (**Figure 1.6**) (Frank 1899). Since Poiseuille's law establishes that resistance is inversely proportional to the blood vessel radius to the fourth power, the resistance to flow in the cardiovascular system is largely confined in the smallest arteries and the arterioles. The peripheral resistance, R, is obtained adding all individual resistances in the microcirculation. The compliant element is mainly characterized by the elasticity of the large arteries and it can be found by adding all the compliances of all vessels and is therefore termed total arterial compliance, C. The two-element Windkessel calculates that during the diastolic phase of the cardiac cycle, when the aortic valve is closed,

pressure will decay exponentially with a characteristic decay time which equals RC. The Windkessel is a lumped model that describes the entire arterial system, using a pressure-flow relation at its inlet. Using this model, the wave travel and reflection phenomena cannot be taken into account. Moreover, the two-element Windkessel does not accurately predict the relationship between flow and pressure during systole. When flow measurements and Fourier analysis became available, the input impedence could be calculated (Westerhof et al. 1972; Milnor, Nichols 1975; Nichols et al. 1977) and a three-element Windkessel, comprising R, C and aorta characteristic impedance (Z_c), was proposed (**Figure 1.6**) (Westerhof et al. 1973). The three-element Windkessel can be seen as the first attempt to relate the lumped Windkessel model and wave travel phenomena since characteristic impedance equals wave speed times blood density divided by (aortic) cross-sectional area. Although the overall calculated pressure waveforms are similar to the measured ones, the high frequency details of the waveforms such as the inflection point and the augmentation in aortic pressure cannot be described by the three-element Windkessel model (Westerhof et al. 2009). Burattini and Gnudi (Burattini, Gnudi 1982) suggested adding another element in order to overcome the inaccuracy of the three-element Windkessel. Stergiopulos et al (Stergiopulos et al. 1999) proposed the four-element Windkessel, adding to the previous model an inertance element (**Figure 1.6**), which is the summation of all the inertances in the entire arterial system. The new element only affects the mean term and very low frequency behavior of the input impedance. However, due to the challenge of estimating the total inertance, the four-element Windkessel is not as successful as the three-element model (Westerhof et al. 2009).

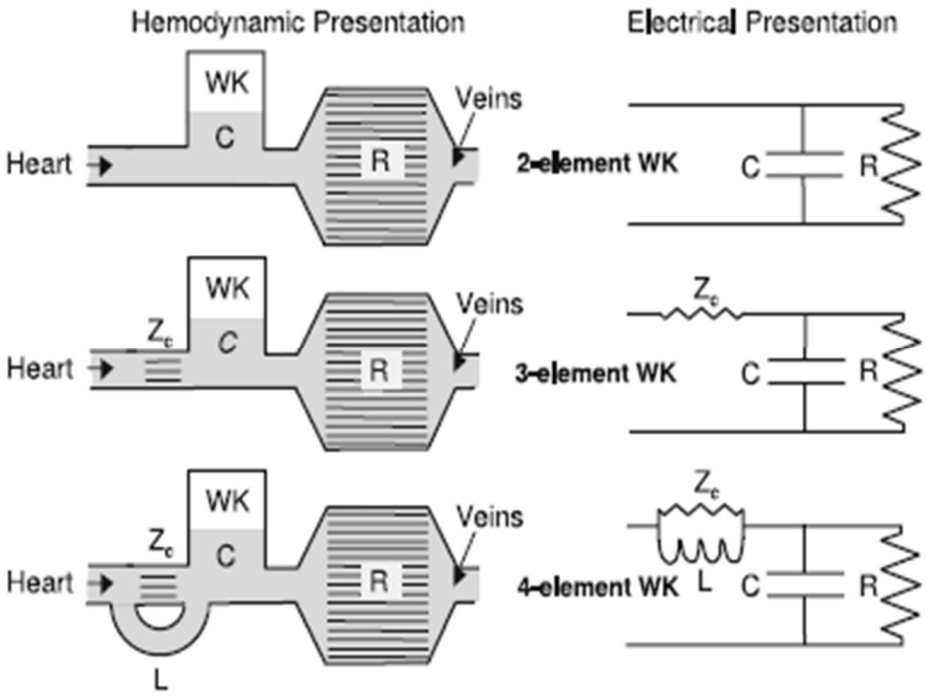

Figure 1.6: The two-element (top), the three-element (middle) and the four-element (bottom) Windkessel (WK) models presented in hydraulic and electrical form. R is the peripheral resistance, C the compliance, Z_c is the aortic characteristic impedance and L is the inertance (Taken from Westerhof et al. 2009).

1.5.2 Wave propagation in the time domain: Wave intensity analysis

Wave intensity analysis (WIA) for studying wave propagation in arteries was introduced by Parker and Jones in 1988 (Parker, Jones et al. 1988). It is based on the method of the characteristics (Riemann 1860) and, in its unseparated form, it does not assume any linearity or periodicity. WIA is an analysis in time domain and it represents the waveforms of pressure and velocity as successive wavefronts (small incremental waves) rather than the summation of sinusoidal wavetrains. Wavefronts are the elemental waves in wave intensity analysis. They can join each other as they propagate, causing waves to increase, or they can separate causing the wave to become less steep as it propagates. **Figure 1.7** shows an example of aortic pressure waveforms decomposed into sinusoidal wavetrains and successive wavefronts.

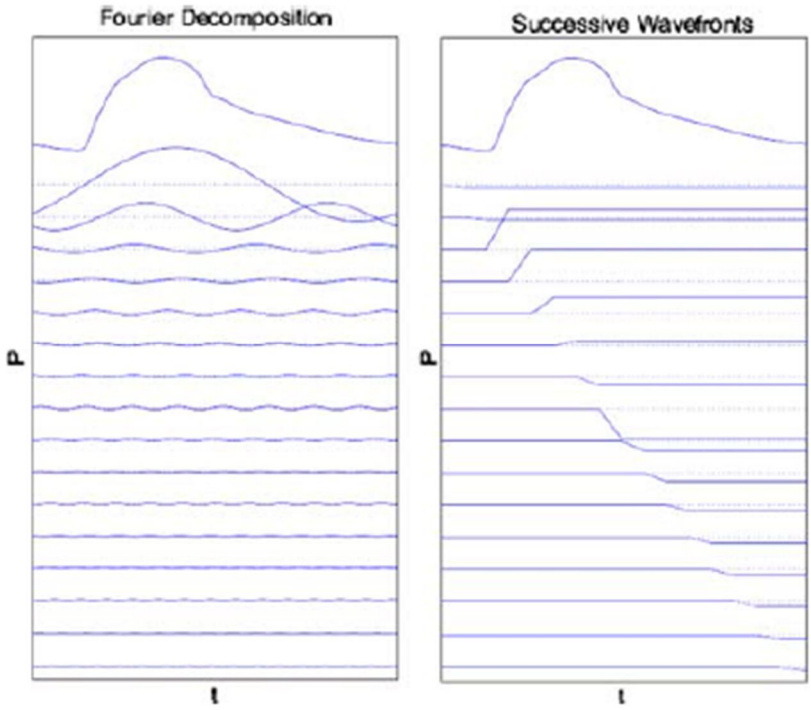

Figure 1.7: Measured pressure waveform in a human aorta (top of both pictures) and decomposition into sinusoidal wavetrains (left) and successive wavefronts (right). (Taken from Parker 2009).

Wave intensity (dI) is calculated as change in pressure times change in velocity

$$dI = dPdU$$

It has the dimensions of power/unit area and it is the flux of energy per unit area carried by the wave as it travels. This definition implies that the wave intensity values depend on the sampling rate. In order to overcome this problem an alternative definition of wave intensity can be used

$$dI = \frac{dP}{dt}\frac{dU}{dt}$$

A wave can be also characterized by the integral of the peak, $\int_{t_{start}}^{t_{end}} dIdt$. The result of the integration is called the wave energy. This quantity is associated with the energy carried by the wave and is generally much less than the total kinetic and potential energy associated with the wave (Parker 2009). **Figure 1.8** shows an example of wave intensity analysis performed in the human ascending aorta from the measured pressure and velocity. Positive values of dI correspond to forward waves and negative values to

backward waves. From the figure it is possible to identify three main peaks. The first peak is the initial compression (or acceleration) wavefront due to the contraction of the left ventricle. In mid-systole there is a negative peak indicating the reflection of the previous contraction wavefront. Then there is a second positive peak representative of a dominant forward wavefront at the end of systole that is a decompression (or deceleration) wave produced by the relaxation of the left ventricle.

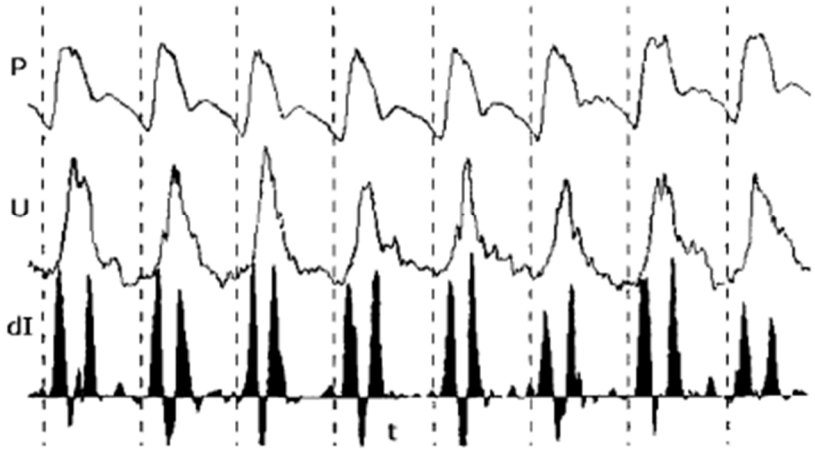

Figure 1.8: First measurement of wave intensity in man. Measured pressure P (top) and velocity U (middle) and net wave intensity dI (bottom). (Taken from Parker 2009).

WIA is a 1-D theory, thus it assumes the arteries are long, thin and elastic tubes. As a consequence of this assumption the variation of velocity across the cross-section is neglected and the no slip condition at the wall is not considered. An important property for the clinical use of wave intensity is that it is calculated in the time domain and thus it is easy to determine when waves are present at the measurement site, their time of arrival and their magnitude. Since the impedance method results are in the frequency domain it is difficult to define when the waves arrive.

1.5.2.1 Non-invasive wave intensity analysis

Feng and Khir (Feng & Khir 2010) developed another technique for studying the propagation of waves in flexible tubes based on noninvasive and simultaneous measurements of diameter (D) and U to separate diameter, velocity and wave intensity waveforms into their forward and backward components. The new wave intensity,

based on D and U measurements, was defined as the product of dD and dU. It has the same advantages of the traditional wave intensity analysis being positive for forward waves and negative for backward waves. While its reliability has been assessed in laboratory on hydraulic bench experiments (Feng & Khir 2010; Li & Khir 2011), the applicability in a clinical setting and using routine clinical measuring equipment has not been demonstrated.

1.5.3 Wave speed

To separate the wave intensity into its forward and backward components, the wave speed (c) must be known (Parker & Jones 1990). The wave speed (also called pulse wave velocity, PWV) is the speed at which disturbance travels along the medium and it depends on the mechanical and geometrical properties of the vessel and on the density of the blood (Milnor & Bertram 1978). Thomas Young (Young 1809) was the first scientist that determined this parameter for an arterial segment as the change in pressure and distensibility. Wave speed is an important clinical parameter because it is an indicator of arterial stiffness and cardiovascular disease. For this reason several methods have been developed to determine it. Theoretically, wave speed in a thin walled elastic tube filled with an incompressible fluid can be determined using the Moens-Kortweg equation, $c = \sqrt{\frac{Eh}{\rho D}}$, (Korteweg 1878; Moens 1879), where, c is the wave speed, E is the Young's modulus of the tube wall, h is the wall thickness, ρ is density of liquid and D is the diameter of tube. In clinical practice the most used method to calculate the wave speed is the "foot-to-foot" method, which implies pressure measurements in two different sites at known distance and the transit time of the wave. This technique gives an averaged wave speed along the path. Usually measurements are taken at the carotid and femoral level (**Figure 1.9)**.

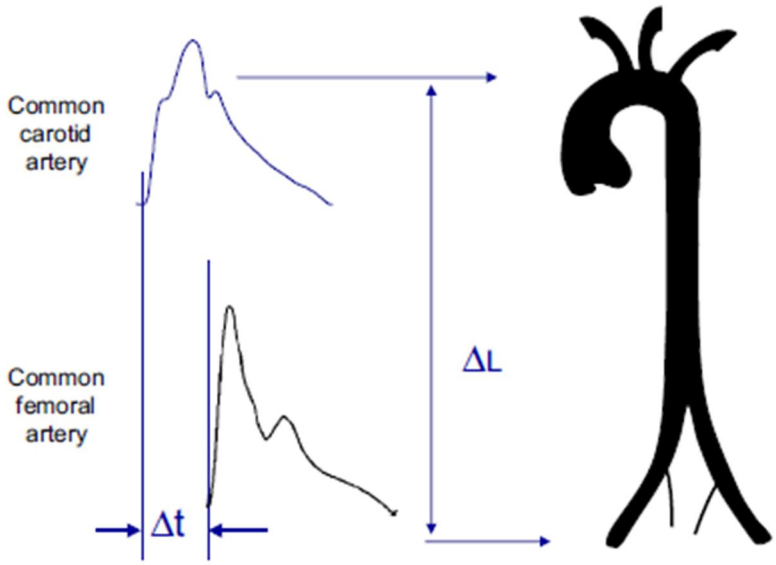

Figure 1.9: Foot-to-foot technique. The method implicates the measurement of the time that the wave takes to travel from one site to another (Δt) at known distance (ΔL). In this example the common carotid artery and the common femoral artery are the two sites and the reference point to calculate the time difference is the foot of the wave (Taken from Laurent et al. 2007).

In the past few decades other methods to determine the local wave speed using single point measurements have been developed:

- *PU-loop method*. Khir et al. (Khir et al. 2001) introduced the PU-loop method that consists of the determination of the slope of the linear portion of the loop at early systole where most probably only forward waves are present. The slope equals ρc, where ρ is blood density;
- *Area-Flow method*. Another technique to determine the wave speed in a specific point of the arterial tree is the area-flow method (Rabben et al. 2004); this is based on the definition of the characteristic impedance;
- *Sum of Squares method*. Davies et al. (Davies et al. 2006) extended the PU-loop principle deriving a formula that minimizes the net wave energy over a complete cardiac cycle using simultaneously P and U measurements in a single position. This technique was developed to overcome the problem of the determination of local wave speed in coronary arteries;

- *lnDU-loop method*. Another method that relies only on diameter and velocity measurements was introduced by Feng and Khir (Feng, Khir 2010). Local wave speed is determined from the slope of the linear portion of the lnDU-loop in early systole, which is equal to ½ c. The advantage of this method is that it does not rely on the pressure measurement that cannot be acquired non-invasively in all the arteries.
- *D^2P-loop method*. Alastruey (Alastruey 2011) proposed the D^2P-loop that consists of the determination of the slope of the linear part of the loop in diastole assuming the arterial wall as a Voigt-type visco-elastic material. The slope is equal to $D_0/\rho c^2$ (with D_0, mean arterial diameter).

1.6 Reservoir-wave approach

The Windkessel model, proposed in 1899 by Frank mentioned in section 1.5.1.1 (Frank 1899, Sagawa et al. 1990), shows the importance of the aortic compliance in turning the discontinuous cardiac output into a more continuous pressure and flow in the downstream arteries, storing about 50% of the left ventricular stroke volume during systole and forwarding it to the peripheral circulation during diastole (Belz 1995). The Windkessel model clarifies very well the diastolic part of the pressure waveform, but is not particularly accurate for the systolic one because it does not take into account the wave contribution. To explain these two phases and the differences in shape of pressure and flow waveforms a new time domain approach, that is a combination of the Windkessel model and the wave propagation theory, was proposed (Wang et al. 2003). The authors considered the measured pressure in the aorta (P) as the sum of a reservoir pressure (P_r) and a pressure due to the waves that is termed excess pressure (P_e). An example is shown in **Figure 1.10**. This new approach resolves the self-cancelling waves that appear in the separation of the flow waveforms using the measured pressure that can only be explained by self-cancelling forward and backward waves of nearly equal magnitudes (Davies et al. 2007; Tyberg et al. 2009).

The main findings of the study of Wang et al. (Wang et al. 2003) were: P_r is proportional to the aortic volume and the P_e waveform has the same shape of the aortic flow. In a separate study, wave intensity analysis was performed in the canine aorta using P_e and U (Tyberg et al. 2009). The results have shown that there are no significant backward-traveling waves to the aortic root at basal conditions. Although several

studies have been carried out using the reservoir-wave approach, the physical meaning of these new components of the measured pressure is still not completely understood as well as how these components change in healthy and non-healthy subjects has to be further investigated.

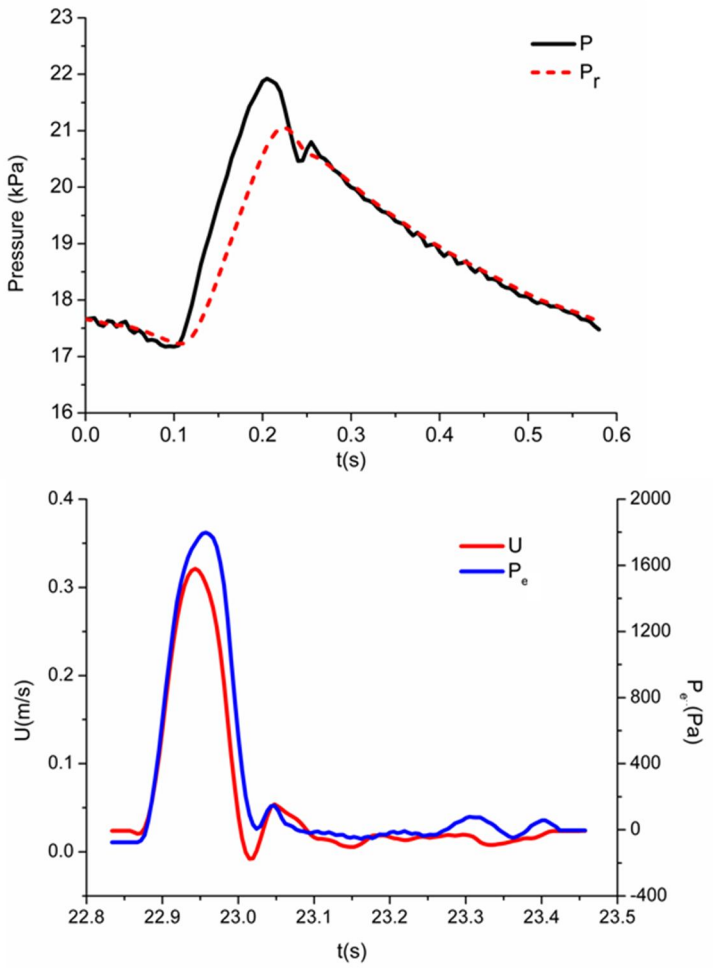

Figure 1.10: Example of reservoir pressure (P_r, top figure in red) calculated from a pressure waveform (P, top figure in black) measured in the aorta of a dog. In the bottom figure, excess pressure (P_e, in blue) and velocity (U, in red) measured at the same site are plotted together to show the similarity between the two curves.

1.6.1 Reservoir-wave approach at an arbitrary location

The reservoir-wave theory as first introduced by Wang et al. (Wang et al. 2003), is based on the assumption that the flow is zero during diastole. This is true only at the aortic root when the aortic valve closes at the beginning of diastole. To use the same approach at different locations along the arterial tree, the concept of the reservoir-wave

theory has been further developed by Aguado-Sierra et al. (Aguado-Sierra et al. 2008a) assuming a similar exponential decay in diastole at different sites of the arterial system. They showed that it is possible to separate both the measured pressure in the reservoir and the excess components along the aorta; they also developed the reservoir-wave approach to the velocity waveforms, introducing the concept of reservoir and excess velocity (**Figure 1.11**). Note that in the original paper of Aguado–Sierra et al. (Aguado-Sierra et al. 2008a) the reservoir pressure and velocity are termed $\overline{P}$ and $\overline{U}$, respectively, and the excess components *p* and *u*, respectively. In this thesis the reservoir pressure and the velocity components are called P_r and U_r and the excess components P_e and U_e.

The hemodynamics in other locations of the arterial system using the reservoir-wave approach has not been studied yet.

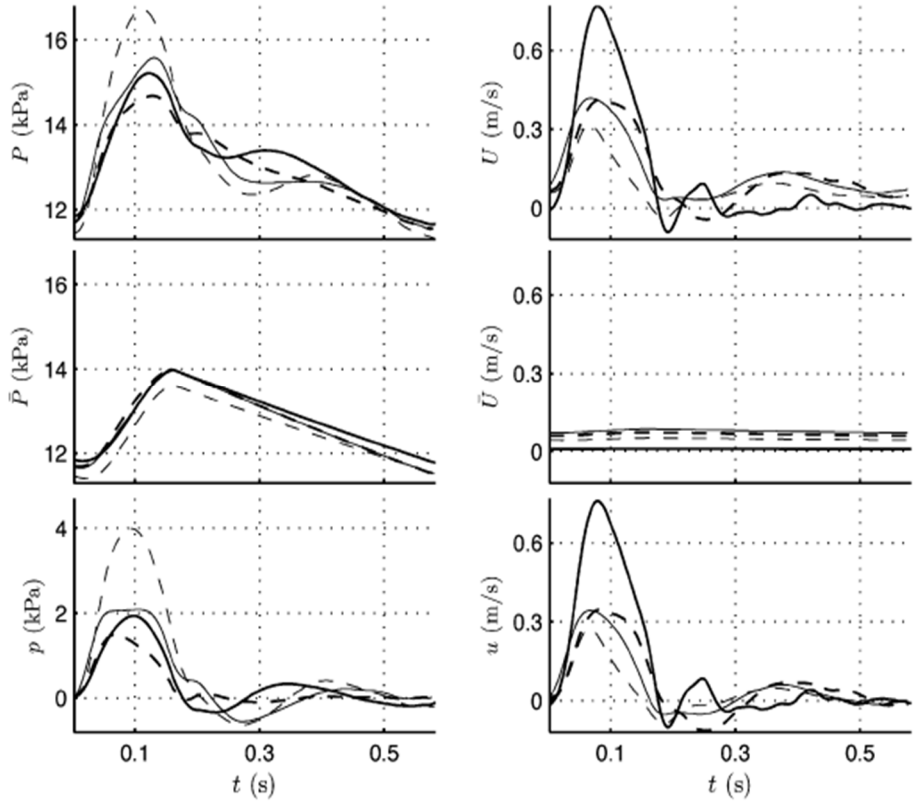

Figure 1.11: Simultaneous pressure (P) and velocity (U) measurements at different aortic locations in a dog and their corresponding reservoir–wave separated components. Pressures are shown on the left and the velocities on the right. Thick solid curves, ascending aorta; thick dashed curves, aortic arch; thin solid lines curves, thoracic aorta; thin dashed curves, abdominal aorta (Taken from Aguado-Sierra et al. 2008a).

1.7 Importance of wave speed and wave intensity analysis in clinical practice

Wave speed is a parameter of particular physiological and clinical interest as it gives a direct measure of arterial stiffness. Increased stiffness of large elastic arteries is an early risk factor for cardiovascular diseases (Blacher et al. 1999; Cohn 2006; Vlachopoulos et al. 2010) and it has been reported that it is related to the following conditions: aging (Avolio et al. 1983; Mitchell et al. 2004; O'Rourke, Nichols 2005), hypertension (Benetos 1997), diabetes (Schram et al. 2004), atherosclerosis (Van Popele et al. 2001), heart failure (Kawaguchi et al. 2003) and others (Rubin et al. 2005). Wave intensity analysis is a relevant hemodynamic parameter in clinic practice for understanding how the waves travel along the arterial tree. This is a useful tool to evaluate the working conditions of the heart interacting with the arterial system (Ramsey, Sugawara 1997; O'Rourke 2002, Penny et al. 2008; Sugawara et al. 2009). In 2003 Ohte et al. (Ohte et al. 2003) used WIA in the carotid artery to assess left ventricular systolic and early diastolic performance in subjects with suspected coronary artery disease. They found a strong correlation between the magnitude of the first positive peak of the wave intensity with the maximum rate of left ventricle pressure rise and between the second positive peak and the time constant of the left ventricle relaxation. In the same year Bleasdale et al. (Bleasdale et al. 2003) established a new index of cerebral vasomotor tone using WIA at the common carotid artery in a population of healthy subjects. The WIA applied at different peripheral arteries has shown differences in wave patterns (Zambanini et al. 2005). Wave intensity analysis shows also differences between normal and pathological subjects. In particular, Curtis et al. (Curtis et al. 2007) found that the energy carried by the forward compression wave is significantly reduced in subjects with heart failure and the one carried by the backward wave was increased. A more recent study has found that the wave reflection index calculated from the wave intensity analysis is a predictor of future cardiovascular events in hypertensive subjects (Manisty et al. 2010).

So far the majority of the methods to determine c and WI are based on pressure waveforms that cannot be determined noninvasively in all arteries. In 2000, Sugawara et al. discovered a linear relationship between diameter and pressure waveforms in the carotid artery during systole (Sugawara et al. 2000). This finding led to the development of a non-invasive real-time measurement system of wave intensity (Harada et al. 2002) where diameter changes are measured with an echo-wall tracking system and used as a

surrogate for pressure changes. Systolic and diastolic blood pressures are used to convert the diameter waveform into pressure. The blood flow velocity is measured with range-gated Doppler signals.

The non-invasive wave intensity analysis and the lnDU-loop method for the determination of c introduced in sections 1.5.2.1 and 1.5.3, respectively, contrary to Harada's technique, have the advantage to not assume any linear relationship between pressure and diameter. The introduction of these techniques in clinical routine would be potentially useful as screening tool for cardiovascular diseases. For this reason, a study of the application of these non-invasive methods in healthy and non-healthy human has to be carried out.

1.8 Relevance of the reservoir-wave approach in clinical practice

The concept of two separate components of the measured pressure related to two different phenomena attracted the interest of other authors that tried to investigate the potential use of the new approach in clinical routine. Davies et al. (Davies et al. 2010a) found that the magnitude of the reservoir pressure increases with age and is the major determinant of the aortic augmentation index, which was considered to be caused mainly by the reflection waves. The same authors, also, reported that the time integral of the excess pressure is a predictor of cardiovascular events (Davies et al. 2010b). These studies demonstrated that the reservoir and excess pressure seem to be a promising tool to be used clinically for prevention, diagnosis or treatment of cardiovascular diseases. Therefore, the potential of this new approach has to be further investigated.

1.9 Motivation for research

As it has been discussed previously in this chapter, it appears evident that wave speed is an important measure of the arterial stiffness. Even though the wave speed was widely studied, most of the techniques employed to determine wave speed are based on pressure measurement, which is not easy to measure non-invasively in all the arteries. For this reason it is difficult to apply these techniques of wave speed determination into the clinical examination practice. The introduction of the lnDU-loop method, proposed by Feng and Khir (Feng 2008; Feng, Khir 2010), could be very promising for routine examination since it is based only on D and U measurements that can easily be recorded

non-invasively in the clinical environment with an ultrasound system. Moreover, the method does not make any assumptions about the relation between pressure and diameter and it does not require the measurement of the pressure waveform, nor of its systolic, diastolic or mean value in order to calibrate the diameter waveform of another artery. The lnDU-loop has been already validated *in vitro* (Li, Khir 2011; Li 2012), but a human study is still lacking.

The reservoir-wave approach seems to have resolved the self-cancelling wave that appears in the linear separation of the flow waveforms and the subtraction of the reservoir pressure allows the study of wave propagation employing wave intensity analysis using the excess pressure (Wang et al. 2003; Davies et al. 2007; Tyberg et al. 2009). However, recently some investigators have questioned the validity of this theory (Mynard et al. 2012; Segers et al. 2012). In particular, Maynard et al. performed wave intensity analysis on computational and animal data and found that using the reservoir-wave approach the wave pattern is not reproduced faithfully by the wave intensity analysis after the subtraction of the reservoir pressure. On the contrary, some other investigators have demonstrated that a paradoxical pattern of wave reflection could appear if the reservoir pressure is not taken into account (Wang et al. 2011). The debate about the more correct model to be used for describing the wave propagation in arteries is still open in the literature.

However, the use of the reservoir wave approach at different vascular locations and the concepts of a reservoir and excess velocity seem to open a new perspective in arterial hemodynamics. Moreover, the findings related to the potential use of reservoir and excess pressure as screening and diagnostic parameters (Davies et al. 2010a; Davies et al. 2010b) are promising, but a wider study in physiological and pathological condition is still needed.

1.10 Aims and objectives

The aim of this thesis therefore is to improve the understanding of wave propagation in central and peripheral arteries using different approaches for determining wave speed, intensities and other hemodynamic parameters in healthy human and in simulated pathological conditions. Furthermore, another aim of this thesis is to introduce a non-invasive technique for determining the mechanical properties of the arterial wall and wave intensities in humans.

The specific objectives of this thesis are:

1) To give a contribution to the debate about the more correct model for describing the wave propagation; quantifying the differences between the wave-only and the reservoir-wave models in describing the wave propagation in the ascending aorta when clear reflection sites are present;

2) To study the arterial distensibility and other hemodynamic parameters in more accessible arteries that can be examined in clinical practice using a new non-invasive technique based on diameter and flow velocity measurements;

3) To investigate non-invasively the changes of elastic and muscular arteries in relation to age and gender in healthy subjects;

4) To separate the velocity waveform into the reservoir and excess components related to the corresponding reservoir and excess components of the pressure and to investigate the changes of these parameters in the carotid artery of healthy human in relation to age and gender;

5) To investigate the effects of the ageing process and pathological conditions on reservoir and excess pressure components in central arteries.

1.11 Thesis outline

In order to achieve the above mentioned aims and objectives this work has been structured in the following way:

- Chapter 2: This chapter is entitled “Theoretical background” and covers all the mathematical formulation for the theories used throughout this thesis.
- Chapter 3: This chapter is entitled “Comparison between wave-only and reservoir-wave approach for the analysis of arterial waves in the canine aorta”. To provide a contribution to the debate about the correct approach to describe wave propagation in arteries, in this chapter, the hemodynamics of the canine aorta in control condition and during total aorta occlusion at four different levels (thoracic, diaphragm, abdominal and iliac) was studied measuring pressure and velocity invasively at the aortic root. Similarities and differences between the wave-only

theory and the reservoir-wave approach in the determination of wave speed and intensities in these conditions were assessed.

- Chapter 4: This chapter is entitled “Non-invasive determination of local wave speed and intensities in carotid and femoral arteries of healthy human”. In this chapter the hemodynamic of central and peripheral human arteries was investigated. Carotid and femoral arteries are more superficial vessels compared to the ascending aorta and thus more suitable for clinical examination. A new non-invasive technique based on diameter and velocity measurements was used here to determine arterial distensibility, wave speed and intensity in the carotid and femoral arteries of healthy human. In this chapter the changes of these hemodynamic parameters with age and gender were also investigated and differences between elastic and muscular arteries were assessed.
- Chapter 5: This chapter is entitled “Reservoir pressure and velocity in the human carotid artery”. In this chapter the reservoir-wave approach was applied to study the hemodynamics of the carotid artery in the same population used in chapter 4. The carotid artery is an elastic artery relatively close to the heart and thus the hemodynamics of this vessel is related to the left ventricle function. Pressure and flow velocity measurements were separated into their reservoir and excess components using an algorithm that allows for the use of this approach not only at the aortic root but also in other locations of the arterial tree. Effects of age and gender on the reservoir/excess components of velocity and pressure, and wave intensities were investigated.
- Chapter 6: This chapter is entitled “Reservoir and excess pressure changes with vascular compliance and stroke volume”. Whilst in the previous study the reservoir and excess components of the pressure were investigated in healthy subjects; in this chapter they were investigated in relation to a change of aortic compliance and stroke volume in order to simulate the ageing process and pathological conditions. These changes were studied *in vitro,* in the ascending aorta of a mock circulatory system of the arterial circulation.
- Chapter 7: This chapter is entitled “Conclusions and future work”. It contains a general discussion, a summary of conclusions related to chapters 3-6 and future works.

Chapter 2 : Theoretical Background

2.1 Introduction

A one-dimensional model to describe fluid flow in elastic tubes has been developed by Euler in 1775 (Euler 1775). The equations of motion for fluid of the model are complex, hyperbolic partial differential equations. They were solved in 1860 when Riemann proposed the method of characteristics (Riemann 1860). The work of Riemann provided the basis for the development of wave intensity analysis (WIA) which has been briefly discussed in chapter 1. WIA relies on the solution of Euler's mathematical model and equations using the method of characteristics (Parker, Jones 1990).

In this chapter the analytical details to derive the wave intensity analysis from the conservation laws that each arterial segment must respect are reported. The two main assumptions that are made when the one-dimensional model is applied to the flow in arteries are:

1) Blood is considered as an incompressible fluid because its compressibility is small in comparison to the large distensibility of the arterial wall (Lighthill 1978, Pedley 1980).
2) The arterial radius expansion and contraction have to be small compared to its undisturbed value, which means that radial fluid motion is negligible compared to the longitudinal one (Lighthill 1978).

2.2 Governing flow equations

Blood flow in arteries follows the laws of conservation for mass and momentum.

Mass law: The conservation law states that an equal quantity of incompressible fluid flowing into a system must flow out, since mass can neither be created nor destroyed

$$\frac{\partial A}{\partial t} + \frac{\partial (AU)}{\partial x} = 0 \qquad (2.1)$$

where A is the cross-sectional area, t is time, U is the spatially averaged velocity and x is the axial distance along the tube .

Momentum law: it is derived from Newton's second law that is Force = mass x acceleration (Newton 1687) that can be rearranged to become Force = rate of change of momentum, which equals the resultant force acting on the body.

$$\frac{\partial U}{\partial t} + U\frac{\partial U}{\partial x} + \frac{1}{\rho}\frac{\partial P}{\partial x} = 0 \tag{2.2}$$

where P is the spatially averaged pressure and ρ is the density of the fluid.

Blood vessels are considered as impermeable elastic tubes with uniform and constant properties and the effects of viscous dissipation are assumed to be negligible. As the cross-sectional area of the tubes changes during systole and diastole as a result of the variation in pressure and the elastic properties of the wall, the values rely on the instantaneous pressure only (Parker & Jones 1990). Accordingly, A can be defined as a function of P that itself is a function of x and t. Equation 2.3 describes the tube law which is the relationship between transmural pressure and cross sectional area

$$A = A\,(P(x,t)) \tag{2.3}$$

And if we expressed this as rate of change of the cross-sectional area at time (t) and distance (x)

$$\frac{\partial A}{\partial t} = \frac{dA}{dP}\frac{\partial P}{\partial t} \quad \text{and} \quad \frac{\partial A}{\partial x} = \frac{dA}{dP}\frac{\partial P}{\partial x} \tag{2.4}$$

The substitution of equation 2.4 into equation 2.1 leads to

$$\frac{dA}{dP}\frac{\partial P}{\partial t} + \frac{dA}{dP}U\frac{\partial P}{\partial x} + A\frac{\partial U}{\partial x} = 0 \tag{2.5}$$

That divided by the arterial segment compliance and rearrange gives

$$\frac{\partial P}{\partial t} + U\frac{\partial P}{\partial x} + \frac{A}{dA/dP}\frac{\partial U}{\partial x} = 0 \tag{2.6}$$

which is a first order hyperbolic partial differential equation, which can be solved using the method of characteristics (Riemann 1860). Matrix notation can be used to express equations 2.2 and 2.6 as

$$\omega t + \Omega\omega x = \Phi \tag{2.7}$$

where $\omega = \begin{pmatrix} P \\ U \end{pmatrix}$ and $\Omega = \begin{pmatrix} U & \frac{1}{D_s} \\ \frac{1}{\rho} & U \end{pmatrix}$

where D_s is the distensibility of the vessel wall which can be defined as the rate of change of A per change of the P over the initial area

$$D_s = \frac{1}{A}\frac{dA}{dP} \tag{2.8}$$

The eigenvalues, λ, of the matrix Ω, are solutions of the characteristic polynomial

$$\left|\Omega - \lambda I\right| = 0 \tag{2.9}$$

where I is the identity matrix and the eigenvalues represent speed of propagation

$$\Omega = \begin{bmatrix} (U-\lambda) & \frac{1}{D_s} \\ \frac{1}{\rho} & (U-\lambda) \end{bmatrix} = (U-\lambda)^2 = \frac{1}{\rho D_s} \tag{2.10}$$

The left term of the equation 2.10 can be defined as c^2, thus

$$c^2 = \frac{1}{\rho D_s} \quad \text{and also,} \quad c^2 = (U-\lambda)^2 \tag{2.11a) and (2.11b)}$$

consequently, the eigenvalues of the matrix Ω are

$$\lambda_{\pm} = U \pm c \tag{2.12}$$

where c is the local wave speed.

The characteristic directions are

$$\frac{dx}{dt} = U \pm c \tag{2.13}$$

and they can be used to convert partial differential equations (PDE) into a system of ordinary differential equations (ODE) assuming that the waves run in the space-time plane along the characteristic directions

$$\frac{dU}{dt} \pm \frac{1}{\rho c}\frac{dP}{dt} = 0 \tag{2.14}$$

Considering the wave speed is a function of local pressure this equation can be rewritten as Riemann function terms

$$R_{\pm} = U \pm \int_{P_0}^{P} \frac{dP}{\rho c} \tag{2.15}$$

where R is the Riemann invariant, P_0 is an arbitrary pressure and (+) and (-) indicate the direction of wave travel (+ indicates forward and – backward direction). The differential form of equation 2.15 is

$$dR_{\pm} = dU \pm \frac{dP}{\rho c} = 0 \tag{2.16}$$

2.2.1 The water-hammer equation

In order to show more clearly the straightforward relationship between pressure and velocity equation 2.16 can be written as

$$dP_{\pm} = \pm \rho c dU_{\pm} \tag{2.17}$$

which is the well-known water-hammer equation that enables one to calculate the pressure dependent wave speed of a wavelet when travel is only unidirectional.

2.2.2 The pressure-velocity loop method

In order to separate the waves into backward and forward components, the knowledge of c is essential. In **Figure 2.1** pressure P is plotted against velocity U over a whole cardiac cycle in order to obtain a PU-loop. In the early ejection phase, where only unidirectional waves are present, the relationship between pressure and velocity is linear and the slope of this linear part equals ρc as predicted by integration of the water hammer equation

$$P_+ - P_0 = \rho c U_+ \tag{2.18}$$

where P_0 is the diastolic pressure.

The PU-loop method has been shown to give accurate results in both *in vivo* (Khir et al. 2001) and *in vitro* experiments (Khir & Parker 2002). This technique to calculate wave speed has been used in chapters 4, 5 and 6.

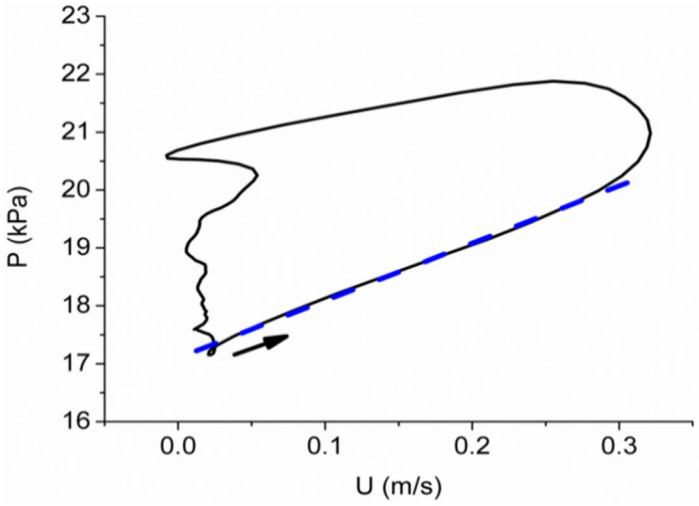

Figure 2.1: Example of PU-loop in a dog during thoracic occlusion. The blue line is the linear fitting of the linear part of the loop in early systole and arrow indicates the direction of the loop.

2.2.3 Wave separation

All measured pressure and velocity values are derived from forward and backward wavefronts that intersect at a precise time and plane. Assuming that the increments in pressure and velocity are the linear summation of variation of P and U in forward and backward directions we can write

$$dP = dP_+ + dP_- \text{ and } dU = dU_+ + dU_- \qquad \text{(2.19) and (2.20)}$$

Replacing the water-hammer equation in equations 2.19 and 2.20 we can calculate dP and dU in forward and backward direction as

$$dP_\pm = \frac{1}{2}\left(dP \pm \rho c dU\right) \qquad (2.21)$$

$$dU_\pm = \frac{1}{2}\left(dU \pm dP \big/ \rho c\right) \qquad (2.22)$$

Integrating equations 2.21 and 2.22

$$P_+ = P_0 + \sum_{t=0}^{T} dP_+ \quad P_- = P_0 + \sum_{t=0}^{T} dP_- \qquad (2.23)$$

$$U_+ = U_0 + \sum_{t=0}^{T} dU_+ \quad U_- = U_0 + \sum_{t=0}^{T} dU_- \qquad (2.24)$$

where P_0 and U_0 are integration factors and T is the duration of the whole beat. P_0 has been assumed equal to the diastolic pressure for P_+ and all the other integration factors have been assumed to be equal to zero.

2.2.4 Wave intensity

The intensity of the wave can be calculated as dI=dPdU and is the flux of energy carried by the waves per unit area. Forward and backward intensities can be defined as $dI_+=dP_+dU_+$ and $dI_-=dP_-dU_-$, respectively. If c is known, then the intensity of the waves can be separated in the forward and backward component

$$dI_{\pm} = \pm\frac{1}{4\rho c}\left(dP \pm \rho c dU\right)^2 \tag{2.25}$$

Wave intensity is always positive for forward waves and negative for those that are travelling in backward direction. Equation 2.25 can be integrated to obtain the energy of the wave

$$I_{\pm} = \int_0^T dI_{\pm} dt \tag{2.26}$$

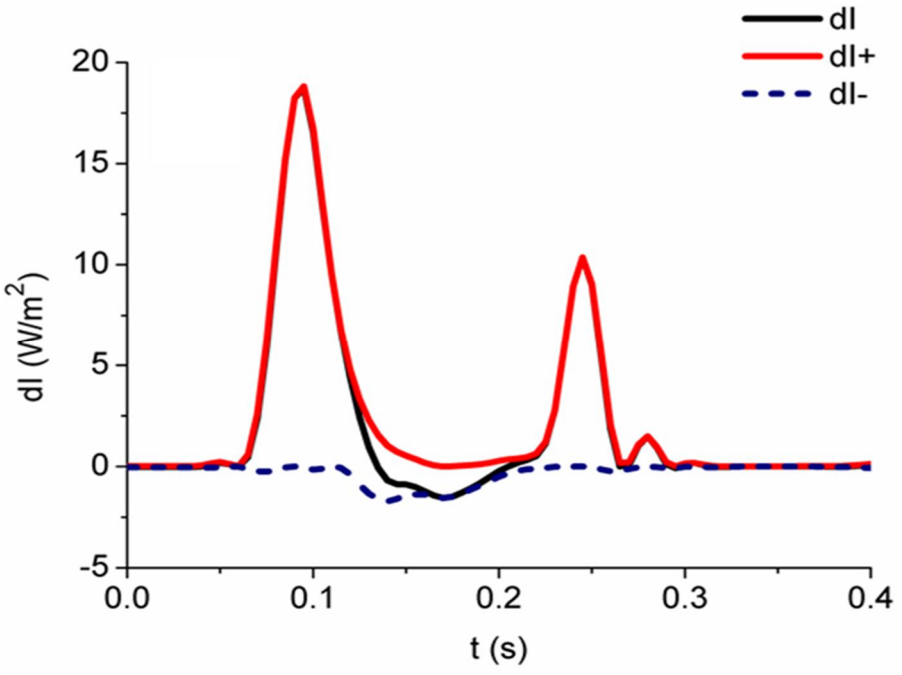

Figure 2.2: Example of wave intensity in the aorta of a dog. Net (dI, black), forward (dI_+, red) and backward (dI_-, dashed blue) wave intensities.

Figure 2.2 shows an example of wave intensity analysis in a canine aorta; the net intensity (dI) is separated into its forward (dI_+) and backward (dI_-) component using equation 2.25. Two main positive waves can be detected; one in early systole that is the forward compression wave due to the ventricular ejection and one in late systole that is the forward expansion wave due to the reduction in left ventricle rate of contraction. In

mid-systole a negative wave is predominant, which is the backward compression wave due to the reflections from the periphery. The area under these curves gives the energy of the waves.

2.2.5 Non-invasive determination of wave speed using diameter and velocity

As discussed in chapter 1, determination of wave speed is useful in clinical environment because it is a marker of vascular disease (Blacher et al. 1999; Mitchell et al. 2010). However, a pressure waveform cannot be obtained in a non-invasive way in all arteries. For this reason, a mathematical formulation for wave speed determination that involves diameter (D) and velocity measurements has been recently developed (Feng 2008; Feng & Khir 2010). This new technique has been already validated *in vitro* (Li & Khir 2011; Li 2012) and an *in vivo* study is part of chapter 4.

The formulation for the assessment of c using D and U follows. If we consider a vessel circular cross sectional area we can write

$$\frac{dA}{A} = \frac{2dD}{D} \tag{2.27}$$

where D in the change in diameter. Replacing equation 2.27 in 2.11a and rearranging we have

$$dP = \rho c^2 \frac{2dD}{D} \tag{2.28}$$

Assuming dD as the linear summation of diameter changes due to changes in the forward and backward diameter changes,

$$dD = dD_+ + dD_- \tag{2.29}$$

substituting equation 2.29 in equation 2.28 and considering equation 2.18, we can write

$$dP_+ + dP_- = \frac{2\rho c^2}{D}\left(dD_+ + dD_-\right) \tag{2.30}$$

which can be expressed in terms of D and U only using the water-hammer equation (equation 2.17)

$$c = \frac{D}{2}\left(\frac{dU_+ - dU_-}{dD_+ + dD_-}\right) \tag{2.31}$$

Assuming that dD/D = dlnD, which is the incremental hoop strain, c can be determined as

$$c = \pm\frac{1}{2}\frac{dU_\pm}{d\ln D_\pm} \tag{2.32}$$

Plotting lnD against U gives a lnDU-loop with a linear portion in early systole, as the PU-loop. In this case the slope of the linear part equals equals ½ c. In **Figure 2.3** a typical example of a lnDU-loop is shown.

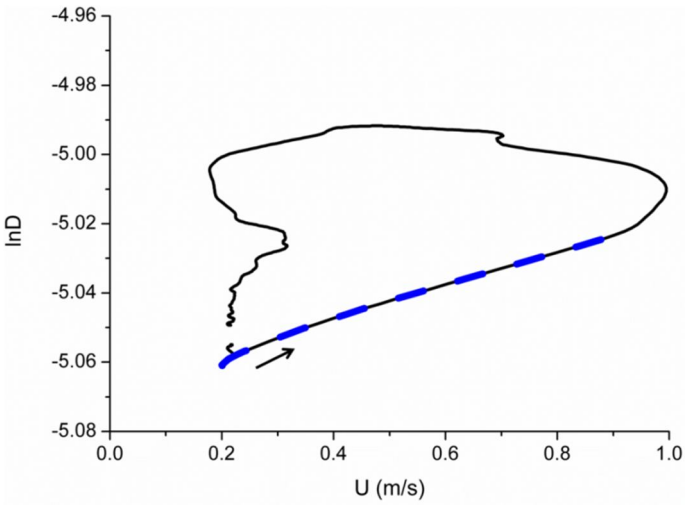

Figure 2.3: Example of lnDU-loop in the femoral artery of a healthy human. The blue line is the linear fitting of the linear part of the loop in early systole and arrow indicates the direction of the loop. The diameter in expressed in (m).

2.2.6 Non-invasive wave intensity analysis

Based on the above formulation also the wave separation and a non-invasive wave intensity analysis ($_n$dI) have been developed (Feng & Khir 2010). Using the water-hammer equation (2.17) in equation 2.28 in order to have the expression in terms of D and U only and considering unidirectional waves lead to

$$dD_{\pm} = \frac{D}{2c} dU_{\pm} \tag{2.33}$$

Since the change in velocity is a linear summation of velocity changes in forward and backward directions (equation 2.20) we can write

$$dD_{\pm} = \frac{1}{2}\left(dD \pm \frac{D}{2c} dU \right) \tag{2.34}$$

$$dU_{\pm} = \frac{1}{2}\left(dU \pm \frac{2c}{D} dD \right) \tag{2.35}$$

Integration of equations 2.34 and 2.35 leads to

$$D_{+} = D_0 + \sum_{t=0}^{T} dD_{+} \quad D_{-} = D_0 + \sum_{t=0}^{T} dD_{-} \tag{2.36}$$

$$U_+ = U_0 + \sum_{t=0}^{T} dU_+ \quad U_- = U_0 + \sum_{t=0}^{T} dU_- \tag{2.37}$$

where D_0 and U_0 are integration factors and T is the duration of the whole beat. D_0 has been assumed equal to the diastolic diameter for D_+ and all other integration factors have been assumed equal to zero.

Non-invasive wave intensity can be calculated as ${}_n$dI=dDdU and can be separated in forward and backward direction as for the traditional wave intensity analysis

$${}_n dI = \pm \frac{1}{4(D/2c)} \left(dD \pm \frac{D}{2c} dU \right)^2 \tag{2.38}$$

Non-invasive wave intensity is always positive for forward waves and negative for those that are travelling in backward direction. Equation 2.38 can be integrated to obtain the energy of the wave as in equation 2.26.

2.2.7 Wave classification

Waves can be classified in four different classes based on their nature (compression and expansion) and direction (forward and backward). Compression waves are related to an increase in pressure and diameter that induces acceleration if the wave is travelling in the forward direction and deceleration in case of backward direction. On the other hand, expansion waves are associated with a decrease in pressure and diameter, which induces acceleration if the wave is running in the backward direction and deceleration for the forward direction. In **Table 2.1** the wave classification is reported.

Table 2.1: Wave classification.

Direction	Wave	dP	dU	dD	dI	${}_n$dI
Forward	**Compression**	>0	>0	>0	>0	>0
	Expansion	<0	<0	<0	>0	>0
Backward	**Compression**	>0	<0	>0	<0	<0
	Expansion	<0	>0	<0	<0	<0

2.2.8 Reservoir-wave theory

In this section, the mathematical formulation of the model proposed by Wang et al. (Wang et al. 2003) is reported. Throughout the thesis this model will be called reservoir-wave model.

The authors assumed that the measured pressure at the aortic level (P) is the linear summation of a pressure due to the waves that they called excess pressure (P_e) and a reservoir pressure due to the elastic properties of the aorta (P_r),

$$P(x,t) = P_e(x,t) + P_r(t) \tag{2.39}$$

where P_r varies with time only.

Variation of aortic P_r can be defined as

$$\frac{dP_r(t)}{dt} = \frac{dP_r}{dV_r}\frac{dV_r}{dt} = \frac{Q_{in}(t) - Q_{out}(t)}{C} \tag{2.40}$$

where V_r is the reservoir volume, Q_{in} is the aorta inflow, Q_{out} the outflow and C is the compliance of all the arterial tree. Q_{out} can be described by the follow equation

$$Q_{out}(t) = \frac{P_r(t) - P_\infty}{R} \tag{2.41}$$

where P_∞ is the asymptotic pressure of the diastolic exponential decay and R is the resistance of the peripheral systemic circulation. Substituting equation 2.41 in equation 2.40

$$\frac{dP_r(t)}{dt} + \frac{P_r(t) - P_\infty}{RC} = \frac{Q_{in}(t)}{C} \tag{2.42}$$

leads to the general solution

$$P_r(t) - P_\infty = (P_0 - P_\infty)e^{-1/RC} + e^{-t/RC}\int_{t_0}^{t} \frac{Q_{in}(t')}{C} e^{t'/RC} dt' \tag{2.43}$$

where t_0 and P_0 are time and pressure at the beginning of the ejection. Q_{in} was considered zero during the diastole.

Once P_r has been subtracted from the measured pressure, P_e can be used instead of P to determine the wave speed (P_eU-loop method), to separate the waves in forward and backward direction and to calculate the wave intensity as $dI=dP_e dU$. This model has been used in chapter 3 to assess the differences with the traditional wave theory in the canine aorta and in chapter 6 to study the reservoir and excess pressure components in the aortic root of a mock circulatory system.

2.2.9 Extension to reservoir velocity

In this section the extension of the reservoir-wave model to an arbitrary location is reported (Aguado-Sierra et al. 2008a).

They assumed that also velocity is the sum of a reservoir (U_r) and an excess (U_e) component

$$U(x,t) = U_e(x,t) + U_r(x,t) \tag{2.44}$$

Note that U_r depends also on the position while P_r depends only on time.

To determine U_r, it has to be assumed that it is directly proportional to $P\text{-}P_\infty$ in the diastolic part where the reservoir effect is prevailing and the wave activity negligible. U_r is given as

$$U_r = \frac{P - P_\infty}{\overline{R}} \tag{2.45}$$

where $\overline{R}$ is the effective resistance of the vessels downstream of the measurement site and can be determined from the linear portion of the PU-loop in diastole or as $\overline{R} = (< P > - P_\infty) / < U >$ where <P> and <U> are the time-averaged pressure and velocity between the dicrotich notch time, T_n, and the end of the beat, T. Once $\overline{R}$ is determined, U_r can be determined at any time $0 < t < T$ as

$$U_r = \frac{P_r - P_\infty}{\overline{R}} \tag{2.46}$$

and is equal to the velocity due to the reservoir pressure only in the case of negligible compliance downstream of the measurement site. U_e can be calculated as $U_e = U - U_r$ (2.47)

U_e can be used instead of U to determine the wave speed (P_eU_e-loop method), to separate the waves in forward and backward direction and to calculate the wave intensity as $dI = dP_e dU_e$. This model was used in chapter 5 to study the carotid hemodynamics in healthy subjects.

Chapter 3 : Comparison between wave-only and reservoir-wave approach for the analysis of arterial waves in the canine aorta

3.1 Introduction

As mentioned at the end of chapter 1, this chapter compares two different models for describing wave propagation in arteries, during aortic occlusion. In particular, the two techniques are the traditional wave intensity analysis and the more recent reservoir-wave approach.

The Windkessel model, proposed in 1899 by Frank (Sagawa et al. 1990), shows the importance of aortic compliance in turning the discontinuous cardiac output into a more steady flow in the microcirculation; about half of the volume flow rate during systole is stored in the compliant arteries which contract during diastole making the volume flow rate through the microcirculation much more uniform (Belz 1995). The model consists of a resistance to flow through the microcirculation (R) that depends on the peripheral vessels and a compliance (C) determined mainly by the elasticity of the large arteries. The model predicts that the arterial pressure will decay exponentially during diastole with a time constant RC. The Windkessel model, as originally presented, describes the diastolic part of the pressure waveform very well, but is not particularly accurate for systole because it does not take into account the contribution of waves (Westerhof et al. 2009).

The addition of the characteristic impedance to the two-element Windkessel was proposed to link the lumped model and the wave propagation in the arterial system (Westerhof et al. 1969; Westerhof et al. 1971). However, the three-element Windkessel is not able to describe high frequency details such as the inflection point and the augmentation shoulder in aortic pressure (Westerhof et al. 2009).

Wave intensity analysis (WIA) is a time-domain technique based on the classical one-dimensional flow equations in flexible tubes, and was introduced as an alternative to the frequency-domain techniques (Parker, Jones 1990; Parker et al. 1988, Parker 2009). Both WIA and impedance methods can be used for the separation of pressure and flow waveforms into their forward and backward components; producing results

that are almost identical (Hughes, Parker 2009). WIA, however, has the advantage that it does not rely upon the assumption of periodicity that is essential for Fourier analysis techniques (Avolio et al. 2009). However, whilst WIA seems to describe the pattern of waves and their intensities very well, the aortic "reservoir effect" is neglected.

There are some anomalies in the separation of arterial pressure into its forward and backward components using either impedance or wave intensity analysis (Hughes, Parker 2009). This is particularly noticeable in diastole when the pressure decays exponentially while flow at the aortic root is almost zero which, according to wave theory, can only be explained by self-cancelling forward and backward waves of nearly equal magnitudes. This could be the result of standing waves in the aorta, but other evidence, such as the extended exponential pressure decay during extended diastole due to ectopic or missing heart beats, mitigates against this (Figure 6, in (Wang, et al. 2003).

The first time domain approach to couple the reservoir effect and the wave propagation theory at the aortic root was proposed by Wang et al. (Wang et al. 2003). The reservoir-wave model was extended to the venous system (Wang et al. 2006) and was further developed for any arbitrary location in the arterial system (Aguado-Sierra et al. 2008a). This model is based on the heuristic assumption that the measured pressure in the aorta (P) is the sum of a reservoir pressure (P_r), due to the storage of blood in the compliant aorta, and an excess pressure (P_e), due to the waves. This new approach resolves the self-cancelling waves that appear in the separation of the flow waveforms using the measured pressure (Davies et al. 2007; Tyberg et al. 2009). The subtraction of the reservoir pressure, which accounts for the potential energy stored in the aorta, allows the study of wave propagation employing wave intensity analysis (WIA) using P_e instead of P. Since the Windkessel function seems to improve left ventricle relaxation (Ochi et al. 1991) and coronary blood flow (Watanabe et al. 1993), the study of the buffering function of the aorta in terms of P_r could be a useful tool to better understand the mechanics of the heart and the coronary circulation. The reservoir-wave model has been applied to human (Davies et al. 2007), animal (Wang et al. 2006) and numerical data (Aguado-Sierra et al. 2008a). Davies et al. (Davies et al. 2010a) reported that the augmentation index (AIx) in humans depends mainly on the arterial reservoir rather than wave reflection. The authors also found that the reservoir pressure increases with age probably due to the increase in aortic stiffness, which suggests that this is the main reason for the change in morphology of the aortic pressure waveform with age.

Recent work has suggested a slight modification of the definition of reservoir pressure to account for the time of propagation of waves through the aortic system (Parker et al. 2012). They define $P(x,t) = P_r(t - \tau(x)) + P_e(x,t)$ where $\tau(x)$ is the time of wave propagation from the aortic root (x=0) to the location x in the arterial system. Since $\tau=0$ at the aortic root, this definition is consistent with previous work analysing flow in the aortic root, but extends the concept to other parts of the arterial system in a way that overcomes the obvious objection that the reservoir pressure cannot be uniform throughout the arterial system (as assumed in the simple Windkessel model) because arterial wave speeds are finite. Parker et al. showed that P_r, so-defined, represented the pressure waveform that resulted in minimal hydraulic work by the left ventricle to generate a given waveform of flow from the ventricle (Parker et al. 2012).

A study of pressure and flow measurements in the canine aorta has shown that the excess pressure waveform, obtained by subtracting the reservoir pressure from the measured pressure, is virtually identical in shape to the measured flow waveform at control conditions (Wang et al. 2003; Tyberg et al. 2009). The similarity between the waveforms indicates that there are no significant backward waves in the aortic root for those conditions. In contradistinction, another study based on WIA of the measured pressure, not taking P_r into account, showed that backward waves were evident in the canine aortic root (Khir, Parker 2005).

Although the reservoir-wave approach is based on a solid mathematical formulation, some authors have questioned the validity of this technique (Maynard et al 2012; Segers et al. 2012). Mynard et al. showed that the use of P_e for determining the intensity of the waves leads to a reduction or elimination of the backward compression waves and to an increase or artefactual introduction of expansion waves. On the other hand Wang et al. (Wang et al. 2011) demonstrated that the wave pattern after subtraction of P_r is more physiologically consistent than that calculated using traditional WIA. As a contribution to the on-going debate regarding the two models, in this chapter the similarities and differences between the results of two models are assessed, and a physiological explanation based on the anatomy of the arterial system is considered.

Since the subtraction of the reservoir pressure from the measured pressure results in a smaller component of the pressure due to local waves, it can be hypothesised that using the reservoir-wave approach would produce smaller values of wave speed and intensities than those produced using the measured pressure. The aim of this work is

thus to provide a detailed, quantitative study of the differences when arterial flow properties are calculated using the measured pressure (wave-only technique) and using the excess pressure (reservoir-wave technique). The data are from measurements in the canine ascending aorta when the effects of total occlusion at four different sites were studied (Khir, Parker 2005). This enables us to study the effect of the reservoir pressure in normal conditions and in conditions where reflected waves are certain to be present.

3.2 Material and Methods

3.2.1 Wave only and reservoir-wave theory

The mathematical equations used in this chapter for the wave only analysis are reported in chapter 2, section 2.2.1, 2.2.2, 2.2.3 and 2.2.4. The equations used for the reservoir-wave analysis are reported in chapter 2, sections 2.2.8.

3.2.2 Experimental protocol

Experiments were performed in 11 anaesthetised mongrel dogs (average weight 22 ± 3 kg, 7 males). All experiments were performed at the University of Calgary (Alberta, Canada) by Professor Tyberg's Cardiovascular Research Group. The surgery was executed by dog surgeons Cheryl Meek and Gerry Groves and the data were collected by Ashraf Khir and Greg Nelson (Page 2009). All experiments in this study adhered to the University of Calgary's guiding principles in the care and use of animals and were approved by the appropriate ethics committee. These data that were used to investigate the size and effect of reflections in the systemic arterial system using WIA (Khir & Parker 2005) are suitable for the work presented here since they provide a strong and clear reflection.

The dogs were anaesthetised with sodium pentobarbital, 30 mg/kg-body weight intravenously and a steady dose of 75 mg/h was given throughout the experiment. The dogs were endotracheally intubated and mechanically ventilated using a constant-volume ventilator (Model 607, Harvard Apparatus Company, Millis, MA, USA).

An ultrasonic flow probe (Model T201, Transonic Systems Inc., Ithaca, NY, USA) was fixed around the ascending aorta approximately 1 cm distal to the aortic valve. Pressure at the aortic root, just downstream of the flow probe, was measured with a high-fidelity pressure catheter (Millar Instruments Inc., Houston, Texas, USA) inserted from the right or left brachial artery. Snares were placed at four different sites:

the upper descending thoracic aorta at the level of the aortic valve (thoracic); the lower thoracic aorta at the level of the diaphragm (diaphragm); the abdominal aorta between the renal arteries (abdominal) and the left iliac artery, 2 cm downstream from the aorta iliac bifurcation (iliac). The right iliac artery was occluded throughout each experiment to allow for inserting a transducer-tipped pressure catheter used for measuring the pressure upstream of each occlusion. **Figure 3.1** illustrates the aorta and the occlusion sites. Data were collected for 30 s before the occlusion (control) and during the occlusion; 3 min after the snare was applied. An interval of 10–15 min was allowed between each occlusion in order to return to control conditions (Van Den Bos et al. 1976). The sequence of the four occlusions was varied between dogs using a 4X4 Latin-square to remove possible time effects. In order to convert the measured flow rate into velocity, the circumference of the ascending aorta was measured post-mortem. All data were recorded at a sampling rate of 200 Hz and stored digitally. The relative time delay between the P and U signals due to the phase differences of the transducers and to the small displacement between their locations was eliminated by the appropriate shifting of the velocity signal (Swalen & Khir 2009).

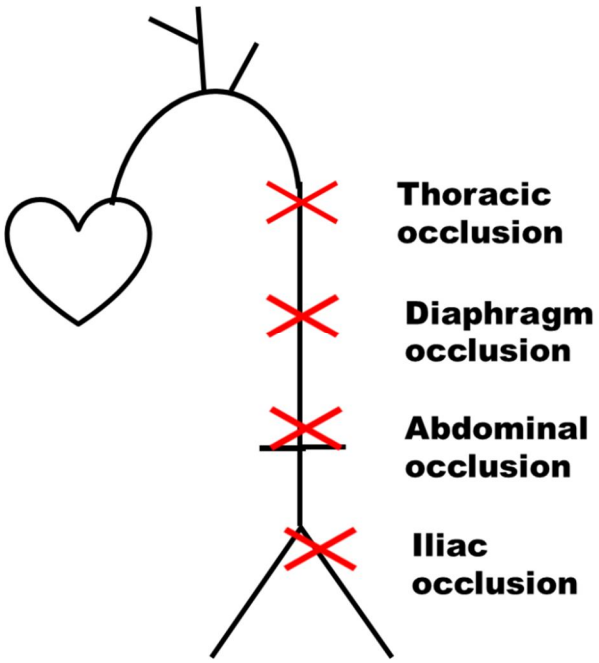

Figure 3.1: Schematic representation of the aorta and the sites where it was occluded.

3.2.3 Analysis

The reservoir pressure was calculated using an algorithm similar to that described in (Aguado-Sierra et al. 2008a). Briefly, the start of diastole is defined as the time of the first point of inflection in the measured pressure after the systolic peak (minimum of the first derivative of the measured pressure). The diastolic pressure is fitted to the model $P(t) - P_\infty = (P_0 - P_\infty)\, e^{-t/RC}$, where P_0 is the pressure at the start of diastole, to find the time constant RC and the asymptotic pressure P_∞. The method is based on the two assumptions that (i) the arteries are well-matched for forward waves and (ii) the volume flow rate into the aorta is proportional to the excess pressure $P_e(t)$. The value of this constant of proportionality is determined iteratively by minimising the mean square error between the model and the measured pressure during the whole cardiac period. Given this constant, $P_r(t)$ and $P_e(t)$ can be calculated directly. In **Figure 3.2** P, P_r and P_e and the separation in forward and backward waves are shown for control and all occlusions. In **Table 3.1**, the averaged values of measured pulse pressure (PP), reservoir pulse pressure (PP_r) and excess pulse pressure (PP_e) are reported together with the averaged value of diastolic pressure (P_d).

Wave speed in the ascending aorta, was determined from the slope of the linear part of the PU-loop (c) and P_eU-loop (c_e), before and during total occlusion (**Figure 3.3**). The net wave intensity was calculated using P (dI) and P_e (dI_e) in all of the experimental conditions and was then separated in forward (dI_{+}, dI_{e+}) and backward (dI_{-}, dI_{e-}) wave intensity. In all cases the forward wave intensity displayed a positive peak at the start of systole indicating a forward compression wave (FCW) and another at the end of systole indicating a forward expansion wave (FEW). In some conditions a negative peak in the backward wave intensity was discernible during mid-systole indicating a backward compression wave (BCW). The magnitude of the forward peaks (dI_{FCW}, dI_{eFCW} and dI_{FEW}, dI_{eFEW}) and backward peaks (dI_{BCW}, dI_{eBCW}) and the Reflection Indices (RI and RI_e), calculated as dI_{BCW}/dI_{FCW} and dI_{eBCW}/ dI_{eFCW}, were determined. Also, the time of the peaks (t_{FCW}, t_{eFCW}, t_{BCW}, t_{eBCW}, t_{FEW}, t_{eFEW}) and the onset time of the backward compression ($t_{BCWonset}$, $t_{eBCWonset}$) and forward expansion waves ($t_{FEWonset}$, $t_{eFEWonset}$) were determined using the two models and the results were compared.

Wave speed and intensity calculated with P and P_e before and during the total occlusion are the average of all cardiac beats over the 30 s period of measurement. Four control recordings were sampled in each dog; one before each occlusion. Since there were no significant differences between these four control measurements, they were pooled for each dog and considered the control state. Data are presented in the text as mean values ± SD and in figures as mean values ± SEM (mean was calculated by averaging the mean values of all dogs). Paired two-sided t-tests were used to assess differences between parameters calculated using P and P_e. Paired t-tests were also used to assess differences between parameters calculated during control and occlusion conditions. The relationship between PP_r and PP with the stroke volume ($V_{in,}$ calculated by integrating the area of under the flow waveform during systole) was assessed using bivariate correlation. Values of $p<0.05$ were considered statistically significant. Statistical analyses were performed using SPSS 17.0 (SPSS Inc., Chicago, Illinois, USA).

Table 3.1: Aortic pulse pressures and diastolic pressure.

Pressure (mmHg)	Control (n = 11)	Thoracic (n=10)	Diaphragm (n=11)	Abdominal (n=11)	Iliac (n=9)
PP	37 ± 11	64 ± 18**	40 ± 17	33 ± 10	37 ± 10
PP_+	31 ± 10	43 ± 10*	27 ± 11	28 ± 10	31 ± 10
PP_-	15 ± 5	27 ± 8**	19 ± 8	15 ± 5	16 ± 6
PP_r	30 ± 9	52 ± 20*	35 ± 16	28 ± 8	28 ± 9
PP_e	20 ± 8	21 ± 7	17 ± 6	17 ± 8	21 ± 9
P_d	83 ± 19	112 ± 21**	104 ± 21**	88 ± 18	82 ±0

Values are mean ± SD. * indicates $p<0.05$ compared to the control and ** indicates $p<0.001$ compared to the control. PP, PP_+ and PP_r are calculated as the difference between the peak and the diastolic values.

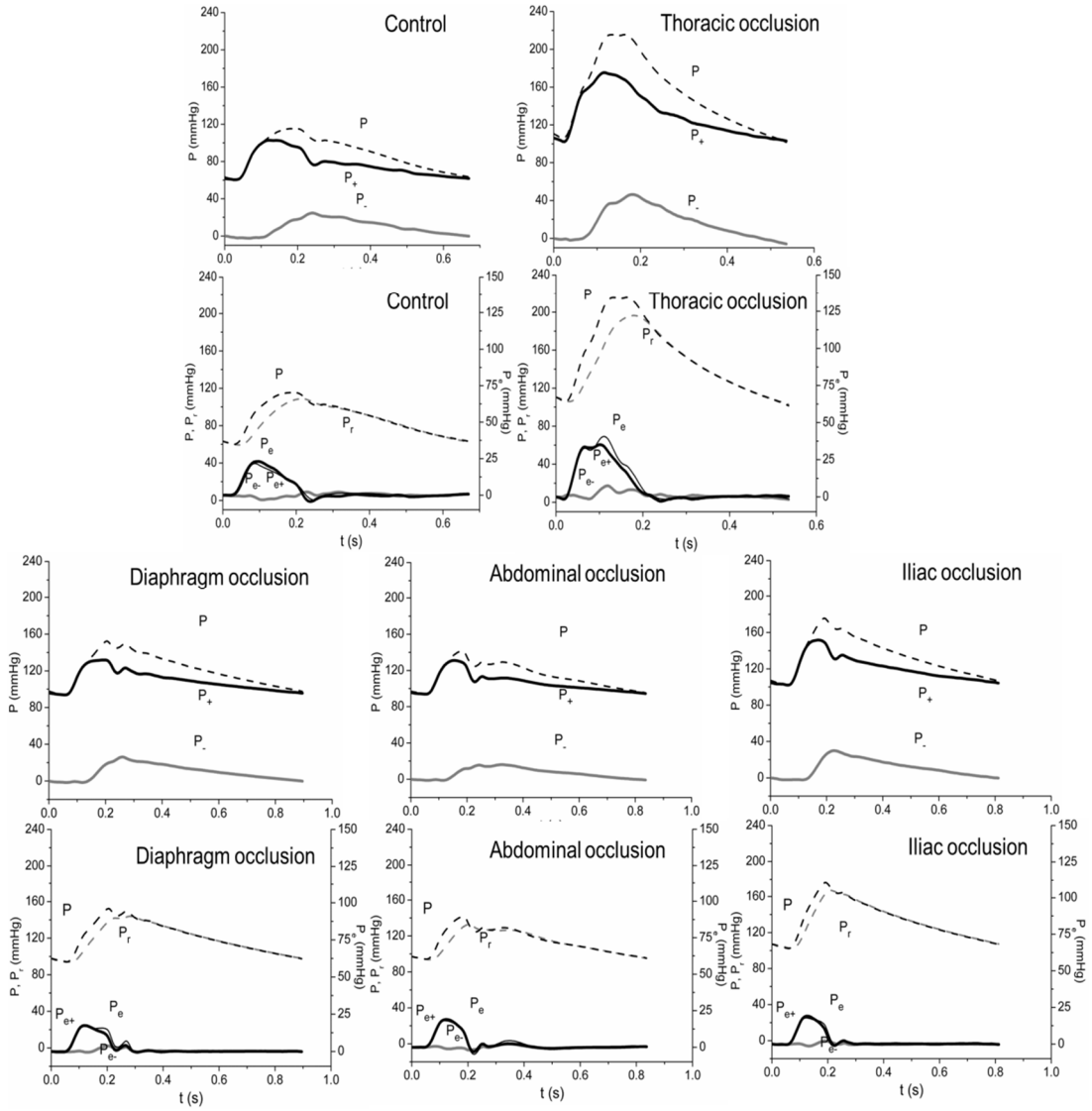

Figure 3.2: Examples of pressure waveforms in control and during the four occlusions. In the upper panel of each condition is shown the measured pressure (P, dashed black) separated into its forward (P_+, solid black) and backward (P_-, gray) components and in the lower panel the excess pressure (P_e, thin black) separated into its forward (P_{e+}, solid black) and backward (P_{e-}, gray) components (right axis), measured pressure (P, dashed black) and reservoir (P_r, dashed gray) component (left axis).

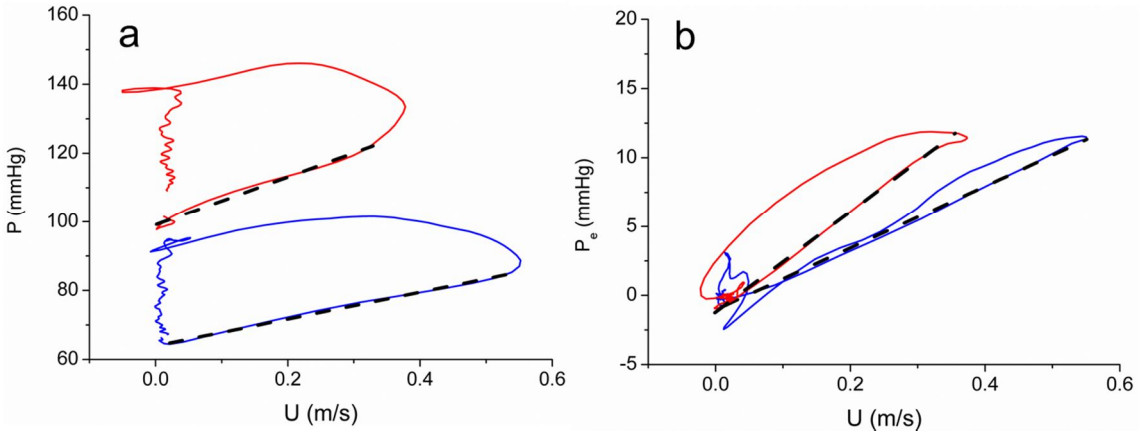

Figure 3.3: a) Typical examples of a PU-loop in the control (blue) and during thoracic occlusion (red). b) Examples of a P_eU-loop in the control (blue) and during thoracic occlusion (red). The dashed black line is the linear part of the loop used to calculate the wave speed. Note the different scales between a and b.

3.3 Results

3.3.1 Wave speed

There is a significant difference in the morphology of the PU and P_eU loops in all cases. The PU-loop is a distinct loop with large hysteresis between the systolic and diastolic portions of the curve. The P_eU-loop exhibits much less hysteresis and in many cases, such as the control conditions shown in **Figure 3.3**, the loop collapsed almost completely to a single curve. In all cases, the early systolic portion of the loop was linear enabling a measurement of the wave speed from the slope. In every condition the wave speed determined from the PU-loop, c, was greater than the wave speed determined from the P_eU-loop, c_e, and all of the differences were statistically significant. c_e is 29% smaller than c in the control state and 44%, 31%, 36% and 27% smaller during the thoracic, diaphragm, abdominal and iliac occlusions respectively. The values of c and c_e and their ratio are reported for all conditions in **Table 3.2**. The wave speeds determined during the four occlusions are shown, together with the control conditions, in **Figure 3.4**. We also see that c during the thoracic occlusion is significantly higher than in control conditions (9.9±2.5 m/s vs. 6.0±2.6 m/s, $p<0.05$). c_e calculated during the thoracic occlusion was also higher than in the control, but the difference was not statistically significant. There were no significant differences between either c or c_e during any of the other occlusions compared to control conditions.

Table 3.2: Averaged values of wave speed and intensity parameters calculated using P_e and P and their percentage ratio.

	Control	Thoracic	Diaphragm	Abdominal	Iliac
c (m/s)	5.8 ± 1.8	9.9 ± 2.6	5.8 ± 1.3	5.8 ± 1.5	5.9 ± 3.0
c_e (m/s)	4.1 ± 1.7	5.5 ± 1.6	4.0 ± 1.2	3.7 ± 1.3	4.3 ± 1.6
c_e/c (%)	71	56	69	64	73
dI_{FCW} (W/m^2)	51.2 ± 47.4	34.3 ± 27.2	34.9 ± 38.2	49.2 ± 48.3	53.6 ± 49.8
dI_{eFCW} (W/m^2)	32.2 ± 31.7	24.4 ± 19.3	23.4 ± 25.2	29.5 ± 34.8	32.2 ± 33.2
dI_{eFCW}/dI_{FCW} (%)	63	71	67	60	60
dI_{FEW} (W/m^2)	34.7 ± 15.5	22.5 ± 12.6	23.9 ± 12.6	29.3 ± 14.8	41.4 ± 20.9
dI_{eFEW} (W/m^2)	25.7 ± 13.3	21.6 ± 12.1	20.8 ± 10.4	20.5 ± 13.5	27.7 ± 16.3
dI_{eFEW}/dI_{FEW} (%)	74	96	87	70	67
dI_{BCW} (W/m^2)	4.4 ± 3.5	8.7 ± 7.7	10.2 ± 9.0	4.1 ± 3.4	4.3 ± 4.0
dI_{eBCW} (W/m^2)	1.1 ± 1.6	2.0 ± 2.5	2.4 ± 2.8	1.3 ± 2.0	1.3 ± 2.2
dI_{eBCW}/dI_{BCW} (%)	24	23	24	32	31
RI	0.10 ± 0.05	0.25 ± 0.15	0.33 ± 0.12	0.11 ± 0.06	0.09 ± 0.04
RI_e	0.03 ± 0.03	0.07 ± 0.04	0.12 ± 0.06	0.04 ± 0.03	0.03 ± 0.02
RI_e/RI	29	30	36	37	30

Values are mean ± SD.

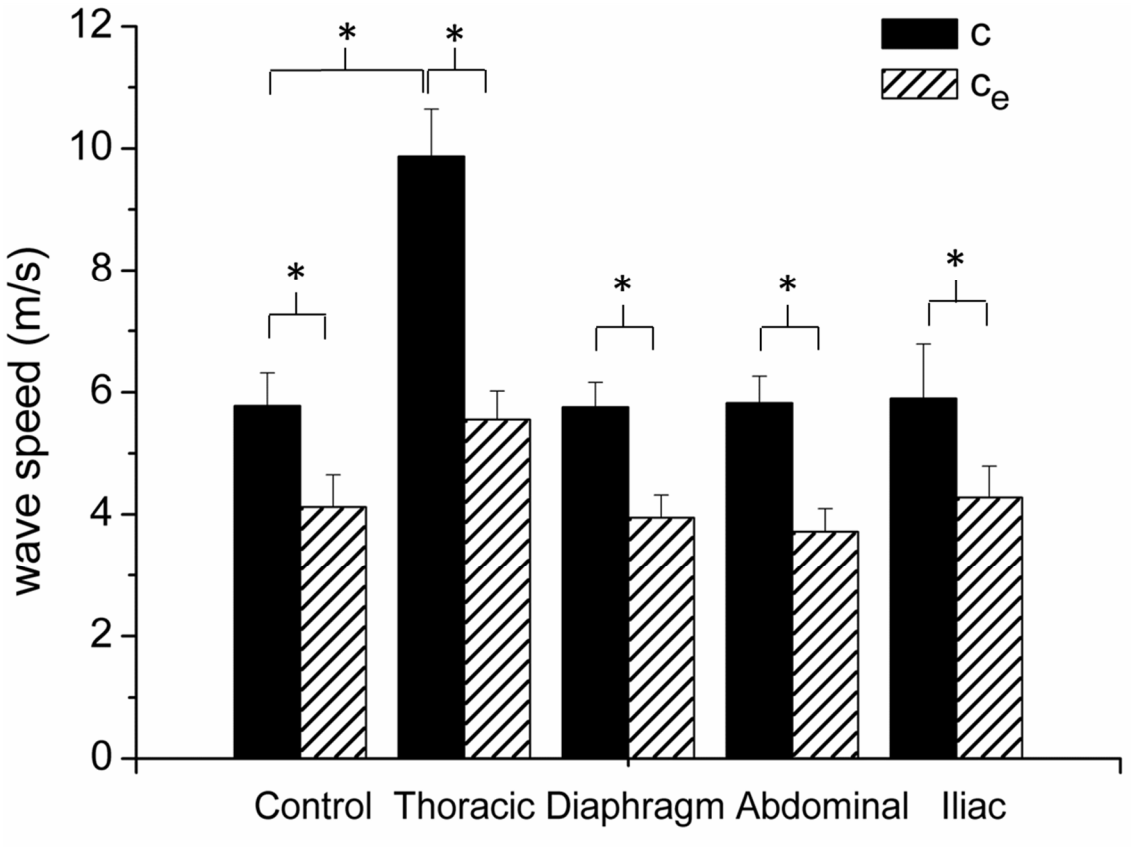

Figure 3.4: Wave speed calculated using measured pressure (c, black) and excess pressure (c_e, dashed) at control and during occlusions at thoracic, diaphragm, abdominal and iliac levels. Bars are SEMs, * indicates $p < 0.05$.

3.3.2 Wave intensity and reflection index

As seen in **Figure 3.5**, there were both similarities and differences between the wave intensity calculated with P, $dI = dPdU$, and with P_e, $dI_e = dP_edU$. In all cases, the forward wave intensities, dI_+ and dI_{e+}, were similar in shape with large peaks at the start (FCW) and end (FEW) of systole. As discussed below, the morphology of these peaks was unchanged, but there were differences in their magnitudes. However, the backward wave intensities, dI_- and dI_{e-}, showed large differences with no peaks discernible in the dI_{e-} waveforms for many of the cases. The magnitude of the three main wave intensity peaks, dI_{FCW}, dI_{FEW}, dI_{BCW}, dI_{eFCW}, dI_{eFEW} and dI_{eBCW} are shown in **Figure 3.6**. For both of the forward waves, FCW and FEW, $dI > dI_e$ and the difference is statistically significant in all cases except for the thoracic and diaphragm occlusions for the FEW wave. dI_{eFCW} is 37% smaller than dI_{FCW} in the control and 29%, 33%, 40% and 40%

smaller during the thoracic, diaphragm, abdominal and iliac occlusions, respectively. dI_{eFEW} is 26% smaller than dI_{FEW} in control and 29% and 33% smaller for abdominal and iliac respectively during occlusions. The results for the BCW are qualitatively different from the results for the forward waves. In all cases $dI_e << dI$ with the differences being highly significant statistically. dI_{eBCW} is 76% smaller than dI_{BCW} in control condition and 77%, 76%, 68% and 69% smaller during the thoracic, diaphragm, abdominal and iliac occlusions, respectively. The percentage ratio between the magnitudes of the three main wave intensity peaks calculated using P and P_e are shown in **Table 3.2**.

The reflection index, which is related to the effective reflection coefficient, shows a similar pattern. For control conditions the difference between RI and RI_e is large and statistically significant, as shown in **Figure 3.6**. In particular RI_e is 71% smaller than RI in control conditions and is 70%, 64%, 63% and 70% smaller for thoracic, diaphragm, abdominal and iliac occlusions respectively. The values of percentage ratio of RI_e/RI in all conditions are reported in **Table 3.2**.

The times of the forward and backward peak intensities and the times of the onset of the BCW and FEW when calculated using the reservoir-wave and the wave only model are reported in **Table 3.4**. As can be seen from the table, there is no significant difference in time between the two analyses in all conditions apart from the time of the onset of the forward expansion wave that comes earlier when the analysis is performed with P_e, both, in control and during the four occlusions.

Comparing wave intensities and reflection indices between occlusion and control conditions a broadly similar pattern emerges. For both the FCW and the FEW there is a slight but statistically significant decrease in the peak values of dI when the occlusion is in the thoracic and diaphragm positions and no significant differences when the occlusion is in the more distal locations. This is true for the wave intensity calculated using the measured pressure dI or the excess pressure dI_e. For the BCW there is a large and highly significant increase in the dI for the thoracic occlusion, an even larger increase for the diaphragm occlusion and no significant difference for the abdominal and iliac occlusions. Although dI_e is significantly smaller than dI for all of the cases, this pattern persists for dI_e; a significant increase for the thoracic occlusion, an even larger increase for the diaphragm occlusion and no differences for the two more distal occlusions.

The reflection index shows this pattern more clearly. For the reflection index calculated using P, RI is more than double for the thoracic occlusion, more than triple for the diaphragm occlusion and is not significantly different from control conditions for the abdominal and iliac occlusions. The reflection index calculated using the P_e, RI_e, is significantly smaller than the correspondent RI, but follows the same pattern; a large increase for the thoracic occlusion, an even larger increase for the diaphragm occlusion and no significant difference from control conditions for the two more distal occlusions.

Table 3.3: Wave timing.

Time (ms)	Control	Thoracic	Diaphragm	Abdominal	Iliac
t_{FCW}	29 ± 4	34 ± 5	30 ± 5	28 ± 4	28 ± 6
t_{eFCW}	32 ± 3	32 ± 5	33 ± 2	31 ± 3	34 ± 3
t_{BCW}	92 ± 12	103 ± 9	96 ± 15	89 ± 14	91 ± 23
t_{eBCW}	83 ± 14	98 ± 9	97 ± 14	81 ± 19	81 ± 27
t_{FEW}	161 ± 25	157 ± 19	157 ± 36	150 ± 34	164 ± 23
t_{eFEW}	161 ± 25	157 ± 24	157 ± 27	151 ± 35	165 ± 22
$t_{BCWonset}$	56 ± 7	41 ± 9	48 ± 6	56 ± 11	55 ± 13
$t_{eBCWonset}$	51 ± 6	43 ± 5	46 ± 3	49 ± 4	54 ± 7
$t_{FEWonset}$	87 ± 12	108 ± 12	109 ± 21	77 ± 14	84 ± 14
$t_{eFEWonset}$	71 ± 8**	83 ± 14**	74 ± 18**	65 ± 9**	72 ± 6*

Values are mean ± SD. * indicates $p<0.05$ compared to the traditional wave intensity analysis based on P and ** indicates $p<0.001$ compared to wave intensity analysis based on P.

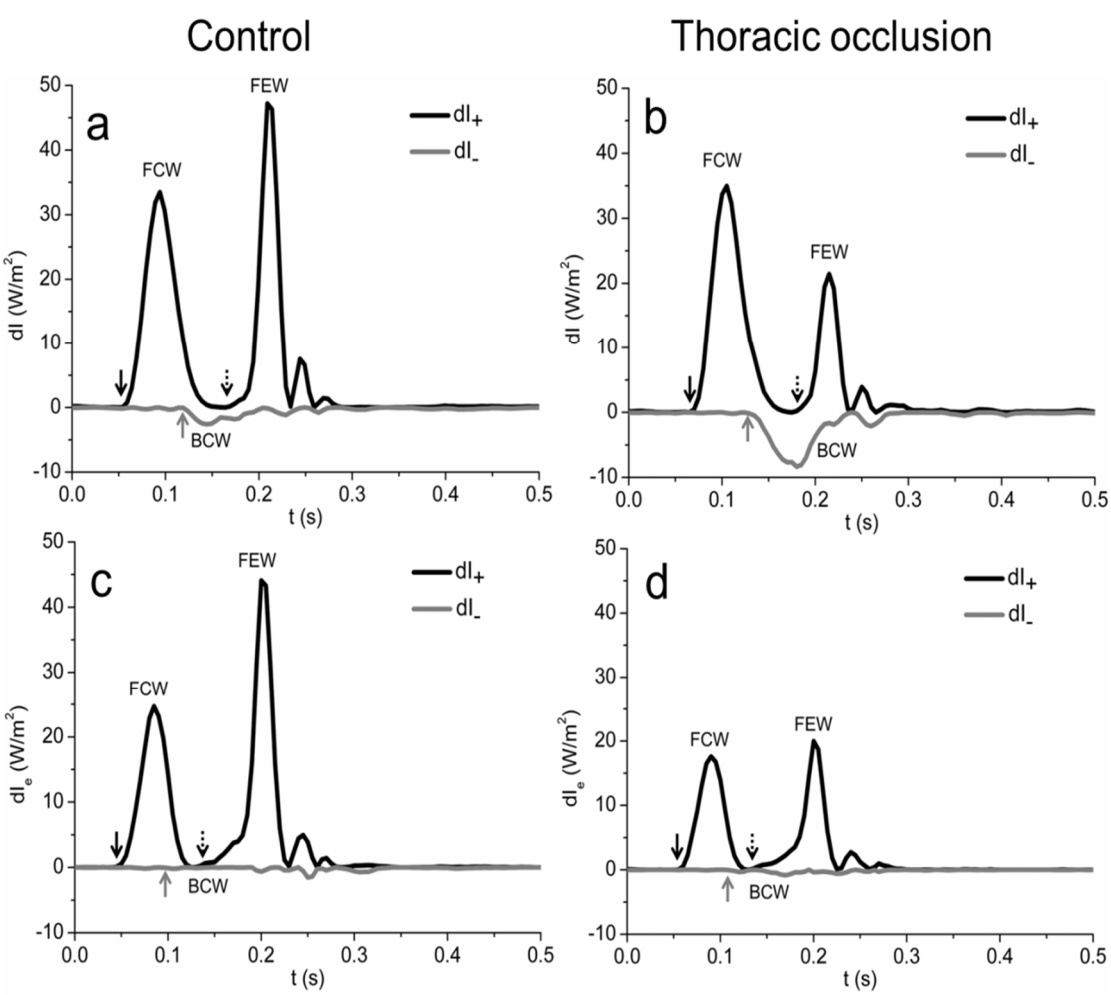

Figure 3.5: a and b) Typical example of wave intensity analysis in control condition calculated with P and P_e, respectively. c and d) wave intensity analysis during the thoracic occlusion using P and P_e, respectively . Black lines are forward intensities (dI_+ and dI_{e+}) and gray lines backward intensities (dI_- and dI_{e-}). Solid black arrows indicate the onset of the forward compression wave (FCW), gray arrows indicate the onset of the backward compression wave (BCW) and the dashed black arrow show the onset of the forward expansion wave (FEW).

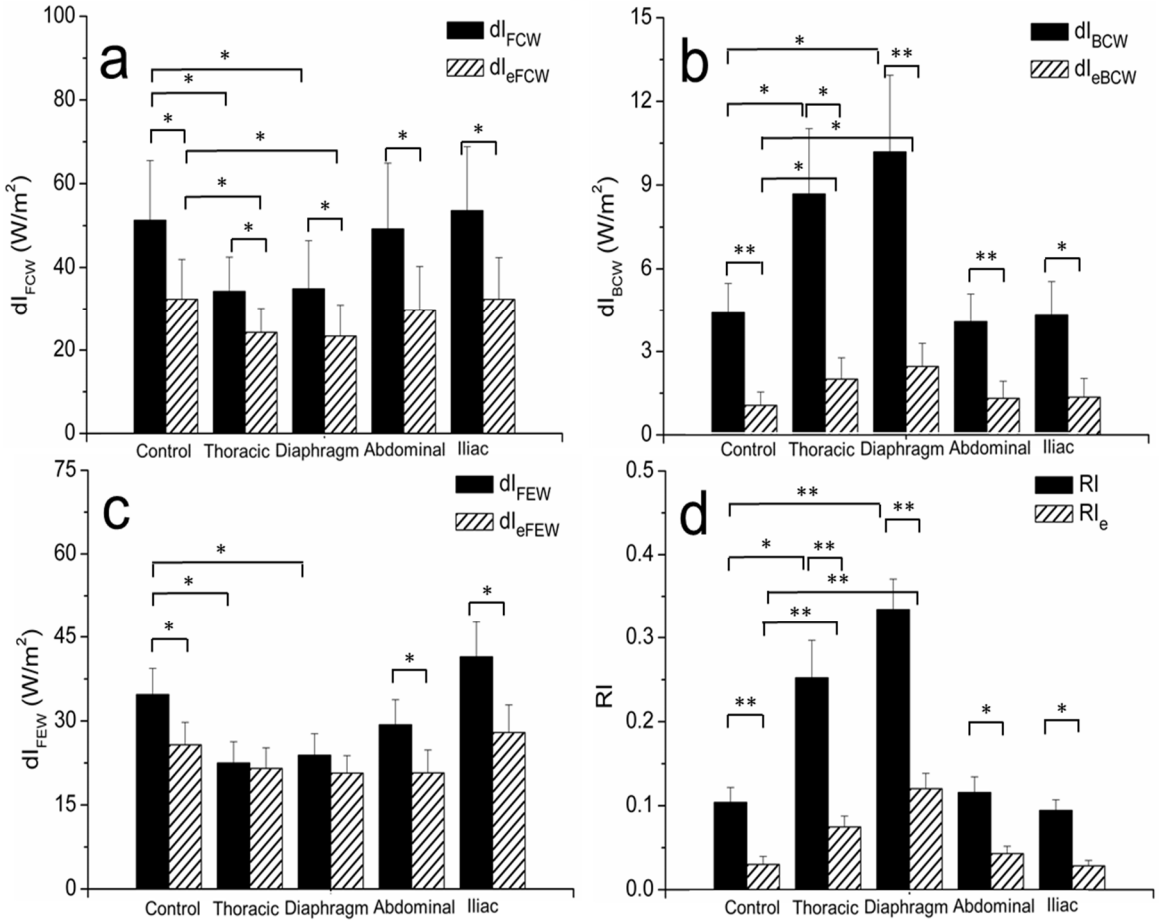

Figure 3.6: a) Peak of forward compression (dI_{FCW}), b) peak of backward compression (dI_{BCW}), c) peak of forward expansion (dI_{FEW}) wave intensities and d) reflection index (RI) calculated using P (black) and P_e (dashed) at control and during occlusions at thoracic, diaphragm, abdominal and iliac levels. Bars are SEMs,* indicates $p < 0.05$ and ** indicates $p<0.001$.

3.3.3 Reservoir pressure

P, P_r and P_e in the ascending aorta for a typical case are shown in **Figure 3.2**. As seen in the figure, the aortic pressure increased significantly when the occlusion was in the thoracic aorta. There was a smaller increase when the occlusion was at the diaphragm position and there were no significant differences from control when the occlusion was in the abdominal or iliac position. The averaged values of measured, reservoir and excess pulse pressures (PP, PP_r and PP_e, respectively) and diastolic pressure P_d for all conditions are reported in **Table 3.1**. As can be seen from the table, PP and PP_r are significantly higher during thoracic occlusion compared to the control,

while PP_e does not change significantly compared to the control state for all the other occlusion conditions.

Figure 3.7 shows the relationship between the reservoir pulse pressure (PP_r) and the stroke volume (V_{in}) in the control condition and during the occlusions for each dog. The Pearson correlation factors between these two parameters were 0.70, 0.83, 0.87, 0.70, 0.72 in control and during thoracic, diaphragm, abdominal and iliac occlusion ($p<0.05$ in all conditions). The slope of the linear regression is higher for the thoracic occlusion than the control, even higher for the diaphragm occlusion but not significantly different from the control for the abdominal and iliac occlusions. A similar relationship is also found between pulse pressure and stroke volume (correlation coefficients were 0.76, 0.85, 0.87, 0.78, 0.74 for control and occlusions, $p<0.05$ in all conditions) (**Figure 3.8**).

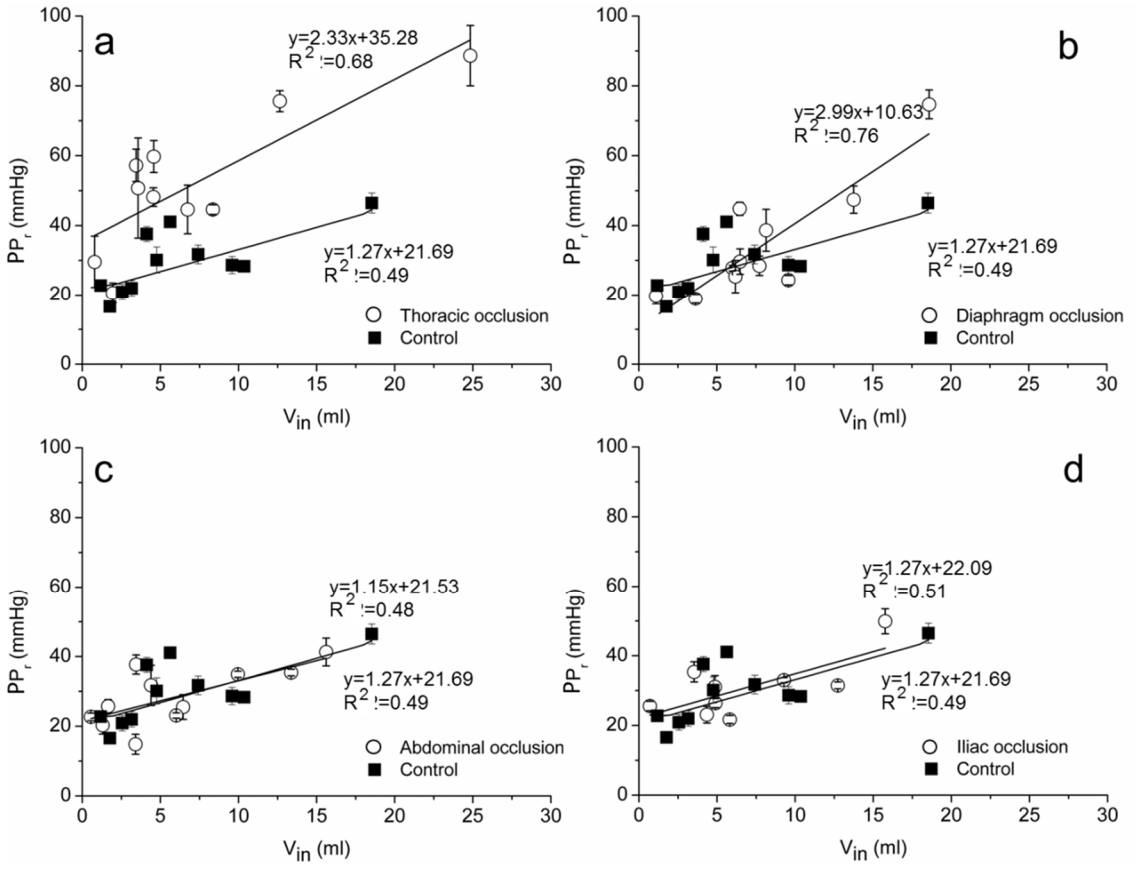

Figure 3.7: Relationship between reservoir pulse pressure (PP_r) and stroke volume (V_{in}) in control condition and during occlusions at the thoracic (a), diaphragm (b), abdominal (c) and iliac (d) level.

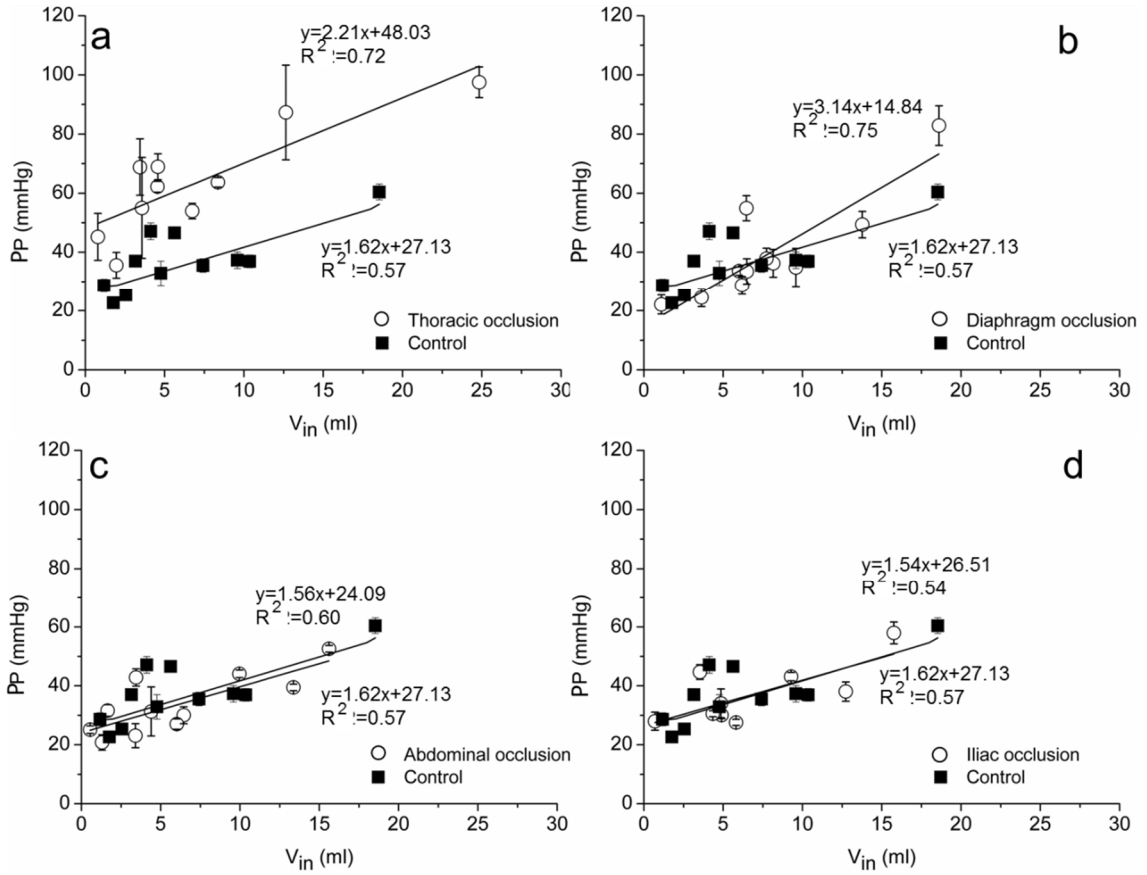

Figure 3.8: Relationship between pulse pressure (PP) and stroke volume (V_{in}) in control condition and during occlusions at the thoracic (a), diaphragm (b), abdominal (c) and iliac (d) level.

3.4 Discussion

This study compares measures of various hemodynamic parameters in the ascending aorta of the dog calculated using P and P_e, which is obtained by subtracting the reservoir pressure as proposed by Wang et al. (Wang et al. 2003). The data used in this analysis were originally used to investigate hemodynamics in the ascending aorta using WIA and the experiment has been designed to provide definitive reflection sites at different locations along the aorta to increase the magnitude of reflected waves seen in the ascending aorta (Khir & Parker 2005). A similar experiment was originally carried out by Van den Bos et al. (Van Den Bos et al. 1976a) who analysed the data using impedance analysis (Westerhof et al. 1972; Westerhof et al. 1971). In this chapter, the reservoir-wave model is applied for the first time in these atypical conditions and the similarities and differences between this model and the wave only model are investigated.

The wave speed calculated from the slope of the P_eU-loop (c_e) was less than the wave speed calculated from the PU-loop (c) in all cases (see **Table 3.2** and **Figure 3.4**). For the control condition the ratio was $c_e/c = 71\%$ and was not significantly different from those calculated during all of the occlusions except for the thoracic occlusion where the reduction was even greater ($c_e/c = 56\%$). The aortic pressure was significantly greater during the thoracic occlusion and this increase in pressure probably influenced the wave speed in the ascending aorta due to its dependence on pressure (Histand, Anliker 1973). c_e was higher during thoracic occlusion than in control but the increase was not statistically significant.

Very few significant differences were seen in the arrival times of the waves calculated using P_e compared to those calculated using P. The notable exception is the arrival time of the FEW, where the arrival time is earlier when calculated from dI_e than for dI (**Table 3.3**) because the maximum of P_e generally occurs early than the maximum of P.

The wave intensities calculated for the three main waves, the forward compression wave (FCW) at the start of systole, the forward expansion wave (FEW) at the end of systole and the backward compression wave (BCW) during mid-systole are reported in **Table 3.2** and **Figure 3.6**. In every case the magnitude of dI_e was less than the magnitude of the corresponding peak of dI. For the forward waves the ratio of magnitudes was similar to the ratio of wave speeds, ($dI_{eFCW}/dI_{FCW} \sim 60\%$) and ($dI_{eFEW}/dI_{FEW} \sim 70\%$). For the backward wave the decrease was much greater ($dI_{eBCW}/dI_{BCW} \sim 25\%$). Unsurprisingly, the reflection index, which is related to the magnitudes of the backward and forward wave intensity peaks, showed a similarly marked decrease ($RI_e/RI \sim 30\%$).

Another finding, common to the two methods, is that the averaged values of RI during diaphragm occlusions are slightly higher than during the thoracic occlusion (**Figure 3.5**) and in some dogs reflections due to the diaphragm occlusion are bigger than those due to the thoracic occlusion. Due to the more proximal position of the thoracic occlusion and thus, less dissipation in travelling back, bigger reflected waves at the aortic root during this condition were expected. A possible explanation of this result is that during this proximal occlusion the aortic arch branches (subclavian and brachiocephalic arteries) play a greater role than during the diaphragm occlusion. Westerhof et al. (Westerhof et al. 1973) previously suggested that the behaviour of the

aorta clamped at the diaphragm level is more similar to a uniform tube with a closed end compared to the aorta occluded at a more proximal location, such as the thoracic level. The authors explained this finding by considering the uniform tube when clamped proximally as "short-circuited" because of the considerable role of the cephalic vessels and collaterals in this condition.

Despite the decrease in the magnitude of the wave intensity calculated using P_e, the pattern of the magnitudes measured during the different occlusions was remarkably similar. For the FCW, there was a significant decrease in peak wave intensity during the two more proximal occlusions compared to the control conditions and no significant differences during the two more distal occlusions using both dI_e and dI. Also for the FEW, differences from control conditions were seen in dI for the more proximal occlusions but not for the more distal occlusions, but these differences were not seen using dI_e. Interestingly, the difference between dI_e and dI were not statistically significant for the two more proximal occlusions whereas a statistically significant decrease was observed for all other conditions including control.

For the BCW, although the magnitude of dI_e was much smaller than dI, the variations from control conditions during the different occlusions were strikingly similar. The magnitude of dI_e was approximately doubled during the more proximal occlusions compared to control conditions and not significantly different during the more distal occlusions; almost exactly the same pattern of results previously reported using dI (Khir, Parker 2005). The pattern for RI_e and RI were similar except that values during the more proximal occlusions were approximately three times as large as during control conditions.

Similar results in WIA using the two techniques have been recently reported (Mynard et al. 2012). The authors performed WIA in computational and animal data and found lower values of backward compression waves and reflection coefficient when the reservoir-wave system was applied compared to the traditional WIA. These results are in line with the findings here reported. However, they also found bigger backward expansion waves using the reservoir-wave approach that were not present in this study.

The decrease of the backward compression wave intensity calculated using P_e is one of the most significant results of this chapter. The previous study based on the measured pressure found a significant increase in the backward wave during the thoracic and diaphragm occlusions and no increase during the abdominal and iliac

occlusions (Khir & Parker 2005). Since the experiment was designed to produce significant reflections, this lack of reflected waves from the distal occlusions was a surprise, although it was consistent with the lack of differences in the impedance spectra reported by Van den Bos et al. (Van Den Bos et al. 1976).

Despite the reduction in the magnitude, dI_{eBCW} and dI_{BCW} showed a similar pattern with significant reflections during the more proximal and no reflections from the more distal occlusion. The substantial reduction of backward compression waves using the reservoir.wave approach can be explained if we consider that the arterial system is well-matched in the forward but not in the backward direction (Gosling et al. 1971; Newman et al. 1972; Greenwald & Newman 1982; Papageorgiou et al. 1990). We calculated the reflection coefficients from the trifurcation of the aortic arch (**Figure 3.9**) in forward direction as

$$R_{+} = \frac{Y_0 - Y_1 - Y_2 - Y_3}{Y_0 + Y_1 + Y_2 + Y_3} \tag{3.1}$$

and for the backward direction as

$$R_{-} = \frac{Y_3 - Y_1 - Y_2 - Y_0}{Y_0 + Y_1 + Y_2 + Y_3} \tag{3.2}$$

where Y_0, Y_1, Y_2, Y_3, are the characteristic admittances ($Y=1/Z=A/\rho c$) for the ascending aorta, brachiocefalic artery, left subclavian artery, and descending aorta, respectively. These values were calculated using the characteristic impedances for the different vessels reported by Cox and Pace (Cox & Pace 1975) in anesthetized dogs in control condition, in which values of vascular impedance have been calculated by averaging between 8 and 15 Hz. It was found that the reflection coefficient is 0.02 in the forward direction and -0.48 in the backward direction. This means that approximately half of the energy carried by a backward wave in the thoracic aorta will be reflected in the aortic arch. This may be the main reason for the observation of small backward waves at the aortic root, even during the occlusion, using the reservoir-wave model.

The pulse of the reservoir pressure is strongly related to the stroke volume as shown in **Figure 3.7**. In particular, a different linear relationship can be observed during occlusion of the aorta at the thoracic and diaphragm level compared to the control for both pressures, caused by the different pulse pressure in these conditions.

Davies et al. (Davies et al. 2010a) studied the contribution of reservoir and excess pressure in humans in relation with age. They found that the contribution of the

reservoir pressure to the increase of AIx with age is larger than that of the reflected wave contribution; the increase is largely due to the decrease of the aorta compliance and other elastic vessels. The results reported here are related to their findings since the increase of pulse pressure due to the thoracic occlusion can be compared to the increase of pressure due to age or to cardiovascular diseases such as hypertension. The findings of this chapter confirm that the reservoir pressure makes a larger contribution to the pressure waveform than the excess pressure (**Table 3.1**) as previously reported by other authors (Davies et al. 2010a, Vermeersch et al. 2009).

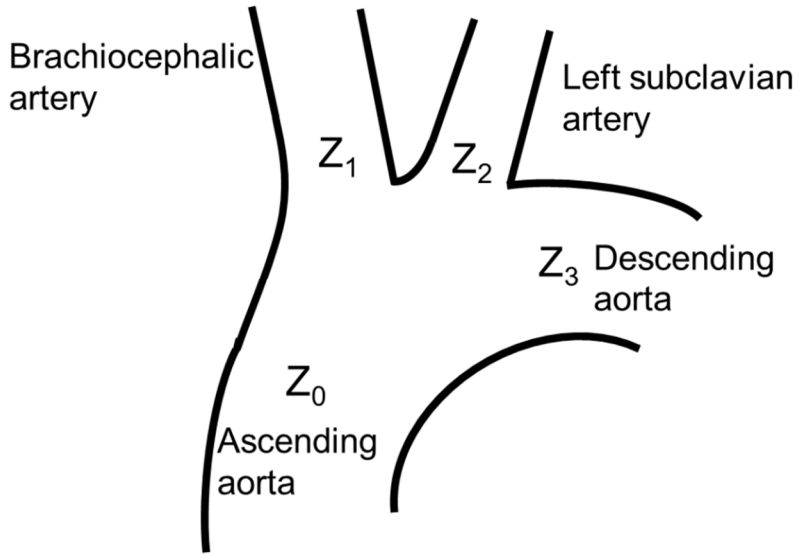

Figure 3.9: Schematic representation of the aortic arch. $Z_{0,}$ characteristic impedance of the ascending aorta; Z_1, characteristic impedance of the brachiocephalic artery; Z_2 characteristic impedance of the left subclavian artery and $Z_{3,}$ characteristic impedance of the descending aorta.

3.5 Conclusion

The reservoir-wave and the wave only analyses produce remarkably similar WIA curves, although the magnitudes are strikingly different. Both models lead to the conclusion that distal occlusions have little or no effect on hemodynamics in the ascending aorta. The models yield different values of wave speed and different wave magnitudes, despite using the same analytical techniques of the pressure-velocity loop and WIA. The reservoir-wave model always yielded lower values for all hemodynamic parameters studied.

The separation of aortic pressure into reservoir and excess components gives information about the Windkessel and wave contribution. The small magnitude of BCW in the aortic root during occlusions, using the reservoir-wave analysis, could be explained by considering the geometry of the aortic arch and reflection coefficients, although this requires a larger study to confirm this observation. The differences found between the results of WIA based on the measured pressure and the reservoir/excess pressures do not mean that the values based on excess pressure are erroneous. In the absence of other independent technique or evidence it is currently not possible to decide which of the two models compared in this work is more correct.

Chapter 4 : Noninvasive determination of wave speed and intensity in healthy human

4.1 Introduction

As mentioned at the end of chapter 1, this chapter investigates the potential use of a new non-invasive technique to determine wave speed and separate the waves in human arteries and the changes of mechanical properties of carotid and femoral arteries with age and gender. Part of this chapter was published in Borlotti et al. 2012 (see list of publication).

There is an increasing interest in assessing arterial mechanical properties as they offer valuable prognostic information. Of particular physiological and clinical interest is the "pulse wave velocity" (PWV) or wave speed (c) as it gives a direct measure of arterial distensibility. c is widely used to determine arterial stiffness, which is considered an early phenotype of vascular damage and a potential prognostic factor in assessing cardiovascular risk (Blacher et al. 1999, Laurent et al. 2001, O'Rourke et al. 2002, Laurent et al. 2006). PWV has also been used as a surrogate marker for cardiovascular disease including atherosclerosis (Meaume et al. 2001) and proposed as an independent risk factor for cardiovascular events such as coronary disease and stroke (Laurent et al. 2007, Boutouyrie et al. 2008). Although carotid-femoral PWV is widely used in clinical practice, it gives regional information about the lumped properties of the vessels. A better understanding of the local properties of the arterial wall would be useful. For this reason in the past few decades several methods have been introduced to determine local c. Khir et al. (Khir et al. 2001) introduced the PU-loop method, which requires simultaneous measurements of pressure (P) and velocity (U) at the same site. The method relies on the linear relationship between pressure and velocity in the absence of reflections; the slope of the initial linear portion of the loop equals ρc, where ρ is blood density. Rabben et al., used a similar technique; flow–area loop, which is based on the definition of the characteristic impedance (Rabben et al. 2002). To accommodate the co-existence of incident and reflected waves, Davies et al. introduced the sum of squares technique (Davies et al. 2006), although the effectiveness of this

technique in the coronary circulation has been questioned (Kolyva et al. 2008).

To understand the propagation of waves along the arterial system in the time domain, Parker and Jones, introduced the theoretical basis of Wave Intensity Analysis (WIA) (Parker & Jones 1990). The method requires the simultaneous measurements of P and U at the same site, and has been successfully applied to several locations along the arterial system; aorta (Parker et al. 1988; Khir & Parker 2005; Ramsey & Sugawara 1997); coronary and carotid arteries (Davies et al. 2006; Sun et al. 2000; Niki et al. 2002; Zambanini et al. 2002); venous system (Wang et al. 2006); left and right ventricles (MacRae et al. 1997; Smolich et al. 2010); and intra-operatively in patients using the intra-aortic balloon pump (Kolyva et al. 2009). The usefulness of this analysis has been recently documented (Sugawara et al. 2009), including the evaluation of the working conditions of the heart and its interaction with the arterial system. To by-pass the invasive nature of acquiring pressure, applanation tonometry has been used to provide pressure waveforms by calibrating arterial pressure waveforms (Segers et al. 2005). However, applanation tonometry can only be used with superficial arteries as well as the need to accept the assumption that diastolic, and mean or systolic pressure at the brachial artery are equal to those at the measurement site.

To avoid the difficulties of acquiring invasive measurements of P and U for the calculation of local c and WIA, Feng and Khir presented the theoretical basis of non-invasive techniques that require the measurements of diameter (D) and U (Feng & Khir 2010). Local c is determined from the slope of the linear portion of the lnDU-loop and the non-invasive wave intensity ($_{n}dI$) is defined as the product of change of diameter and change of velocity. Similar to traditional WIA, the method allows for the separation of waves into their forward and backward components and has recently been validated *in vitro* (Li & Khir 2011). In this chapter the method is used for the first time with clinical data acquired using ultrasound measurements of D and U in the carotid and femoral arteries.

As mentioned in chapter 1, in this section the wave speed and intensity were determined noninvasively in a population of healthy subjects. The overall aim of this study is to use the new non-invasive techniques to quantify the effect of age and gender on the arterial mechanical properties and hemodynamic parameters in the carotid and femoral arteries of a population of healthy subjects. The specific objectives are to non-invasively 1) determine local c using direct measurements of D and U, from which

distensibility can be calculated, 2) separate D and U waveforms into their forward and backward components, and 3) carry out the non-invasive wave intensity analysis in healthy human vessels.

The main aims of this investigation are to study the lnDU-loop method in humans and the changes of some hemodynamic parameters with age and gender.

4.2 Material and Methods

4.2.1 The Asklepios population

The Asklepios Study is a longitudinal population study aiming to investigate the interaction between ageing, cardiovascular haemodynamics and inflammation in (preclinical) cardiovascular disease (Rietzschel et al. 2007). The total cohort included 2524 participants (1301 women) of 35–55-year-old individuals, free from overt cardiovascular disease at study initiation, randomly sampled from the twinned Belgian communities of Erpe–Mere and Nieuwerkerken. Measurements were performed during a continuous 2-year period, between October 2002 and September 2004 in Erpe–Mere. The examination was the following for all participants: (1) informed consent and the study questionnaire were revised; (2) measurements of basic clinical data; (3) blood samples examination (4) echocardiographic examination (5) vascular echographic and tonometric measurements. All measurements were single centre, single device and single observer. The study protocol was approved by the ethics committee of Ghent University Hospital and all subjects gave a written informed consent.

4.2.2 Study population

In this study data were drawn from the Asklepios study database and comprised data from 1774 subjects (934 women) aged 35-55 years (average age 45.8±6 years). The data used in this chapter were given to our group with the only purpose of investigating the new non-invasive technique. Only subjects with diameter and flow velocity measurements available both, in carotid and femoral arteries, were considered. Basic clinical and hemodynamic characteristics of the population are presented in **Table 4.1**.

Table 4.1: Physical and hemodynamic characteristics of subjects.

Parameter	Gender	35-40	41-45	46-50	51-56
No.	Male	218	219	219	184
	Female	242	247	221	224
Age (years)	Male	38.3±1.7	43.7±1.4	48.4±1.4	53.7±1.7
	Female	38.2±1.8	42.4± 1.5	48.4±1.5	53.6±1.7
Height (cm)	Male	177.5±5.3	176.0±6.8	175.1±6.3	174.1±5.9
	Female	164.6±6.1$^{\xi}$	164.1± 6.3$^{\xi}$	162.6±5.9$^{*,\xi}$	160.9±5.7$^{*,\xi}$
Weight (kg)	Male	81.8±11.5	81.8±12.2	82.4±11.4	80.9±11.7
	Female	65.5±11.1$^{\xi}$	65.4± 11.3$^{\xi}$	67.5±12.5$^{\xi}$	68.8±12.0$^{\xi}$
SBP (mmHg)	Male	131.5±11.4	128.9±15.0	134.6±14.0	137.8±15.3
	Female	123.4±16.0$^{\xi}$	133.6±12.0$^{*,\xi}$	131.3±15.3$^{\xi}$	135.6±16.7
DBP (mmHg)	Male	75.3±9.4	78.4±10.4*	80.3±10.3	80.6±10.8
	Female	74.3±10.9	76.7± 10.7*	76.7±10.2	78.8±10.8
MAP (mmHg)	Male	98.0±9.6	101.3±11.1*	102.9±11.4	104.4±12.1
	Female	96.0±12.0	99.4±12.0*	100.1±11.8$^{\xi}$	103.6±12.5
PP (mmHg)	Male	56.5±9.3	55.1±7.9	54.9±8.6	57.6±10.1*
	Female	50.1±8.0$^{\xi}$	51.9±9.8$^{\xi}$	54.3±10.6*	57.9±11.8*
HR (beat/min)	Male	61.4±8.6	61.6±9.1	63.5±11.2	61.4±9.9
	Female	65.3± 8.4$^{\xi}$	66.7±8.5$^{\xi}$	65.3±8.4	65.4±9.0$^{\xi}$
Carotid					
SD_c (mm)	Male	7.19±1.19	7.05±0.93	7.27±1.20	7.18±1.03
	Female	6.48±0.81$^{\xi}$	6.51±0.98$^{\xi}$	6.41±0.97$^{\xi}$	6.66±0.95$^{*,\xi}$
MD_c (mm)	Male	6.41±0.60	6.42±0.68	6.65±0.92*	6.69±0.88
	Female	5.83±0.57$^{\xi}$	5.86±0.75$^{\xi}$	5.85±0.65$^{\xi}$	6.10±0.82$^{*,\xi}$
DD_c (mm)	Male	5.90±0.75	5.93±0.75	6.12±1.03	6.14±1.01
	Female	5.41±0.61$^{\xi}$	5.49±0.78$^{\xi}$	5.44±0.69$^{\xi}$	5.75±0.85$^{*,\xi}$
Femoral					
SD_f (mm)	Male	9.13±1.22	9.36±1.30	9.59±1.77	9.71±1.57
	Female	7.35±1.44$^{\xi}$	7.67±1.63$^{\xi}$	7.56±1.42$^{\xi}$	8.09±1.79$^{*,\xi}$
MD_f (mm)	Male	8.70±1.00	8.87±1.19	8.97±1.39	9.08±1.39
	Female	6.86±0.97$^{\xi}$	6.93±1.00$^{\xi}$	6.97±1.00$^{\xi}$	7.27±1.13$^{*\xi}$
DD_f (mm)	Male	8.46±1.03	8.61±1.21	8.72±1.45	8.88±1.42
	Female	6.61±0.98$^{\xi}$	6.68±1.03$^{\xi}$	6.70±1.04$^{\xi}$	6.99±1.18$^{*,\xi}$

Values are mean ± SD. SBP: systolic blood pressure; DBP: diastolic blood pressure; MAP: mean arterial pressure; PP: pulse pressure; HR: heart rate; SD: systolic inner diameter; MD: mean inner diameter; DD: diastolic inner diameter. * indicates significant change ($p<0.01$) compared to the immediate previous half-age group. $^{\xi}$ indicates a significant change ($p<0.01$) between male and female in the same age group.

4.2.3 Vascular echography

The subjects undertook a scan examination of the left and right carotid and femoral arteries using a commercially available ultrasonographic system (VIVID 7; GE Vingmed Ultrasound, Horten, Norway) equipped with a vascular transducer (12L 7.3–11.4 MHz; linear array transducer set at 10 MHz) (Rietzschel et al. 2007).

Subjects were lying in recumbent position with the neck in slight hyperextension and turned approximately 30º contralateral for the carotid artery scan and with the legs slightly apart and exorotated for the femoral artery examination. All measurements were ECG gated and consisted of cineloops or recordings of at least five (up to 30) cardiac cycles during normal breathing. Sweep speeds for M-mode, pulsed wave (PW) or continuous wave (CW) Doppler was set at 100 mm/s. Images and loops were exported in raw DICOM format. All recordings were performed by a single trained sonographer, on a single echo system.

4.2.3.1 Flow velocity measurement

Systolic centreline blood flow velocity was measured (PW Doppler) in the carotid and femoral arteries. At least five ECG-gated cardiac cycles were acquired. Images, in raw DICOM format (**Figure 4.1**), were processed offline with home-written programs in MatLab (The Mathworks, Natick, MA, USA). After a preliminary filtering of the images, a morphological operation derived from a combination of the fundamental morphological operations dilation and erosion was applied in order to smooth image contours. Thus, maximum and minimum velocity envelopes were detected based on a grey scale threshold and the average profile (**Figure 4.2**) was used to calculate the local c using the lnDU-loop method. The correction for the angle between the flow and the ultrasound beam was applied where needed.

4.2.3.2 Diameter measurement

During the vascular echography the sonographer selected a region of interest (ROI) over a section of the artery that includes both the posterior and the anterior walls. Inside the ROI radio frequency data (RF) data at 209 frames/s were acquired along eight beams. B-mode images and RF data were imported in MatLab, one beam was selected and its RF data were shown as an RF M-mode together with a 4 mm-wide section of the B-mode image around the selected beam. At this point, to obtain the diameter waveform, the vessel boundary was selected manually at a given moment in time and its

movement was automatically tracked using a modified autocorrelation estimator (Rabben et al. 2002, Rabben et al. 2004, Segers et al. 2005, Vermeersch et al. 2008). In this study the inner vessel diameter was detected by tracking the lumen-intima boundary on both the anterior and posterior walls. The use of the RF data allowed for a higher axial resolution compared to the conventional M-mode (Rietzschel et al. 2007).

4.2.3.3 Velocity and diameter alignment

U and D were not recorded simultaneously, but they were acquired during the same vascular examination (Rietzschel et al. 2007). To perform the analysis two representative beats for each subject with similar heart rate were selected and aligned using the peak of the R-wave of the ECG.

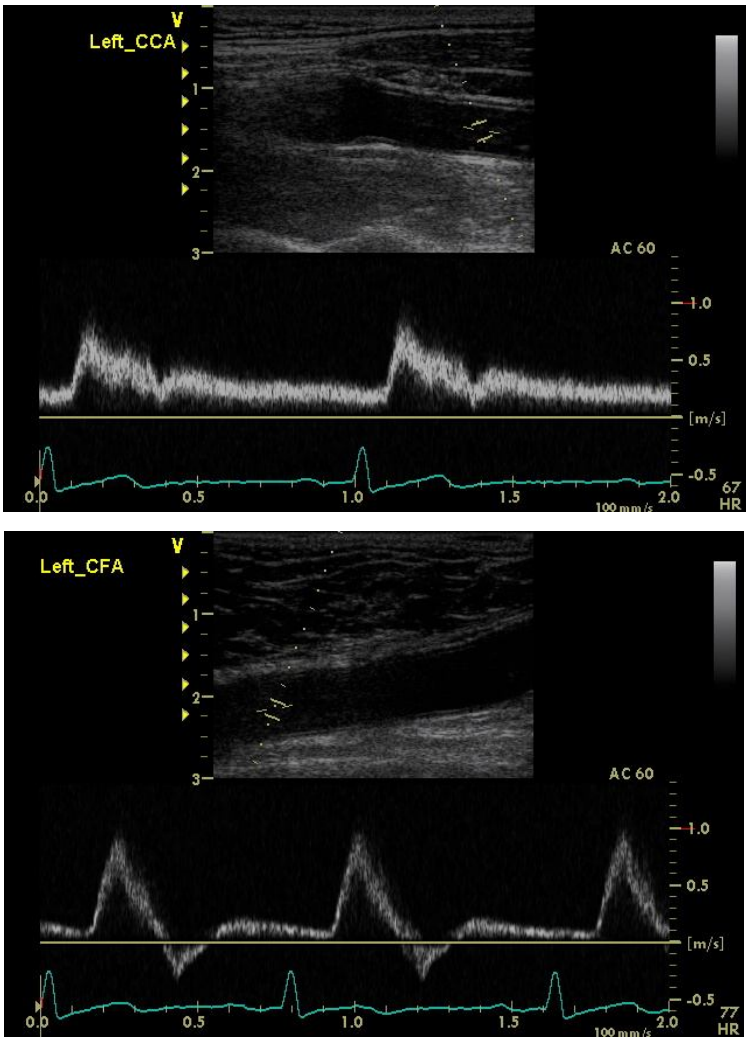

Figure 4.1: Examples of DICOM images of velocity flow waveforms and the ECG in the carotid (top) and femoral (b) arteries of a 45 years old male.

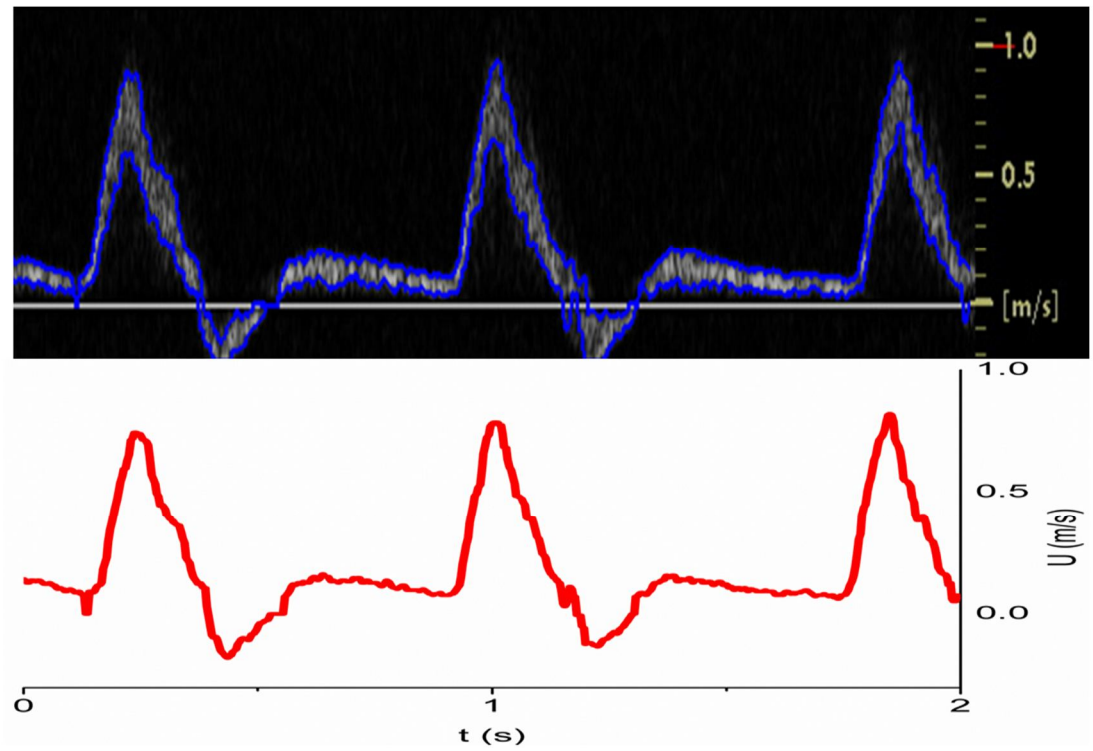

Figure 4.2: The maximum and minimum envelopes (blue lines) detected from the femoral DICOM image of Figure 4.1 (top) and the flow velocity profile (red) obtained by averaging the two envelopes (bottom).

4.2.4 Biochemistry

Serum concentrations of glucose, cholesterol and high-density lipoprotein (HDL) cholesterol were measured using commercial reagents according to the manufacturers' recommendations at 37ºC on a Modular P system (Roche Diagnostics) in an ISO 9002 certified reference laboratory. Serum glucose was evaluated using a standard hexokinase enzymatic method. Total serum cholesterol was assayed by means of the enzymatic colorimetric CHOD–PAP method. Serum HDL cholesterol was assessed by the homogenous enzymatic method that involves the use of dextran sulfate and polyethylene glycol-modified cholesterol esterase and cholesterol oxidase. The coefficient of variation of all tests was < 3%. Biochemical parameters of the population are reported in **Table 4.2.**

Table 4.2: Biochemical data of the subjects.

Parameter	Gender	35-40	41-45	46-50	51-56
Total cholesterol (mg/dl)	Male	211±39	217±36	224±37	223±35
	Female	205±32	208±33$^{\xi}$	215±35	227±36*
HDL cholesterol (mg/dl)	Male	55±14	56±13	57±14	56±13
	Female	71±16$^{\xi}$	70± 18$^{\xi}$	70±18$^{\xi}$	72±17$^{\xi}$
Glycemia (mg/dl)	Male	92±9	93±12	94±12	96±17
	Female	87±7$^{\xi}$	87± 7$^{\xi}$	89±9$^{*,\xi}$	93±19*

Values are mean ± SD. HDL: high density lipoprotein. * indicates significant change ($p<0.01$) compared to the immediate previous half-age group. $^{\xi}$ indicates a significant change ($p<0.01$) between male and female in the same age group.

4.2.5 Determination of local wave speed and distensibility

Local c can be determined using equation 2.32

$$c = \pm \frac{1}{2} \frac{dU_{\pm}}{d \ln D_{\pm}}$$

where dU and dlnD are the changes of velocity and diameter natural logarithm, (+) and (-) indicate the forward and backward directions, respectively. Equation 2.32 describes a linear relationship between lnD and U for unidirectional waves. To identify automatically the linear portion of the loop an algorithm recently proposed has been used (Swalen, Khir 2009). Firstly, diameter and velocity measurements were smoothed using a Savitsky-Golay filter and afterwards the program calculates the local slope at each sampling time from the onset of the pressure waveform and calculates the relative difference between the current slope and the average of all the previous slopes starting from the beginning of the linear part. The procedure stops when the difference between the current slope and the average of the previous ones is larger than a selected threshold. **Figure 4.3** shows two typical examples of lnDU-loops, velocity and diameter waveforms at the carotid and femoral arteries for the same subject.

Substituting Equation 2.32 in the Bramwell-Hill equation allows for the determination of local distensibility ($_n$Ds)

$$_n Ds = \frac{4}{\rho} \left(\frac{d \ln D}{dU} \right)^2 \tag{4.1}$$

where the fluid density ρ is assumed 1050 kg/m^3.

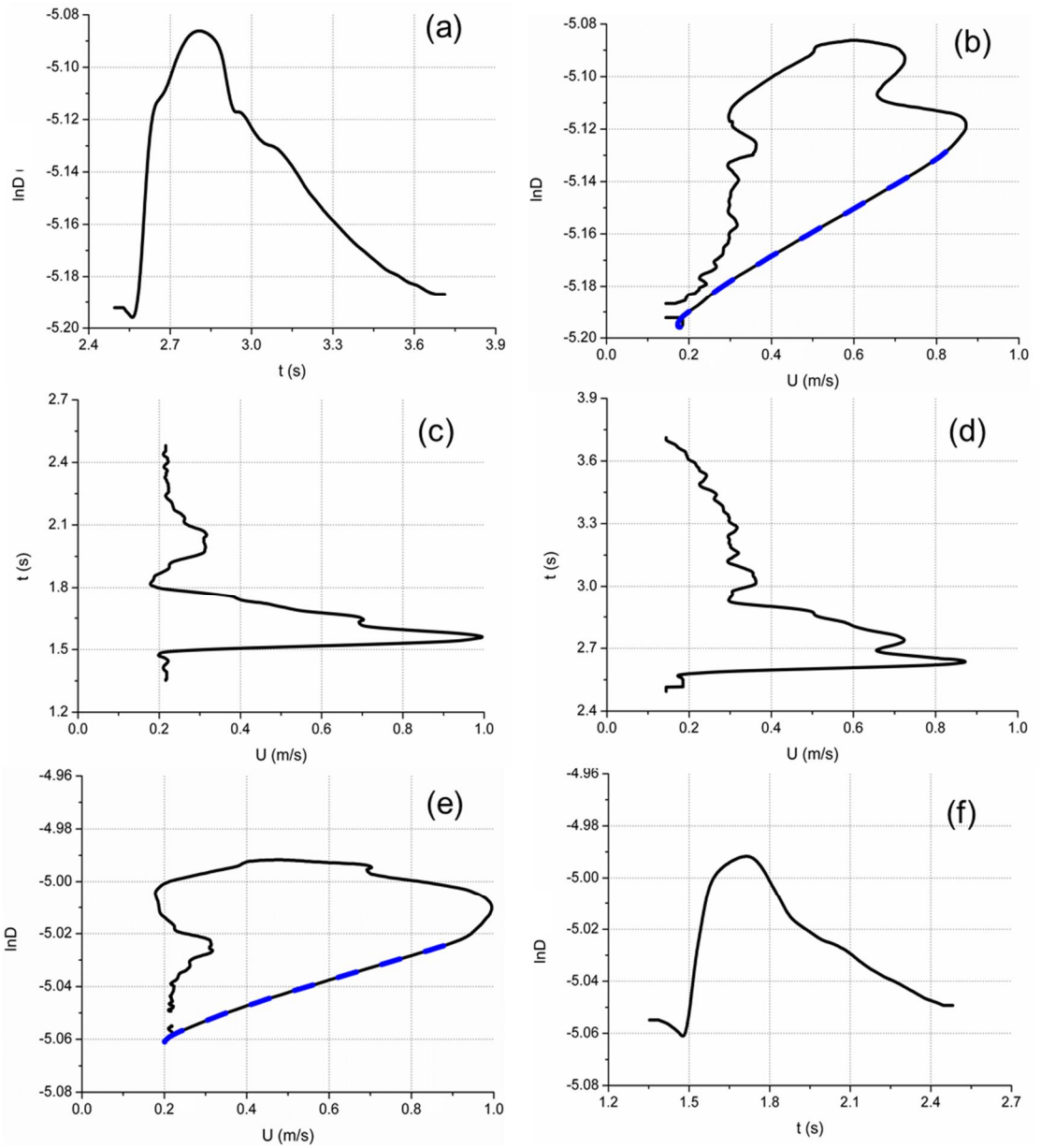

Figure 4.3: (a) Diameter natural logarithm waveforms, (b) lnDU-loop and (c) velocity flow waveform in the carotid artery; (d) velocity flow waveform, (e) lnDU-loop and (f) diameter natural logarithm waveforms in the femoral artery in a 40 years old female. Local wave speed is 5.02 m/s and 9.59 m/s for the carotid and femoral artery, respectively. The dashed blue line indicates the initial linear part of the loop.

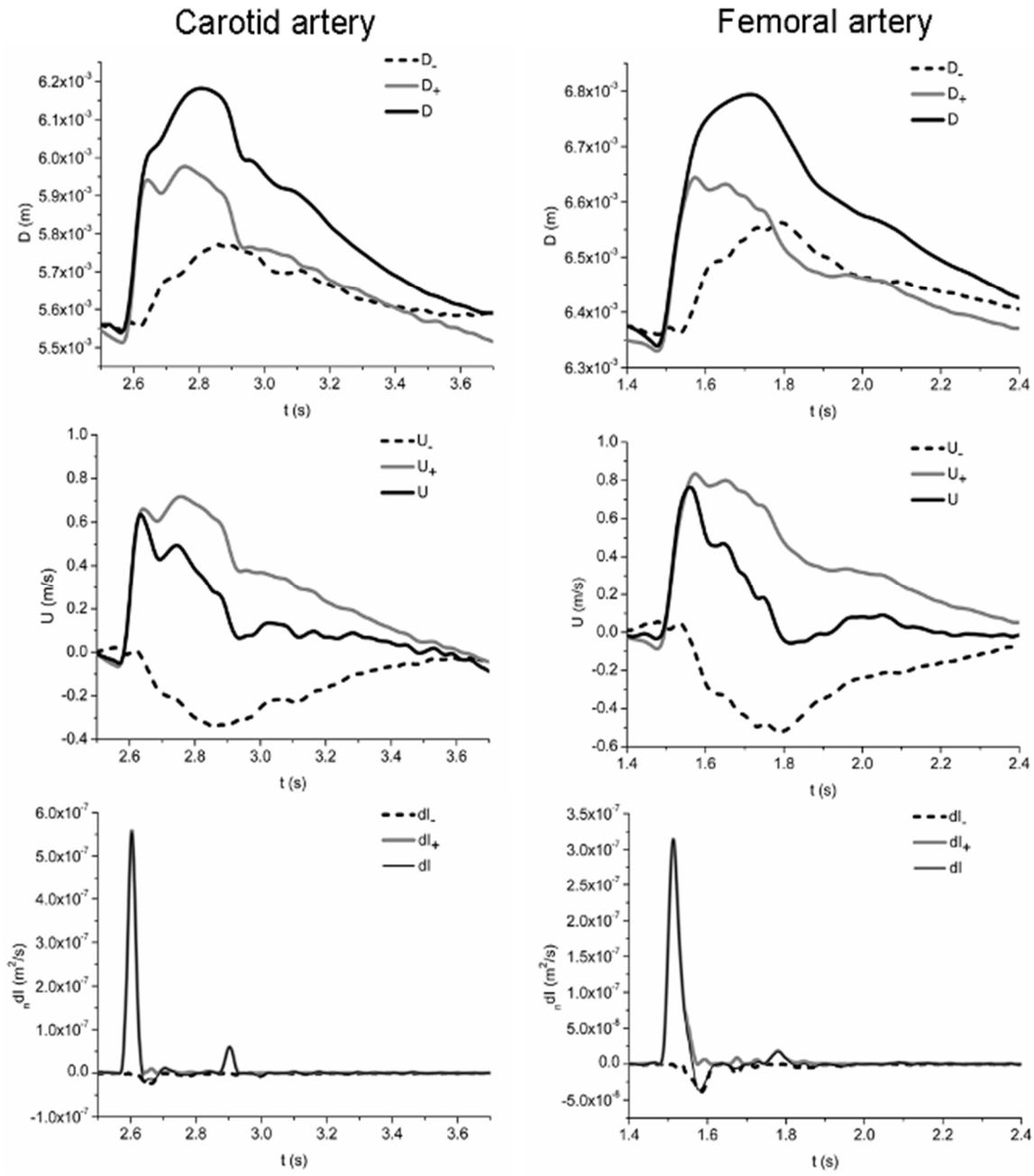

Figure 4.4: The measured, calculated forward (+) and backward (-) diameter (D), velocity (U) and non-invasive wave intensity ($_{n}$dI) in the carotid (left) and in the femoral artery (right) in a 40 years old female. The black solid lines show the measured parameter, gray solid lines show the forward waves and the black dashed lines show the backward waveforms.

4.2.6 Wave separation and intensities of the waves

D and U waveforms can be separated in their forward and backward component using Equations 2.34 and 2.35 described in chapter 2 and the non-invasive wave intensity is determined as $_{n}dI=dDdU$ (Feng, Khir 2010). The knowledge of c, $_{n}dI$ can be separated into its forward and backward components

$$_{n}dI_{\pm} = \frac{1}{4(D/2c)}\left(dD \pm \frac{D}{2c}dU\right)^{2} \quad (4.2)$$

Equation 4.2 shows that the non-invasive wave intensity analysis has the same useful characteristic of the traditional analysis, being positive for forward and negative for backward waves. Peak intensities of the forward and backward compression waves ($_{n}dI_{+max}$ and $_{n}dI_{-min}$) were determined. The ratio of $_{n}dI_{-min}$ to $_{n}dI_{+max}$, termed in this chapter as the Reflection Index ($_{n}RI$), was calculated at the carotid and at the femoral sites. **Figure 4.4** shows two examples of D, U and wave intensity separation in the carotid and in the femoral artery.

4.2.7 Statistical analysis

Data are presented as mean values ± SD and bars in figures are SEM. The population has been subdivided by gender into four half-decades of age: 35-40, 41-45, 46-50 and 51-55 years. Effects of age and gender on c, $_{n}Ds$, $_{n}dI_{+max}$, $_{n}dI_{-min}$ and $_{n}RI$ were studied using analysis of the covariance technique (ANCOVA). These parameters were adjusted for mean arterial pressure (MAP) that was calculated as the averaged value of the calibrated brachial artery waveforms, heart rate (HR) and body height. The analysis was carried out also including glycemia, total cholesterol and HDL cholesterol as covariates. Paired Student's t-tests were used to asses any significant difference between the same parameter in carotid and femoral artery. Values $p<0.01$ were considered statistically significant. Statistical analyses were performed using SPSS 17.0 (SPSS Inc., Chicago, Illinois, USA). All data were collected by the same operator and analysed by one analyser. Reproducibility analysis was not carried out.

4.3 Results

4.3.1 Local wave speed

Figure 4.3 shows two typical examples of lnDU-loops, velocity and diameter waveforms at the carotid and femoral arteries for the same subject. In the femoral artery

c was on average higher than that at the carotid (10.98±4.70 m/s vs. 4.03±1.64 m/s, p<0.001).

4.3.1.1 The effects of age and gender on the wave speed

In the carotid artery c increased significantly with age (p<0.001) but the difference between male and female was not statistically significant. In the femoral artery c did not change with age but was found higher in men than women (11.43±5.07 m/s vs. 10.52±4.92 m/s, p<0.001). Both, carotid and femoral wave speeds did not reveal an age-gender interaction. When the biochemistry parameters were included to the analysis as covariates, the differences between male and female c in the femoral artery was attenuated. **Figure 4.5** shows the changes of c with age and gender at the carotid and femoral arteries.

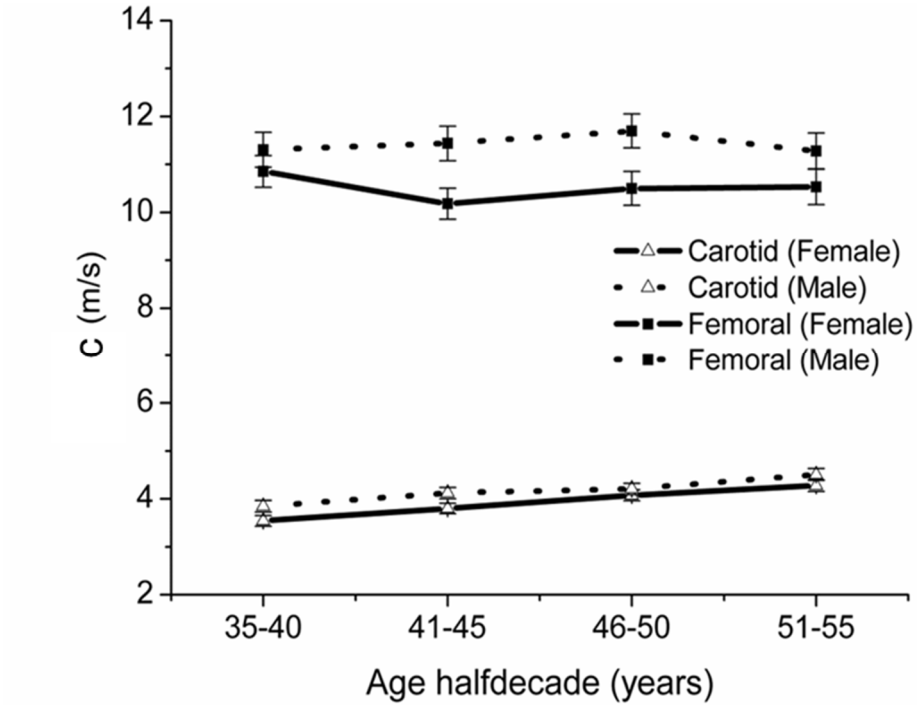

Figure 4.5: Local wave speed, c, is shown as a function of age and gender at the carotid and femoral arteries. c was adjusted for mean arterial pressure (MAP), heart rate (HR) and body height. Error bars are SEMs.

4.3.2 Local distensibility

Carotid artery $_{n}$Ds was on average higher than that of the femoral artery ($87\pm67\cdot10^{-3}$ kPa^{-1} vs. $15\pm14\cdot10^{-3}$ kPa^{-1}, p<0.001).

4.3.2.1 The effects of age and gender on the arterial distensibility

Carotid $_nDs$ decreased with age (apart from men age 41-45 and 46-50, $p<0.001$) and it was higher in female than males ($91\pm74\cdot10^{-3}$ kPa^{-1} vs. $77\pm53\cdot10^{-3}$ kPa^{-1}, $p<0.01$). In the femoral artery, $_nD_s$ did not change with age and was higher in females than males ($17\pm15\cdot10^{-3}$ kPa^{-1} vs. $13\pm11\cdot10^{-3}$ kPa^{-1}, $p<0.001$). Inclusion of glycemia, total cholesterol and HDL cholesterol to the analysis led to a decrease in the distensibility differences between male and female at the femoral artery. **Figure 4.6** shows the changes of $_nDs$ in the carotid and femoral arteries with age and gender.

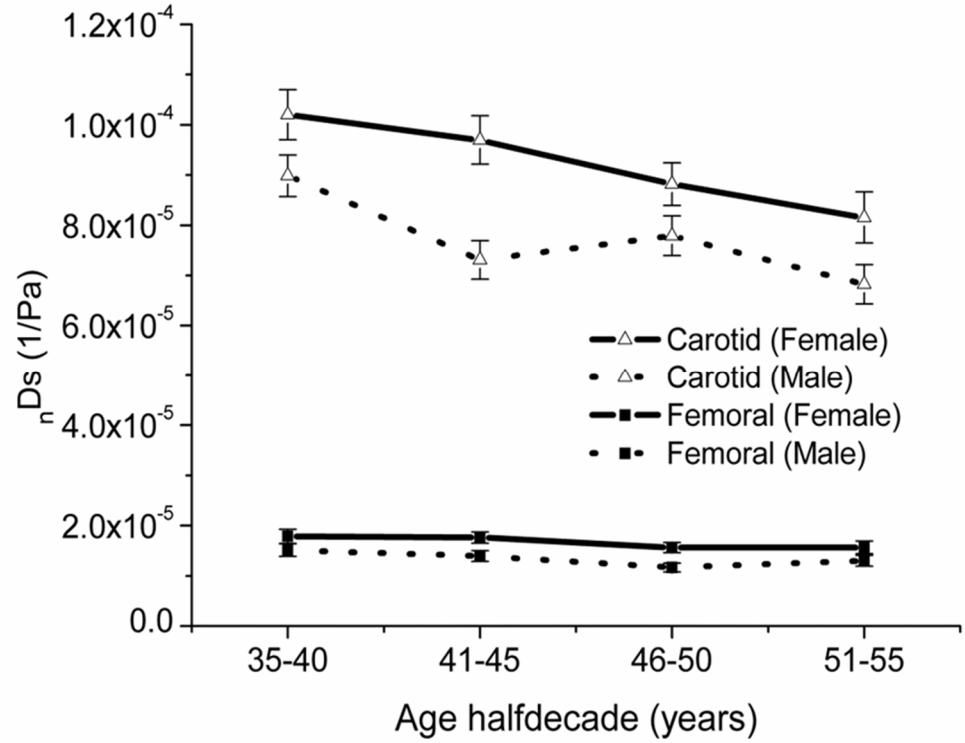

Figure 4.6: Local distensibility $_nDs$ is shown as a function of age and gender at the carotid and femoral arteries. $_nDs$ was adjusted for mean arterial pressure (MAP), heart rate (HR) and body height. Error bars are SEMs.

4.3.3 Wave intensity parameters

Figure 4.4 shows a typical D, U and $_ndI$ waveforms in the carotid and femoral arteries, separated into their forward and backward components. Examining $_ndI$ waveforms, three peaks can be identified: a forward compression wave in early systole (first positive peak) due to the left ventricle (LV) contraction, a backward compression wave in mid-systole (negative peak) due to reflections from the periphery, and a forward expansion wave at the end of systole (second positive peak) due to the

reduction in LV rate of contraction. Those peaks are similar in shape and timing to those of traditional WIA. The average peak intensities of the forward compression wave were $2.60\pm1.41\cdot10^{-7}m^2/s$ and $2.08\pm1.14\cdot10^{-7}$ m^2/s for the carotid and femoral artery, respectively and those of the backward compression wave were $0.38\pm0.30\cdot10^{-7}m^2/s$ and $0.42\pm0.34\cdot10^{-7}$ m^2/s.

4.3.3.1 The effects of age and gender on the intensities of the compression waves

Average peak forward and backward wave intensities decreased with age in the carotid ($p<0.001$) and a significant dependence of the peak intensity of the forward compression wave on gender in this vessel was found; higher in males ($2.92\pm1.51\cdot10^{-7}$ m^2/s vs. $2.29\pm1.10\cdot10^{-7}$ m^2/s, $p<0.001$). In the femoral artery average peak forward and backward wave intensities did not change significantly with age and peak intensity of the forward compression wave is higher in females than males ($2.28\pm1.50\cdot10^{-7}$ m^2/s vs. $1.93\pm1.16\cdot10^{-7}$ m^2/s, $p<0.001$). **Figure 4.7** displays the changes of peak intensity of the forward ($_ndI_{+max}$) and backward ($_ndI_{-min}$) compression wave with halfdecade age and gender at the carotid (top) and femoral (bottom) arteries.

4.3.3.2 The effects of age and gender on the reflection index

$_nRI$ indicating wave reflections from the left leg were higher than those in the carotid artery indicating reflections from the head (0.22 ± 0.14 vs. 0.15 ± 0.12, $p< 0.001$). The reflection indices for both genders did not change significantly with age but in the carotid artery $_nRI$ is higher in females than males (0.16 ± 0.11 vs. 0.14 ± 0.11, $p<0.01$). Changes with age and gender of the $_nRI$ from the head and left leg are shown **Figure 4.8**.

4.4 Discussions

In the present chapter, newly introduced non-invasive methods have been applied to determine local c, distensibility and wave intensity in the carotid and femoral arteries in a population of healthy human subjects. The technique has already been validated in flexible tubes using *in vitro* experiments for the determination of c and $_ndI$ (Li & Khir 2011). However, the new techniques are applied in this work for the first time *in vivo* to assess the mechanical properties of arteries in a relatively large healthy population. Local c was determined using the lnDU-loop method and then was used with the Bramwell-Hill equation to determine local distensibility. Non-invasive wave

intensity analysis was carried out and peak intensity and the reflection index were calculated. Changes of these parameters with age and gender were investigated in 4 halfdecade classes.

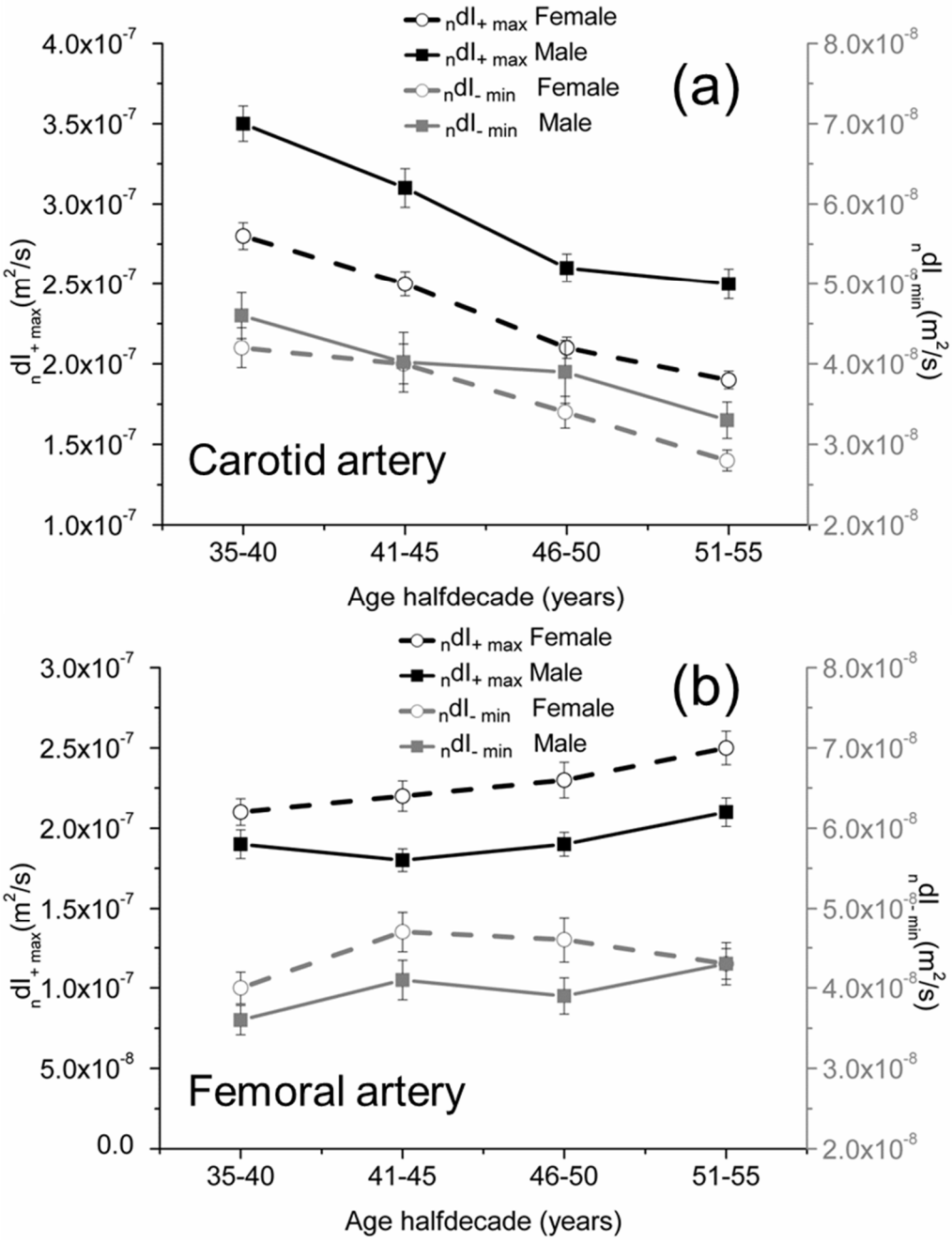

Figure 4.7: Forward (black scale and lines) and backward (gray scale and lines) compression wave intensities ($_{n}dI_{+max}$ and $_{n}dI_{-min}$) at the carotid (top) and femoral arteries (bottom) as a function of age and gender. Parameters were adjusted for mean arterial pressure (MAP), heart rate (HR) and body height. Error bars are SEMs.

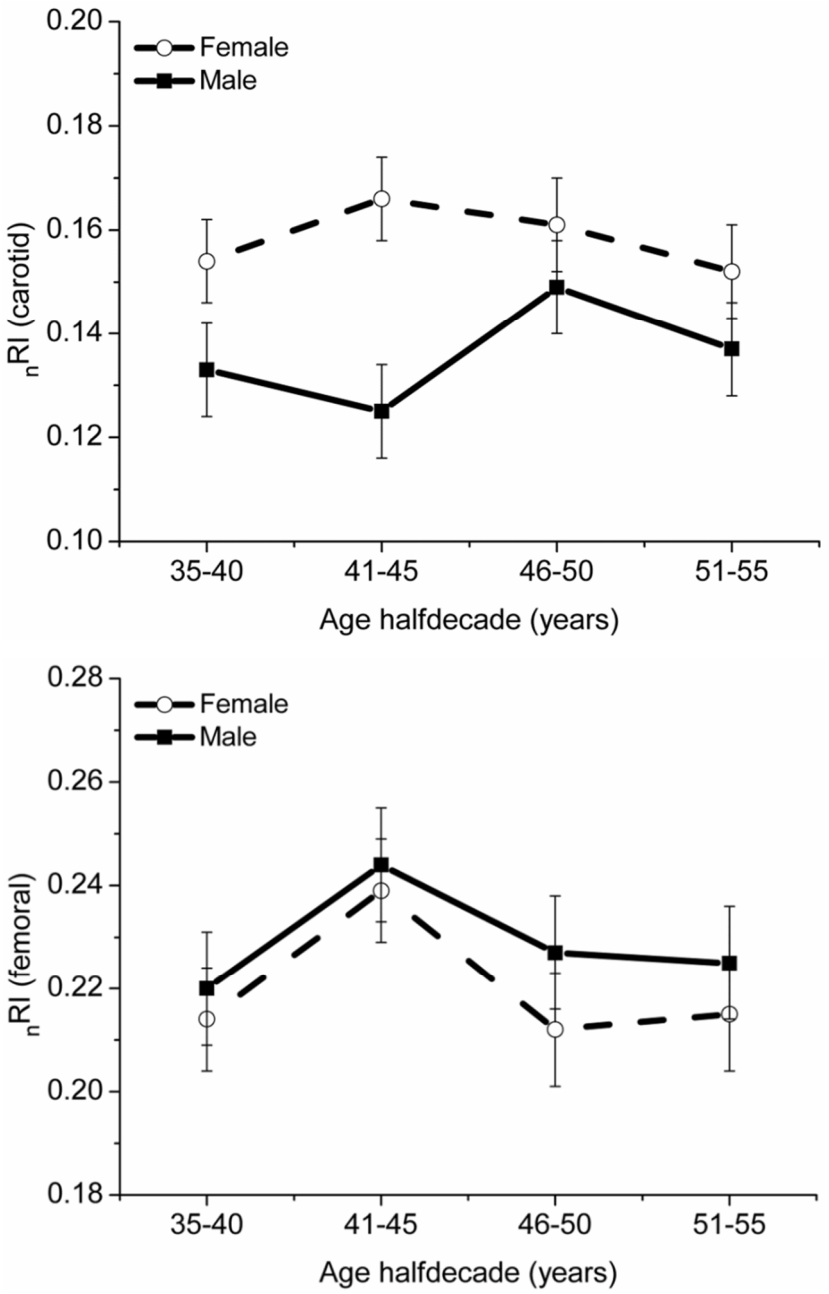

Figure 4.8: Changes of reflection index ($_nRI$) from the upper (top) and from the lower (bottom) part of the body with age and gender. Reflection index was adjusted for mean arterial pressure (MAP), heart rate (HR) and body height. Error bars are SEMs.

Local c in the femoral artery is on average higher and the distensibility is lower than in the carotid artery. These dissimilarities between the two arteries were somewhat expected and can be explained taking into account their different geometry and wall composition. The femoral artery internal diameter is on average larger than that of the carotid artery (7.9±1.6 mm and 6.2±0.7mm respectively, $p<0.001$). Also, content of smooth muscle in the femoral artery is higher than that in the carotid artery (Learoyd &

Taylor 1966).

The results show an increase of carotid local c and decrease of distensibility with age. In contrast, it has been found that local c and distensibility in the femoral artery do not change with age but are higher and lower in men than women, respectively. The results presented in this chapter are in line with those reported by Vermeersch et al. (Vermeersch et al. 2008) who used the same population and derived local carotid and femoral distensibility and local PWV using applanation tonometry and ultrasound wall tracking techniques. Other investigators (Benetos et al. 1993, Bortolotto et al. 1999) that have studied the different behavior of elastic and muscular arteries reported that in general elastic arteries are more affected by aging process than the muscular one. In particular, Benetos et al., studying the mechanical properties of carotid and femoral arteries in normotensive and hypertensive subjects, found that the carotid artery is a very compliant vessel in young subjects, but with age and increasing blood pressure, the distensibility of this artery decreases dramatically (Benetos et al. 1993). This decrease is partially limited by the increase in diameter with age. On the other hand, they found that the femoral artery is less compliant, but is not affected by either age or high blood pressure. Further, Bortolotto et al. compared the mechanical properties of central and peripheral arteries (Bortolotto et al. 1999). In this case the comparison was made between an old and a young group of subjects. Their findings showed that age affects the carotid but not the radial mechanical properties. Since they found that both arteries dilated with age, they concluded that at the level of the carotid artery, the increase in diameter does not compensate for the change in the elastic properties of the vessel. However, as seen in **Table 4.1**, these results indicate the increase in diameter with age is not significant. This is most likely due to the narrow age range of our population. The causes behind the effect of age on central arteries are still not certain; elastic fibers can degenerate with age which can lead to the dilation of the vessel but also atherosclerosis could be a key factor with the increase of age (Safar 1990).

Whether or not including biochemical parameters (HDL-cholesterol, total cholesterol and glycemia) in the analyses would impact either the findings on gender, or the results on the differential carotid and femoral age-dependencies differences has been considered. Overall, inclusion of these biochemical parameters (which are heavily lifestyle-influenced) did not materially affect the findings. Only, the small gender difference in femoral c and distensibility were attenuated by including HDL-cholesterol

in the model (as could in part be expected because of the known, pronounced gender difference in HDL-cholesterol).

In this study the vessel inner diameter has been detected by tracking the intima-lumen boundary for consistency with the mathematical formulation. This boundary may give a greater relative change in diameter compared to the media-adventitia due to the assumption of wall incompressibility (Tanaka et al. 2009). Therefore, higher values of local c and lower values of distensibility using the outer diameter are expected. Arterial diastolic diameter is on average larger in males than females in both sites (6.02±0.90 mm vs. 5.52±0.75 mm, $p<0.001$ at the carotid and 8.65 mm±1.29 vs. 6.74 mm±1.07 mm mm, $p<0.001$ at the femoral). However, significant dependence of local c on gender has been found only at the femoral artery. This is most likely due to the greater difference in diameter between males and females at this site (28% vs. 9% at the femoral and carotid arteries, respectively).

The travelling of waves in arteries implicates an exchange between the kinetic energy of the blood and the potential energy of the distending vessel wall. Therefore, changes in P, U and D in arteries are inextricably related. Any perturbation of one of these parameters will cause a change in the other two. Since the distension of the arterial wall is linked with a change in pressure, waves can be defined as pressure-velocity waves or as diameter-velocity waves. In the present work WIA is defined in terms of D and U for the useful, non-invasive benefits. Therefore, although the reported intensity values may not have an apparent physical meaning the non-invasive WIA is still considered a natural approach that does not contradict any of the other methods reporting intensity using P and U with different units (Parker & Jones 1990, Sugawara et al. 2009).

Examination of the basic mathematical formulation of invasive; dI=dPdU and non-invasive; $_{n}$dI=dDdU wave intensity indicated a potentially useful relationship between both techniques. Considering the relation between the changes in pressure and diameter, $dD = \frac{D}{2\rho c^2} dP$; equation (3) in Feng and Khir (Feng & Khir 2010), it can be shown that $_{n}dI = \frac{D}{2\rho c^2} dI$. Niki et al. (Niki et al. 2002) studied wave intensity analysis at the carotid artery using the P and U traditional formulation in a population of 135 healthy subjects, with an age range of under 25 to above 65 years. In agreement with the

findings reported here of the significant increase of local c with age, Niki et al., found a significant increase in the stiffness parameter β with age, but the authors did not find significant changes in dI indices with age. Therefore the wave intensity results of the two studies are in line and the results presented here follow the theoretical prediction; using the no significant change of dI reported by (Niki et al. 2002), together with the results of no significant change in D (apart from female in the last age halfdecade, **Table 4.1**) and a significant increase of c, all with respect to age, lead to a significant decrease in $_{n}$dI. Since this is the first detailed study of measurement of non-invasive wave intensity in human, there are no other similar results available for comparison.

Traditional WIA has already been used to determine the ratio of the reflected wave to that of the incident wave energy (Jones et al. 2002, Manisty et al. 2009) as an indicator of reflection. In this study the ratio of peak intensity of the reflected wave to that of the forward compression wave was termed as the Reflection Index ($_{n}$RI). The $_{n}$RI carries a similar physical meaning to that of the well-established reflection coefficient. The latter provides a theoretical measure of the local reflection (at a single mismatched bifurcation, for example) and is calculated as the ratio of the local reflected to the incident pressure, however, the former gives an estimation of the accumulative reflected intensities (from several mismatched discontinuities, for example) arriving back at the measurement site. $_{n}$RI can therefore give information about the peripheral arteries downstream of the measurement site. The results show that $_{n}$RI in the left femoral artery, indicating reflections from the left leg, is higher than in the carotid, indicating wave reflections from the head (0.22±0.14 vs. 0.15±0.12 respectively, $p<0.001$). This difference is most likely due to the different geometry of the bifurcations that the incident wave encounters along its path and the different mechanical properties of the vessel downstream. Changes of $_{n}$RI with age are not statistically significant.

4.4.1 Methodological considerations

Several methods to assess local c non-invasively in human have been developed over the years. Some methods require either a linear relationship between brachial pressure waveform or the diameter waveform at the measurement site (Sugawara et al. 2000: Harada et al. 2002; Reneman & Hoeks 1996; Meinders & Hoeks 2004). Some other methods convert the diameter waveform of a local superficial artery into the local pressure waveform by calibrating the former using SBP, DBP or MAP at the brachial

artery (Vermeersch et al. 2008; Papaioannou et al. 2009). The lnDU-loop method does not make any assumptions about the relation between pressure and diameter and it does not require the measurement of the pressure waveform, its systolic, diastolic or mean value in order to calibrate the diameter waveform of another artery. The main advantage of the new technique is that it is based only on D and U measurements that can be easily recorded non-invasively in the clinical environment with an ultrasound system.

The lnDU-loop and the $_{n}$dI methods provide an integrated analytical system that allows for the non-invasive assessment of local c and intensity in any location along the arterial tree. Moreover, diameter, velocity and intensity waveforms can be separated into the forward and backward components to study the propagation of waves and obtain useful hemodynamic information about the downstream events, for example from the arrival time of reflected waves.

4.5 Limitations

Although the theoretical basis of wave intensity analysis requires simultaneous acquisition of the D and U waveforms, the measurements of this study were not synchronised. D and U were aligned using the peak of the R-wave of the ECG in similar heart rate beats. Furthermore, due to the shortness of the interval time between the two recordings of D and U, it can be safely assumed that hemodynamics parameters did not alter significantly.

4.6 Conclusion

This work demonstrates that local c and wave intensity can be calculated in the human carotid and femoral arteries from direct non-invasive measurements of vessel diameter and flow velocity. The lnDU-loop and the $_{n}$dI are potential relevant tools to assess local arterial distensibility and the nature of wave reflections in the clinical environment as they can be obtained totally non-invasively. Another important feature of these methods is that, relying only on diameter and velocity waveforms, it can be carried out with ultrasonographic measurements, which are nowadays readily available in clinical practice. The new techniques allow also for the separation of diameter, flow velocity and non-invasive intensity waveforms into their forward and backward components, which enables the determination of the Reflection Index. The carotid artery is more affected by the aging process than the femoral artery, even in healthy subjects. Local c, distensibility and hemodynamic wave intensity parameters (except

$_n$RI) have strong correlations with age at the carotid artery. The mechanical properties and hemodynamics parameters of the femoral artery are not significantly age-dependent, but local c, distensibility and forward wave intensity are significantly gender-dependent. The validation of these findings strengthens the reliability and robustness of the new proposed technique.

Chapter 5 : Reservoir pressure and velocity in the human carotid artery

5.1 Introduction

This chapter focuses on the potential use of the reservoir-wave approach to study the hemodynamics in the carotid artery of healthy human investigating the changes of the reservoir and excess pressure and velocity components with age and gender. Also, in this chapter a study of the effect of the arterial asymptotic pressure on reservoir and excess components of pressure and velocity is presented.

The reservoir-wave approach proposed by Wang et al. that has been applied in chapter 3 separates the measured pressure in a component due to the elastic properties of the aorta and another component due to the waves (Wang et al. 2003). This approach relies on the assumption that the flow is zero during diastole, which is true only at the aortic root. This concept has been further developed by Aguado-Sierra et al. (Aguado-Sierra et al. 2008a) to use this approach at different locations along the arterial tree. Their work further extends the reservoir-wave approach to study the concept of reservoir (U_r) and excess (U_e) velocities related to the reservoir (P_r) and excess (P_e) pressures, respectively. They proposed a new algorithm, based on empirical hypotheses to derive the reservoir pressure from pressure measurements alone at an arbitrary arterial location and to separate velocity flow waveforms. The empirical hypotheses are based on two observations; a) the pressure waveform decay measured at different locations in the arterial system is very similar in diastole and b) the P_e at the aortic root is very similar in shape to the flow waveform (Q).

The same authors applied this approach to the left and right carotid arteries of a small population of 8 young healthy subjects in order to study wave speed and intensities using P_e and U_e (Aguado-Sierra et al. 2008b). In this chapter the hemodynamics of the left carotid artery using the reservoir-wave approach will be studied in the same healthy population used in chapter 4, where pressure was measured using the applanation tonometry technique. The large number of subjects involved in this study will allow for an in depth investigation of the changes of pressure, velocity and intensities parameters with age and gender and for a better understanding of the

physical meaning of these components. The overall aim of this chapter is to give a new physiological insight into the carotid hemodynamics considering the two components of pressure and velocity.

In chapter 3, a reservoir-wave algorithm that allows for the determination of the arterial asymptotic pressure (P_∞) from the fitting of the exponential pressure decay was used. However, Vermeersch et al. (Vermeersch et al. 2009) studying the reservoir pressure component in the same population used in this chapter reported that the values found by the free fitting algorithm were not physiological. In their work they decided to fix P_∞ to the venous pressure that they assumed to be 0 mmHg.

Since the reservoir-wave approach was introduced, different assumptions about P_∞ were considered; Veermersch et al. (Vermeersch et al. 2009) and Aguado-Sierra et al. (Aguado-Sierra et al. 2008a) used 0 mmHg assuming P_∞ equal to the venous pressure. In another work, Aguado-Sierra et al. (Aguado-Sierra et al. 2008b) used 25 mmHg referring to the work of Schipke et al. (Schipke et al. 2003). Sridharan et al. (Sridharan et al. 2012) used 35 mmHg that was the value found by Wang et al. (Wang et al. 2006) in dogs using a free fitting algorithm.

It can be hypothesized that using a free fitting method and fixing a value for P_∞ lead to different values of the hemodynamic parameters studied in this chapter. For this reason, also a parametric study using the free fitting algorithm and using a fixed value of P_∞ is presented here.

5.2 Material and Methods

5.2.1 Study population

The data were drawn from the Asklepios study database and involved data from 2003 subjects (1024 women) aged 35-55 years (average age 46±6 years). Only subjects with pressure and flow velocity measurements available in the carotid artery were considered. Basic clinical and hemodynamic characteristics of the population are presented in **Table 5.1**.

5.2.2 Applanation tonometry

The detailed description of the applanation tonometry procedure used to measure carotid pressure can be found in (Rietzschel et al. 2007). Applanation tonometry was performed with a Millar pentype tonometer (SPT 301; Millar Instruments, Houston,

Texas, USA). All tonometry data were recorded continuously for 20 s with a sampling rate of 200 samples/s.

Table 5.1: Physical and hemodynamic characteristics of subjects.

Parameter	Gender	35-40	41-45	46-50	51-56
No.	Male	252	249	248	230
	Female	253	265	253	253
Age (years)	Male	38±2	44±1	48±1	54±2
	Female	38±2	43±1	48±1	54±2
Height (cm)	Male	178±7	176±6	175±7	174±6
	Female	165±6$^{\xi}$	164±6$^{\xi}$	163±6$^{*,\xi}$	161±6$^{*,\xi}$
Weight (kg)	Male	82±12	80±12	83±12	81±11
	Female	65±11$^{\xi}$	65±11$^{\xi}$	66±12$^{\xi}$	67±11$^{\xi}$
SBP (mmHg)	Male	132±11	133±12	135±14	138±16
	Female	125±15$^{\xi}$	128±15$^{*,\xi}$	131±15$^{\xi}$	137±18
DBP (mmHg)	Male	75±10	79±10*	80±10	81±11
	Female	74±11	76±11*	76±10	78±11
MAP (mmHg)	Male	98±10	101±11*	103±11	105±13
	Female	96±12	99±12*	100±12$^{\xi}$	104±13
PP (mmHg)	Male	57±9	55±8	55±9	57±11*
	Female	50±8$^{\xi}$	52±10$^{\xi}$	55±11*	58±13*
HR (beat/min)	Male	61±9	62±9	64±11	62±10
	Female	65±8$^{\xi}$	66±9$^{\xi}$	65±9	65±9$^{\xi}$

Values are mean ± SD. SBP: systolic blood pressure; DBP: diastolic blood pressure; MAP: mean arterial pressure; PP: pulse pressure; HR: heart rate. Pressure was recorded at the brachial artery. * indicates significant change ($p<0.01$) compared to the immediate previous halfdecade group. $^{\xi}$ indicates a significant change ($p<0.01$) between males and females in the same age group.

The signal was filtered and divided into individual beats using the foot of the wave as a starting point of individual cardiac cycles. An ensemble average curve was calculated and considered as the tonometry recording for that measuring location. Tonometry was first performed at the brachial artery, and the tonometric recording was calibrated by appointing the peak and trough of the waveform the value of systolic blood pressure (SBP)ba and diastolic blood pressure (DBP)ba (obtained through oscillometric recordings), respectively, leading to a scaled brachial artery pressure tracing, Pba. Mean arterial pressure (MAP)ba was calculated by numerically averaging the curve. Next, tonometry was performed at the carotid artery, assuming that diastolic and mean pressures remain fairly constant in the large arteries. Thus, the trough and

mean of all tonometric recordings were assigned the values of DBPba and MAPba giving scaled carotid artery pressure waveforms (P).

5.2.3 Flow velocity measurements

The flow velocity measurements used in this chapter were the same used in chapter 4. The sequence of cardiac cycle was divided in single beats and an ensemble average beat was calculated as done for the pressure measurements. The two measurements were aligned using the algorithm proposed by (Swalen, Khir 2009).

5.2.4 Determination of reservoir and excess pressure

Reservoir pressure (P_r) was determined from the measured pressure (P) using the algorithm proposed by (Aguado-Sierra et al. 2008a). P_r at an arbitrary location can be determined using the following equations:

$$\frac{dP_r}{dt} = a\left(P - P_r\right) - b\left(P_r - P_\infty\right) \tag{5.1}$$

where, a and b ($1/\tau$) are the rate constants of the system and P_∞ is the asymptotic pressure.

The solution of equation 5.1 is given by:

$$P_r - P_\infty = \left(P_r\left(T_N\right) - P_\infty\right) e^{\left(-b\left(t-T_N\right)\right)} \qquad T_N < t < T \tag{5.2}$$

$$P_r = \frac{b}{a+b}P_\infty + e^{\left(-(a+b)t\right)}\left[\int_0^t aP\left(t'\right)e^{\left((a+b)t'\right)}dt' + P_r\left(t=0\right) - \frac{b}{a+b}P_\infty\right] \quad 0 < t < T_N \tag{5.3}$$

where T is duration of the cardiac cycle and T_N is time of the dicrotic notch.

The constant parameters $P_r(T_N)$, P_∞ and b can be determined by minimizing the sum of squares of the error between fitted and measured pressure data using equation 5.2. An unconstrained nonlinear optimization routine (fminsearch in Matlab) was used. To estimate the parameter a, continuity of P_r at $t=T_N$ is enforced (equation 5.3) and a is fitted from experimental data using the fminsearch Matlab routine. P_r is then obtained for the entire period from equations (5.2) and (5.3). Excess pressure (P_e) was subsequently calculated as the difference between P and P_r. An example of P separated in its reservoir and excess components is shown in **Figure 5.1a**. From **Figure 5.1b** it is possible to observe the similarity between P_e and U. The peaks of the measured (Ppeak), reservoir ($P_r$peak) and excess ($P_e$peak) pressure were determined. The pulse of the measured and the reservoir pressure (PP and PP_r, respectively) were calculated as the difference between the corresponding peaks and the diastolic pressure (P_d). Also the

integral of reservoir and excess pressure (PRI and PEI, respectively) were determined as the area under P_r and P_e curves (**Figure 5.1a**).

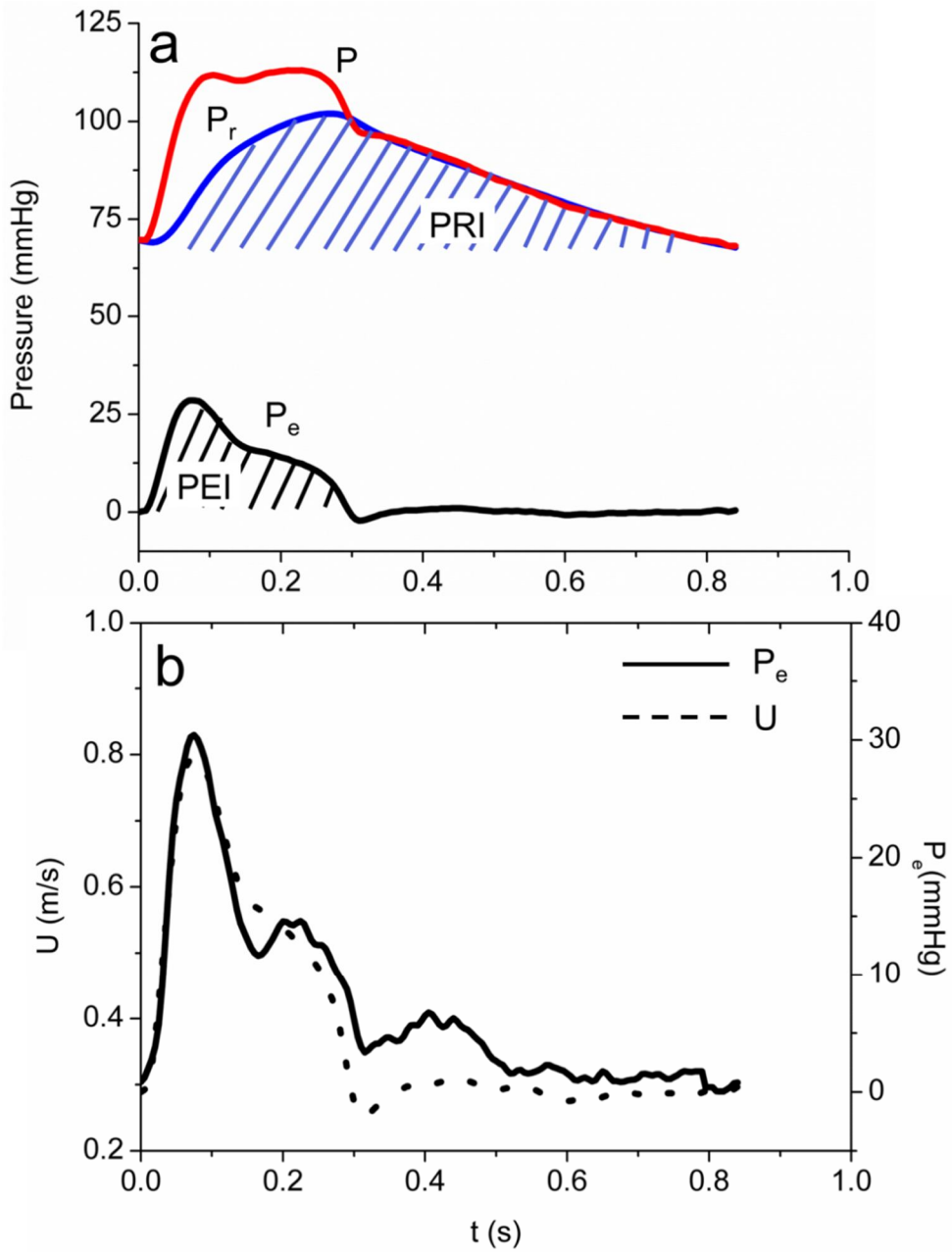

Figure 5.1: a) Example of measured (P, red), reservoir (P_r, blue) and excess (P_e, black) pressures in the carotid artery of a 39 years old female. PRI and PEI are the integral of the reservoir and excess pressures. b) P_e and U in the same subject.

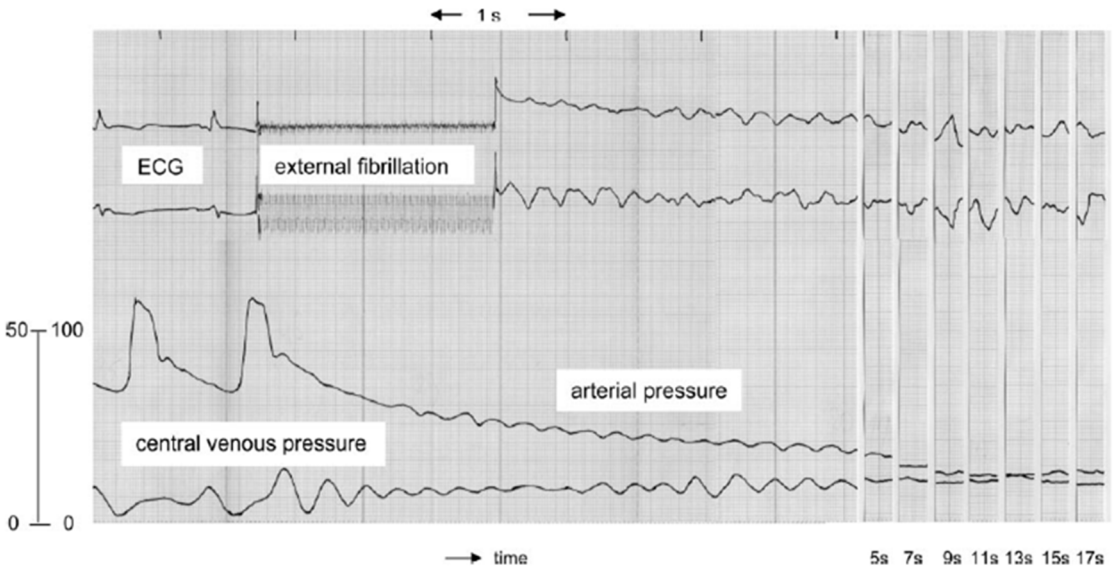

Figure 5.2: Arterial and venous pressures recorded in a subject during the implantation of defibrillator devices (taken from Schipk et al. 2003).

5.2.4.1 Asymptotic pressure (P_∞)

Vermeersch et al. pointed out that a free fitting of P_∞ in the Asklepios population results in non-physiological values of this parameter in many cases (Vermeersch et al. 2009). The reason behind this finding could be related to the procedure used to derive the carotid pressure from the brachial waveform or it might depend on a too short diastolic time that does not allow for a precise estimation of the asymptotic pressure. To overcome this problem the authors in their work decided to set P_∞ (that they called venous pressure, P_v) to 0 mmHg for the entire dataset (Vermeersch et al. 2009). However, it was reported in several studies that when the heart stops the arterial pressure decays exponentially to a value that is higher compared to the venous pressure (Schipke et al. 2003; Jellinek et al. 2000) and that the equilibrium is not reached even after 20 s. The explanation of this phenomenon is still unknown, but some authors have speculated that it can be due to a waterfall effect (Permutt et al. 1963), to a Starling resistor (Starling 1897) or the different compliance of the arterial and venous compartment (Jellinek et al. 2000). Due to ethical restrictions not many studies have been performed in human to find out a reference value of the arterial asymptotic pressure when the heart stops. Recently, two groups managed to record the arterial pressure after stopping the heart in patients undergoing implantation of defibrillator devices (Schipke et al. 2003; Jellinek et al. 2000). From Figure 1 in Jellinek et al. (Jellinek et al. 2000) it is possible to estimate that the asymptotic arterial pressure is

about 14 mmHg before the heart starts again. According to Shipke et al., the arterial pressure decays to a value of 24.2 mmHg after 13 s from stopping the heart (Schipke et al. 2003). **Figure 5.2** shows an example of the decay of the arterial pressure and the venous pressure recorded when the heart stopped pumping. In this chapter, two analysis are reported; once the analysis was carried out using a free fitting algorithm of P_∞ and separately setting P_∞ =19 mmHg which is the average of the two values found in the literature in humans. **Figure 5.3** shows an example of P and the correspondent P_r calculated by free fitting and by setting P_∞ to 19 mmHg.

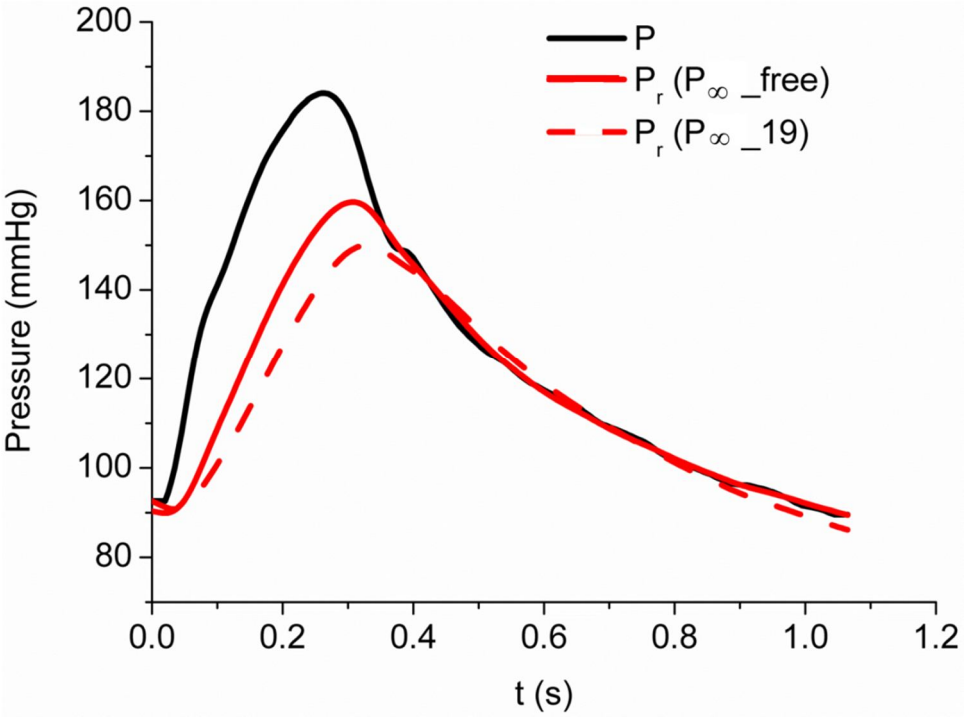

Figure 5.3: Example of measured pressure (black) and the correspondent reservoir pressures calculated by free of fitting P_∞ (solid red) and by setting P_∞=19 mmHg (dashed red). P_∞ calculated using the free fitting algorithm in this case was 80 mmHg.

5.2.5 Determination of reservoir and excess velocity

The measured velocity (U) was separated into the reservoir (U_r) and excess (U_e) components using the equations presented in (Aguado-Sierra et al. 2008a; Aguado-Sierra et al. 2008b) and reported here in section 2.2.8 of chapter 2. In their paper, two methods to determine the downstream resistance ($\overline{R}$) are suggested; 1) calculate $\overline{R}$ from the slope of the linear part of the PU-loop during the diastolic phase of the cardiac

cycle and 2) determine it as $\overline{R} = \left(< P > - P_{\infty} \right) / < U >$ where <P> and <U> are the time-averaged pressure and velocity in diastole. In this work the second approach was chosen since it was difficult to detect the linear part of the loop in diastole in many cases. Maximum velocity peaks, Upeak, $U_r$peak and $U_e$peak were calculated as the peaks of the corresponding waveforms.

In subjects where the diameter waveform was available, also the flow (Q) and the volume (V) were calculated. The former was determined as UA (with A the cross-sectional area, calculated as $\pi D^2_d/4$, where D_d is the diastolic diameter) and the latter was estimated from the area under the Q curve.

5.2.6 Wave speed and wave intensity analysis

Wave speed (c_{ee}) was determined using the P_eU_e-loop method and the wave intensity was performed replacing P and U with P_e and U_e in equation 2.25 of chapter 2 (Aguado-Sierra et al. 2008a). Peaks of forward and backward compression (FCW and BCW) waves were determined.

5.2.7 Statistical analysis

Data are presented as mean values ± SD in tables and text and bars in figures are SEMs. The population has been subdivided by gender into four halfdecades of age: 35-40, 41-45, 46-50 and 51-55 years. Effects of age and gender on Ppeak, $P_r$peak $P_e$peak, PP, PP_r, PRI, PEI, Upeak, $U_r$peak, $U_e$peak, τ, c_{ee}, FCW and BCW were studied using analysis of the variance technique (ANOVA) and the covariance technique (ANCOVA). Pearson correlation factors were calculated in order to assess any correlation between hemodynamic parameters. Values $p<0.01$ were considered statistically significant. Statistical analyses were performed using SPSS 17.0 (SPSS Inc., Chicago, Illinois, USA).

5.3 Results

As shown in **Figure 5.4** systolic pressure in the carotid artery increases significantly with age ($p<0.001$) both in males and females. Diastolic pressure (P_d) increases as well with age ($p<0.001$), but also a significant difference between gender was found ($p<0.001$) with males having a higher diastolic pressure than females (**Figure 5.5**). Pulse pressure (PP) increases significantly with age ($p<0.001$), but the increase is more pronounced in women than in men (in the first three age halfdecades PP does not

increase in men) (**Figure 5.6**). **Figure 5.7** shows the changes of the velocity peak with age and gender. It decreases significantly with age and is significantly higher in males than females (both p<0.001).

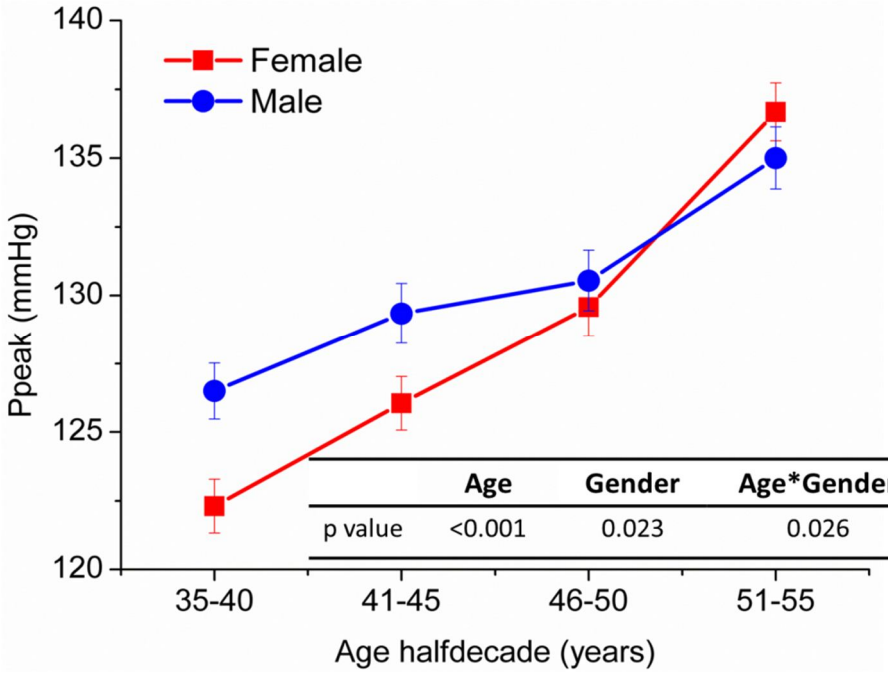

Figure 5.4: Changes of systolic peak pressure (Ppeak) in the carotid artery with age and gender. In the table the p values are reported. Ppeak increases significantly with age.

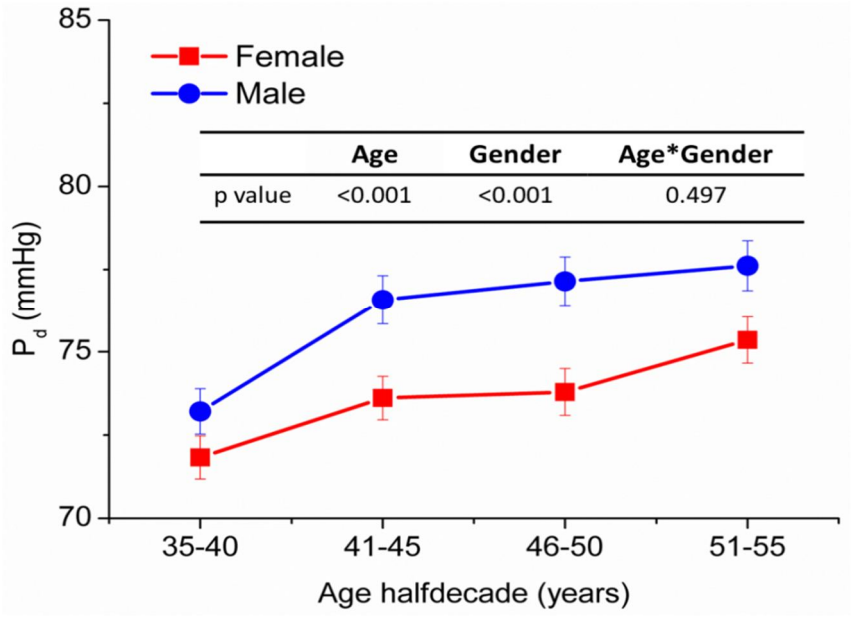

Figure 5.5: Changes of diastolic pressure (P_d) in the carotid artery with age and gender. P_d increases significantly with age and is higher in males than females.

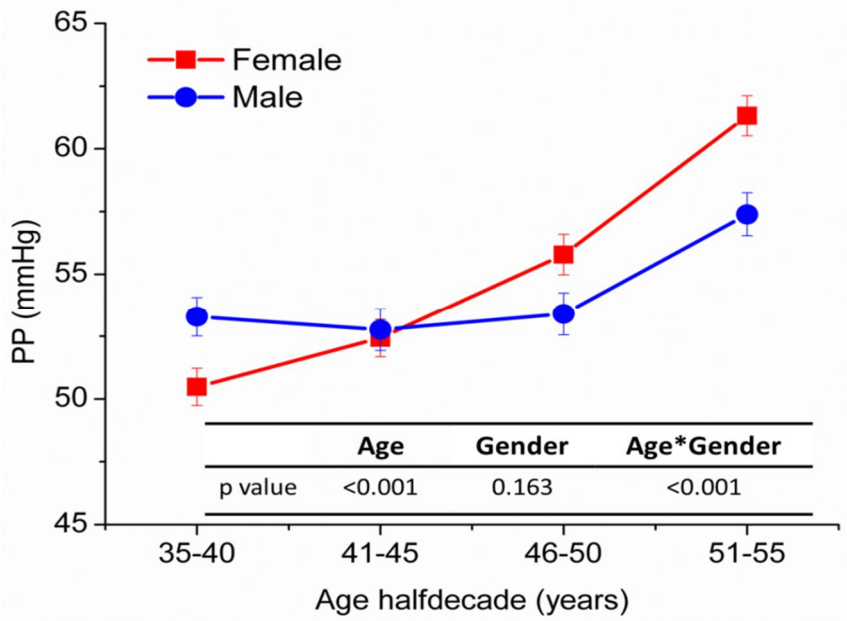

Figure 5.6: Changes of pulse pressure (PP) in the carotid artery with age and gender. PP pressure increases significantly with age and in females more than males. Also a significant interaction between age and gender was found.

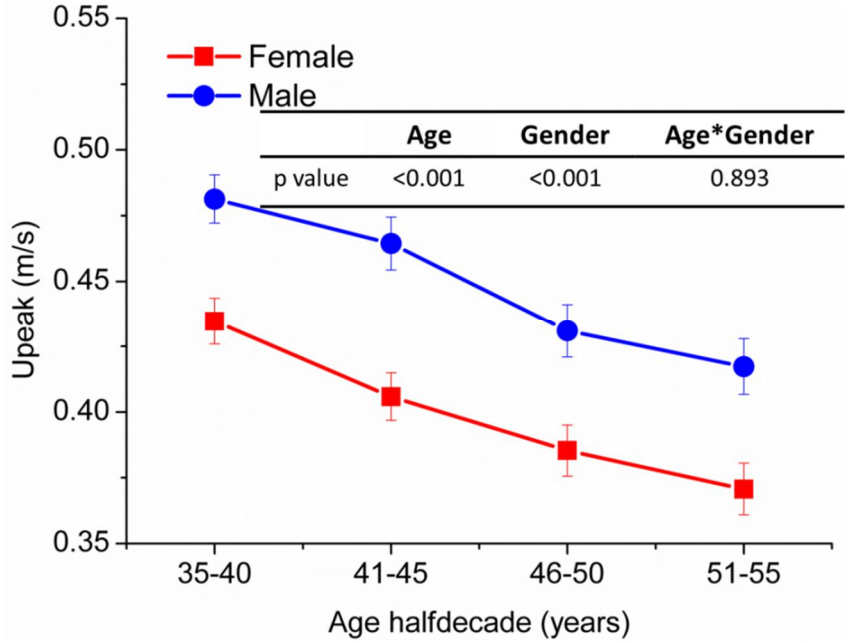

Figure 5.7: Changes of peak velocity (Upeak) in the carotid artery with age and gender. Upeak decreases significantly with age and is significantly higher in males than females.

5.3.1 Changes of reservoir and excess pressure with age and gender

Figure 5.8 shows the changes of P_∞ with age and gender as calculated using the free fitting method. The average values of P_∞ are relatively high for both males and

females and in all age halfdecades (50-60 mmHg). P_∞ increases significantly with age both, in men and women ($p<0.001$).

As shown in **Figure 5.9**, in both analyses $P_r$peak increases significantly with age and is higher in male than female. PP_r increases significantly with age ($p<0.001$), but the increase is more pronounced in women than in men (**Figure 5.10**). Both trends are very similar to Ppeak and PP, respectively. Even though the changes are very similar using the two analyses, setting P_∞ to a fixed value led to smaller values of $P_r$peak and PP_r compared to the free fitting. **Figure 5.11** shows the changes of the reservoir pressure integral (PRI) with age and gender. A statistically significant increase of PRI with age ($p<0.001$) and a significant difference between male and female ($p<0.001$) were found using both techniques. PRI calculated using the free fitting method is higher than PRI calculated setting P_∞. In **Figure 5.12** the changes of $P_e$peak with age and gender are reported. In this case the two techniques led to different results; no significant differences with age and gender were found using the free fitting method, but a significant difference with age was found setting P_∞ ($p<0.001$), increasing in females and decreasing in males. The excess pressure integral (PEI) increases significantly with age ($p<0.001$) and is higher in females than males ($p<0.001$) using both techniques (**Figure 5.13**). $P_e$peak and PEI calculated setting P_∞ are higher than that calculated using the free fitting method.

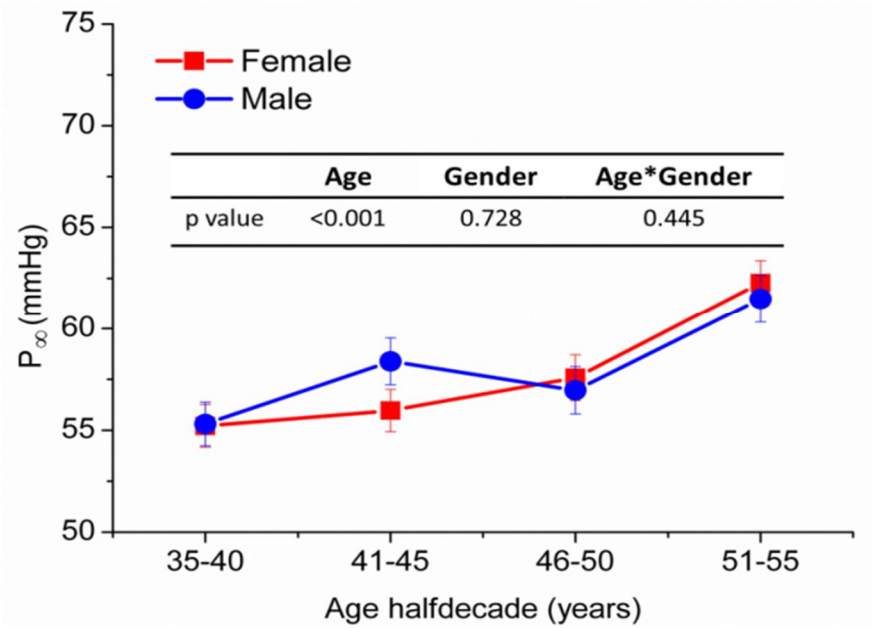

Figure 5.8: Changes of P_∞ calculated using the free fitting method with age and gender. P_∞ increases significantly with age. It was adjusted for P_d.

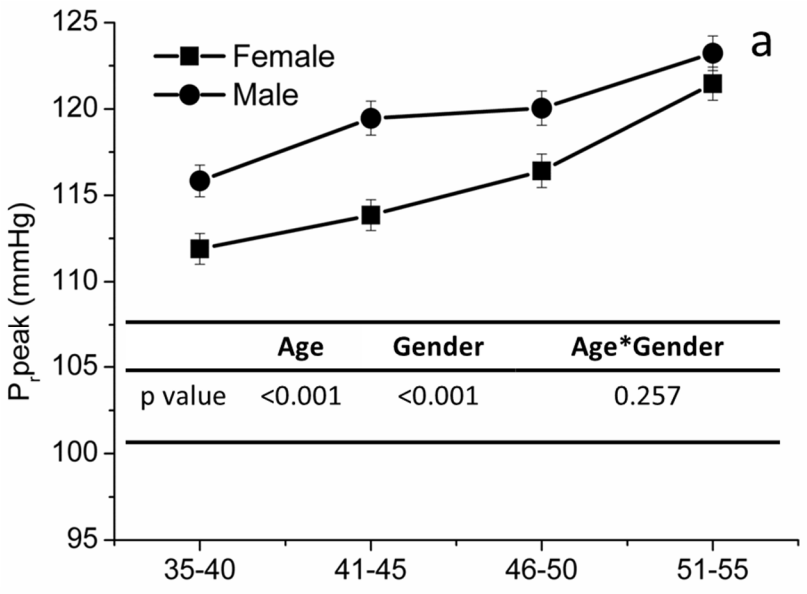

	35-40	40-45	45-50	50-55
Female	115%	114%	114%	114%
Male	114%	113%	113%	112%

Figure 5.9: Changes of peak reservoir pressure ($P_r$peak) in the carotid artery with age and gender using the free fitting algorithm (a) and setting P_∞=19 mmHg (b). $P_r$peak increases significantly with age and is higher in males compared to females in both cases. $P_r$peak is higher using the free fitting method than setting P_∞=19 mmHg. Percentage ratios between the values in (a) and (b) are reported in the table (c).

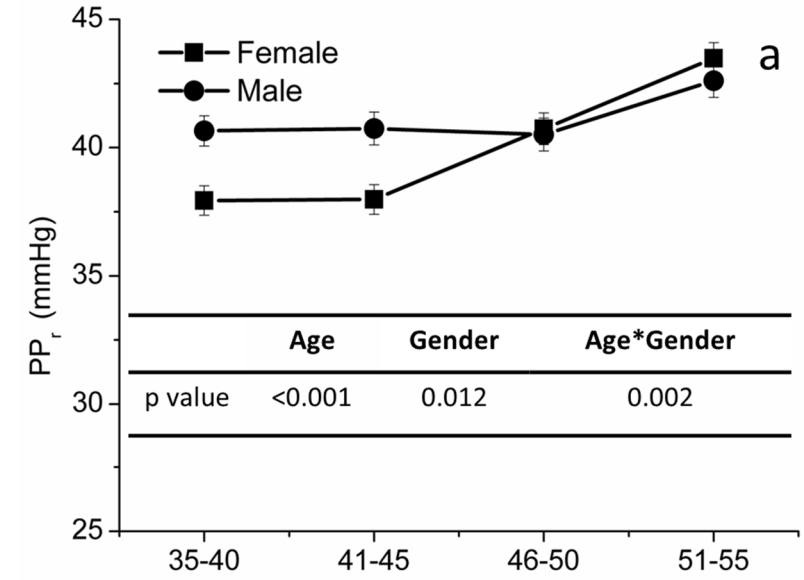

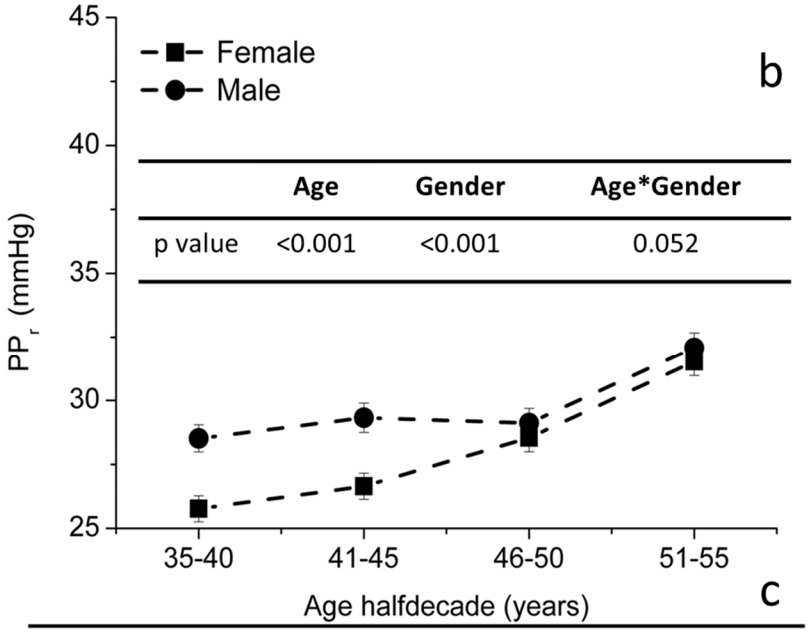

	35-40	40-45	45-50	50-55
Female	147%	143%	143%	138%
Male	143%	139%	139%	133%

Figure 5.10: Changes of pulse reservoir pressure (PP_r) in the carotid artery with age and gender using the free fitting algorithm (a) and setting P_∞=19 mmHg (b). PP_r increases significantly with age and is higher in males than females in both cases. A significant age-gender interaction was found only in (a). PP_r is higher using the free fitting method than setting P_∞=19 mmHg. Percentage ratios between the values in (a) and (b) are reported in the table (c).

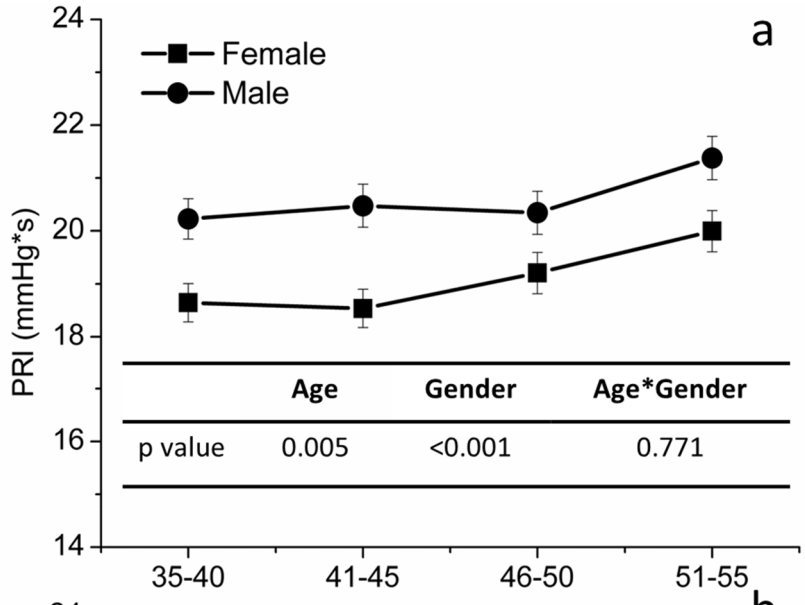

c

	35-40	40-45	45-50	50-55
Female	122%	122%	121%	114%
Male	116%	114%	119%	114%

Figure 5.11: Changes of reservoir pressure integral (PRI) in the carotid artery with age and gender using the free fitting algorithm (a) and setting P_∞=19 mmHg (b). PRI increases significantly with age and is higher in males than females in both cases. PRI is higher using the free fitting method than setting P_∞=19 mmHg. Percentage ratios between the values in (a) and (b) are reported in the table (c).

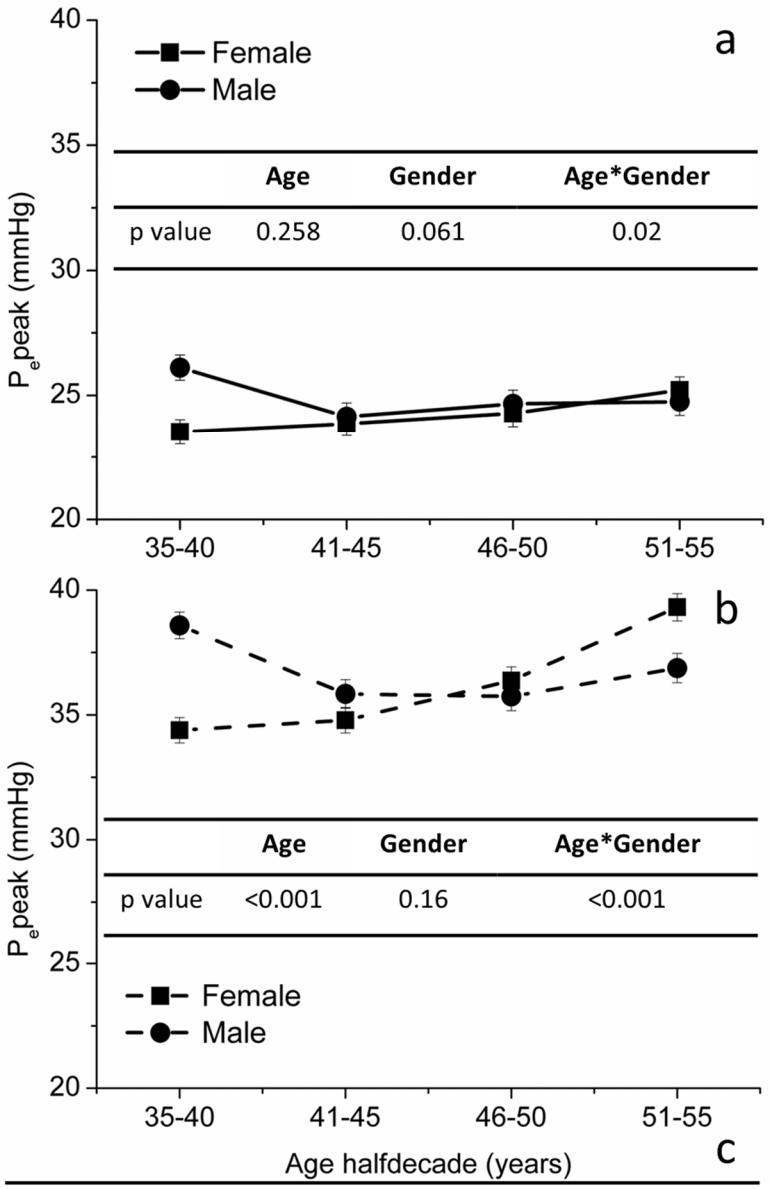

	35-40	40-45	45-50	50-55
Female	68%	69%	67%	64%
Male	68%	67%	69%	67%

Figure 5.12: Changes of peak excess pressure ($P_e$peak) in the carotid artery with age and gender using the free fitting algorithm (a) and setting P_∞=19 mmHg (b). $P_e$peak does not change significantly with age or gender in (a), but changes significantly with age in (b). A significant age-gender interaction was found in (b). $P_e$peak is smaller using the free fitting method than setting P_∞=19 mmHg. Percentage ratios between the values in (a) and (b) are reported in the table (c).

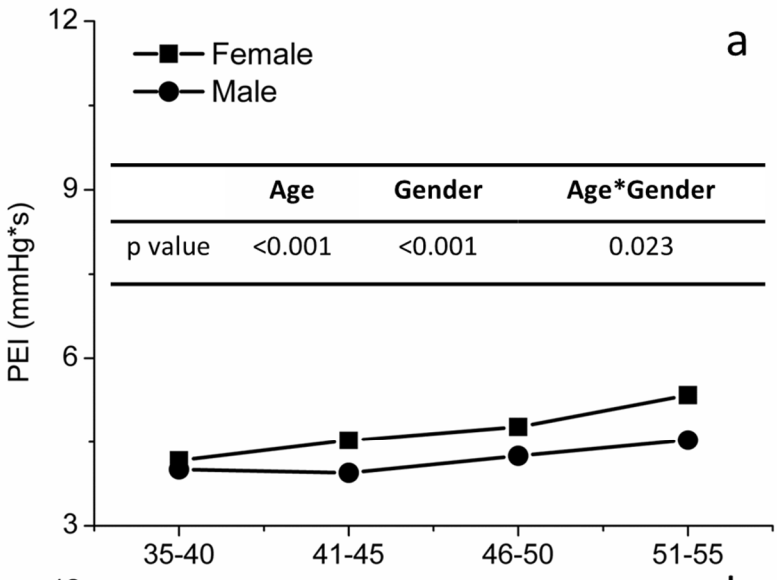

c

	35-40	40-45	45-50	50-55
Female	44%	47%	47%	48%
Male	43%	43%	46%	48%

Figure 5.13: Changes of excess pressure integral (PEI) in the carotid artery with age and gender using the free fitting algorithm (a) and setting the value of P_{∞}=19 mmHg (b). PEI increases significantly with age and is higher in females than males in both cases. A significant age-gender interaction was found in (a). PEI is smaller using the free fitting method than setting P_{∞}=19 mmHg. Percentage ratios between the values in (a) and (b) are reported in the table (c).

5.3.2 Changes of reservoir and excess velocity with age and gender

Examples of velocity separation into the U_r and U_e components are shown in **Figure 5.14** for the two algorithm used to calculate P_r. A strong positive correlation was found between the volume (V), estimated as the area under the carotid flow curve, and $U_r$peak (**Figure 5.15**), but not with Upeak and $U_e$peak with both techniques.

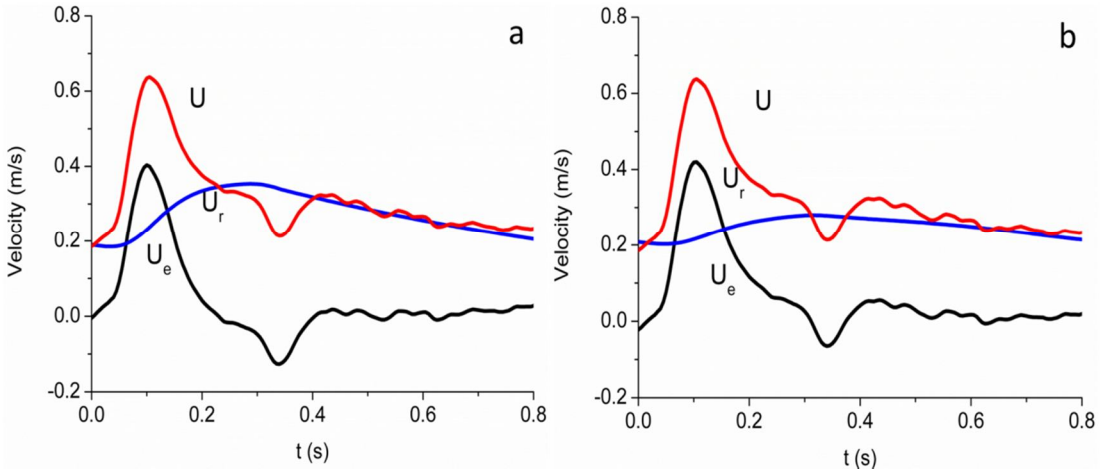

Figure 5.14: Examples of velocity waveform (U, red) separated into reservoir (U_r, blue) and excess (U_e, black) components using the free fitting algorithm (a) and setting P_∞=19 mmHg.

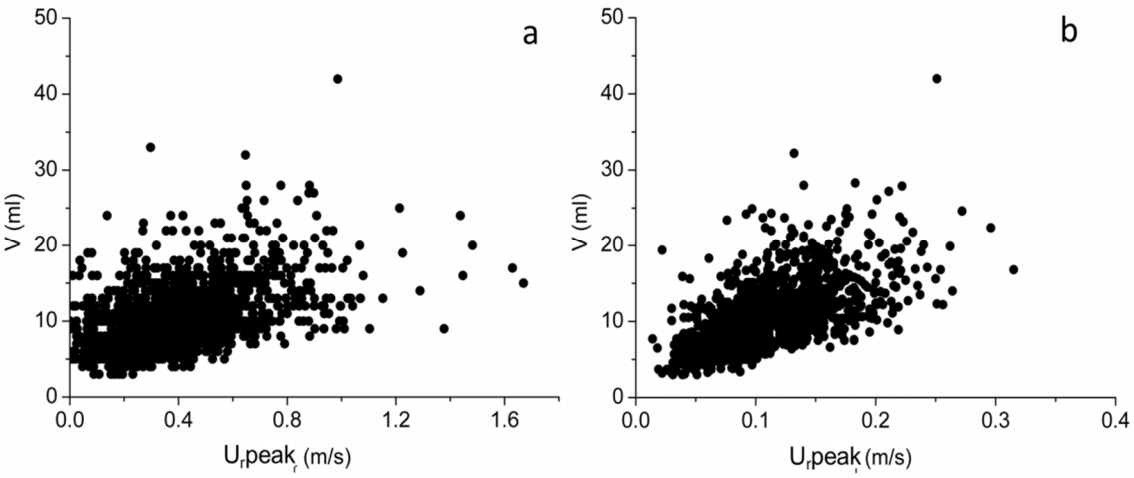

Figure 5.15: Relationship between volume and reservoir peak velocity using the free fitting algorithm (a) and fixing P_∞ (b). The Pearson correlation coefficient is 0.479 for (a) and 0.636 for (b). p values are <0.001 in both cases.

Figure 5.16 shows the changes of $U_r$peak with age and gender. A significant increase of this parameter with age was found only using the free fitting method ($p<0.001$). No difference with gender was found in both cases. $U_r$peak calculated using the free fitting algorithm is much higher than that calculated fixing the value of the asymptotic pressure. This is due to the fact that the determination of U_r depends on $\overline{R}$ that depends on P_∞. As previously discussed, generally, P_∞ determined by the free fitting algorithm leads to values that appear non-physiological because too high (Vermeersch et al. 2009). The $U_e$peak trend is similar to the Upeak in both cases with a significant decrease with age ($p<0.001$) and significant difference between male and female ($p<0.001$, higher in male than female) (**Figure 5.17**). As expected the values of $U_e$peak are different using the different techniques to determine P_r, being higher when P_∞=19 mmHg.

5.3.3 Time constant decay (τ)

The time constant decay decreases significantly with age and is different between male and female (higher in male than female) in both analyses (**Figure 5.18**). As expected, τ is different in the two techniques because it is affected by P_∞. Using the free fitting algorithm τ is smaller than that calculated setting P_∞; the time to reach a plateau is shorter using the free fitting method since the asymptotic pressure is higher. A strong negative relationship was found between τ and the parameter related to the excess pressure component, $P_e$peak and PEI, but only in the analysis where P_∞ is set to 19 mmHg (**Figure 5.19**).

5.3.4 Changes of wave speed and intensities with age and gender

Wave speed (c_{ee}), calculated using the pressure and velocity components due to the waves (P_e and U_e), is shown in **Figure 5.20** as function of age and gender. c_{ee} increases significantly with age only using the free fitting algorithm ($p=0.01$) and there is no difference between males and females in both cases. c_{ee} calculated using the free fitting algorithm is slightly smaller than c_{ee} calculated setting P_∞=19 mmHg, the average ratio between the two wave speeds is 90% (**Figure 5.20c**).

The intensity of the forward compression wave (FCW) decreases significantly with age and is higher in males than females in both cases (**Figure 5.21**). Using the free fitting algorithm intensity values are smaller than setting P_∞. Whilst, the intensity of the

backward compression wave (BCW) does not change significantly with age and gender in both cases (**Figure 5.22**).

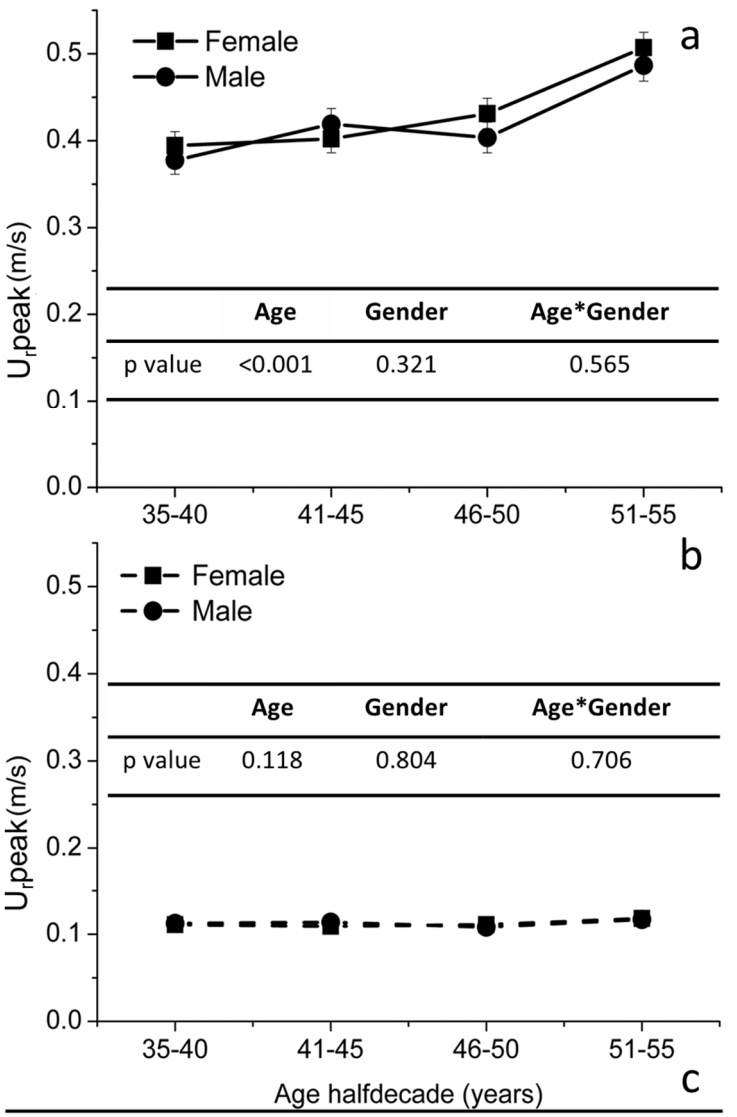

	35-40	40-45	45-50	50-55
Female	355%	369%	389%	430%
Male	366%	368%	373%	417%

Figure 5.16: Changes of reservoir peak velocity ($U_r$peak) in the carotid artery with age and gender using the free fitting algorithm (a) and setting the P_∞=19 mmHg (b). $U_r$peak increases significantly with age only in (a). $U_r$peak is higher using the free fitting method than setting P_∞=19 mmHg. Percentage ratios between the values in (a) and (b) are reported in the table (c).

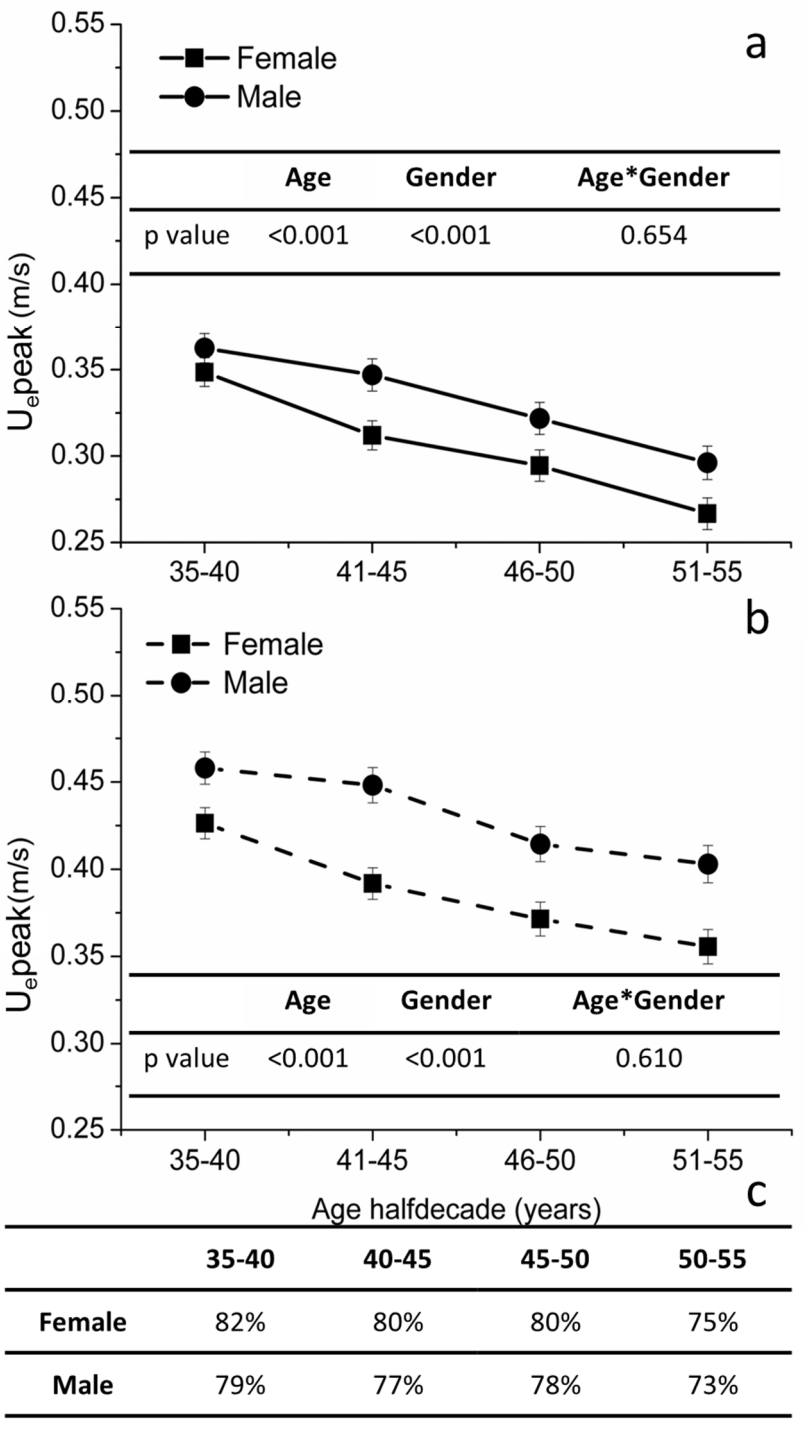

	35-40	40-45	45-50	50-55
Female	82%	80%	80%	75%
Male	79%	77%	78%	73%

Figure 5.17: Changes of excess peak velocity ($U_e$peak) in the carotid artery with age and gender using the free fitting algorithm (a) and setting P_∞=19 mmHg (b). $U_e$peak decreases significantly with age and is higher in maleS compare to femaleS in both cases. $U_e$peak is higher using the free fitting method than setting P_∞=19 mmHg. Percentage ratios between the values in (a) and (b) are reported in the table (c).

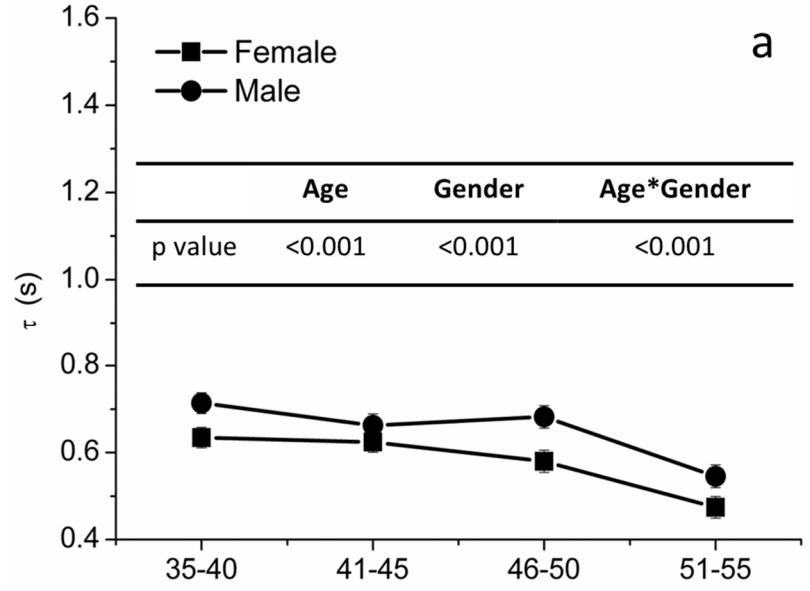

	35-40	40-45	45-50	50-55
Female	50%	50%	47%	41%
Male	54%	50%	53%	42%

Figure 5.18: Changes of τ in the carotid artery with age and gender using the free fitting algorithm (a) and setting P_∞=19 mmHg (b). τ decreases significantly with age and is higher in males than females in both cases. Also a significant age-gender interaction was found. τ is smaller using the free fitting method than setting P_∞=19 mmHg. Percentage ratios between the values in (a) and (b) are reported in the table (c). τ was adjusted for diastolic pressure P_d.

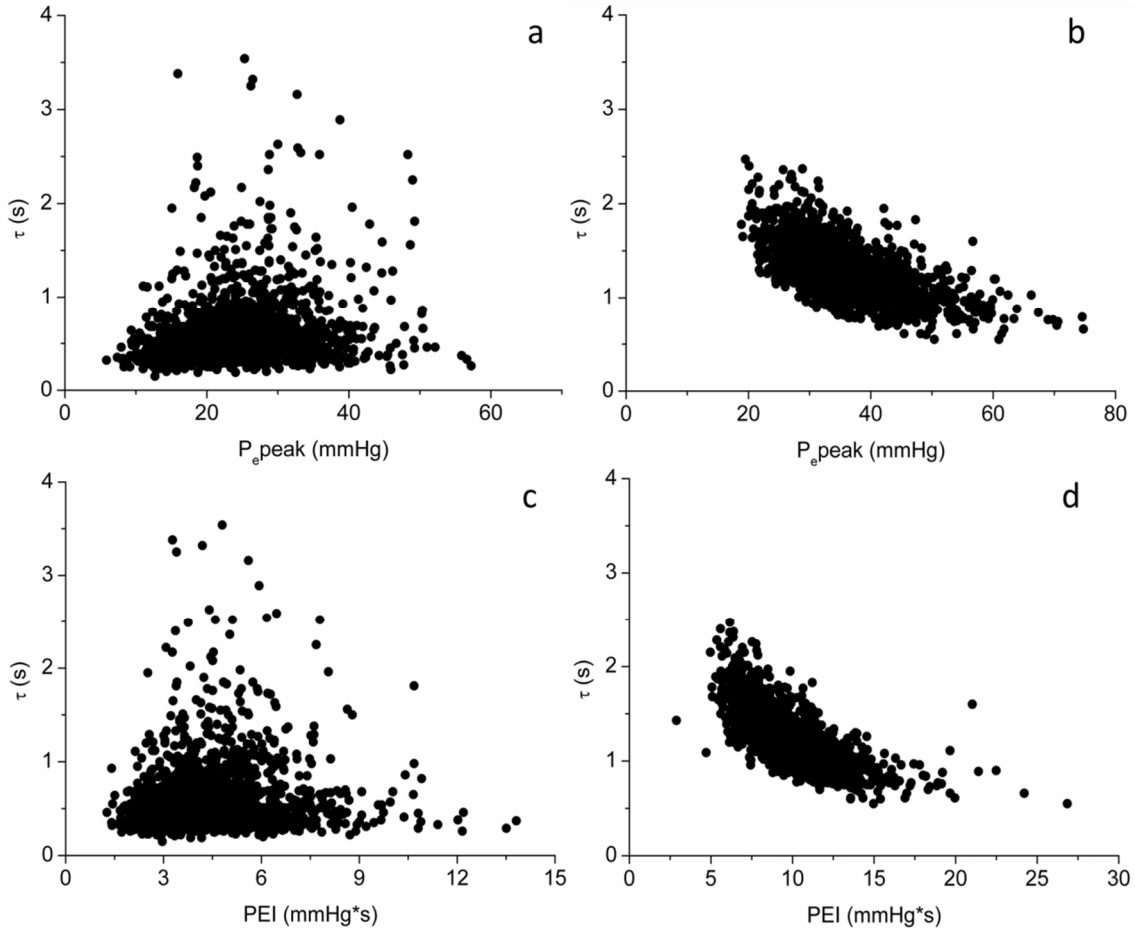

Figure 5.19: Relationship between τ and the $P_e$peak using the free fitting algorithm (a) and fixing P_∞ (b). Relationship between τ and PEI using the free fitting algorithm (c) and fixing P_∞ (d). A strong negative correlation was found only when a value for the asymptotic pressure was set. The Pearson correlation coefficient is -0.712 for (b) and -0.623 for (d). p values are <0.001 in both cases.

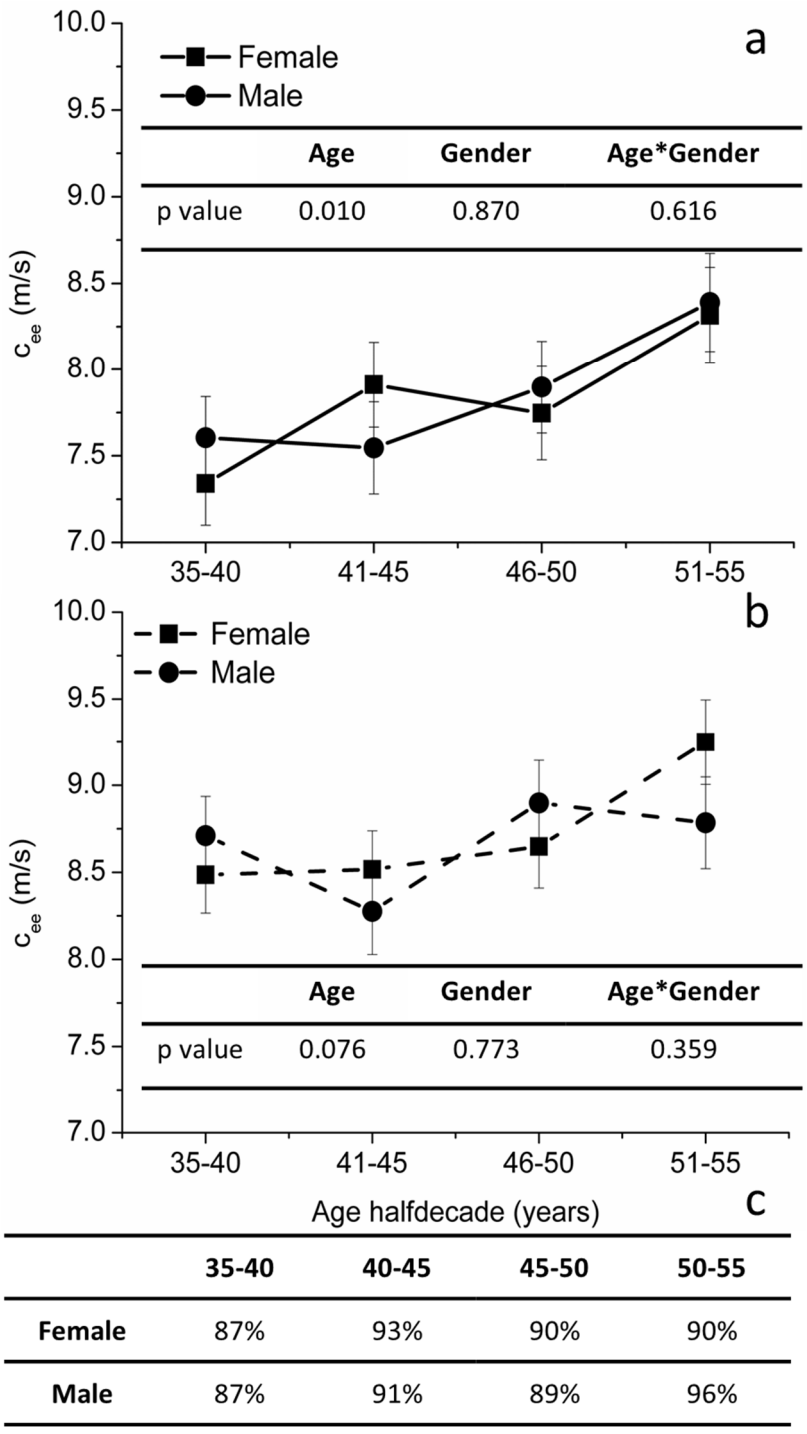

	35-40	40-45	45-50	50-55
Female	87%	93%	90%	90%
Male	87%	91%	89%	96%

Figure 5.20: Changes of wave speed (c_{ee}) in the carotid artery with age and gender using the free fitting algorithm (a) and setting P_{∞}=19 mmHg (b). c_{ee} increases significantly with age only in (a). c_{ee} is smaller using the free fitting method than setting P_{∞}=19 mmHg. Percentage ratios between the values in (a) and (b) are reported in the table (c). c_{ee} was adjusted for mean arterial pressure MAP.

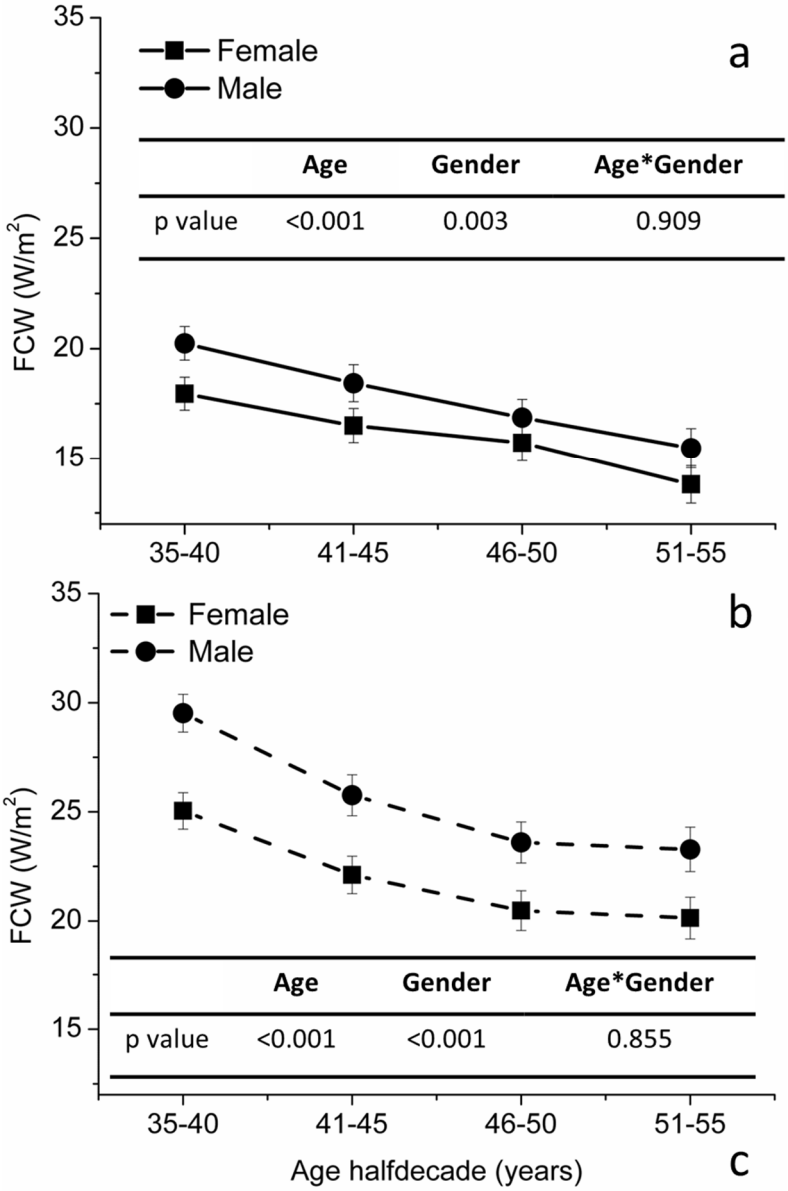

	35-40	40-45	45-50	50-55
Female	72%	75%	77%	69%
Male	69%	72%	71%	66%

Figure 5.21: Changes of the intensity of the forward compression wave (FCW) in the carotid artery with age and gender using the free fitting algorithm (a) and setting P_∞=19 mmHg (b). FCW decreases significantly with age and is significantly higher in male than female in both cases. FCW is smaller using the free fitting method than setting P_∞=19 mmHg. Percentage ratios between the values in (a) and (b) are reported in the table (c). FCW was adjusted for mean arterial pressure MAP.

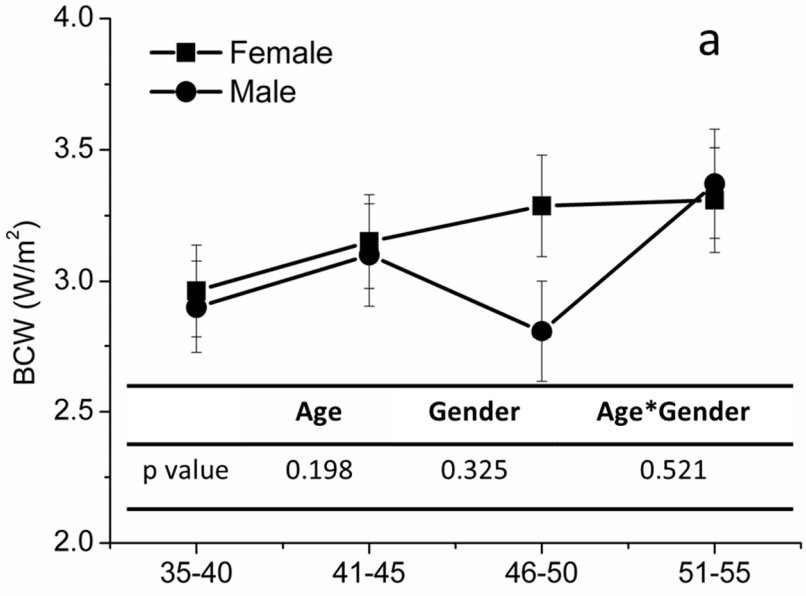

c

	35-40	40-45	45-50	50-55
Female	87%	97%	107%	117%
Male	81%	101%	92%	110%

Figure 5.22: Changes of the intensity of the backward compression wave (BCW) in the carotid artery with age and gender using the free fitting algorithm (a) and setting P_∞=19 mmHg (b). No significant differences were found with age and gender in both cases. Percentage ratios between the values in (a) and (b) are reported in the table (c). BCW was adjusted for mean arterial pressure MAP.

5.4 Discussion

In this chapter the hemodynamics of the carotid artery in healthy subjects was studied using the reservoir-wave approach and changes of excess/reservoir components with age and gender were investigated. The findings presented in chapter 4 showed that carotid artery is affected by the ageing process also in healthy subjects. The results reported in this chapter confirm the previous findings; most of the hemodynamic parameters studied here change significantly with age. Reservoir pressure parameters, $P_r$peak and PP_r, significantly increase with age (particularly in women) following the trend of Ppeak and PP. The same result was found in the same population setting the asymptotic pressure to 0 mmHg and considering the carotid pressure waveform a surrogate of the central pressure waveform (Vermeersch et al. 2009). Also PRI increases significantly with age both in males and females. All the reservoir parameters are significantly higher in males than females. $P_e$peak significantly changes with age only in the analysis where the asymptotic pressure was set to a fixed value. In this case, it seems to increase in females and decrease in males. No differences between men and women were found in both cases. PEI increases significantly with age and is higher in women than men. This is an important hemodynamic parameter since it has been found to be a marker of cardiovascular events in hypertensive treated subjects (Davies et al. 2010b).

Recently the changes of reservoir and excess central pressure with age of 43 asymptomatic subjects aged 20-69 years old were reported (Bia et al. 2011). The ascending aortic pressure was derived from the radial pulse, measured by applanation tonometry, using a transfer function. The authors divided the population in age decades and found that the maximum of the reservoir pressure increases almost linearly with age. From the decade 30-39 years old to the 50-59 one it increases around 12 mmHg. Averaging the mean value for men and women in the first and last half-age decade of the population studied in this chapter the increase is around 9 mmHg in both analyses. They found a significant increase of the maximum of the excess pressure only in the last age decade (60-69 years), and it is almost constant from the 30-39 to the 50-59 years old age decade. Also Davies et al. (Davies et al. 2010a) reported an increase of reservoir pressure in 18 patients scheduled for coronary angiography (averaged age 54±10 years old). Further, it found that maximum excess pressure is statistically higher in male than female and that the maximum of reservoir pressure is not different between men and

women in a population of 22 asymptomatic subjects (averaged aged 20 years old) (Cymberknop et al. 2011). On the contrary, the analysis reported here showed that differences in gender are statistically significant in the reservoir but not in the excess component.

The use of the algorithm applied allows also for the separation of the velocity in its component due to the elasticity of the large vessels (reservoir velocity) and that due to the travelling wave (excess velocity). Aguado-Sierra et al. (Aguado-Sierra et al. 2008b) have already separated the velocity waveforms in the carotid artery, but the number of subjects used in the study (8 subjects) was too small to investigate the changes of this parameters with age or gender and to assess any relationship with other hemodynamic parameters. In this study a full investigation of these parameters with age and gender is reported.

Upeak and $U_e$peak decrease with age in both male and female and are significantly higher in male. $U_r$peak increases significantly with age but only using the algorithm of free fitting P_∞ and there is no difference in gender in both analyses. It was also found that there is a strong positive relation between the volume entering the carotid artery, estimated as the area under the flow curve, and $U_r$peak. This is an important finding since the physical meaning of the reservoir and excess components is still not fully understood. This relationship indicates that the reservoir velocity is related to the buffering capacity of the elastic vessels.

The time constant decay, τ, was also studied in relation with age and gender. It was found that it is strongly affected by the ageing process; in particular it decreases significantly with age. τ is equal to RC and decreases because the compliance of the vessel decreases with age, since R, estimated as the mean pressure over mean flow, does not change significantly with age (**Figure 5.23**). τ was found to be different between males and females (higher in males than females). The time constant decay is negatively related to the excess pressure parameters, $P_e$peak and PEI, but only in the analysis where P_∞ was fixed. This is a surprising finding since τ is related to the diastolic part of the cycle, while the excess pressure has a larger contribution in the systolic part. Moreover, τ depends on global resistance and compliance whilst it is believed that P_e is stronger related to the local property of the vessel.

In this chapter, also the changes of wave speed and intensity determined using the pressure and velocity components due to the waves were investigated for the first time

as function of age and gender. c_{ee} increases with age only using the free fitting algorithm and there is no significant difference between males and females in both cases. c_{ee} is almost double compared to the wave speed found in the same population using the lnDU-loop. Since a gold standard for the determination of the local wave speed in arteries has not been established yet, is not possible to say which calculation is more correct. It might be possible that in this particular case, the measurements of pressure, flow velocity and diameter were taken too close to a positive reflection site. This situation has been demonstrated, to lead to an overestimation of the real wave speed if calculated using the PU-loop (Li et al. 2011) and it might lead to an underestimation using the lnDU-loop.

The peak of the forward compression wave decreases significantly with age and is higher in males than females. This finding may be related to a decrease of ventricular contractility with age. The peak of the backward compression wave seems not to be affected by the ageing process.

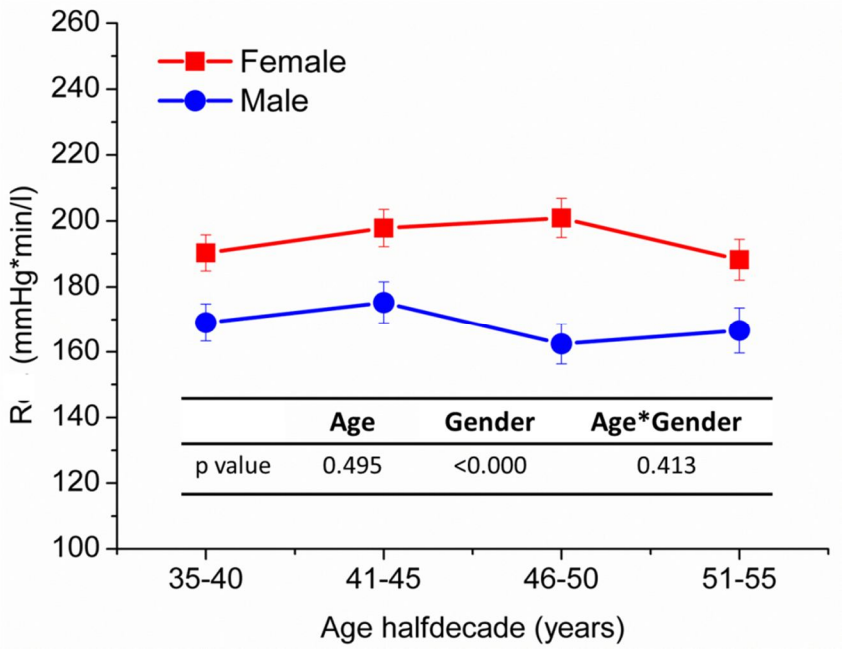

Figure 5.23: Changes of resistance (R) with age and gender. R is significantly higher in male than female, but it does not change significantly with age.

In this chapter the same data were analysed using two different methods to calculate P_r. One method is based on the free fitting of the asymptotic pressure, P_{∞}, from the diastolic decay of the measured pressure. This method, as previously reported by

Vermeersch et al., leads to high value of P_∞ in the specific case of this population (Vermeersch et al. 2009). The reason for this is unknown but it can be related to the technique used to derive the carotid pressure from the brachial pressure or to the fact that the diastolic decay is too short and the fitting is not precise. Wang et al. (Wang et al. 2003) found a P_∞ around 35 mmHg using a free fitting algorithm to derive P_r in dogs when a long beat was generated.

Many studies were carried out in animals (Guyton et al. 1954; Drees & Rothe 1974; Samar & Coleman 1978; Yamamoto et al. 1980; Sylvester et al. 1981; Versprille et al. 1985) to find the mean circulatory filling pressure that is, according to Guyton, "the pressure that would be measured at all points in the entire circulatory system if the heart were stopped suddenly and the blood were redistributed instantaneously in such a manner that all pressures were equal" (Guyton et al. 1954). The average value found from these studies was 8 mmHg, but in most of these cases the arterial and the venous pressure were forced to equilibrium after the heart stopped pumping. More recent studies in humans have shown that the arterial and the venous pressure do not reach the same value even after 20 s (Schipke et al. 2003; Jellinek et al. 2000). The pressure of the arterial side is higher than the venous side. The average of the values found in these two works was used as P_∞ in the second analysis performed in this chapter.

Generally, the trends and the changes with age and gender were not affected by the choice of the algorithm used (apart from P_e and U_r), but the averaged absolute values were largely dependent on P_∞. P_r was larger using the free fitting method and peak of P_e was smaller resulting in higher $P_r$peak, PP_r, PRI and smaller $P_e$peak and PEI. The reservoir and excess components of the measured velocity were greatly affected by P_∞ because their determination depends on the resistance that was calculated using the asymptotic pressure. Using the free fitting algorithm U_r is much higher than that calculated fixing P_∞ and in some cases the peak of this velocity was higher than the measured velocity peak.

Also τ was affected by the choice of the analysis. In particular, the average values were almost half when P_∞ was free fitted. That means that the arterial pressure reaches an asymptotic value earlier compared to the method were P_∞ was set to 19 mmHg. This result was expected since free fitting P_∞ leads, on average, to values higher than 19 mmHg.

5.5 Conclusion

In this chapter the hemodynamic of the carotid artery in healthy was studied using the reservoir-wave approach. Here for the first time, both pressure and velocity were separated in their reservoir and excess components and their changes with age and gender were investigated. Most of the hemodynamic parameters related to pressure and velocity studied here are affected by the ageing process, confirming the results presented in chapter 4 where the non-invasive technique was applied to the same population.

A strong positive relationship was found between the volume entering the carotid artery and the velocity component due to the buffering capacity of vessels and a strong negative relationship between the constant decay and pressure component due to the waves.

A free fitting algorithm to estimate P_∞ and another algorithm where P_∞ was set to a certain value were tested here. The results of the two techniques are different mostly in the absolute values, but the pattern of changes with age and gender are very similar.

The reservoir-wave approach can be used also at arbitrary location of the arterial system to describe the local hemodynamic of the vessel. Here the study was performed in a healthy population of subjects included in a relatively narrow age range; a comparison of these parameters in an older or pathological population would be interesting in order to investigate potential markers of cardiovascular diseases that can be used to detect the pathology earlier.

Chapter 6 : Reservoir and excess pressure changes with vascular compliance and stroke volume

6.1 Introduction

As mentioned in chapter 1, the main aim of this chapter is to study the reservoir (P_r) and excess (P_e) pressure components of the measured aortic pressure and their respective changes with compliance and stroke volume in a mock circulatory system (MCS).

As previously discussed, the concept of a reservoir pressure due to the buffering effect of the aorta and an excess pressure due to the traveling waves, is relatively new and needs further investigation. Recent studies have shown that the pulse pressure is predominantly due to Windkessel properties (Wang et al. 2003, Mohiuddin et al. 2012) and that reservoir pressure increases with age (Davies et al. 2010a, Vermeersch et al. 2009) because of the increasing stiffness of the aorta with age. Davies et al. also found that the reservoir pressure is the main determinant of the Augmentation Index (AIx) and they have also reported that the integral of the excess pressure is a good predictor of cardiovascular events in a population of treated hypertensive patients (Davies et al. 2010b). The clinical and physiological relevance of P_r and P_e is not yet fully understood. It would be useful from a clinical point of view to relate these parameters with particular pathological hemodynamic conditions, in order to use them as screening or diagnostic parameters.

For this purpose, the aim of this work is to study the effect of aortic compliance and stroke volume on P, P_r and P_e. Aortic compliance is related to physiological (age) and pathological (such as hypertension, atherosclerosis and arterial wall diseases) events and stroke volume is related to left ventricle contractility. Both, compliance and stroke volume are believed to be related to P_r since it is determined by the Windkessel capacity of the aorta and it is related to the volume "trapped" in the aorta that depends on the volume ejected. P_e can be affected by the arterial stiffness as well since a change in the mechanical properties of the vessel is going to affect the wave speed of pressure and

flow waveforms. The way P_r and P_e are affected by the aortic compliance and the stroke volume has not been investigated before.

This study was carried out in a MCS that includes a vascular system and a pumping system that simulates the pumping action of the heart. A similar MCS was previously designed and tested by Kolyva et al. (Kolyva et al. 2012) to be used with the intra-aortic balloon pump; in this work the same MCS was modified in order to suit the purpose of the experiments. The use of a MCS rather than *in vivo* experiments allows for a selective control of the variation of aortic compliance and stroke volume resulting in changes of these variables that are almost independent of each other.

6.2 Material and Methods

6.2.1 Mock circulatory system (MCS)

The MCS is composed of two main units (**Figure 6.1**):

1) The vascular system that includes: the artificial aorta with its main branches, the capillary system (that act as resistances) and the venous return;

2) The pumping system, which includes the left ventricle assist device (LVAD), a stepper motor and a control unit.

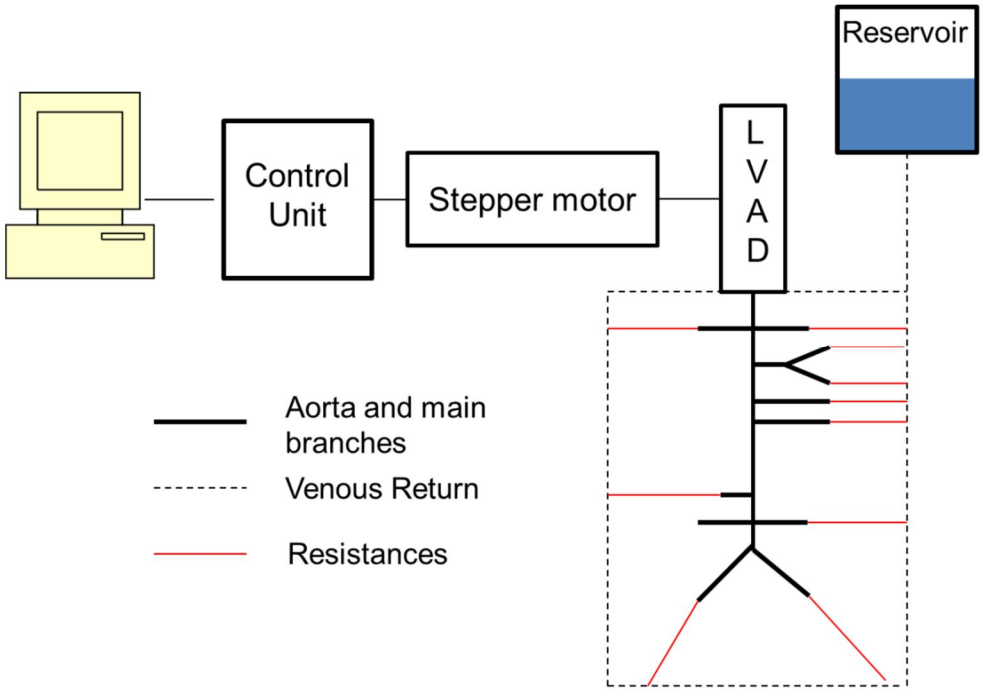

Figure 6.1: Schematic representation of the experimental set-up.

The LVAD was connected respectively to the piston pump through the ventricular connection, to the reservoir by means of the atrial connection and to the

aorta through the aortic valve (**Figure 6.1**). Each branch of the aorta was fitted with the corresponding resistance tube and then to a drainage tube acting as a venous return, which was joined to the overhead reservoir (**Figure 6.2**). All experiments were carried out at room temperature (about 20ºC) and water was used as test fluid. The same artificial aorta was used in all the experiments and its mechanical properties were changed by wrapping it in different ways using different materials. The stroke volume was varied by setting different profiles in the software that controls the LVAD.

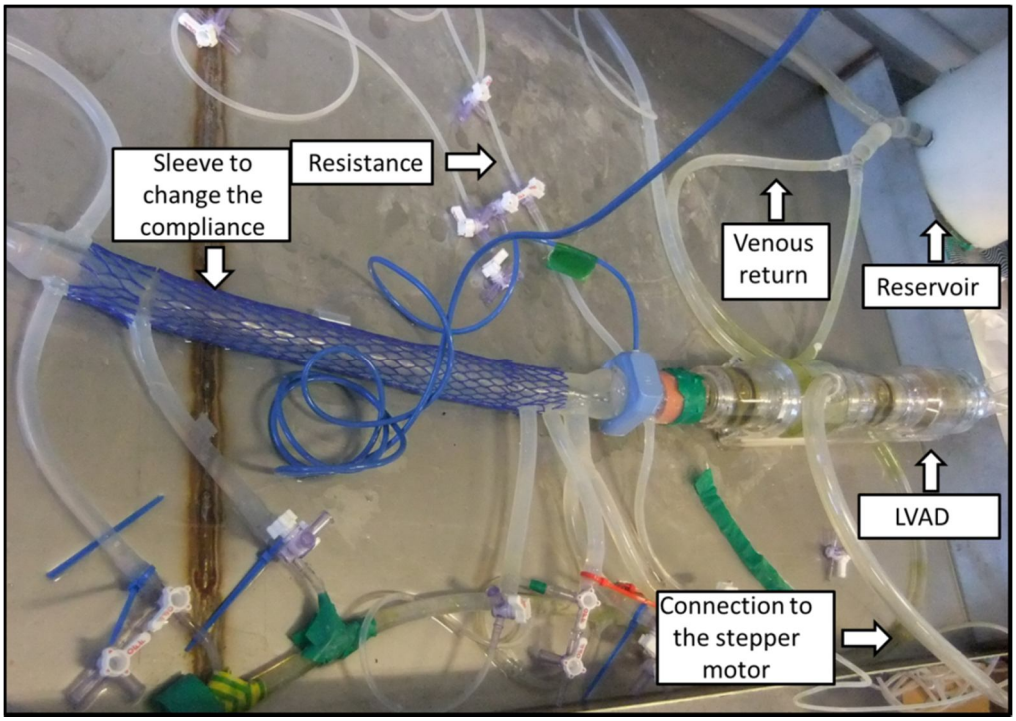

Figure 6.2: Experimental set-up. The artificial aorta is connected to the LVAD and each branch is connected to a capillary tube that acts as terminal resistance. Capillary tubes are connected to the venous return that is joined to the reservoir. The LVAD was connected to the stepper motor with a plastic tube.

6.2.1.1 Artificial aorta

The aorta model used in these experiments is a 1:1 replica of the human aorta and its main branches: left and right coronary arteries; innominate artery bifurcating to the right subclavian and right carotid arteries; left carotid artery; left subclavian artery; celiac artery; left and right renal arteries; aorto-iliac bifurcation leading to left and right iliac arteries. A schematic representation of the model is shown in **Figure 6.3**. In **Table 6.1** dimensions of the aorta and its main branches are given.

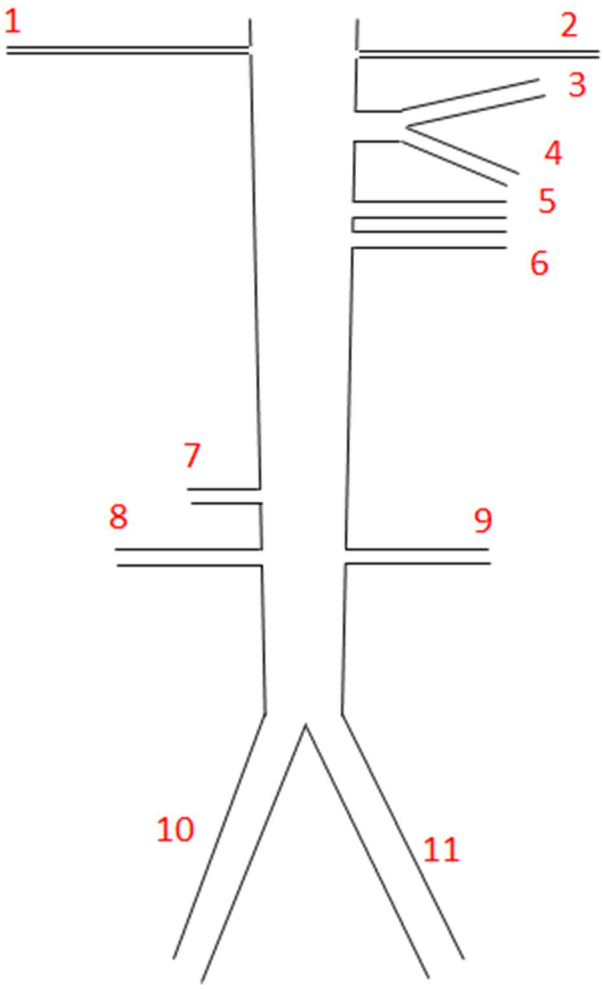

Figure 6.3: Schematic representation of the artificial aorta. Arterial segments: (1) right coronary, (2) left coronary, (3) right subclavian, (4) right carotid, (5) left subclavian, (6) left subclavian, (7) celiac, (8) right renal, (9) left renal, (10) right iliac, (11) left iliac.

6.2.1.2 Resistances and compliances

In order to reproduce the physiological distribution of flow in the artificial aorta, resistances and compliances were implemented in the model. Distribution of resistances and compliances used in this chapter are mainly based on Kolyva's work (Kolyva et al. 2012) that refers to the Stergiopolous model (Stergiopulos et al. 1992).

Total resistance is the sum of a proximal and a terminal resistance. The geometry of the aorta model accounts for the proximal resistance and the capillary tubes connected to the main branches and the venous return account for the terminal resistances reported by Stergiopolous (Stergiopulos et al. 1992). According to Kolyva et al. (Kolyva et al. 2012) the proximal resistance is three orders of magnitude smaller than the terminal one. For this reason total resistance was considered equal to the

terminal one. The same dimensions of capillary tubes calculated in Kolyva's were used in these experiments (Kolyva et al. 2012).

Table 6.1: Dimensions of the arterial segments.

Vessel	Number	Internal Diameter (mm)	Wall Thickness (mm)	Length (cm)
Outflow tract	1	30	1.63	2.0
Coronary artery	2	4	0.05	25.0
Ascending aorta	1	30	1.63	4.0
Arch 1	1	23	1.32	6.3
Innominate artery	1	12	0.86	23.4
Left carotid artery	1	8	0.63	25.9
Left subclavian	1	8	0.67	23.4
Arch 2	1	22	1.27	4.9
Thoracic aorta	1	20	1.20	16.6
Celiac artery	1	8	0.64	12.0
Abdominal aorta 1	1	12	0.84	5.3
Renal artery	2	6	0.52	23.2
Abdominal aorta 2	1	10	0.82	10.4
Iliac artery	2	8	0.63	25.8

The total compliance of the system is also a sum of proximal and terminal (or distal) compliances. The value of proximal compliance is the compliance of the aorta and it gives the main contribution to the total compliance of the model. Distal compliances reported by Stergiopulos were reproduced in Kolyva's by means of trapped volume of air held in syringes. Since the aim of these experiments was to investigate the changes in reservoir and excess components by varying the aortic compliance and as it has been reported that distal compliances do not affect markedly the central waveforms they were not implemented in the system (Matthys et al. 2007). The compliance of the aorta was determined according to a method reported by Segers et al. (Segers et al. 1998). The details are reported in section 6.2.2.

6.2.1.3 The venous return and the reservoir

Each capillary tube was connected to a drainage tube acting as venous return as shown in **Figure 6.2**. An overhead reservoir was joined to the venous return and to the atrial chamber of the LVAD. The height of the water inside the reservoir was about 14 cm in order to provide an atrial pressure of about 10 mmHg.

6.2.1.4 The left ventricular assist device

A left ventricular assist device (LVAD) has been used in order to produce a pulsatile flow inside the mock circulatory system (Abiomed BVS 5000, Abiomed Inc, MA, USA). The LVAD consists of two chambers in series, the left atrium (LA) and the left ventricle (LV) and two valves, the mitral valve placed between LA and LV and the aortic valve that separates LV from the aortic root (**Figure 6.4**). During the experiments the LA was connected to the reservoir. The LV is a silicon sac which is filled and compressed by water from the LA and from the piston which is operated by a stepper motor driver, respectively. **Figure 6.5** illustrates the systolic and diastolic phases of the LVAD. The capacity of the LVAD is 100 ml, but preliminary tests have shown that the stability of the device at high stroke volume is compromised (Hunt 2012). For this reason in these experiments the stroke volume (V) was set to 30 ml, 40 ml, 50 ml and 60 ml.

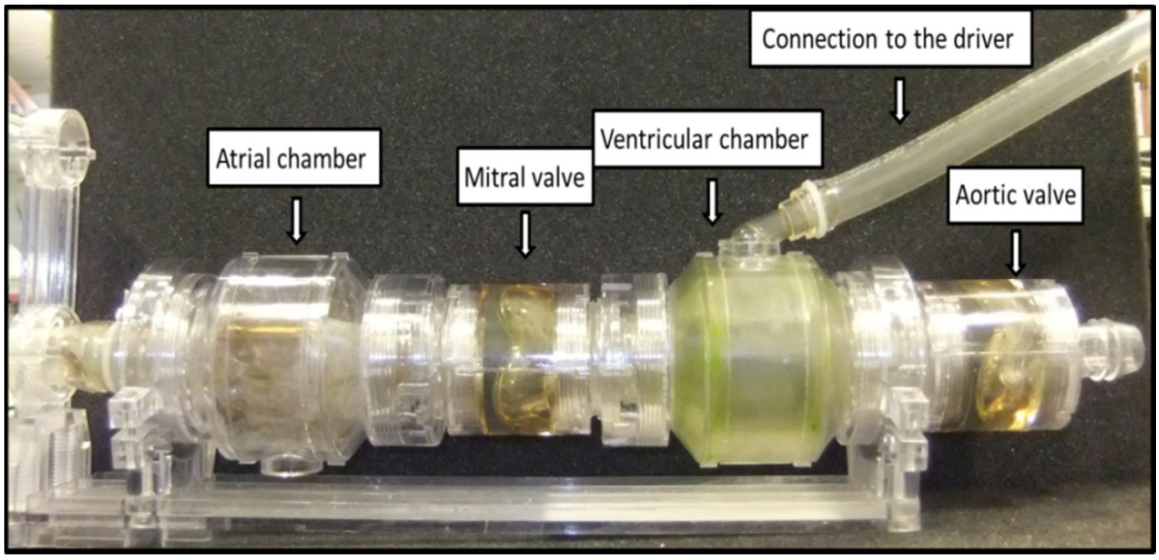

Figure 6.4: LVAD Abiomed BVS 5000.

6.2.1.5 The stepper motor driver and the control unit

An external stepper motor (Heart Pump Simulator, Placepower, Norfolk, UK) was connected to the LV in order to drive the LVAD. The motor is driven by a stepper drive, controlled from a PC using a dedicated software (Easitools, v 1.5, Parker Hannifin Corp, Dorset, UK). In **Figure 6.6** the heart simulator is shown together with the driver and the PC unit. Through the software it is possible to generate different flow profiles controlling V (related to the number of steps of the piston) and the timing of systole and diastole (varying the acceleration and deceleration of the piston movement).

An Excel spread sheet was provided with the driver for the calculation of the required pump performance. In these experiments four values of V were used and acceleration and deceleration values were changed in order to have a cardiac cycle of 1s and a ratio systole/total cycle of approximately 1/3.

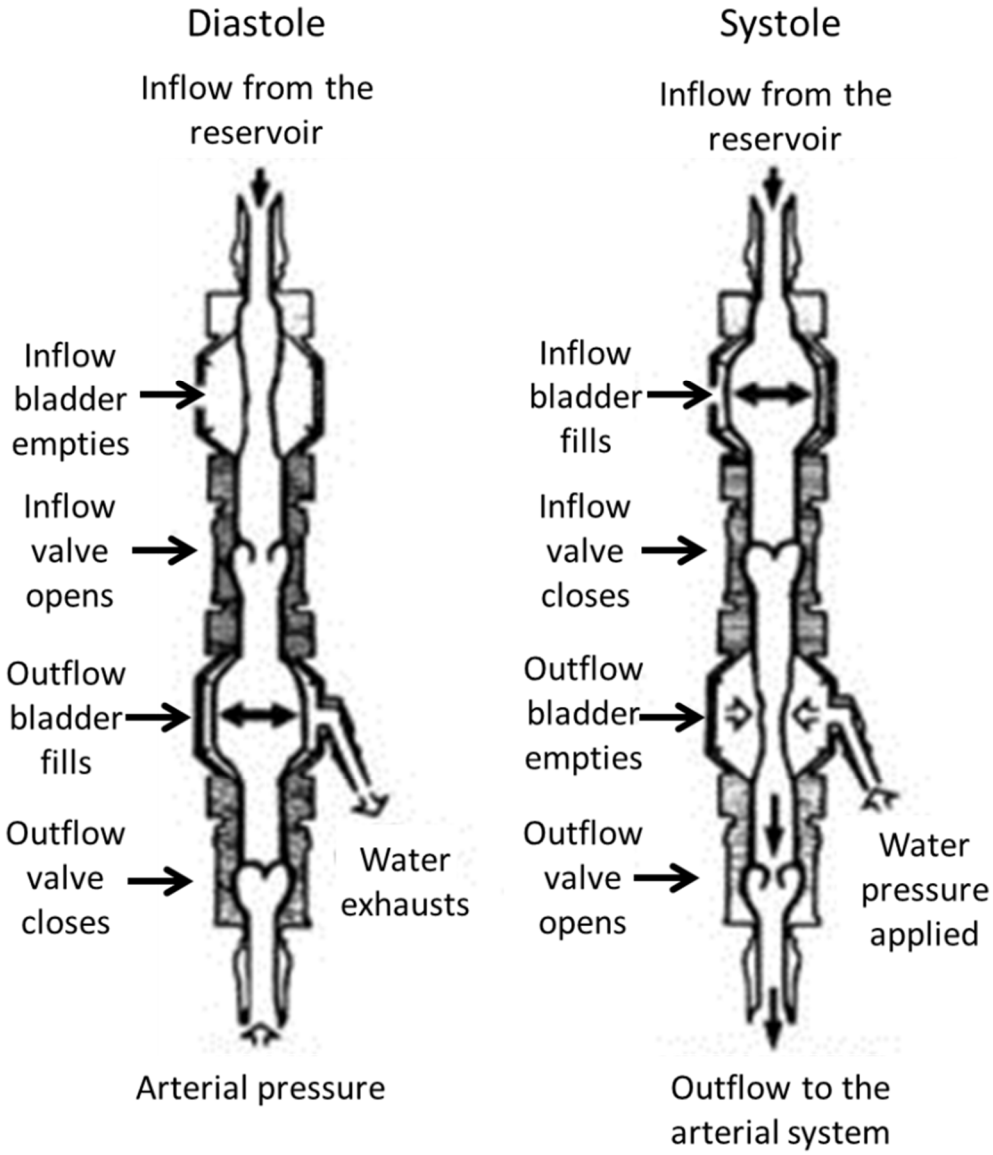

Figure 6.5: Schematic representation of the LVAD during diastolic and systolic phases. (Modified from Dowling & Etoch 2000)**.**

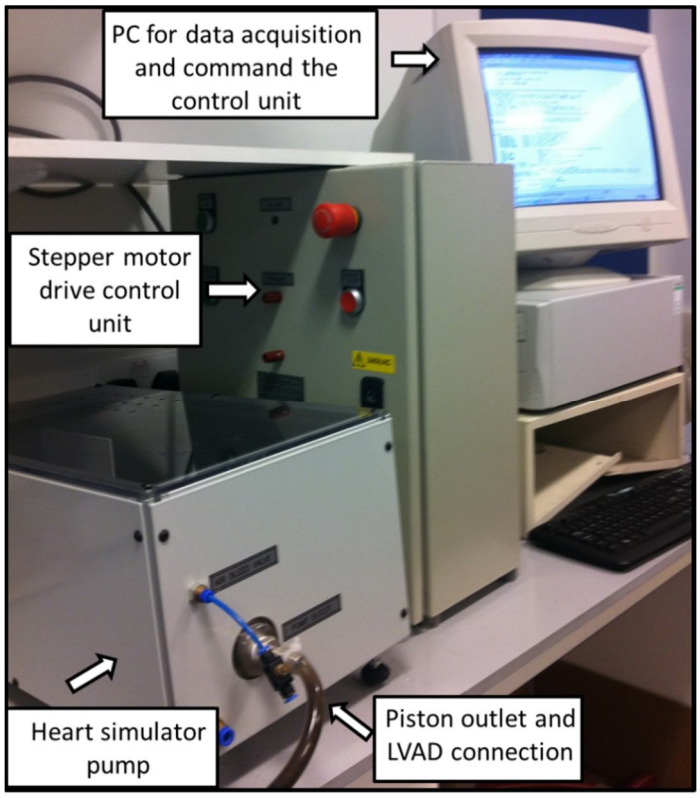

Figure 6.6: Heart Pump Simulator.

Table 6.2: Different preparations used for wrapping the aorta to provide different compliances.

Aorta Preparation	Wrapping
A1	1 plastic net sleeve
A2	2 plastic net sleeves
A3	3 plastic net sleeves
A4	1 plastic net sleeve + 1 fabric sleeve
A5	1 plastic net sleeve + clingfilm
A6	1 plastic net sleeve + tape

A1 is the aorta with the highest value of compliance and A6 the lowest. The aorta was wrapped also in the configuration of highest compliance because the value found for the aorta itself was too high for the aim of the experiments.

6.2.2 Determination of the static compliance (Cs)

In order to vary the aortic compliance, the main trunk of the aorta was wrapped in different ways using sleeves, clingfilm and tape as reported in **Table 6.2**. Six different aorta preparations corresponding to six different values of compliance were obtained (termed A1, A2, A3, A4, A5, A6 from the highest to the lowest compliance).

Compliance is defined as dV/dP (with dV variation of volume and dP variation of pressure). To determine the value of aortic static compliance (Cs) the aorta and the main branches were closed and filled with water. The volume was increased by injecting water in steps of 5 ml using a graduated syringe and was decreased by removing water also in steps of 5 ml.

An 8F transducer-tipped pressure catheter (Millar Instruments Inc., Houston, Texas, USA) was placed inside the aorta and at each step of increased/decreased volume the value of pressure was recorded. For each aorta preparation, the compliance was determined after the experiment in order to reach the pressure values recorded during the experiment. However, it was not always possible to determine the value of Cs in the same range of pressure obtained during the experiment in particular for the aorta with lower values of compliance.

Volume of water was plotted against pressure during the loading and unloading phase as shown in **Figure 6.7.** For the same aorta preparation, the pulse pressure at the aortic root was different for the four different stroke volumes ejected in the system and, as can be observed from **Figure 6.7**, the slope of the curves depends on the pressure range considered. In **Figure 6.7** the ranges of pressure at different volume are also shown. The procedure of loading and unloading was repeated at least three times for each aorta. Values of Cs for each stroke volume were determined by averaging the slopes of the loading and unloading curves in the range of pressure reached during the experiment (**Table 6.3**). It is possible to observe from the table that the values of Cs for the more compliant aorta (A1, A2, A3) are more affected by the pressure range selected to determine the slope and thus by the stroke volume compared to the stiffer aorta (A4, A5, A6). The ratio between the minimum and maximum values calculated for the same aorta preparation are 0.53, 0.60, 0.60, 0.81, 0.96 and 0.88 for A1, A2, A3, A4, A5 and A6, respectively. For A4, A5 and A6, the value of compliance was almost constant throughout the pressure range found in the experiment for each stroke volume. Cs was calculated in the same range of pressure for stroke volumes of 50 and 60 ml.

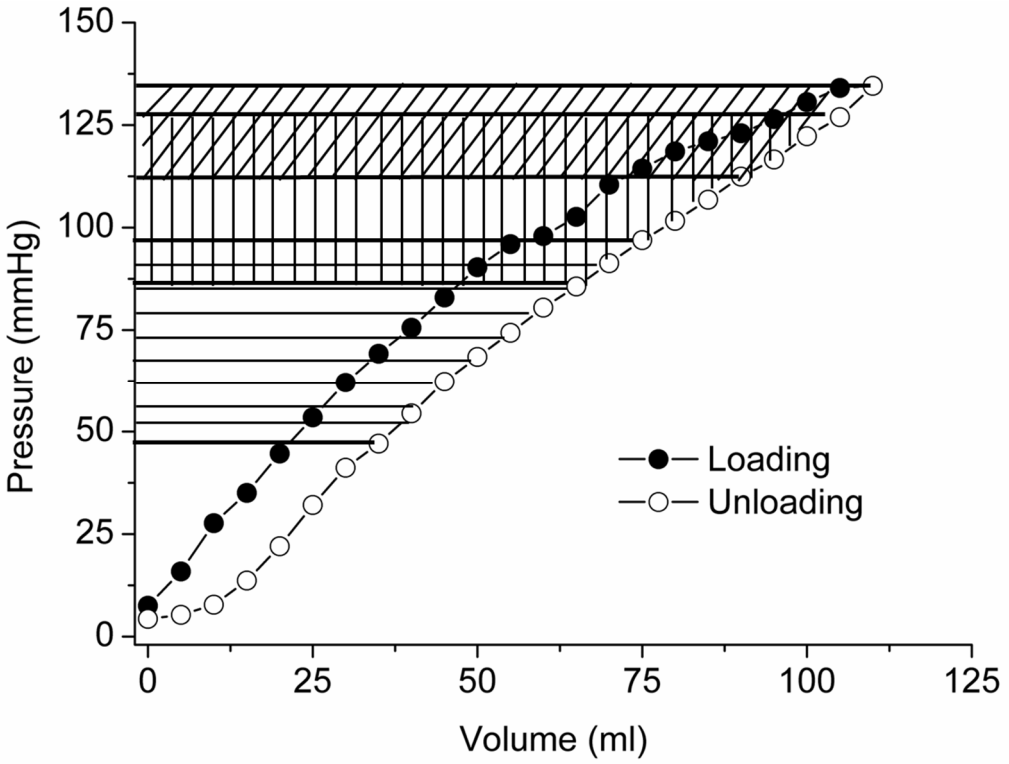

Figure 6.7: Example of calculation of aortic compliance in the third configuration (A3). A pressure-volume curve relating the change in volume and the change in pressure inside the aorta was obtained during the loading and unloading phases. The average of the slopes of linear fits over the loading and unloading curves in the pressure range 55-100 mmHg for 30 ml (horizontal stripes), 90-115 mmHg for 40 ml (vertical stripes) and above 115 mmHg (oblique stripes) for 50 and 60 ml yielded the values of C3. The hysteresis relates to the viscoelastic properties of the material of the aortic wall.

Table 6.3: Values of Cs for each aorta preparation (A1-A6) determined in the range of pressure obtained during the experiments for the different ejected volumes.

	Compliance (Cs)					
Volume (ml)	A1 (ml/mmHg)	A2 (ml/mmHg)	A3 (ml/mmHg)	A4 (ml/mmHg)	A5 (ml/mmHg)	A6 (ml/mmHg)
30	1.29±0.01	1.13±0.03	0.78±0.06	0.63±0.01	0.54±0.02	0.30±0.00
40	1.94±0.12	1.64±0.24	1.07±0.08	0.68±0.07	0.52±0.00	0.32±0.00
50	2.41±0.24	1.87±0.35	1.29±0.18	0.78±0.20	0.53±0.01	0.34±0.00
60	2.41±0.24	1.87±0.35	1.29±0.18	0.78±0.20	0.53±0.01	0.34±0.00

Values are mean ± SD. Cs was calculated by averaging the slopes of the loading and unloading curves in the range of pressure reached during the experiment. The procedure of loading and unloading was repeated at least three times for each aorta preparation.

6.2.3 Pressure and flow measurements

Pressure (P) and flow (Q) were measured at the same position at the aortic root as shown in **Figure 6.8**.

Pressure was measured with an 8F transducer-tipped pressure catheter (Millar Instruments Inc., Houston, Texas, USA) inserted from the iliac artery. The frequency response of the Millar catheter according to manufacturer specifications is: DC to 1000Hz (-3dB).

The pressure transducer was calibrated using the method of a vertical column of water. The transducer output in voltage was recorded after changing the level of water acting on the catheter inside the column. The range of pressure for the calibration was based on the pressure range expected during the experiment. The recorded voltages and applied pressures were plotted and the equation of the regression line relating these values was calculated (**Figure 6.9**). Pressure data during the calibration and the experiments were acquired at 500 Hz with Sonolab software (Sonometrics Corporation, London, Ontario, Canada).

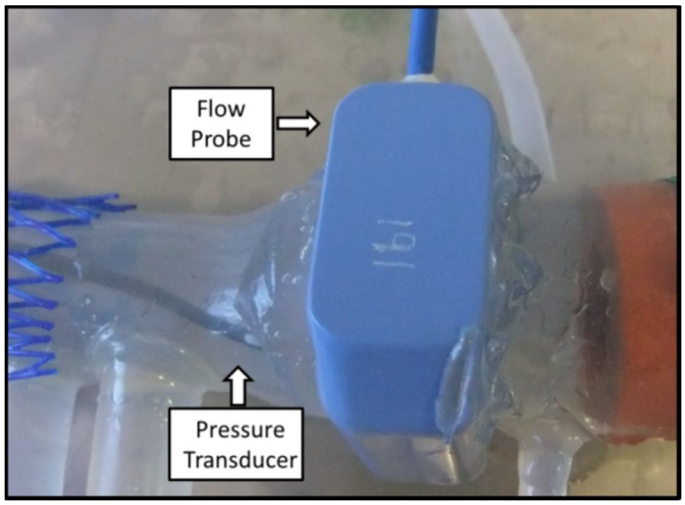

Figure 6.8: Flow probe and pressure catheter at the aortic root measuring P and Q.

Flow was measured with an ultrasonic flow probe 32 mm size (Transonic, Ithaca, NY, USA) placed at the aortic root.

The flow probe was calibrated on the aorta; the inlet of the aorta was connected to a pump that generates continuous flow which was varied using a tap valve placed on the circuit. The fluid was collected for a certain period of time from the venous return using a measuring cylinder whilst the flow measured with the flow probe was recorded.

Flow in voltage was plotted against flow in l/min and the linear regression line for conversion was obtained (**Figure 6.10**). Flow data during the calibration and the experiments were also acquired at 500 Hz with Sonolab sofware (Sonometrics Corporation, London, Ontario, Canada).

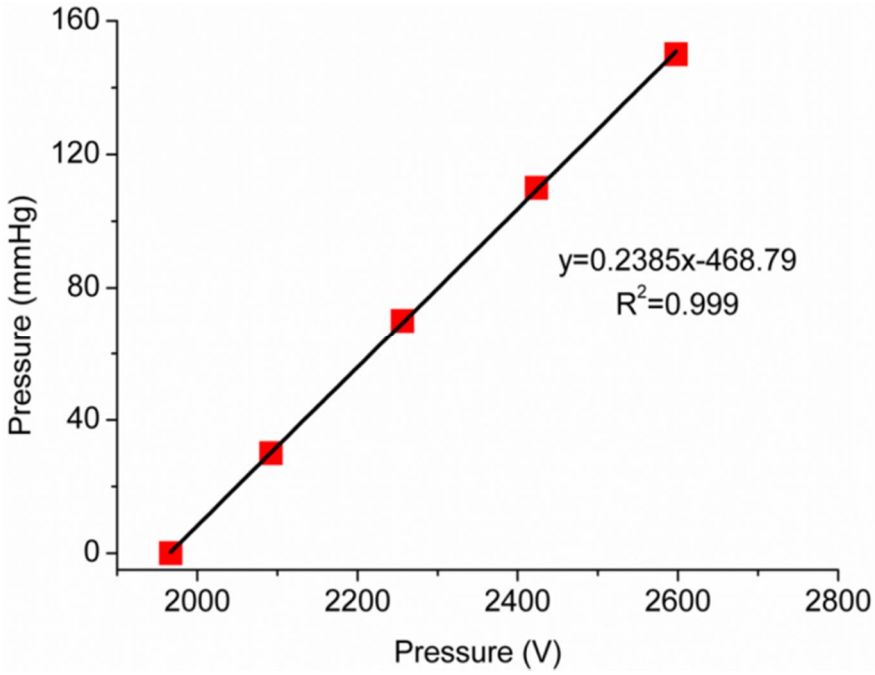

Figure 6.9: Example of the pressure transducer calibration regression line.

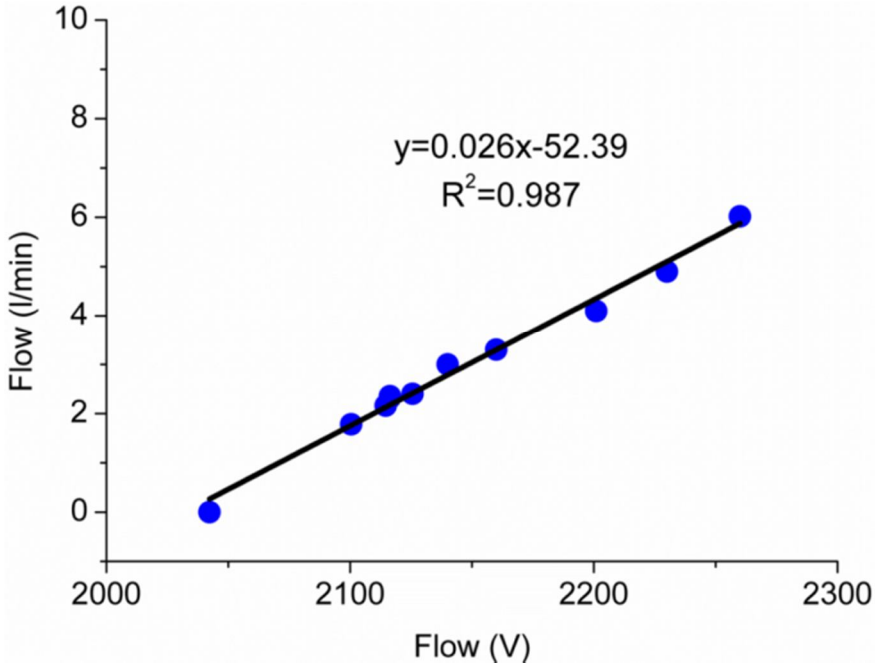

Figure 6.10: Example of the flow transducer calibration regression line.

6.2.4 Experimental procedures

The profiles corresponding to stroke volume of 30, 40, 50, 60 ml were consecutively set in the software that drives the control unit. For each V approximately 10 beats were recorded. After that, the aorta was disconnected from the LVAD, the branches were closed and the compliance was determined as described in section 6.2.2. For all the aorta preparations (A1-A6) the same procedure was followed. **Figure 6.11** shows the comparison of two pressure recordings at the same site to assess the reproducibility of the measurements.

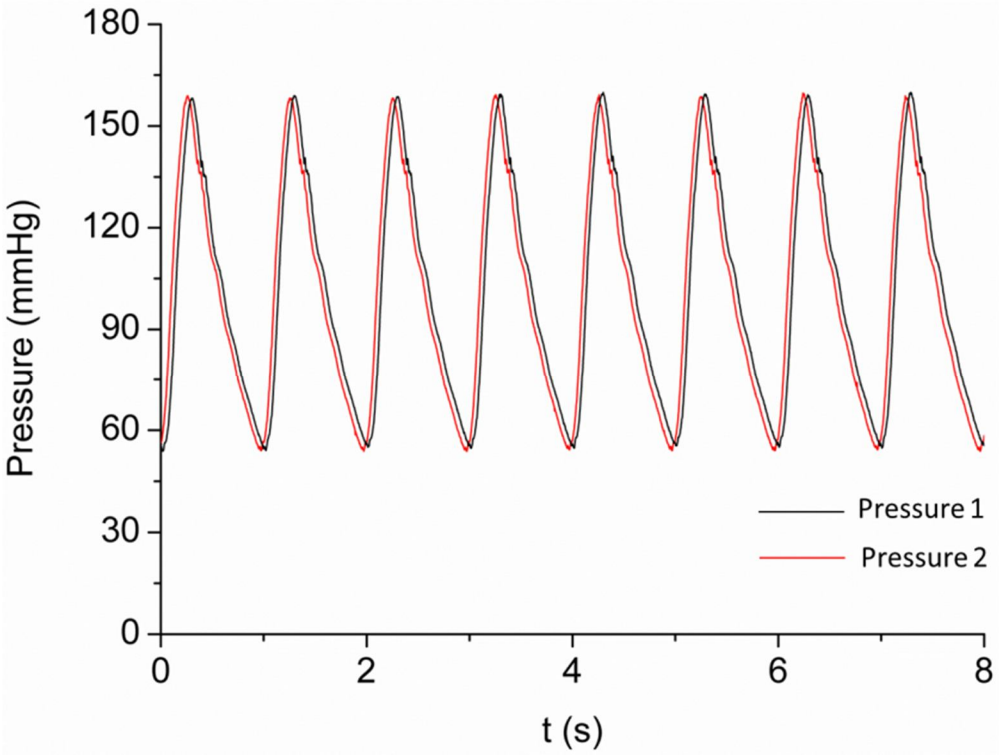

Figure 6.11: Comparison of two pressure measurements at the same site. The waveforms superimpose one another, giving confidence of good reproducibility of measurements.

6.2.5 Analysis

The recorded pressure and flow data were filtered in Matlab by means of a Savitzky-Golay filter and further processed with the same software. P_r was calculated from P as described in Aguado-Sierra et al. (Aguado-Sierra et al. 2008a). Thus, P_e was determined as $P-P_r$. The following parameters were calculated for all the experiment by averaging the values of three beats for each combination Cs-V:

- Ppeak – Maximum of P;
- $P_r$peak – Maximum of P_r;
- $P_e$peak – Maximum of P_e;
- P_d – Diastolic pressure;
- MAP – Mean arterial pressure, calculated as P_d+1/3(Ppeak-P_d) (Li et al. 2006);
- PP – Pulse pressure, calculated as Ppeak-P_d;
- PP_r – Pulse reservoir pressure, calculated as $P_r$peak-P_d;
- PP_r/PP – Ratio of pulse reservoir pressure over pulse pressure;
- P_{inf} – asymptotic pressure, calculated by fitting the diastolic part of the cycle (Aguado-Sierra et al. 2008a);
- τ – Time constant of the pressure exponential decay in diastole, calculated by fitting the diastolic part of the cycle (Aguado-Sierra et al. 2008a);
- c – Wave speed, calculated from the slope of the linear part of the PU-loop (where U is the velocity determined from Q) (Khir, Parker 2001);
- c_e – Wave speed, calculated from the slope of the linear part of the P_eU-loop, as determined in chapter 3;
- Cp – Dynamic compliance calculated as V/PP (Chemla et al. 1998);
- Cpr – Dynamic compliance calculated as V/PP_r.

6.2.5.1 Statistical analysis

The changes of the parameters reported in section 6.2.5 with Cs and V were investigated and the results are reported in section 6.3.2 and 6.3.3, respectively.. Values of Cs are the ones reported in **Table 6.3**. p values <0.05 were considered statistically significant. Note that changes in relation to Cs were plotted with the x-axis reversed (from A1 to A6) to show more intuitively the analogy of reduced compliance with age. In graphs and tables the mean values of three beats ± SD are reported. The experimental data were fitted with linear or exponential curves, based on highest R^2. In graphs the fitting is reported with its equation, its R^2 and the p value of the regression analysis.

6.3 Results

6.3.1 Static vs. dynamic compliance

The values of Cs were compared to the values of compliance estimated using dynamic methods: the stroke volume to pulse pressure ratio (Cp) and the stroke volume to pulse reservoir pressure ratio (Cp_r). In **Figure 6.12** the comparison between the three methods is reported for all the aorta configurations for each value of stroke volume. **Figure 6.12** shows that, at lower stroke volume (lower pressure range) the values of compliance are markedly smaller in the case of a more compliant (A1, A2, A3) aorta. That is due to the higher slope of the pressure-volume curve for high range of pressure (**Figure 6.7**). In **Table 6.4** the percentage difference between Cs and Cp and between Cs and Cp_r are reported. Considering that the volume/pulse pressure ratios are an estimation of the compliance in a single point, different results are expected.

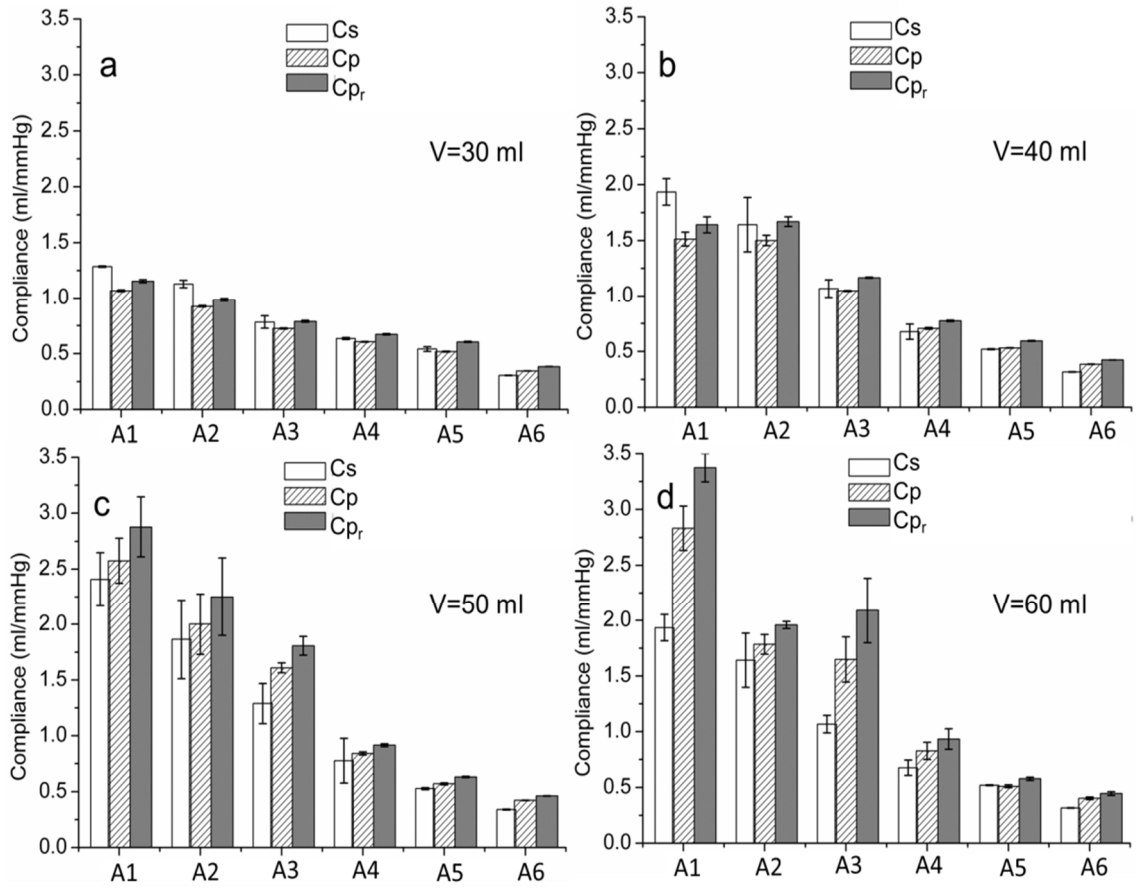

Figure 6.12: Comparison between Cs, Cp and Cp_r, for V=30 ml (a), V=40 ml (b), V=50 ml (c) and V=60 ml (d) for all the aorta preparations.

Table 6.4: Percentage differences between Cs, Cp and Cp_r.

Volume (ml)		A1	A2	A3	A4	A5	A6
30	Cp	17%	18%	7%	5%	4%	-13%
	Cp_r	10%	13%	-1%	-6%	-12%	-26%
40	Cp	22%	7%	2%	-4%	-2%	-22%
	Cp_r	15%	-2%	-9%	-15%	-15%	-34%
50	Cp	-7%	-7%	-25%	-8%	-8%	-24%
	Cp_r	-20%	-21%	-40%	-18%	-20%	-36%
60	Cp	-18%	4%	-28%	-7%	3%	-19%
	Cp_r	-40%	-5%	-62%	-20%	-10%	-31%

The percentage differences were calculated as (Cs-Cp)/Cs)*100 and (Cs-Cp_r)/Cs)*100.

6.3.2 Changes with compliance

6.3.2.1 Measured pressure (P)

Figure 6.13 shows typical measured pressure waveforms recorded at different aorta configurations for a stroke volume of 30 ml. Changes of systolic pressure (Ppeak) with compliances are reported in **Figure 6.14.** As expected, a significant linear increase of Ppeak with decreasing compliance was found (for all the stroke volume, $p<0.05$). In the figure also the linear fitting for each volume is reported. In **Figure 6.15** changes of diastolic pressure (P_d) with compliances are shown. Although there is a decreasing trend of P_d with decreasing compliance, the relationship is not statistically significant. As shown in **Figure 6.16** there is no significant change in MAP with changing compliance for all the stroke volumes. **Figure 6.17** shows the changes of pulse pressure (PP) with compliance. PP exponentially increases with decreasing compliance (for all stroke volume, $p<0.001$).

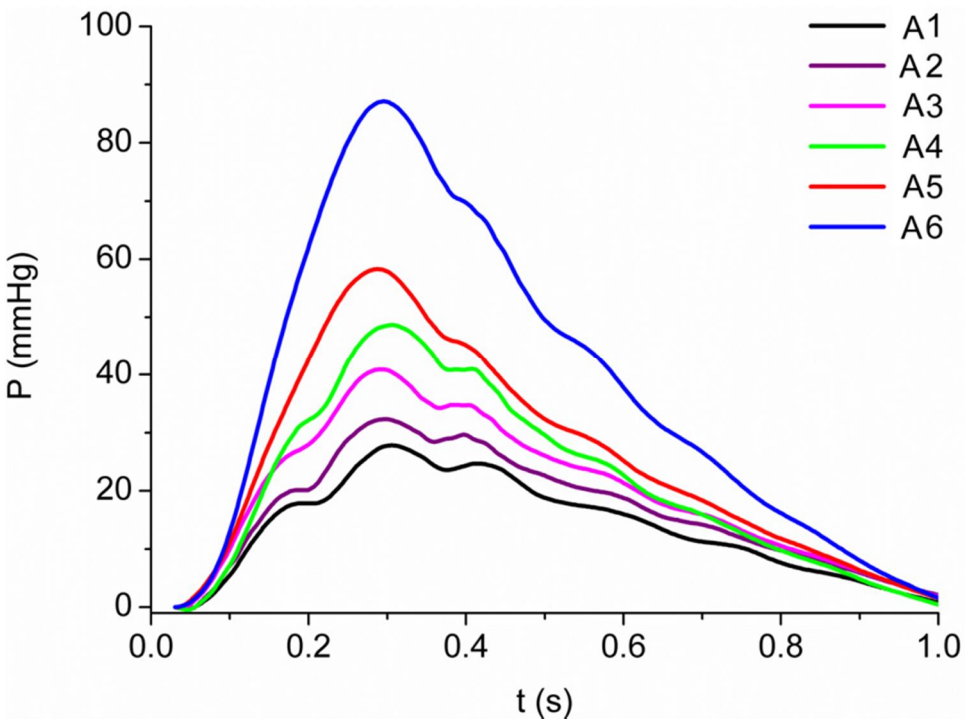

Figure 6.13: Example of measured pressure waveforms at V=30 ml for all the aorta preparations. Diastolic pressure was subtracted from the initial value of pressure. Curves were aligned with the upstroke of the measured pressure.

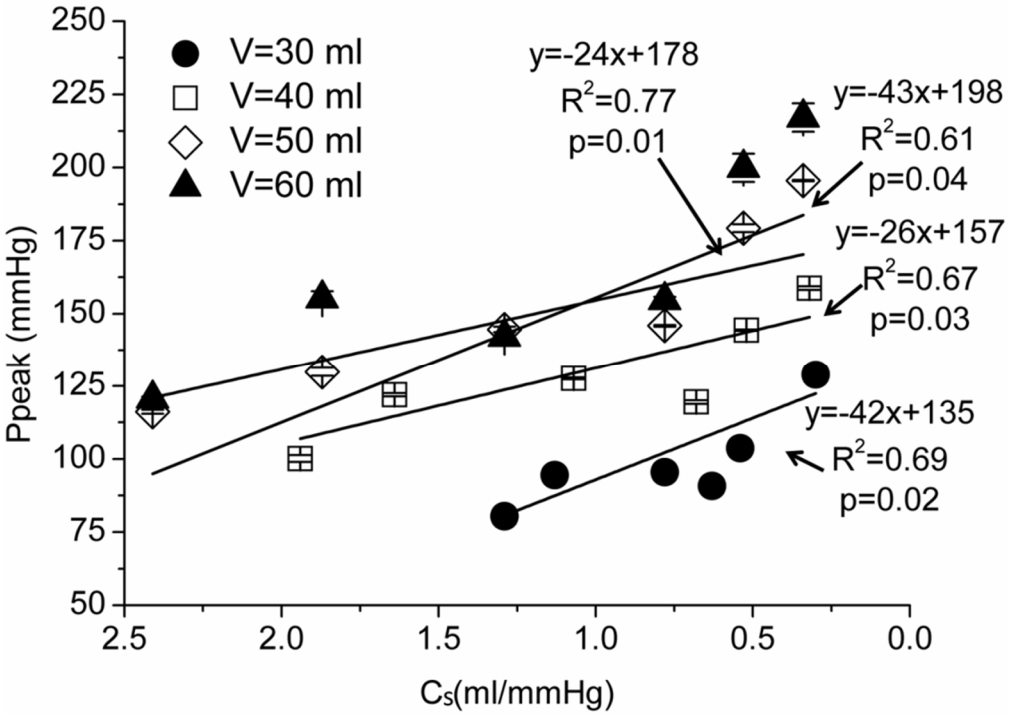

Figure 6.14: Changes of Ppeak with Cs. Ppeak linearly increases with decreasing Cs (for all V $p<0.05$).

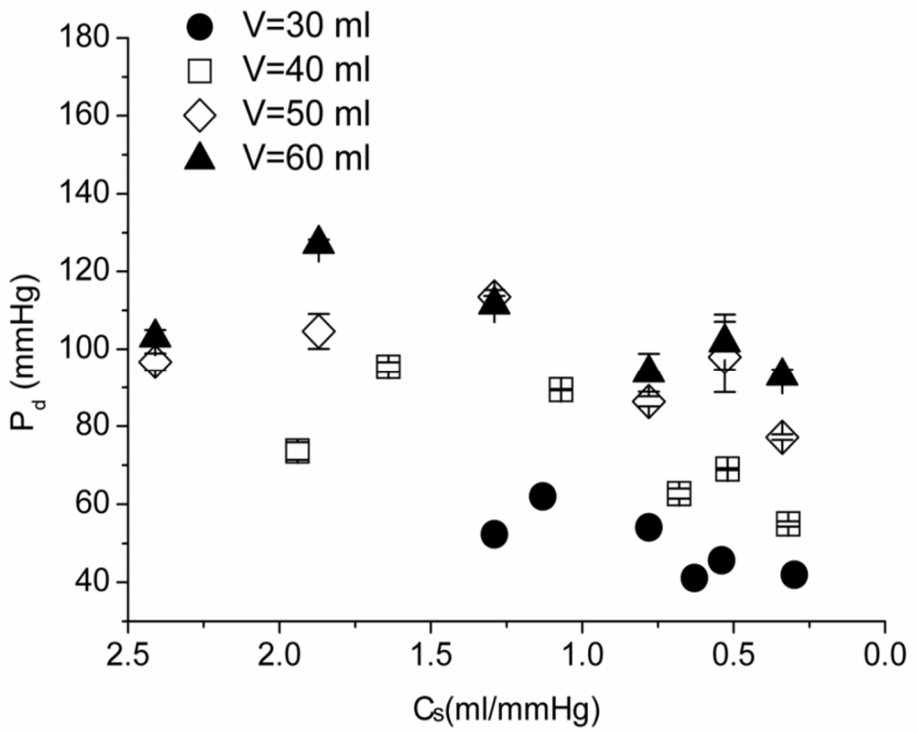

Figure 6.15: Changes of P_d with Cs. No significant relationship between P_d and Cs was found.

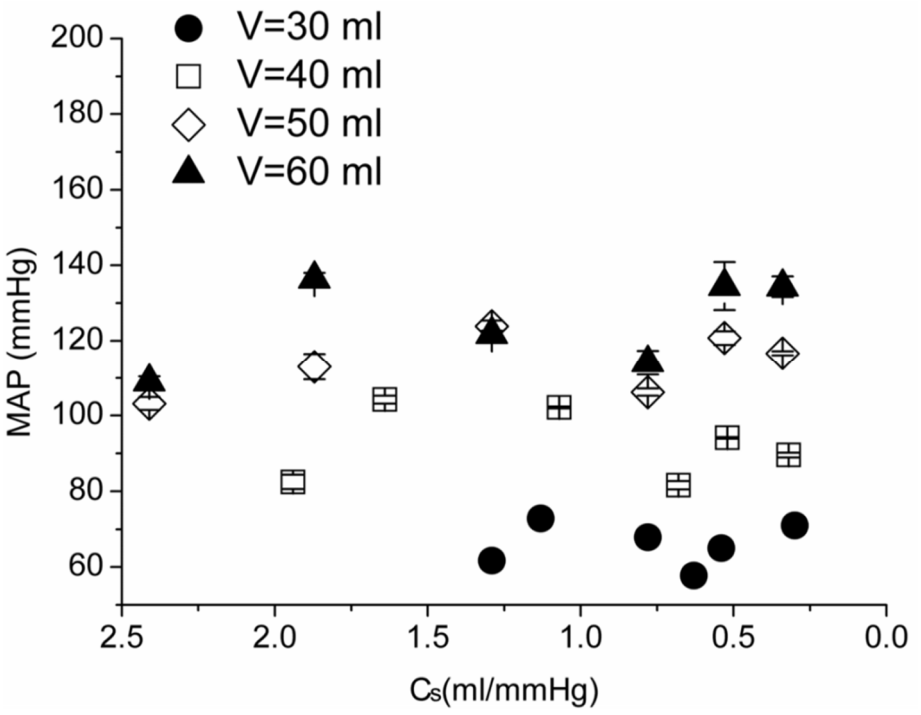

Figure 6.16: Changes of MAP with Cs. No significant relationship between MAP and Cs was found.

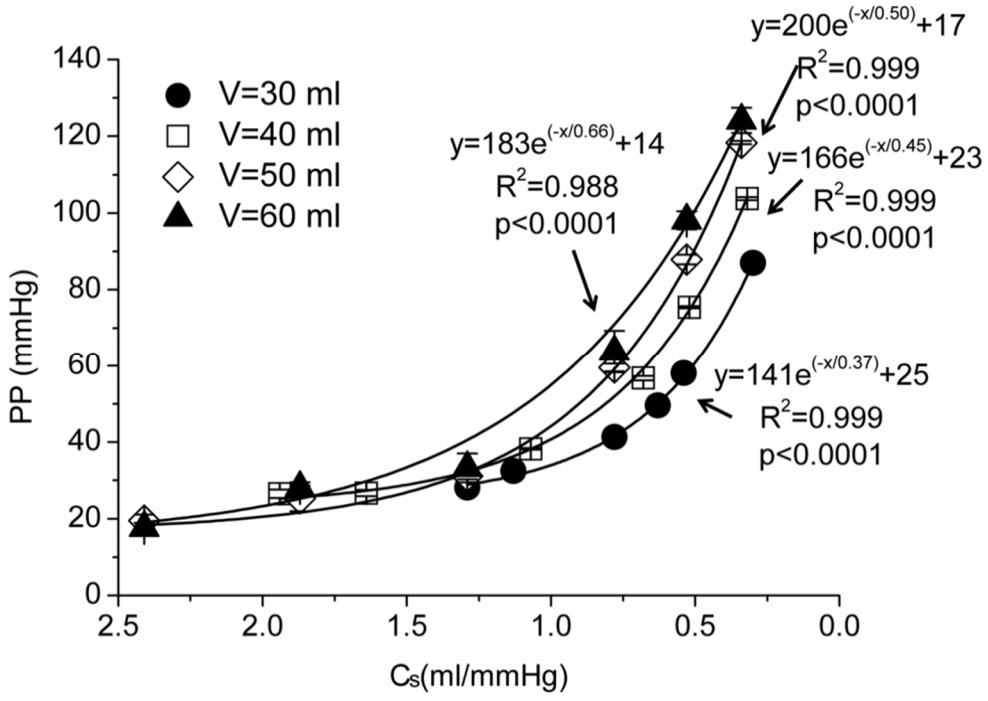

Figure 6.17: Changes of PP with Cs. PP exponentially increases with decreasing Cs (for all V $p<0.05$).

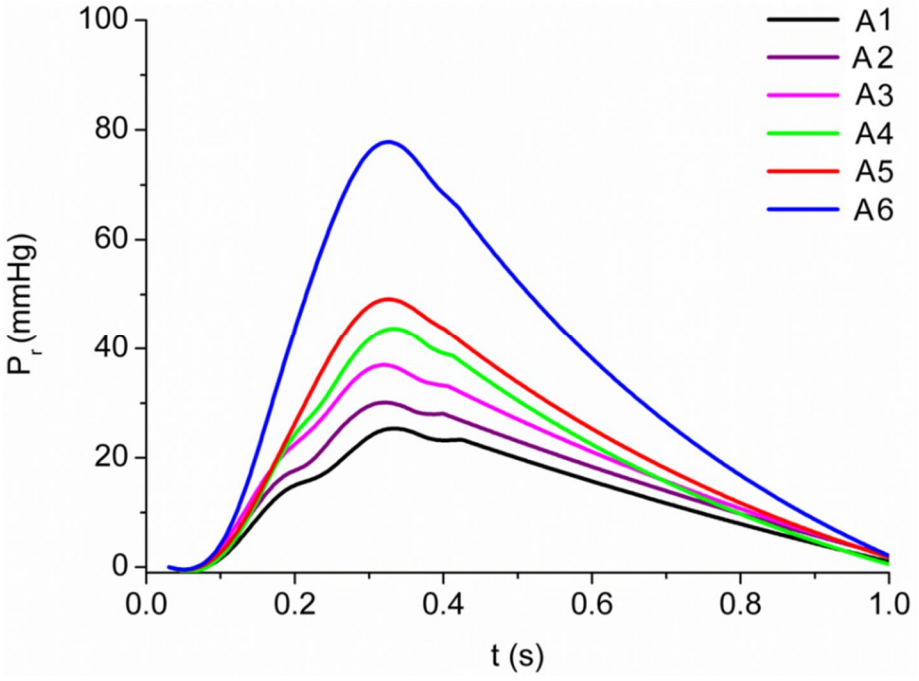

Figure 6.18: Reservoir pressure waveforms at V=30 ml for all the aorta preparations, calculated from the measured pressures reported in **Figure 6.13**. Diastolic pressure was subtracted from the initial value of pressure. Curves were aligned with the upstroke of the measured pressure.

6.3.2.2 Reservoir pressure (P_r)

Figure 6.18 shows the reservoir pressure waveforms calculated from the measured pressures shown in **Figure 6.13** and **Figure 6.19** shows an example of P, P_r and P_e. Changes of peak reservoir pressure ($P_r$peak) with compliances are reported in **Figure 6.20**. A significant linear increase of $P_r$peak with decreasing compliance was found for stroke volume of 40, 50 and 60 ml. An increasing trend was found also for the stroke volume of 30 ml but it was not statistically significant. In **Figure 6.20** the linear fitting for each volume is also reported. **Figure 6.21** shows the changes of pulse reservoir pressure (PP_r) with compliance. PP_r exponentially increases with decreasing compliance (for all stroke volume, $p<0.001$). Changes of the PP_r/PP ratio with compliances are reported in **Figure 6.22**. No significant difference of this parameter was found with compliance.

6.3.2.3 Excess pressure (P_e)

Figure 6.23 shows typical examples of excess pressure waveforms calculated from the measured pressures shown in **Figure 6.13**. Changes of peak excess pressure ($P_e$peak) with compliance are reported in **Figure 6.24**. A significant exponential increase of $P_e$peak with decreasing compliance was found for stroke volume of 40 and 50 ml. An increasing exponential trend was found also for the stroke volumes of 30 ml and 60 ml but it was not statistically significant.

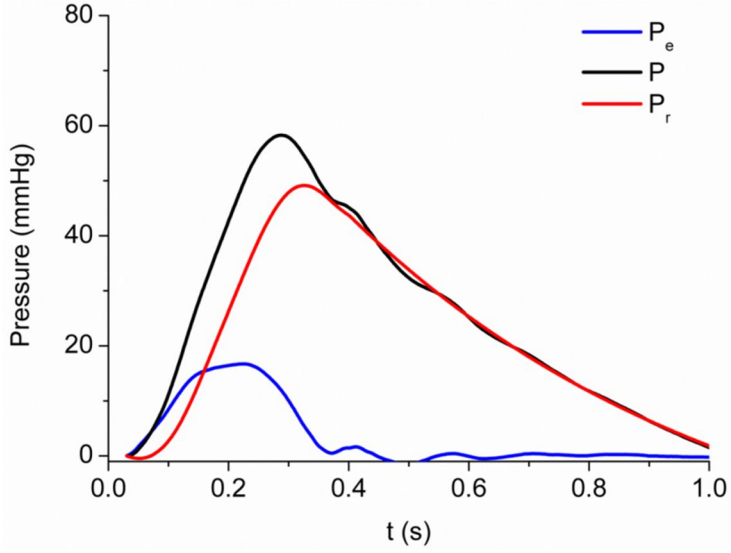

Figure 6.19: Example of measured pressure (black) and calculated reservoir (red) and excess (blue) pressure.

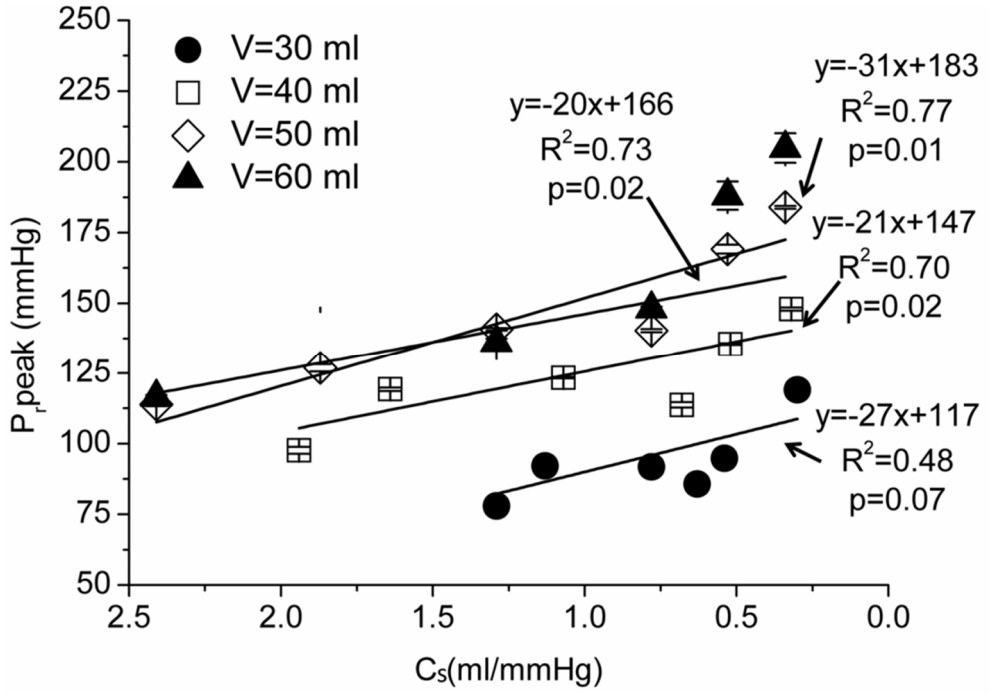

Figure 6.20: Changes of $P_r$peak with Cs. $P_r$peak increases significantly with decreasing Cs (for all V $p<0.05$, a part from V=30ml).

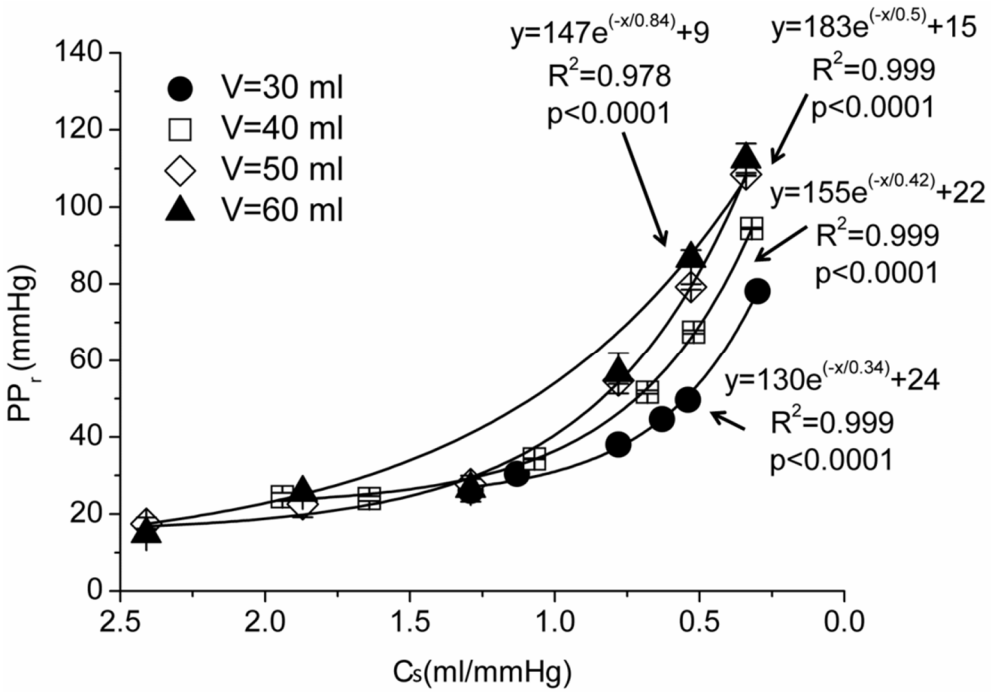

Figure 6.21: Changes of PP_r with Cs. PP_r increases exponentially with decreasing Cs (for all V $p<0.05$).

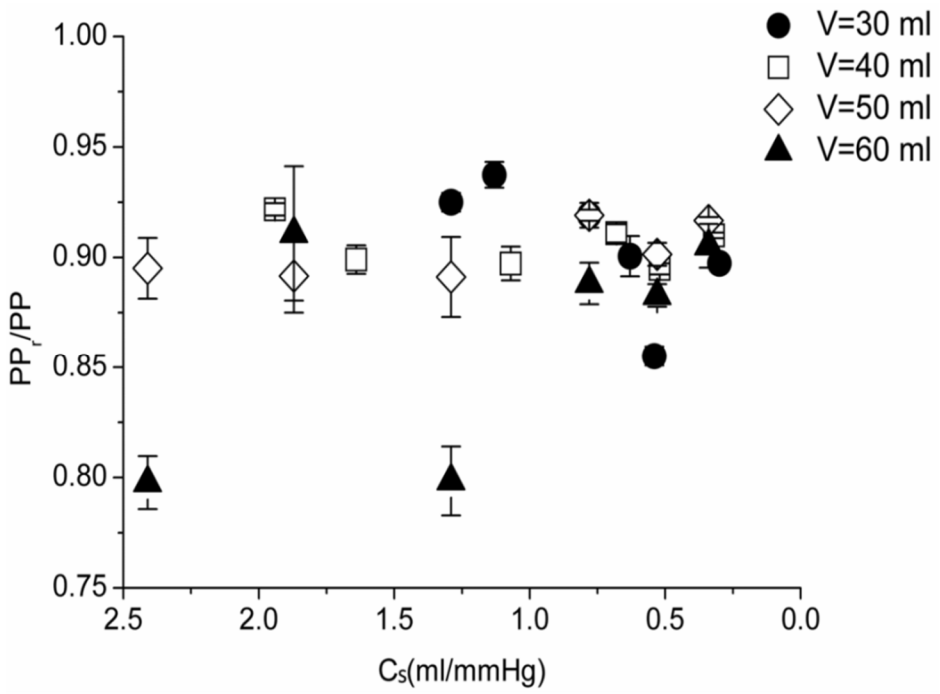

Figure 6.22: Changes of PP_r/PP with Cs. No significant relationship between PP_r/PP and Cs was found.

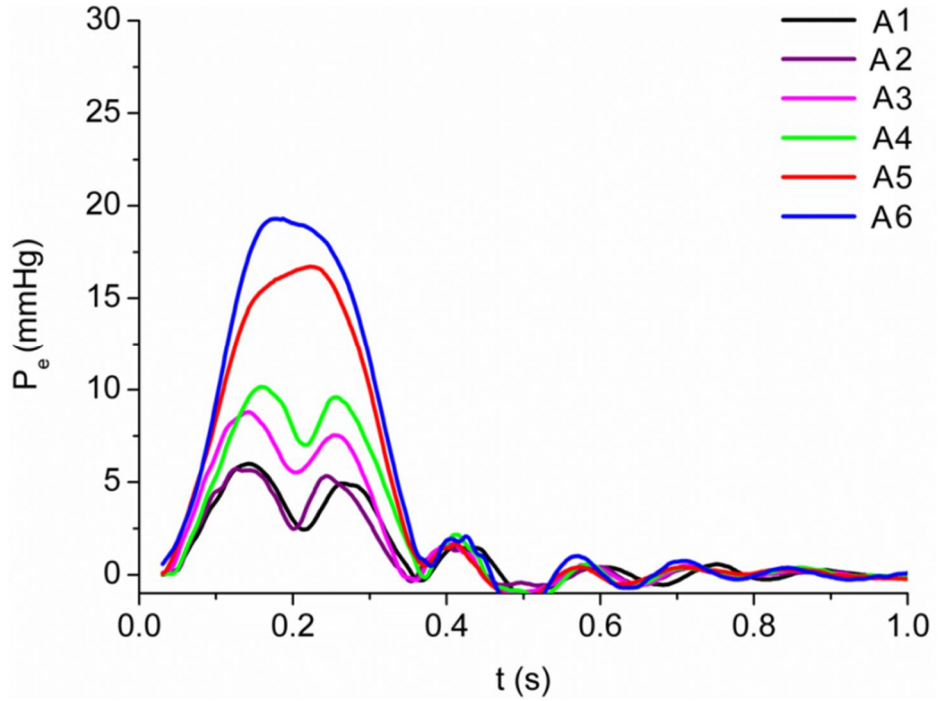

Figure 6.23: Excess pressure waveforms at V=30 ml for all the aorta preparations, calculated from the measured pressures reported in **Figure 6.13**. Curves were aligned with the upstroke of the measured pressure.

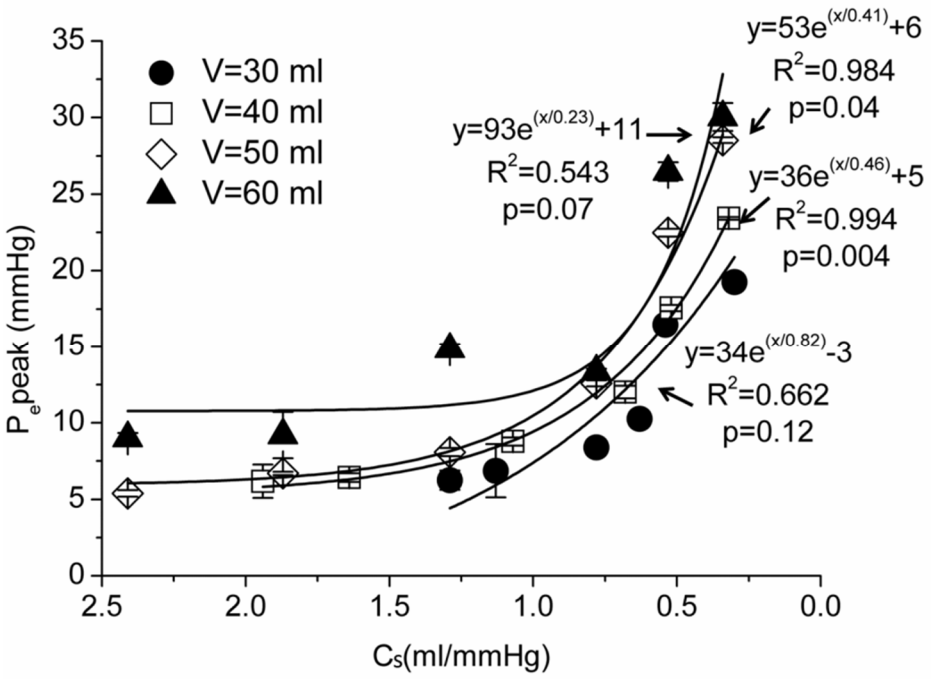

Figure 6.24: Changes of $P_e$peak with Cs. $P_e$peak increases significantly with decreasing Cs for V=40 ml and V=50 ml ($p<0.05$), but not for V=30 ml and V=60 ml.

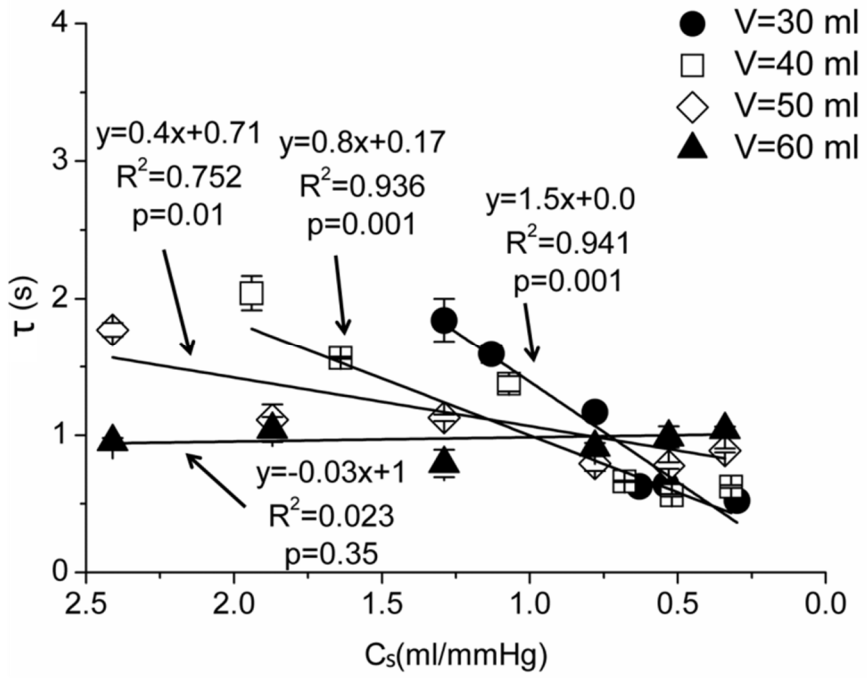

Figure 6.25: Changes of τ with Cs. τ decreases significantly in a linear way with decreasing Cs (for all V $p<0.05$, apart from V=60ml). For V=30 ml, V=40 ml and V=50 ml the best fitting of the experimental data is a linear curve.

Table 6.5. Values of the time constant decay calculated by fitting the exponential decay (τ) and estimated as RC (τ_{RC}).

V (ml)		A1	A2	A3	A4	A5	A6
30	τ (s)	1.8±0.2	1.6±0.1	1.2±0.1	0.6±0.1	0.6±0.0	0.5±0.0
	τ_{RC} (s)	1.4±0.1	1.0±0.0	0.8±0.1	0.7±0.1	0.4±0.1	0.4±0.1
40	τ (s)	2.0±0.1	1.6±0.0	1.4±0.1	0.7±0.0	0.6±0.0	0.6±0.0
	τ_{RC} (s)	2.1±0.1	1.9±0.1	1.3±0.3	0.7±0.0	0.6±0.1	0.4±0.1
50	τ (s)	1.8±0.1	1.1±0.1	1.1±0.0	0.8±0.1	0.8±0.0	0.9±0.1
	τ_{RC} (s)	1.8±0.0	2.6±0.3	1.8±0.0	0.8±0.1	0.5±0.0	0.5±0.1
60	τ (s)	1.0±0.0	1.0±0.1	0.8±0.1	0.9±0.0	1.0±0.1	1.0±0.0
	τ_{RC} (s)	1.8±0.0	1.9±0.3	1.2±0.0	0.7±0.0	0.6±0.0	0.4±0.1

6.3.2.4 Time constant decay (τ)

τ was calculated by fitting the exponential decay of the pressure waveform in diastole. It decreases linearly with decreasing Cs for V of 30, 40 and 50 ml ($p<0.05$) (**Figure 6.25**). The slope of the linear curve decreases from V=30 ml to V=40 ml. For the highest stroke volume no relationship was found between τ and Cs and the linear fitting is very poor.

τ can also be calculated as RC (with R resistance and C compliance). **Table 6.5** includes values of τ found by fitting the exponential decay are reported with the time constant calculated as RC, where R was estimated as the ratio of the time-averaged P over the time-averaged Q and C is Cs.

6.3.2.5 Wave speed

Wave speed calculated using the excess pressure (c_e) is always smaller than that calculated using measured pressure (c) (**Figure 6.26**). Both wave speeds, increase exponentially with a decrease in Cs (all $p<0.05$, apart from c for stroke vol In **Table 6.6** the percentage ratio of the two wave speeds is reported.

6.3.3 Changes with stroke volume (V)

In this section the changes of the same hemodynamic parameter are investigated in relation to a variation of V. Results are reported for each aorta preparation (A1-A6) although for the highest compliances (A1-A3) the value of compliance cannot be considered constant with increasing stroke volume.

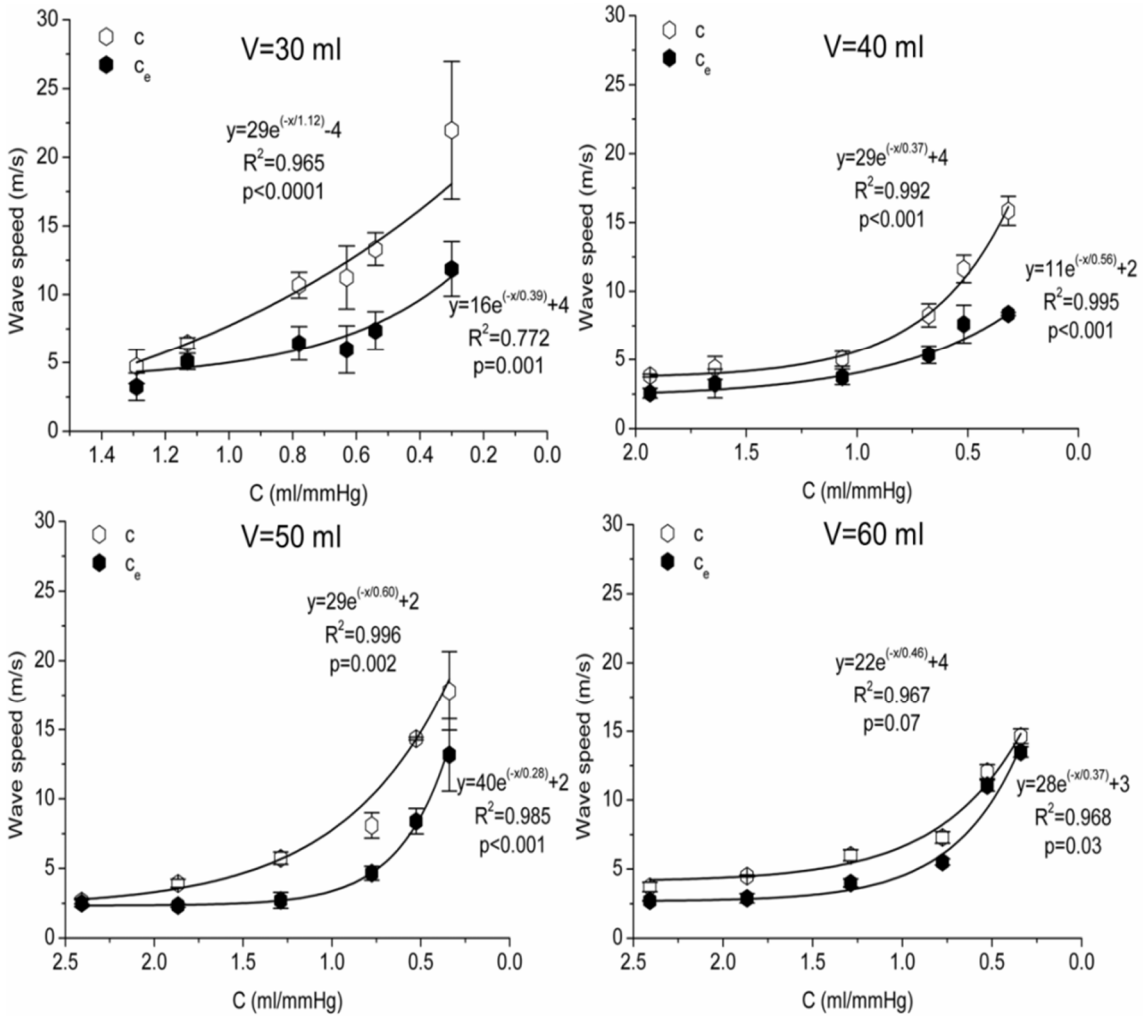

Figure 6.26: Changes of c and c_e with Cs for a) 30 ml, b) 40 ml, c) 50 ml and d) 60 ml. c and c_e increase significantly with decreasing Cs (for all V $p<0.05$, a part from c in case of V=60 ml).

Table 6.6: Percentage ratio of c and c_e, calculated as $c_e/c \cdot 100$.

V (ml)	A1	A2	A3	A4	A5	A6
30	69%	79%	60%	53%	55%	54%
40	67%	74%	74%	65%	65%	53%
50	94%	60%	47%	58%	59%	74%
60	73%	64%	67%	76%	92%	92%

6.3.3.1 Measured pressure

Figure 6.27 shows typical pressure waveforms recorded at different values of stroke volume at the aorta preparation A5. Changes of Ppeak with V are reported in

Figure 6.28. A linear increase of Ppeak with increasing V was found ($p<0.05$ for all the aorta preparations, apart from A2 and A3). In the figure also the linear fitting is reported. In **Figure 6.29** changes of P_d with V are shown. A significant linear increase of P_d with V for all the aorta configurations was found. As shown in **Figure 6.30** also the MAP increases linearly with increasing V (all $p<0.05$, apart from A3). **Figure 6.31** shows the changes of PP with V. Two different behaviors can be observed. For high values of compliance (A1-A3) PP decreases linearly with increasing V ($p<0.05$, apart from C2). For low values of compliance (A4-A6) PP increases linearly with increasing V (all $p<0.05$).

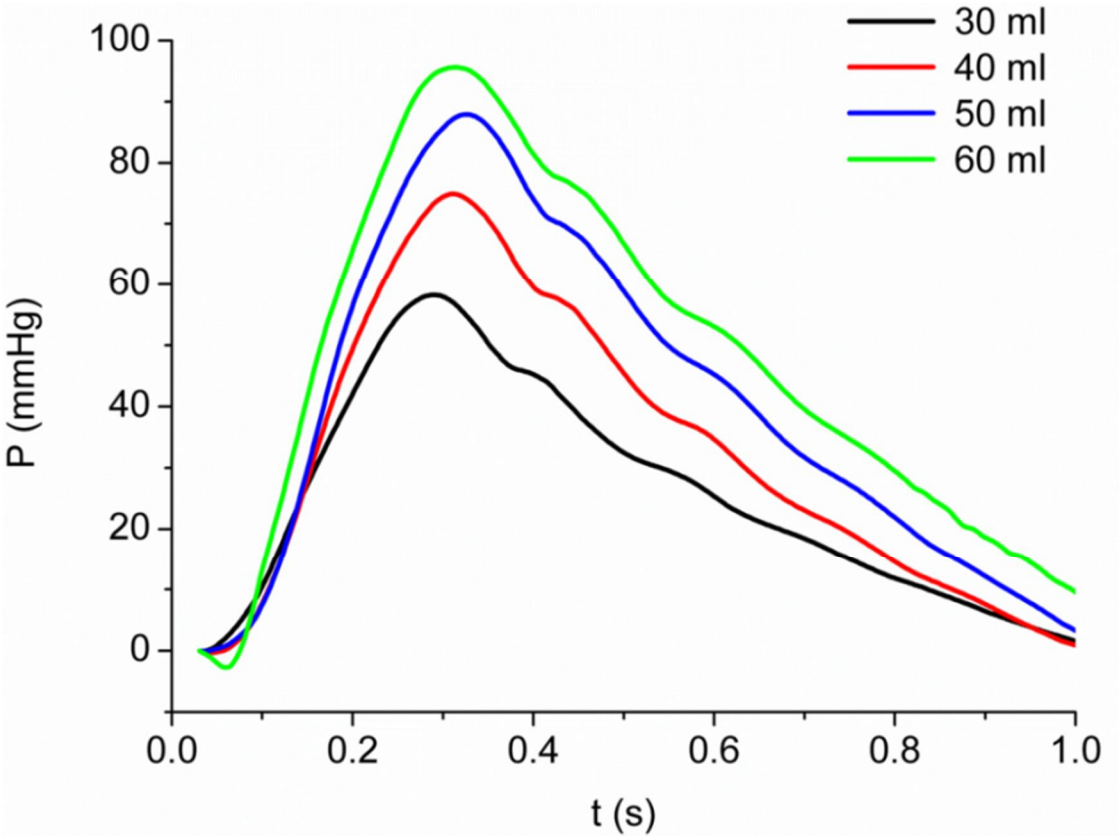

Figure 6.27: Typical example of measured pressure waveforms at different V and at the same aorta preparation (A5). Diastolic pressure was subtracted from the initial value of pressure. Curves were aligned with the upstroke of the measured pressure.

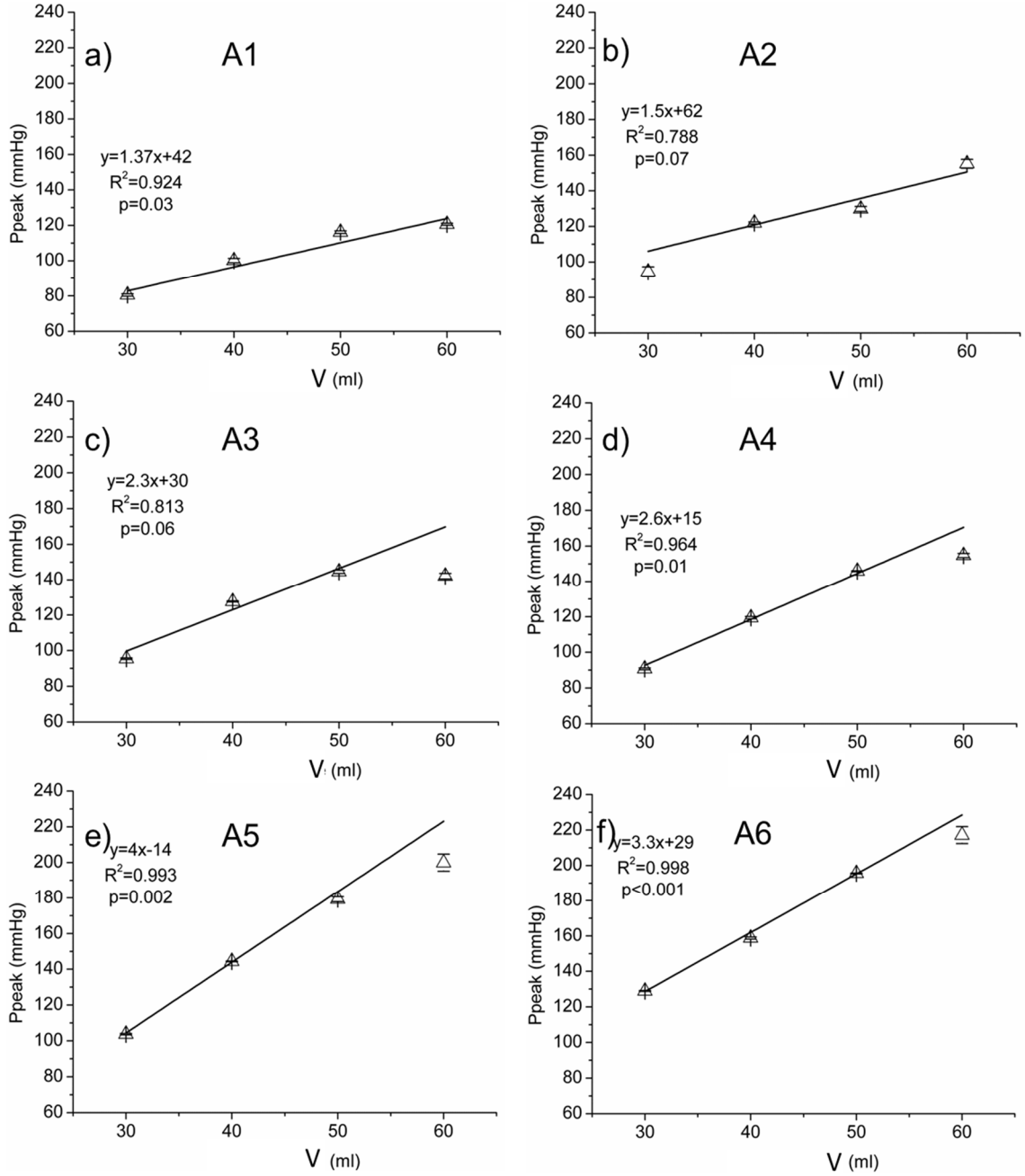

Figure 6.28: Changes of Ppeak with V for a) A1, b) A2, c) A3, d) A4, e) A5 and f) A6. Ppeak increases linearly with increasing V ($p<0.05$, apart from A2 and A3). Black lines are the linear fitting.

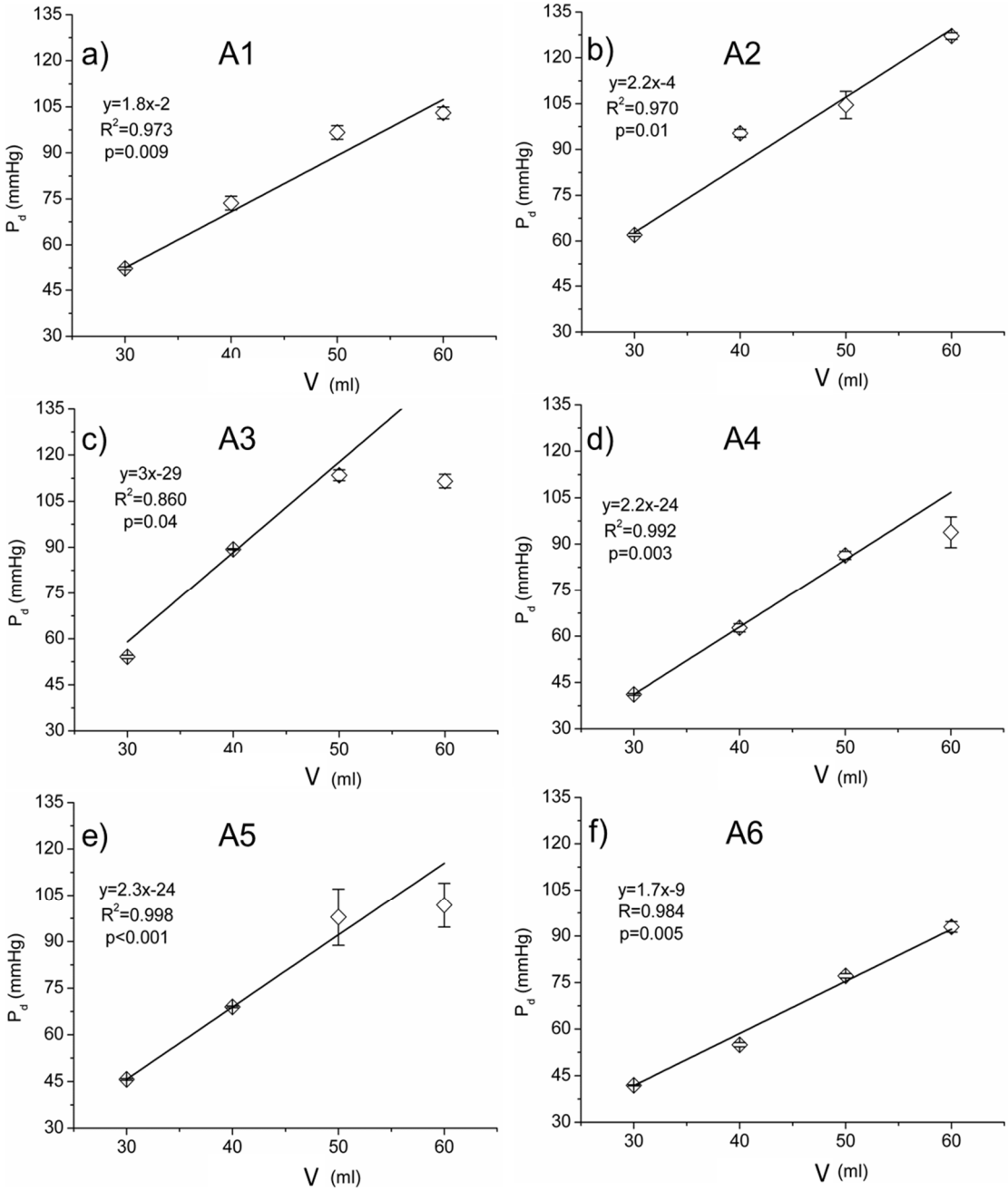

Figure 6.29: Changes of P_d with V for a) A1, b) A2, c) A3, d) A4, e) A5 and f) A6. P_d increases linearly with increasing V (all $p<0.05$). Black lines are the linear fitting.

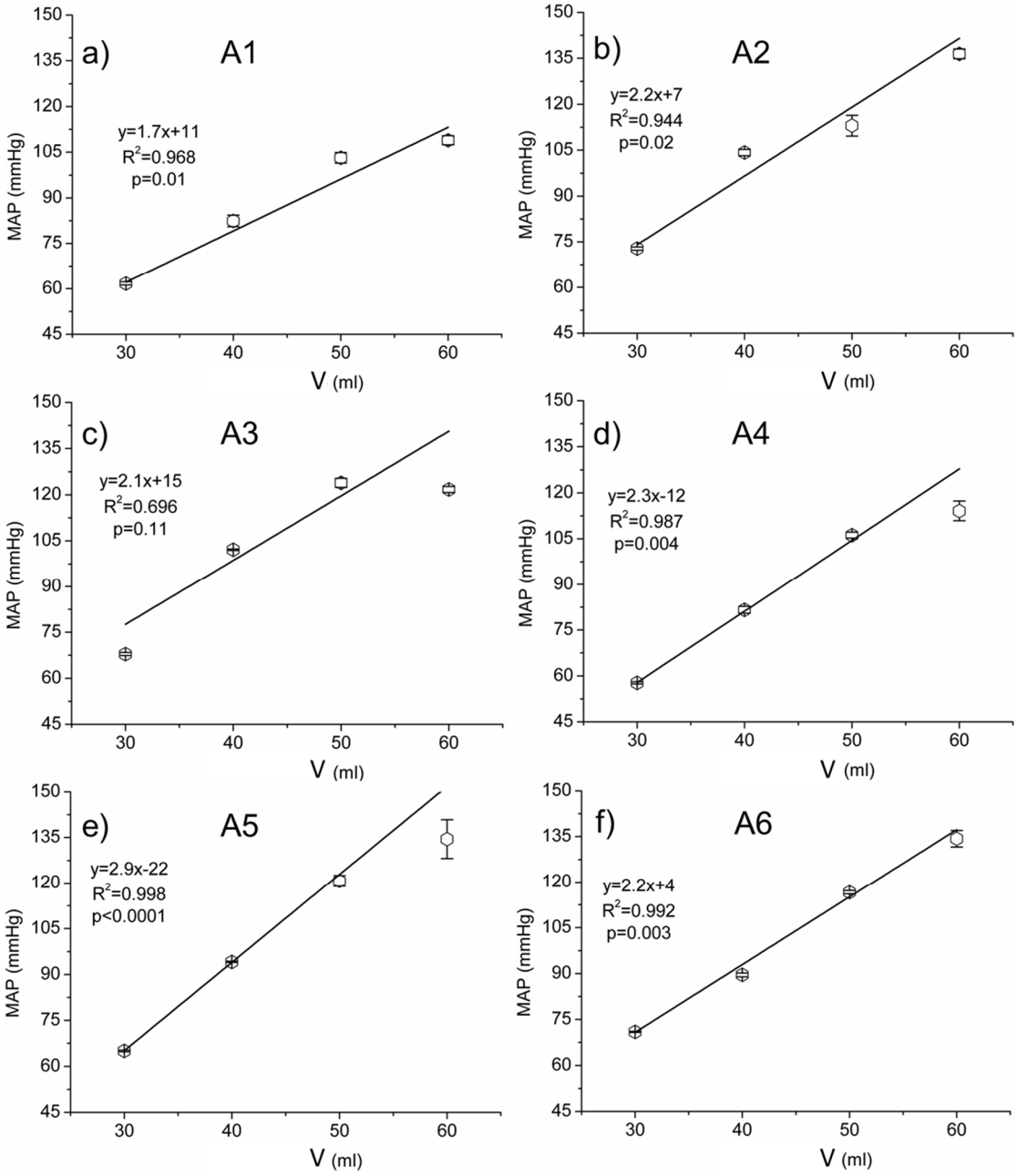

Figure 6.30: Changes of MAP with V for a) A1, b) A2, c) A3, d) A4, e) A5 and f) A6. MAP increases linearly with increasing V (all $p<0.05$, apart from A3). Black lines are the linear fitting.

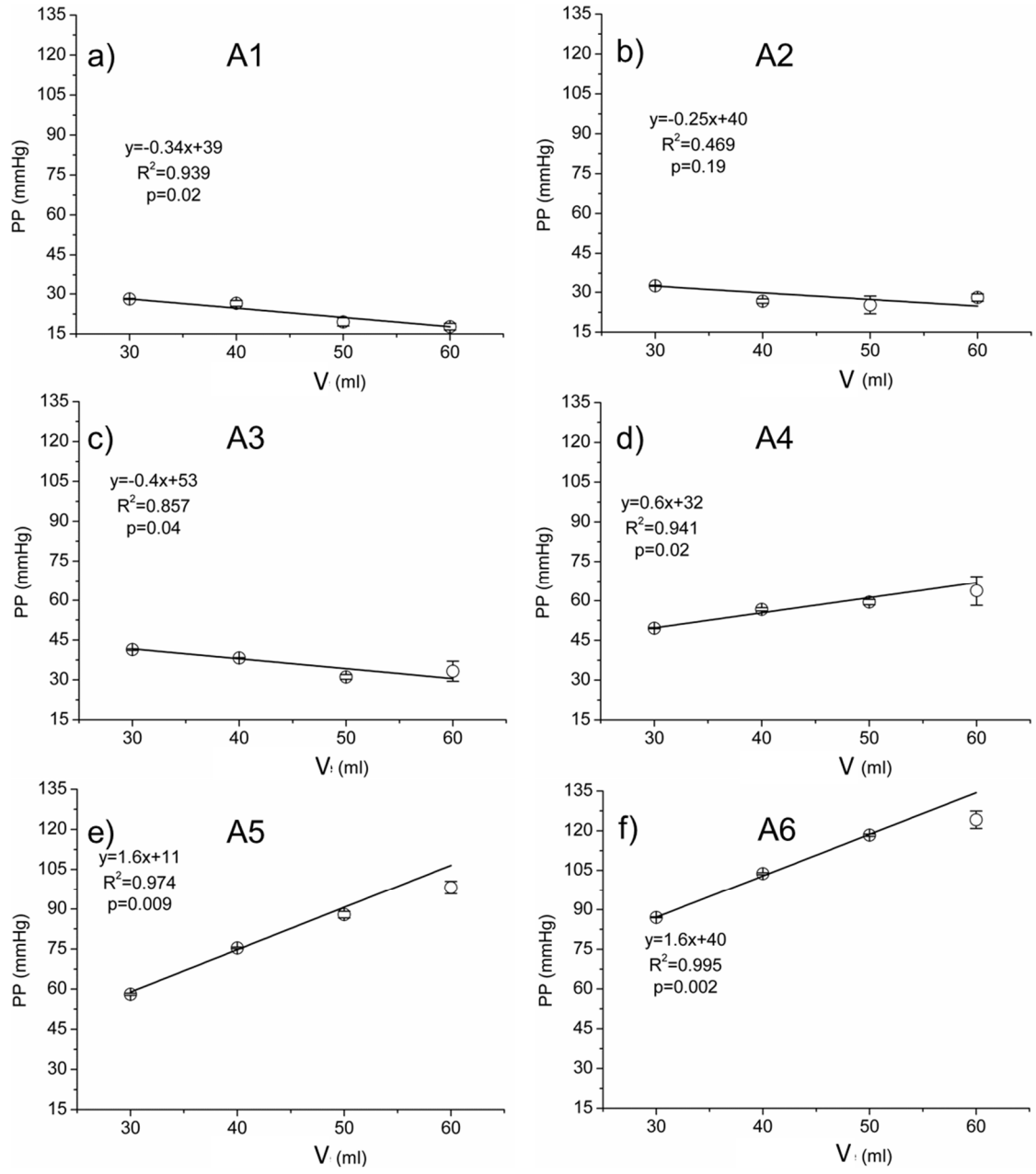

Figure 6.31: Changes of PP with V for a) A1, b) A2, c) A3, d) A4, e) A5 and f) A6. Two different trends can be observed; PP decreases linearly with increasing V for A1, A2 and A3 ($p<0.05$, apart from A2) and it increases linearly for A4, A5 and A6 ($p<0.05$). Black lines are the linear fitting.

6.3.3.2 Reservoir pressure

Figure 6.32 shows typical reservoir pressure waveforms calculated from the measured pressures shown in **Figure 6.27**. Changes of $P_r$peak with volumes are reported in **Figure 6.33**. A linear increase of $P_r$peak with increasing volume was found ($p<0.05$ for all aorta preparations). **Figure 6.34** shows the changes of PP_r with stroke volume. Two different behaviors can be observed as for PP. For high values of compliance (A1-A3) PP_r decreases linearly with increasing V ($p<0.05$, apart from A2). For a stiffer aorta (A4-A6) PP_r increases linearly with increasing V (all $p<0.05$). Changes of the PP_r/PP ratio with V are reported in **Figure 6.35**.

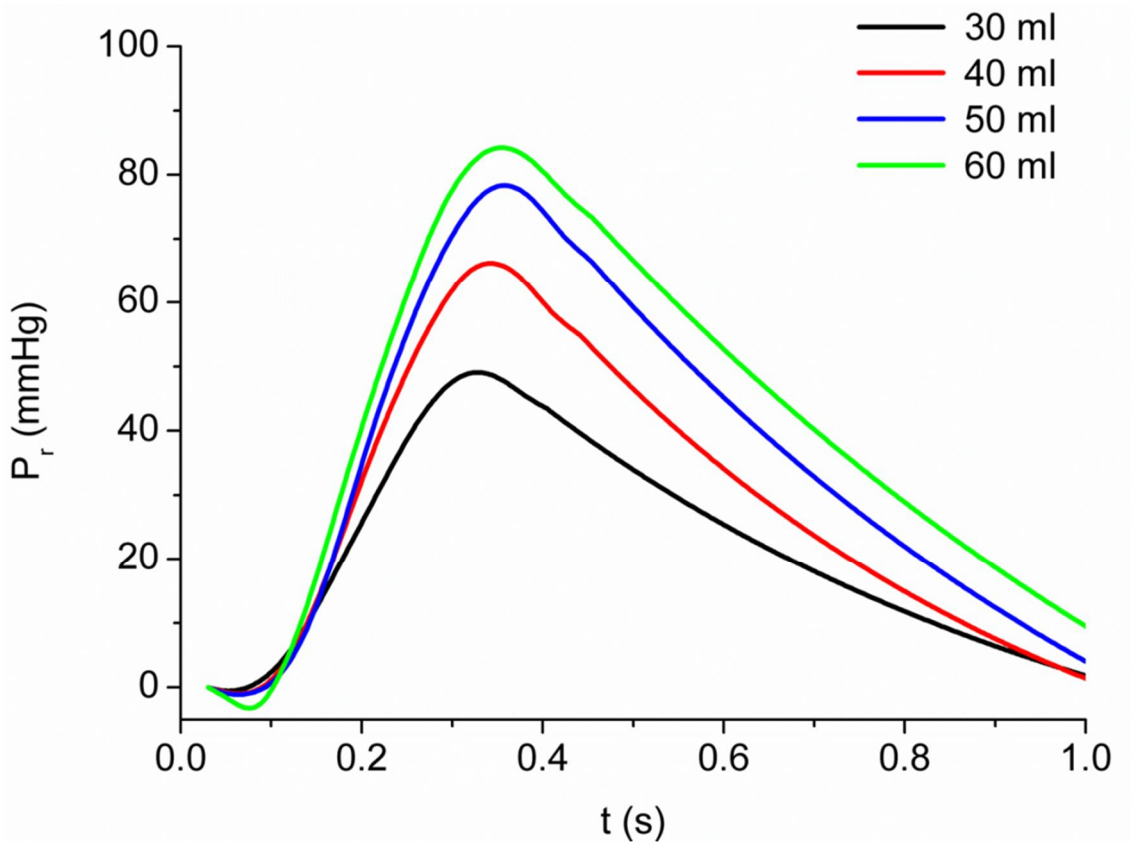

Figure 6.32: Reservoir pressure waveforms calculated from the measured pressure shown in **Figure 6.27**. Diastolic pressure was subtracted from the initial value of pressure. Curves were aligned with the upstroke of the measured pressure.

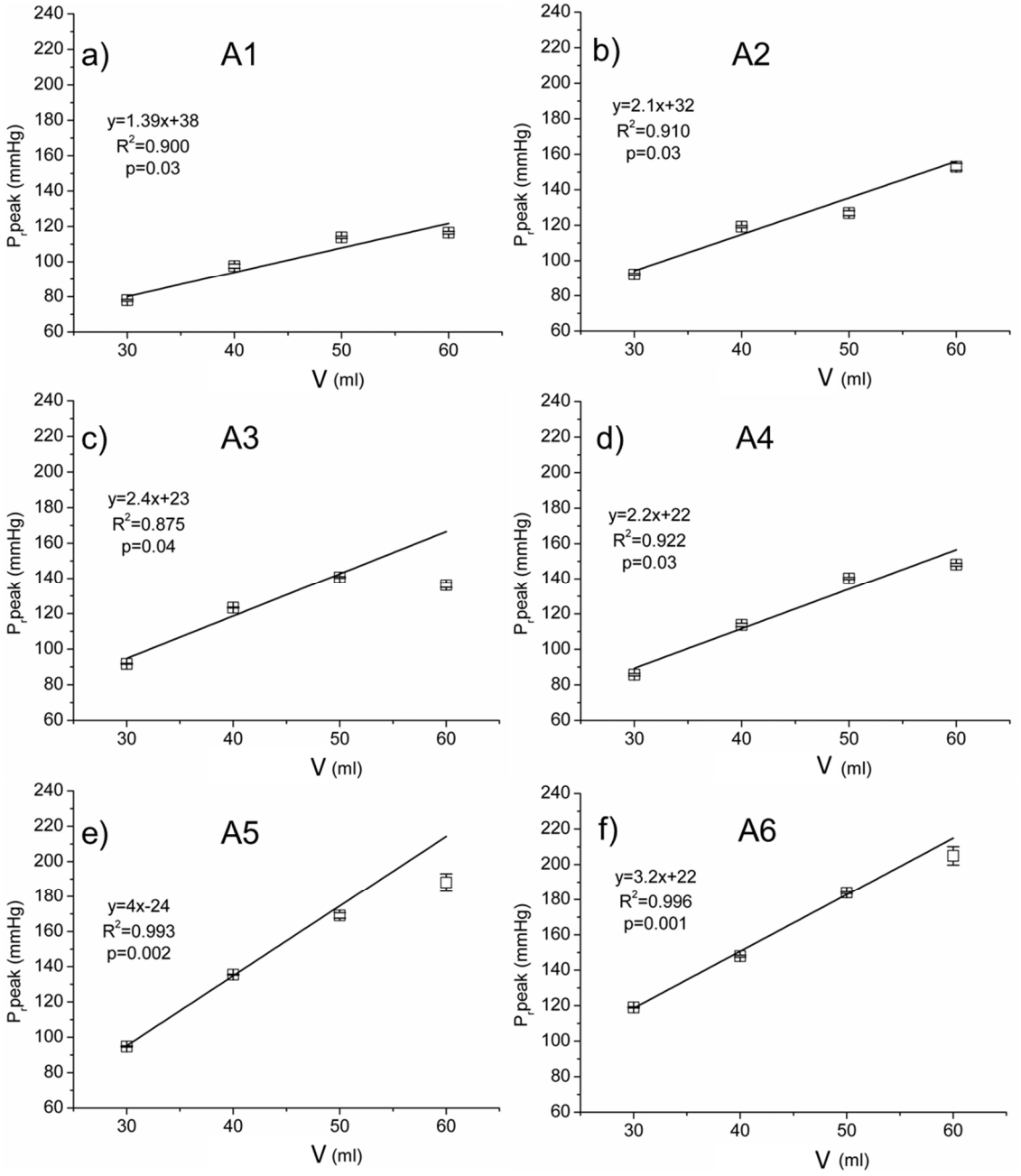

Figure 6.33: Changes of $P_r$peak with V for a) A1, b) A2, c) A3, d) A4, e) A5 and f) A6. $P_r$peak increases with increasing V (all $p<0.05$). Black lines are the linear fitting.

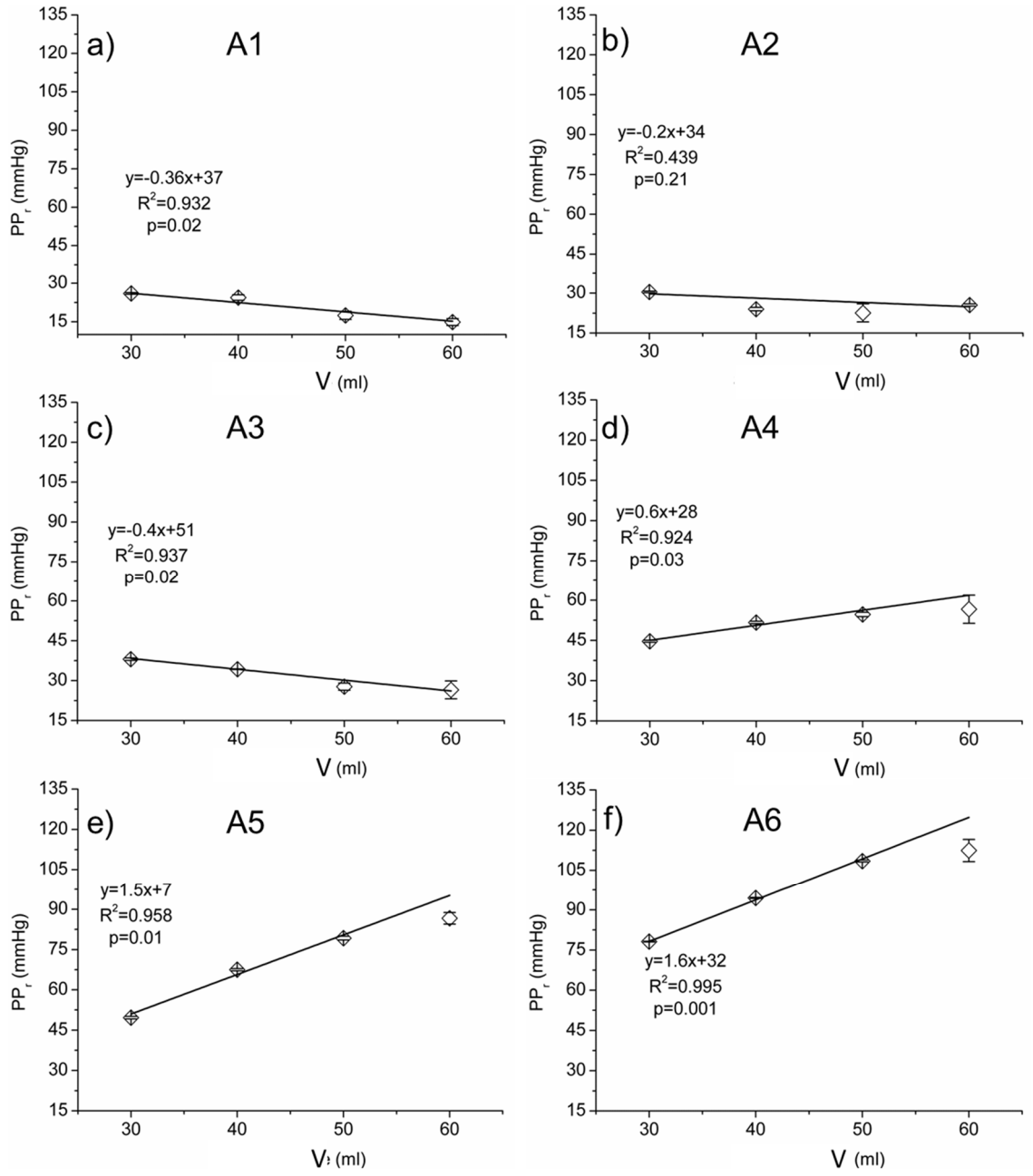

Figure 6.34: Changes of PP_r with V for a) A1, b) A2, c) A3, d) A4, e) A5 and f) A6. Two different trends can be observed; PP_r decreases with increasing V for A1, A2 and A3 ($p<0.05$, apart from C2) and it increases for A4, A5 and A6 ($p<0.05$). Black lines are the linear fitting.

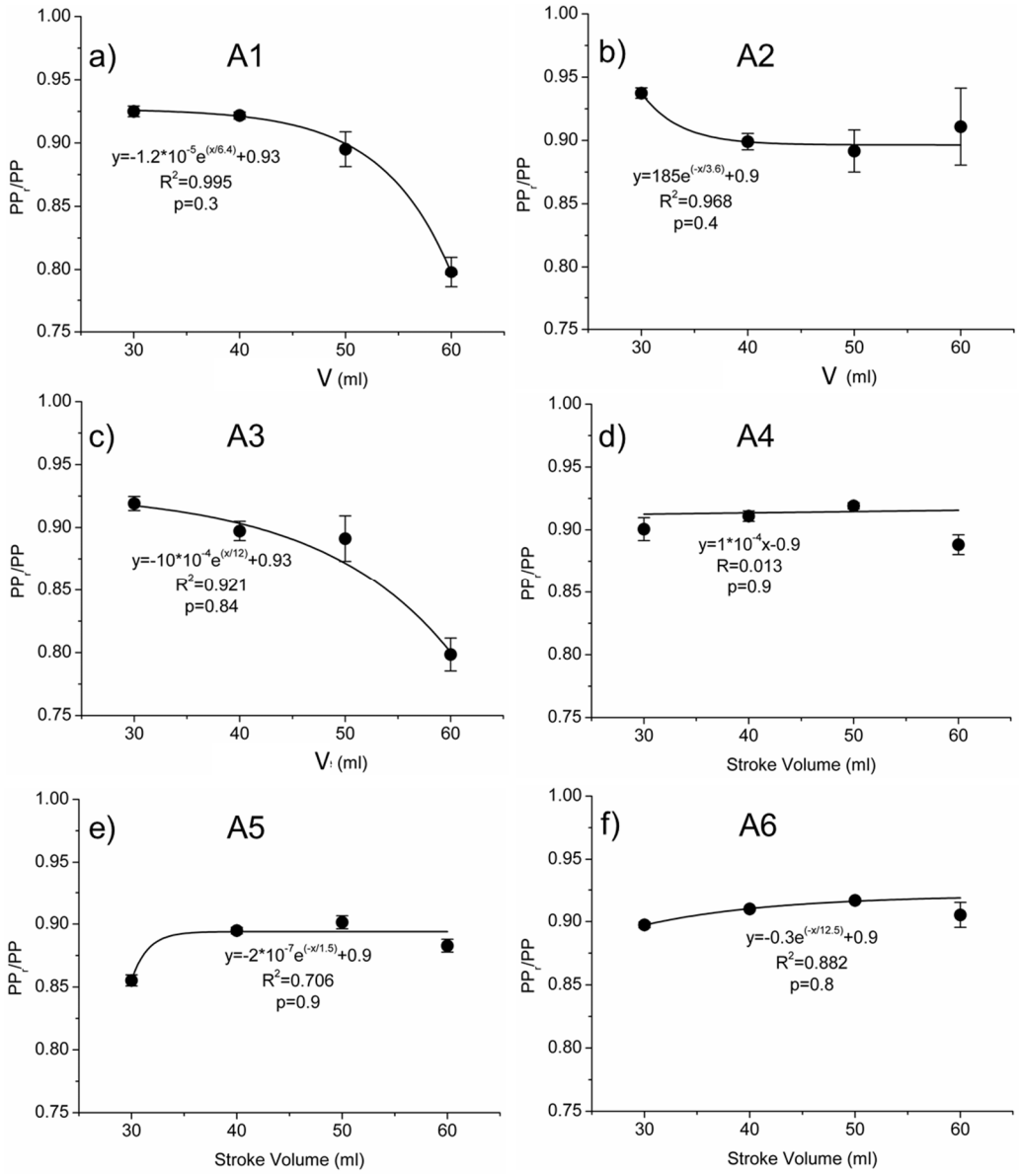

Figure 6.35: Changes of PP_r/PP with V for a) A1, b) A2, c) A3, d) A4, e) A5 and f) A6. Experimental data are well fitted by an exponential curve (apart from A4) but the relationship with V is not significant.

6.3.3.3 Excess pressure

Figure 6.36 shows excess pressure waveforms corresponding to the measured pressures shown in **Figure 6.27**. Changes of peak excess pressure ($P_e$peak) with V are reported in **Figure 6.37**. An increasing pattern of $P_e$peak with increasing V can be identified. For less stiffer aorta experimental data are well fitted by an exponential

curve, but the relationship between the two variables is not significant ($p>0.05$). For stiffer aorta $P_e$peak increases linearly and the increase is significant for A4 and A6.

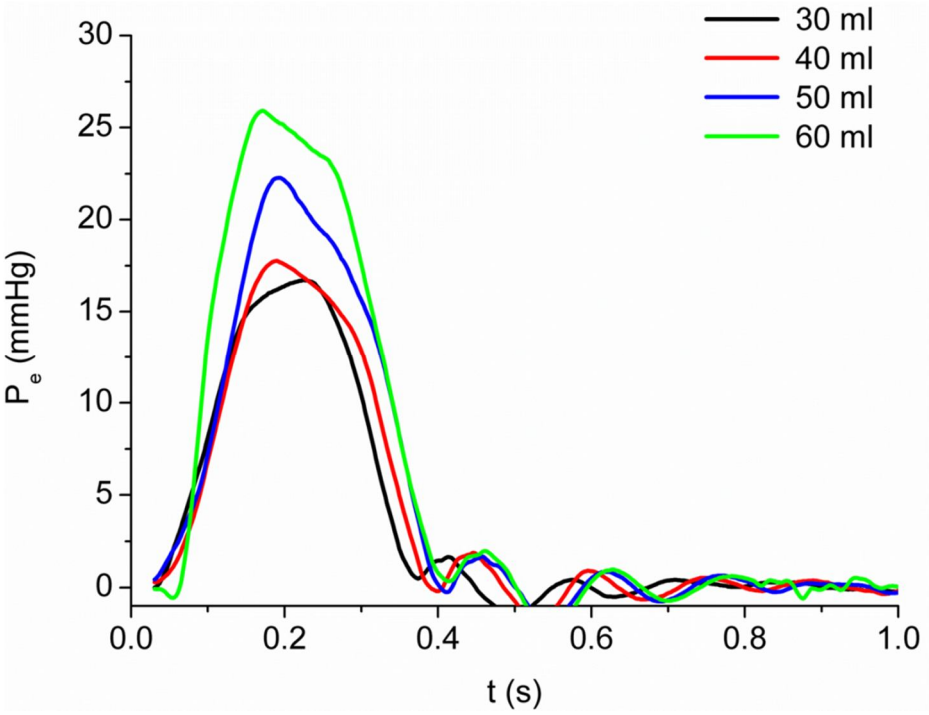

Figure 6.36: Excess pressure waveforms calculated from the measured pressures in **Figure 6.27**. Curves were aligned with the upstroke of the measured pressure.

6.3.3.4 Time constant decay (τ)

Changes of τ with increasing V are reported in **Figure 6.38**. Also in this case two different trends can be noticed; a decreasing pattern for less stiffer aorta and an increasing pattern for the stiffer ones. Apart from A6 none of the increasing trend is statistically significant.

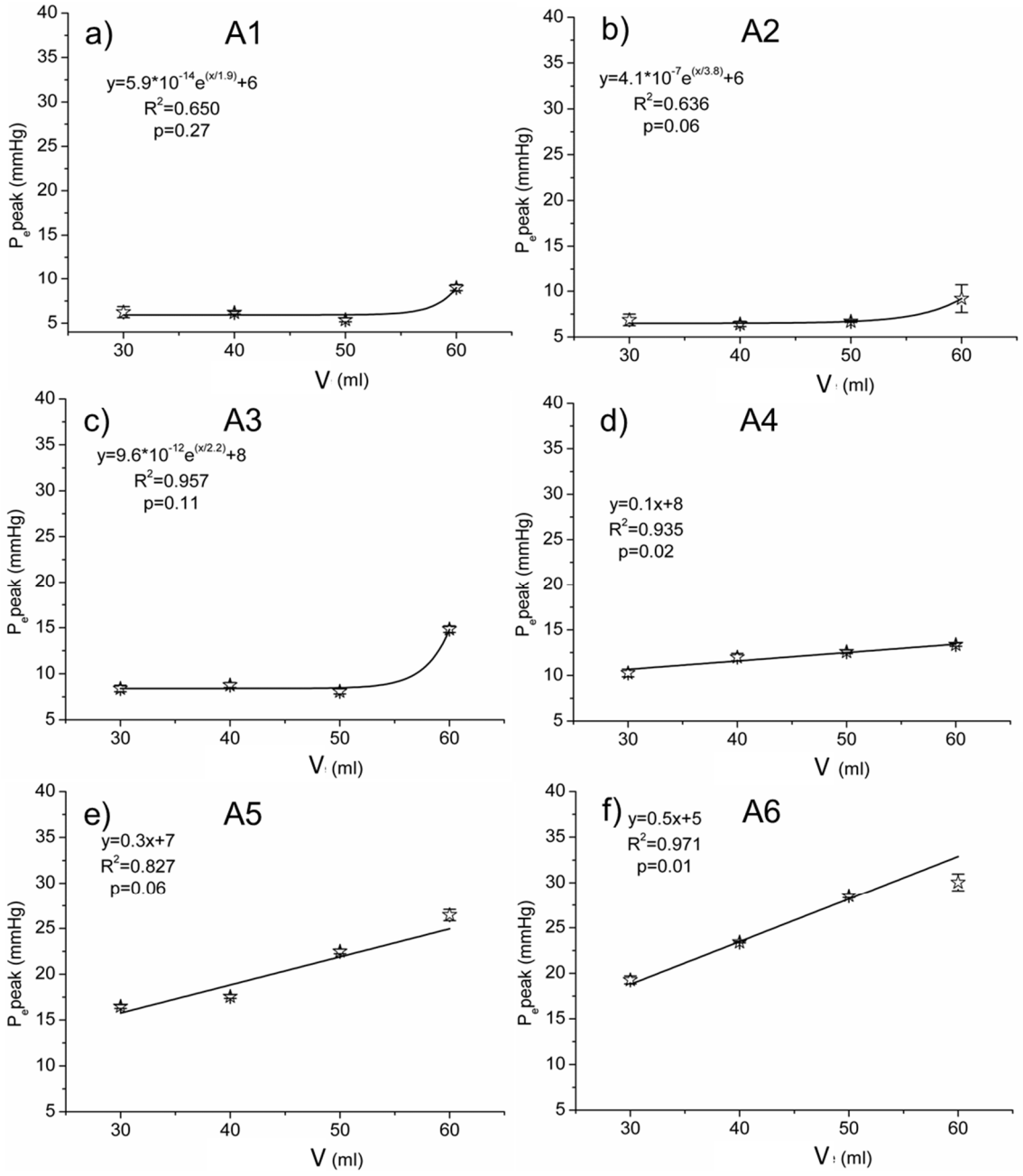

Figure 6.37: Changes of $P_e$peak with V for a) A1, b) A2, c) A3, d) A4, e) A5 and f) A6. $P_e$peak increases with increasing V in two different ways. Experimental data of A1, A2 and A3 are well fitted by an exponential curve, but a relationship between $P_e$peak and V was not found ($p>0.05$). Experimental data of A4, A5 and A6 are well fitted by a linear curve (all $p<0.05$, apart from A5).

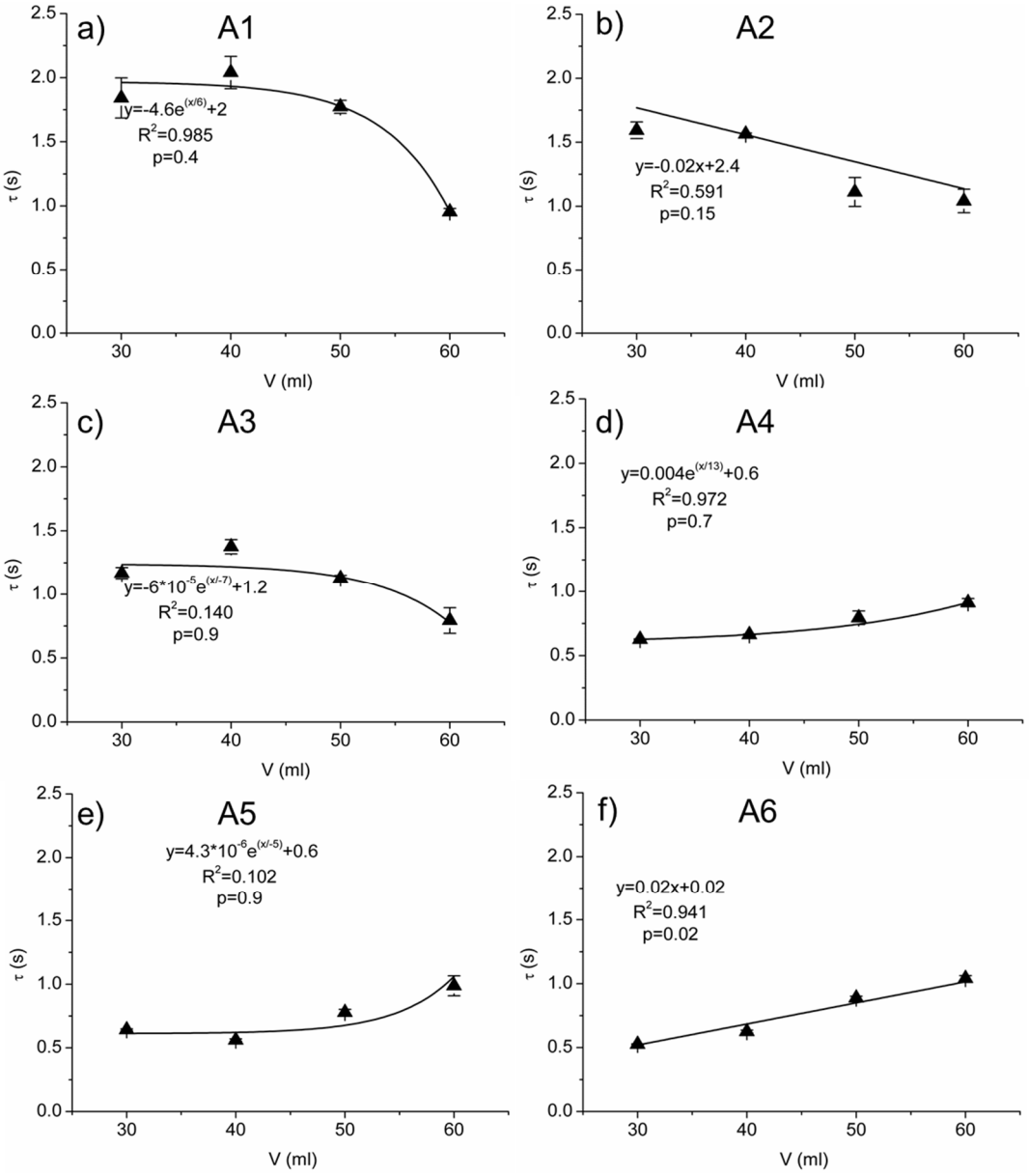

Figure 6.38: Changes of τ with V for a) A1, b) A2, c) A3, d) A4, e) A5 and f) A6. For high values of compliance (A1-A3) τ tends to decrease with increasing volume but changes are not statistically significant ($p>0.05$). For low values of compliance (A4-A6) τ seems to increase, but not significantly, apart from A6.

6.3.3.5 Wave speed

Wave speed changes with V are shown in **Figure 6.39**. There was no significant difference between either c or c_e with V. As previously shown, the differences between c and c_e are larger at high values of compliance.

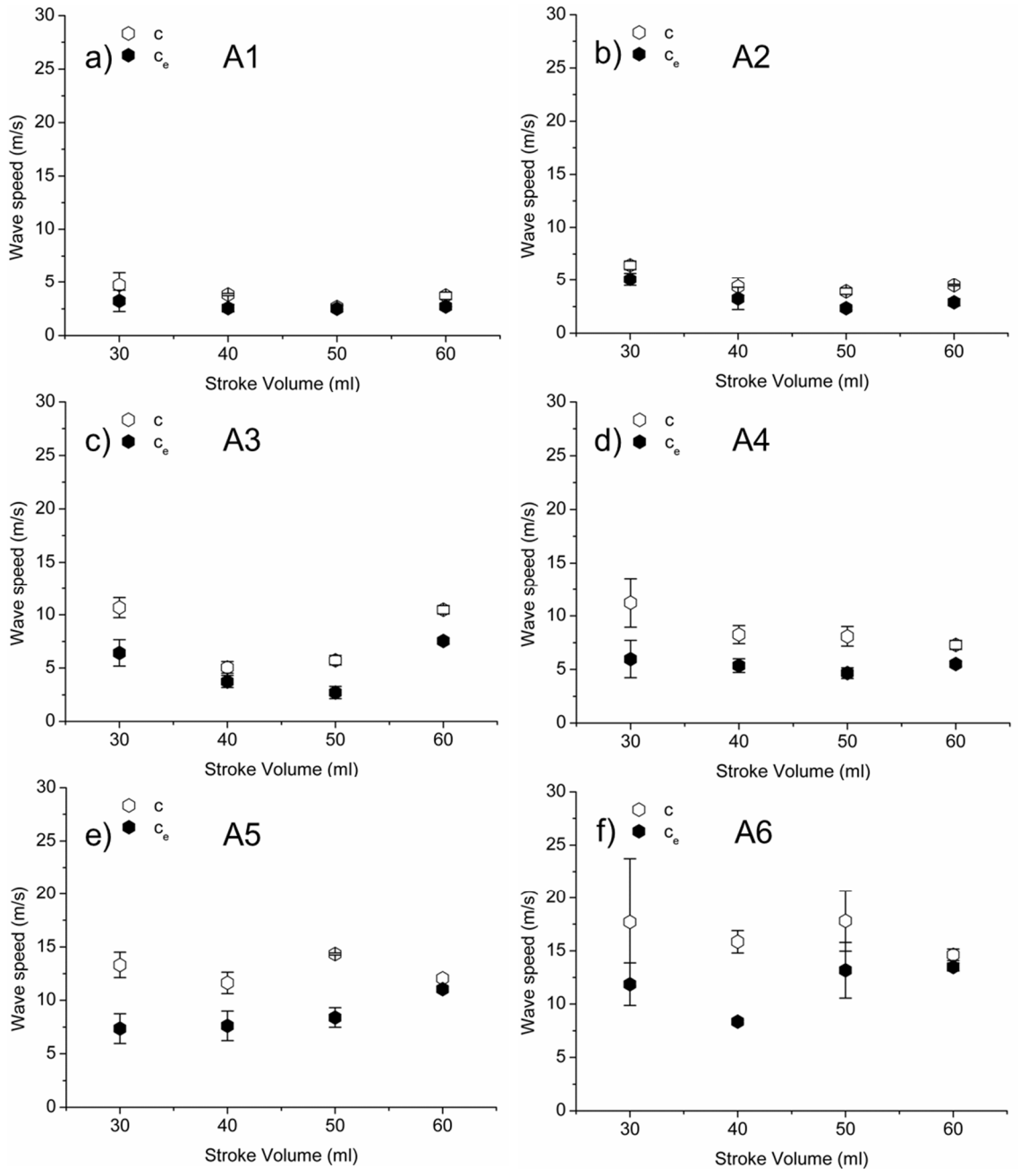

Figure 6.39: Changes of wave speeds (c and c_e) with stroke volume for a) A1, b) A2, c) A3, d) A4, e) A5 and f) A6.

6.4 Discussion

In this chapter the effects of varying vascular compliance and stroke volume on P, P_r, P_e, τ and wave speeds were investigated in a mock circulatory system. To change vascular compliance, the artificial aorta was wrapped and 6 different aortas were obtained. Only aortic compliance was varied because it gives the biggest contribution to total compliance. The range of compliance investigated was 0.30-2.41 ml/mmHg (**Table 6.3**) which is comparable to the range 0.34-2.80 ml/mmHg which was found by Chemla et al. (Chemla et al. 1998) in a population of healthy and non-healthy subjects aged 20-74 years old using the V/PP ratio method.

The use of a mock circulatory system has some advantages compare to in-vivo experiments. First, it allows for a selective variation of compliance and stroke volume. Second, it eliminates confounding effects, such as the change in heart rate that has been shown to affect the Windkessel properties of the arterial system (Mohiuddin et al. 2007) and the arterial tone response of the vessel which in turn may result in a change of peripheral resistance. Third, the volume ejected by the ventricle does not vary with changing compliance.

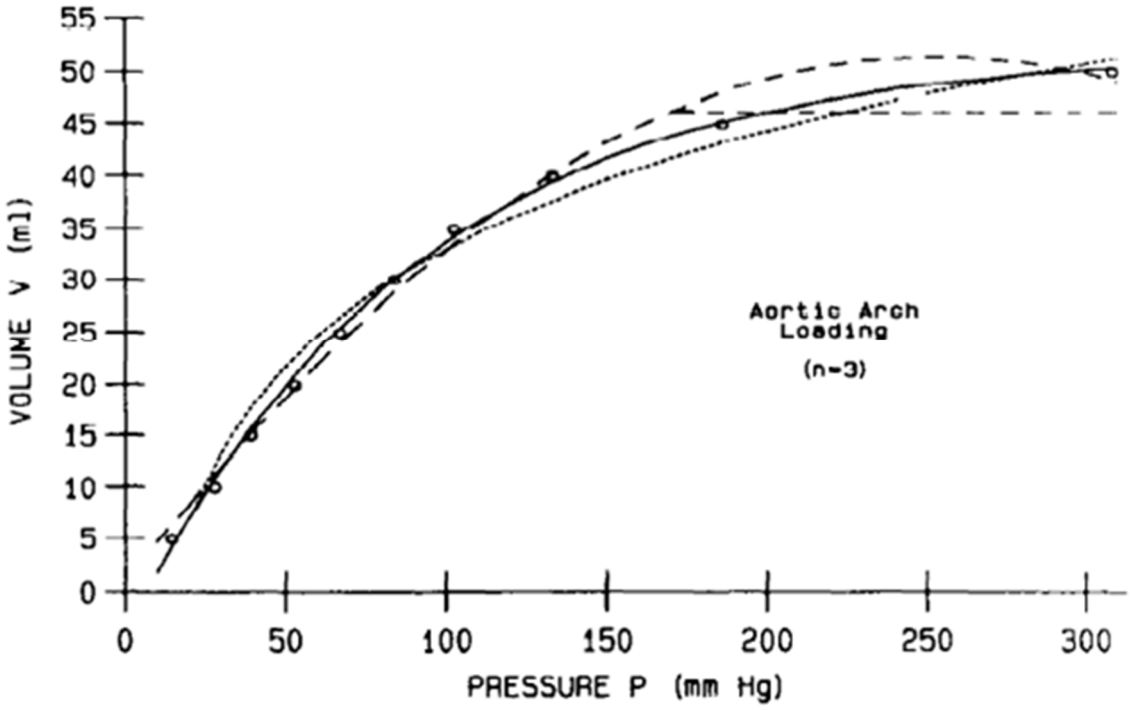

Figure 6.40: In-vivo volume-pressure relationship for a human aortic arch segment during loading phase. Symbols are experimental data and lines are three different types of fitting (Taken from Liu et al. 1986).

It can be observed that the example of pressure-volume curve shown in **Figure 6.7** for the artificial aorta is different from the anatomical aorta volume-pressure curve (**Figure 6.40**, note the axes are reversed). The curve shown in **Figure 6.40** is the pressure-volume curve for a human aortic arch segment during the loading phase found in a very similar static way. Both show a nonlinear behavior, the compliance of the real aorta decreases with increasing pressure while in the artificial aorta the slope of the curve increases with increasing pressure. That is due to the different material of the real and artificial aorta. The *in vivo* aorta is composed by two main components: elastin and collagen. The former acts at low values of strain and the latter at higher values resulting in a nonlinear behavior of the pressure-volume relationship (Metafratzi et al. 2002).

The artificial aorta used in this work showed a linear pressure-volume curve only when it was wrapped to create stiff aorta (A4-A6). **Table 6.3** shows that in these cases the compliance values are almost constant for all the stroke volumes and therefore for different pressure ranges. For higher values of compliance (A1-A3) the pressure-volume relationship is nonlinear (**Figure 6.7**) and the difference between low values of pressure (low stroke volume) and high values of pressure (high stroke volume) can also be 50% (**Table 6.3**). This can explain the two different behaviors between A1-A3 and A4-A6 reported in the results section 6.3.3 for some hemodynamic parameters that will be discussed in section 6.4.2.

Cs was compared to Cp, which was demonstrated to be a good estimator of total arterial compliance (Chemla et al. 1998). However, it was also reported that the dynamic compliance is usually 20-30% smaller than the static one (Langewouters et al. 1984). **Table 6.4** shows that static compliance is higher than the dynamic one in most of the cases. Since the reservoir pressure is related to the volume stored in the aorta during systole, compliance values were also compared to Cp_r. Generally the differences of these values of compliance with the static values were higher than those found comparing Cp and Cs (**Table 6.4**).

6.4.1 Changes of hemodynamic parameters with aortic compliance

Wrapping the artificial aorta in different ways allowed for the investigation of a wide range of values of compliance that can then be compared to different ages or to physiological and pathological (such as hypertension, atherosclerosis) conditions.

The results presented in this chapter show that systolic pressure (Ppeak) increases linearly with decreasing compliance, diastolic pressure (P_d) tends to decrease but not significantly, mean arterial pressure (MAP) does not change and pulse pressure (PP) increases exponentially with decreasing compliance. These trends were expected and are in line with those of the literature (Liu et al. 1989, Cohn 1999, Kuecherer et al. 2000). With decreasing aortic compliance a smaller portion of stroke volume is stored in the aorta during ejection and more is forwarded to the periphery. That causes an increase in systolic and pulse pressure and an increase of the left ventricular workload. The stroke volume stored in the aorta during systole is unloaded during diastole to help maintain diastolic pressure, a decrease of the stroke volume stored results in a decrease in diastolic pressure if the peripheral resistance does not change.

Here, for the first time, a study of the changes of parameters related to P_r and P_e with aortic compliance in a mock circulatory system is reported. A linear increase of the reservoir peak with decreasing aortic compliance and a non-linear increase of the pulse of the reservoir pressure were found. These relationships are very similar to those found for PP and Ppeak. Regarding the relationship of P_e with aortic compliance, a significant exponential increase of its peak with decreasing compliance was found only for a stroke volume of 40 and 50 ml (p values smaller compared to those found for PP_r). It can be speculated that P_r is affected more by the change in aortic compliance than P_e and the pressure component due to the reservoir function is the major determinant of P when the elastic characteristic of the aorta varies. Moreover, from A1 to A6 PP_r increases 3, 4, 6 and 8 times for 30, 40, 50 and 60 ml, respectively while P_e increases 3, 4, 5 and 3 times for 30, 40, 50 and 60 ml, respectively.

Increase of P_r with age was recently reported both in healthy (Vermeersch et al. 2009) and non-healthy subjects (Davies et al. 2010a). Since arterial stiffness increases with age, the results presented here confirm previous findings. Furthermore, the findings reported in this chapter have the advantage of only being dependent on the aortic compliance variation, since others confounding factors like heart rate, peripheral resistance and vascular remodeling were eliminated using the mock circulatory system.

Variation of compliance seems not to affect the PP_r/PP ratio which is always about 0.9.

Another parameter studied here was the diastolic decay time constant (τ) calculated from the exponential pressure decay. As was expected the relationship

between this parameter and the compliance is linear since τ is also equal to RC and R in this study does not vary.

The wave speed at the aortic root was calculated by means of the PU-loop (c) and P_eU-loop (c_e) methods. Wave speeds increase exponentially with decreasing aortic compliance. Trends are significant in all cases apart from c using 60 ml as stroke volume. This result was expected since wave speed is related to the inverse square root of the distensibility (2.11a). As previously shown in chapter 3, **Table 3.2** and **Figure 3.4**, c_e is always smaller than c, but the difference seems to be smaller for high values of compliance.

6.4.2 Changes of hemodynamic parameters with stroke volume

The same hemodynamic parameters were studied at different stroke volumes to simulate different LV contractility. Due to a limitation of the pump, it was not possible to reproduce physiological values of stroke volume. To have a good range of stroke volume it was decided to set the pump at 30, 40, 50 and 60 ml.

It is worth noting that although the changes with stroke volumes were reported for each aorta preparation (A1-A6) in section 6.3.3, for high compliance (A1-A3) the values calculated are quite different at different stroke volumes. That means that it is not possible to draw the same conclusions as for the other aortas (A4-A6) where the values of compliance are almost the same irrespective of stroke volume and changes in the hemodynamic parameters studied depend only on the change in stroke volume.

Systolic, diastolic and mean pressures have a linear relationship with stroke volume ($p<0.05$ in most of the cases). All these parameters increase with increasing stroke volume. For the systolic pressure the increase with stroke volume is steeper when the aorta was stiffer (A4-A6) than for higher compliance (A1-A3). This results in different trends of pulse pressure; it linearly decreases with increasing stroke volume for A1, A2, and A3 and increases linearly with stroke volume for A4, A5 and A6. Decrease in PP for A1, A2 and A3 does not depend on increasing stroke volume but on a substantial increase of compliance from 30 ml to 60 ml (**Table 6.3**).

Also in this case the parameters related to P_r, $P_r$peak and PP_r, follow the same pattern of Ppeak and PP. PP_r/PP ratio does not change significantly with stroke volume. $P_e$peak presents different behaviors for more and less compliant aorta. It does not change significantly with stroke volume for high value of compliance (A1-A3) and it

increases linearly with increasing stroke volume for lower compliance with an increasing steepness of the linear regression from A4 to A6. That means in a stiffer aorta the change in the pressure component due to the waves is more affected by a change in stroke volume than in a more compliant vessel. Both P_r and P_e seems to be highly related to a change in stroke volume.

Generally there are no significant changes of τ and wave speeds with stroke volume in all the aorta preparations.

As discussed before the results for high compliance presented here are biased by a change of compliance although the experiments were carried out in the same aorta preparation due to a nonlinear pressure-volume relationship. For lower compliance the pressure-volume relationship is linear and the values of compliance calculated from the curve do not change at different pressure ranges. Only for A4, A5 and A6 it is possible to say that the hemodynamic parameter trends found here depend on the variation of the stroke volume and not on other factors.

6.5 Conclusion

In this chapter the reservoir and excess components of the measured aortic pressure, τ and wave speeds were investigated whilst changing the aortic compliance and the stroke volume in a mock circulatory system. This allows the study of different physiological and pathological conditions, such as age, hypertension, atherosclerosis and ventricular contractility in relation to vascular compliance and ventricular function. The pressure component due to the buffering activity of the aorta (P_r) and the one due to the wave (P_e) are both significantly related to aortic compliance and stroke volume, but P_r has a stronger relationship with aortic compliance compared with P_e and its magnitude increases more when the aorta becomes stiffer. Moreover, P_r seems to follow the same trend as the measured pressure and it is the major determinant of the total pressure. Increasing the stroke volume the magnitude of P_r and P_e linearly increase. Wave speeds, calculated using PU-loop and P_eU-loop, follow the same pattern, c is always greater than c_e. Wave speed is strongly related to aortic compliance, but does not change with stroke volume.

Chapter 7 : Discussions and Conclusions

The clinical and biomechanical relevance of the thesis is related to its potential application for better understanding the cardiovascular system in healthy and non-healthy subjects, and how the mechanical properties of the arteries changes with age and gender. In particular, this thesis introduces of a new noninvasive technique to determine arterial stiffness in humans and it deeply investigates the changes of other parameters in relation to different hemodynamic conditions that could be related to age, hypertension, stroke and other diseases.

Differences in wave speed, wave intensities and reflection index were observed in the canine aorta in control condition and during occlusions comparing the reservoir-wave and the wave only approaches (chapter 3). In particular, using the reservoir-wave approach wave speed, intensities and reflection index were smaller in all conditions. Notably, the reservoir-wave approach led to surprisingly small values of backward waves and reflection indices also during proximal aorta occlusions, such as at the thoracic level. These findings could be explained considering that the arterial system is well matched in forward but not in backward direction. Both approaches led to the conclusion that distal occlusions (abdominal and iliac) do not affect the hemodynamics of the aorta at the level of the aortic root.

In this study, lnDU-loop technique to determine the wave speed and the noninvasive wave intensity analysis was applied in a relative large population of healthy humans (chapter 4). These techniques were already validated in bench experiments (Li & Khir 2011), but a study in human was lacking. Using the Bramwell-Hill equation the arterial distensibility was determined from the wave speed. These noninvasive methods were used in two different types of artery; in the carotid artery that is an elastic vessel and in the femoral artery that is a muscular vessel to assess how they differently change in relation to age and gender. It was found that the carotid artery is more affected by the ageing process compared to the femoral artery. Since the lnDU-loop and the noninvasive wave intensity analysis methods rely only on the diameter and velocity measurements, which can be both determined noninvasively, they have a potential use for screening and diagnosis in clinical practice.

The reservoir-wave approach was found to be useful also to describe the arterial hemodynamics at arbitrary locations (Aguado-Sierra et al. 2008a). In chapter 5 of this thesis this algorithm was used to investigate the carotid hemodynamics of the same population studied in chapter 4. The use of this approach allows for the separation of the pressure and the velocity into reservoir (related to the buffering capacity of the vessel) and excess (related to the wave propagation) components. The study of the changes of these parameters with age and gender shows that they are affected by age. This finding confirms the results in chapter 4 about the changes of mechanical properties of the elastic vessels with age. However, the wave speed calculated using the lnDU-loop was smaller than the one calculated using the P_eU_e-loop.

Two different analyses were carried out; a free fitting algorithm of the asymptotic pressure and an algorithm where this parameter was set to a fixed value. Generally, the two analyses led to similar results in terms of changes with age and gender, but to different values. In particular the average time constant decay τ is much smaller using the free fitting technique.

In this chapter, the same study carried out in the carotid artery was not repeated for the femoral artery. This is because the algorithm used is based on the assumption that pressure's exponential decay in the location considered is similar to the aortic one. The similarity between carotid and aortic pressure waveforms is established (Segers et al. 2005a), but in the femoral artery the exponential decay can be quite different due to the larger distance from the aorta, the different nature of the vessel and the different reflection wave pattern at that location.

Reservoir and excess pressure components in chapter 5 were studied in healthy and relative young subjects. To investigate how they change in pathological conditions they were also studied in bench experiments using a mock circulatory system which included an artificial aorta with its main branches and an LVAD able to reproduce a cardiac beat (chapter 6). Aortic compliance was changed by wrapping the aorta in different ways to replicate the change of aortic stiffness with age or cardiovascular diseases such as hypertension. Also the stroke volume was changed to mimic different heart contractility. It was found that Ppeak, PP, $P_r$peak, PP_r, $P_e$peak increase with decreasing aortic compliance, but the relationship between compliance and reservoir pressure is stronger than the one between compliance and excess pressure.

Moreover, the aortic wave speed increases exponentially with decreasing compliance. As found in chapter 3, wave speed calculated using excess pressure is always smaller than the wave speed calculated using the measured pressure. Reservoir and excess pressures are highly related with the stroke volume; in particular, if the compliance does not change they increase with increasing volume.

7.1 Conclusions

This thesis has met the objectives set out in section 1.10.

The main findings drawn from this study are:

1) From the comparison of the reservoir-wave and the wave only approach in canine aorta it was found: a) in control condition and during occlusion wave speed and intensities are smaller using the excess pressure rather than the measured one; b) intensities of the reflected waves and the reflection coefficient are surprisingly small also during proximal occlusions using the reservoir-wave approach; c) both methods led to the conclusion that distal occlusions do not affect aortic hemodynamics.

2) The algorithm derived in a previous study (Feng, Khir 2010) for determining wave speed and wave intensity noninvasively using measurement of diameter and velocity at same site has been applied here in carotid and femoral arteries of healthy humans. The findings confirm that elastic arteries are more affected by the ageing process than muscular arteries and the distensibility of the carotid is higher than of the femoral. Moreover, the results are in line with the one reported for the same population obtained using pressure waveforms, although the wave speed found here in the carotid artery is smaller than the one calculated using pressure (Vermeersch et al 2008). These techniques are reliable for the determination of wave speed, distensibility and wave intensities in human arteries.

3) The main advantage of the lnDU-loop technique is that it is based only on diameter and velocity measurements, it does not make any assumptions about the relation between pressure and diameter and it does not require the measurement of the pressure waveform, its systolic, diastolic or mean value in order to calibrate the diameter waveform of another artery. Therefore, it that can be easily used in the clinical environment to determine arterial mechanical properties noninvasively at any location of the arterial tree using only an ultrasound system.

4) An algorithm was used in this thesis to separate pressure and velocity into reservoir and excess components in healthy subjects to study carotid hemodynamics and the changes of these parameters with age and gender. It was found that they are strongly related to the ageing process, also in healthy human. Moreover, when the asymptotic pressure is fixed to a certain value, the time constant decay τ has a strong negative correlation with the excess pressure parameters. The reservoir component of the velocity was found to be positively related to the volume, estimated as the area under the flow curve.

5) The findings of the experiments carried out in the mock circulatory system showed that: a) the reservoir pressure, as the measured pressure, is strongly inversely correlated with compliance; b) wave speed calculated using the excess and measured pressure increases exponentially with decreasing compliance; c) the reservoir and excess pressures increase linearly with increasing stroke volume if the compliance is constant; d) wave speed calculated using the excess and the measured pressure is not correlated with the stroke volume.

6) Throughout the thesis valuable information about arterial hemodynamics in healthy and non-healthy subjects was found. This is relevant in the development of new techniques and new hemodynamic indices that can be used for screening, diagnosis and prognosis of cardiovascular diseases.

7.2 Future works

1) Following the findings of the comparison between the wave propagation in the canine ascending aorta described using the wave-only and the reservoir-wave approach presented in chapter 3 it would be useful to establish which analysis is more correct using a technique independent from reservoir pressure;

2) From the study of the lnDU-loop and the non-invasive wave intensity analysis in carotid and femoral arteries presented in chapter 4 it would be useful to carry out a clinical trial, involving healthy and non-healthy subjects;

3) The hemodynamics of the carotid artery was also studied considering the reservoir and excess components of pressure and velocity in healthy human (chapter 5). A clinical study designed to: a) compare excess and reservoir pressure components in healthy and hypertensive subjects; b) establish a way to distinguish between different

causes of hypertension (wave reflections, aorta compliance, resistances) in order to create a patient specific treatment should be carried out;

4) Following the study presented in chapter 6 it would be useful to investigate the effect of other parameters such as the resistance of the mock circulatory system on P_r, P_e, U_r, U_e, τ and wave speed.

References

AGUADO-SIERRA, J., ALASTRUEY, J., WANG, J.-., HADJILOIZOU, N., DAVIES, J. and PARKER, K.H., 2008a. Separation of the reservoir and wave pressure and velocity from measurements at an arbitrary location in arteries. *Proceedings of the Institution of Mechanical Engineers, Part H: Journal of Engineering in Medicine,* **222**(4), pp. 403-416.

AGUADO-SIERRA, J., DAVIES, J.E., HADJILOIZOU, N., FRANCIS, D., MAYET, J., HUGHES, A.D. and PARKER, K.H., 2008b. Reservoir-wave separation and wave intensity analysis applied to carotid arteries: A hybrid 1D model to understand haemodynamics. *Engineering in Medicine and Biology Society, EMBC, 2008 Annual International Conference of the IEEE*, pp. 1381-1384.

ALASTRUEY, J., 2011. Numerical assessment of time-domain methods for the estimation of local arterial pulse wave speed. *Journal of Biomechanics,* **44**(5), pp. 885-891.

ANLIKER, M., ROCKWELL, R.L. and OGDEN, E., 1971. Nonlinear analysis of flow pulses and shock waves in arteries, Part I: Derivation and properties of mathematical model. Z ang Math Phys **22**, pp 217–246.

ARNETT, D., BOLAND, L., EVANS, G., RILEY, W., BARNES, R., TYROLER, H. and HEISS, G., 2000. Hypertension and arterial stiffness: The atherosclerosis risk in communities study. *American Journal of Hypertension,* **13**, pp. 317-323.

AVOLIO, A., WESTERHOF BE, SIEBES M and TYBERG JV, 2009. Arterial hemodynamics and wave analysis in the frequency and time domains: an evaluation of the paradigms. *Medical & Biological Engineering & Computing,* **47**(2), pp. 107-110.

AVOLIO, A.P., CHEN, S.G. and WANG, R.P., 1983. Effects of aging on changing arterial compliance and left ventricular load in a northern Chinese urban community. *Circulation,* **68**(1), pp. 50-58.

BELZ, G.G., 1995. Elastic properties and Windkessel function of the human aorta. *Cardiovascular Drugs and Therapy,* **9**(1), pp. 73-83.

BENETOS, A., 1997. Large artery stiffness in hypertension. *Journal of Hypertension, Supplement,* **15**(2), pp. S89-S97.

BENETOS, A., LAURENT, S., HOEKS, A.P., BOUTOUYRIE, P.H. and SAFAR, M.E., 1993. Arterial alterations with aging and high blood pressure: A noninvasive study of carotid and femoral arteries. *Arteriosclerosis and Thrombosis,* **13**(1), pp. 90-97.

BIA, D., CYMBERKNOP, L., ZOCALO, Y., FARRO, I., TORRADO, J., FARRO, F., PESSANA, F. and ARMENTANO, R.L., 2011. Age-related changes in reservoir and

excess components of central aortic pressure in asymptomatic adults. *Engineering in Medicine and Biology Society,EMBC, 2011 Annual International Conference of the IEEE*, pp. 6454-6457.

BLACHER, J., ASMAR, R., DJANE, S., LONDON, G.M. and SAFAR, M.E., 1999. Aortic pulse wave velocity as a marker of cardiovascular risk in hypertensive patients. *Hypertension,* **33**(5), pp. 1111-1117.

BLEASDALE, R.A., MUMFORD, C.E., CAMPBELL, R.I., FRASER, A.G., JONES, C.J.H. and FRENNEAUX, M.P., 2003. Wave intensity analysis from the common carotid artery: A new noninvasive index of cerebral vasomotor tone. *Heart and vessels,* **18**(4), pp. 202-206.

BORTOLOTTO, L.A., HANON, O., FRANCONI, G., BOUTOUYRIE, P., LEGRAIN, S. and GIRERD, X., 1999. The aging process modifies the distensibility of elastic but not muscular arteries. *Hypertension,* **34**(4), pp. 889-892.

BOUTOUYRIE, P., LAURENT, S. and BRIET, M., 2008. Importance of arterial stiffness as cardiovascular risk factor for future development of new type of drugs. *Fundamental and Clinical Pharmacology,* **22**(3), pp. 241-246.

British Heart Foundation, BHF Facts. Online sheet. http://www.bhf.org.uk/media/news-from-the-bhf/bhf-facts.aspx. 2012.

BURATTINI, R. and GNUDI, G., 1982. Computer identification of models for the arterial tree input impedance: Comparison between two new simple models and first experimental results. *Medical and Biological Engineering and Computing,* **20**(2), pp. 134-144.

CHEMLA, D., HÉBERT, J., COIRAULT, C., ZAMANI, K., SUARD, I., COLIN, P. and LECARPENTIER, Y., 1998. Total arterial compliance estimated by stroke volume-to-aortic pulse pressure ratio in humans. *American Journal of Physiology - Heart and Circulatory Physiology,* **274**(2), pp. H500-H505.

COHN, J.N., 2006. Arterial stiffness, vascular disease, and risk of cardiovascular events. *Circulation,* **113**(5), pp. 601-603.

COHN, J.N., 1999. Pathophysiologic and prognostic implications of measuring arterial compliance in hypertensive disease. *Progress in cardiovascular diseases,* **41**(6), pp. 441-450.

COX, R.H. and PACE, J.B., 1975. Pressure flow relations in the vessels of the canine aortic arch. *American Journal of Physiology,* **228**(1), pp. 1-10.

CURTIS, S.L., ZAMBANINI, A., MAYET, J., THOM, S.A.M., FOALE, R., PARKER, K.H. and HUGHES, A.D., 2007. Reduced systolic wave generation and increased peripheral wave reflection in chronic heart failure. *American Journal of Physiology - Heart and Circulatory Physiology,* **293**(1), pp. H557-H562.

CYMBERKNOP, L., BIA, D., ZOCALO, Y., FARRO, I., TORRADO, J., FARRO, F., PESSANA, F. and ARMENTANO, R.L., 2011. Gender-related differences in the excess pressure component of central aortic pressure waveform of healthy young, *Engineering in Medicine and Biology Society,EMBC, 2011 Annual International Conference of the IEEE*, pp. 207-210.

DAVIES, J.E., BAKSI, J., FRANCIS, D.P., HADJILOIZOU, N., WHINNETT, Z.I., MANISTY, C.H., AGUADO-SIERRA, J., FOALE, R.A., MALIK, I.S., TYBERG, J.V., PARKER, K.H., MAYET, J. and HUGHES, A.D., 2010a. The arterial reservoir pressure increases with aging and is the major determinant of the aortic augmentation index. *American Journal of Physiology - Heart and Circulatory Physiology,* **298**(2), pp. H580-H586.

DAVIES, J., TILLIN, T., MALAWEERA, A., LACY, H., CRUICKSHANK, K., STANTON, A., COLLIER, D., THURSTON, H., WILLIAMS, B., PARKER, K., THOM, S. and HUGHES, A., 2010b. Excess pressure is higher in Atenolol-treated individuals and independently predicts cardiovascular events in the CAFE substudy of ASCOT. *Journal of Hypertension,* **28**, pp. e247.

DAVIES, J.E., HADJILOIZOU, N., LEIBOVICH, D., MALAWEERA, A., ALASTRUEY-ARIMON, J., WHINNETT, Z.I., MANISTY, C.H., FRANCIS, D.P., AGUADO-SIERRA, J., FOALE, R.A., MALIK, I.S., PARKER, K.H., MAYET, J. and HUGHES, A.D., 2007. Importance of the aortic reservoir in determining the shape of the arterial pressure waveform - The forgotten lessons of Frank. *Artery Research,* **1**(2), pp. 40-45.

DAVIES, J.E., WHINNETT, Z.I., FRANCIS, D.P., WILLSON, K., FOALE, R.A., MALIK, I.S., HUGHES, A.D., PARKER, K.H. and MAYET, J., 2006. Use of simultaneous pressure and velocity measurements to estimate arterial wave speed at a single site in humans. *American Journal of Physiology - Heart and Circulatory Physiology,* **290**(2), pp. H878-H885.

DOWLING, R.D. and ETOCH, S.W., 2000. Clinically available extracorporeal assist devices. *Progress in cardiovascular diseases,* **43**(1), pp. 27-36.

DREES, J.A. and ROTHE, C.F., 1974. Reflex Venoconstriction and Capacity Vessel Pressure-Volume Relationships in Dogs. *Circulation research,* **34**(3), pp. 360-373.

EULER, L., 1775. Principia pro motu sanguinis per arterias determinando. In: EDIDERUNT P.H. FUSS ET N. FUSS PETROPOLI and APUND EGGERS ET SOCIOS., eds, *Opera posthuma mathematica et physica anno 1844 detecta, 2.* pp. 814-823.

FENG, J. and KHIR, A.W., 2010. Determination of wave speed and wave separation in the arteries using diameter and velocity. *Journal of Biomechanics,* **43**(3), pp. 455-462.

FENG, J., 2008. *Wave propagation in flexible tubes,* PhD Thesis Brunel University.

FRANK, O., 1905. Der Puls inden Arterien. *Z Biol,* **46**, pp. 441-553.

FRANK, O., 1899. Die Grundform des arteriellen Pulses. *Z. Biol,* **37**, pp. 483-526.

FRANKLIN, S.S., 2005. Arterial Stiffness and Hypertension: A Two-Way Street? *Hypertension,* **45**(3), pp. 349-351.

FRANKLIN, S.S., JACOBS, M.J., WONG, N.D., L'ITALIEN, G.J. and LAPUERTA, P., 2001. Predominance of Isolated Systolic Hypertension Among Middle-Aged and Elderly US Hypertensives: Analysis Based on National Health and Nutrition Examination Survey (NHANES) III. *Hypertension,* **37**(3), pp. 869-874.

GOSLING, R.G., NEWMAN, D.L., BOWDEN, N.L. and TWINN, K.W., 1971. The area ration of normal aortic junctions. Aortic configuration and pulse-wave reflection. *British Journal of Radiology,* **44**(527), pp. 850-853.

GREENWALD, S.E. and NEWMAN, D.L., 1982. Impulse propagation through junctions. *Medical and Biological Engineering and Computing,* **20**(3), pp. 343-350.

GUYTON, A. and HALL, J., 2006. *Textbook of medical physiology*. 11th edn. the University of Michigan: Elsevier Saunders.

GUYTON, A.C., POLIZO, D. and ARMSTRONG, G.G., 1954. Mean Circulatory Filling Pressure Measured Immediately After Cessation of Heart Pumping. *American Journal of Physiology,* **179**(2), pp. 261-267.

HALES, S., 1733. *Statistical Essays: Containing Haemastaticks.* Reprinted in 1964 edn. New York: Hafner.

HARADA, A., OKADA, T., NIKI, K., CHANG, D. and SUGAWARA, M., 2002. On-line noninvasive one-point measurements of pulse wave velocity. *Heart and vessels,* **17**(2), pp. 61-68.

HARVEY, W., 1628. *Exercitatio anatomica de motu cordis et sanguinis in animalibus.* 1st edn. Francofurti Edition.

HISTAND, M.B. and ANLIKER, M., 1973. Influence of flow and pressure on wave propagation in the canine aorta. *Circulation research,* **32**(4), pp. 524-529.

HUGHES, A. and PARKER, K., 2009. Forward and backward waves in the arterial system: impedance or wave intensity analysis? *Medical & Biological Engineering & Computing,* **47**(2), pp. 207-210.

HUNT, A., 2012. *Effect of Vascular Nitric Oxide Bioactivity and Vascular Ageing on Arterial Blood Pressure and Flow Waveforms,* PhD Thesis Imperial College.

JELLINEK, H., KRENN, H., OCZENSKI, W., VEIT, F., SCHWARZ, S. and FITZGERALD, R.D., 2000. Influence of positive airway pressure on the pressure gradient for venous return in humans. *Journal of applied physiology,* **88**(3), pp. 926-932.

JONES, C.J.H., SUGAWARA, M., KONDOH, Y., UCHIDA, K. and PARKER, K.H., 2002. Compression and expansion wavefront travel in canine ascending aortic flow: Wave intensity analysis. *Heart and vessels,* **16**(3), pp. 91-98.

KAWAGUCHI, M., HAY, I., FETICS, B. and KASS, D.A., 2003. Combined ventricular systolic and arterial stiffening in patients with heart failure and preserved ejection fraction: Implications for systolic and diastolic reserve limitations. *Circulation,* **107**(5), pp. 714-720.

KHIR, A.W., O'BRIEN, A., GIBBS, J.S.R. and PARKER, K.H., 2001. Determination of wave speed and wave separation in the arteries. *Journal of Biomechanics,* **34**(9), pp. 1145-1155.

KHIR, A.W. and PARKER, K.H., 2005. Wave intensity in the ascending aorta: Effects of arterial occlusion. *Journal of Biomechanics,* **38**(4), pp. 647-655.

KHIR, A.W. and PARKER, K.H., 2002. Measurements of wave speed and reflected waves in elastic tubes and bifurcations. *Journal of Biomechanics,* **35**(6), pp. 775-783.

KOLYVA, C., PANTALOS, G.M., GIRIDHARAN, G.A., PEPPER, J.R. and KHIR, A.W., 2009. Discerning aortic waves during intra-aortic balloon pumping and their relation to benefits of counterpulsation in humans. *Journal of applied physiology,* **107**(5), pp. 1497-1503.

KOLYVA, C., SPAAN, J.A.E., PIEK, J.J. and SIEBES, M., 2008. Windkesselness of coronary arteries hampers assessment of human coronary wave speed by single-point technique. *American Journal of Physiology - Heart and Circulatory Physiology,* **295**(2), pp. H482-H490.

KOLYVA, C., BIGLINO, G., PEPPER, J.R. and KHIR, A.W., 2012. A Mock Circulatory System With Physiological Distribution of Terminal Resistance and Compliance: Application for Testing the Intra-Aortic Balloon Pump. *Artificial Organs,* **36**(3), pp. E62-E70.

KORTEWEG, D.J., 1878. Ueber die Fortpflanzungsgeschwindigkeit des Schalles in elastischen Röhren. *Annalen der Physik,* **241**(12), pp. 525-542.

KUECHERER, H.F., JUST, A. and KIRCHHEIM, H., 2000. Evaluation of aortic compliance in humans. *American Journal of Physiology - Heart and Circulatory Physiology,* **278**(5), pp. H1411-H1413.

LANGEWOUTERS, G.J., WESSELING, K.H. and GOEDHARD, W.J.A., 1984. The static elastic properties of 45 human thoracic and 20 abdominal aortas in vitro and the parameters of a new model. *Journal of Biomechanics,* **17**(6), pp. 425-435.

LAURENT, S., BOUTOUYRIE, P., ASMAR, R., GAUTIER, I., LALOUX, B., GUIZE, L., DUCIMETIERE, P. and BENETOS, A., 2001. Aortic stiffness is an independent predictor of all-cause and cardiovascular mortality in hypertensive patients. *Hypertension,* **37**(5), pp. 1236-1241.

LAURENT, S., COCKCROFT, J., VAN BORTEL, L., BOUTOUYRIE, P., GIANNATTASIO, C., HAYOZ, D., PANNIER, B., VLACHOPOULOS, C., WILKINSON, I. and STRUIJKER-BOUDIER, H., 2006. Expert consensus document on arterial stiffness: Methodological issues and clinical applications. *European heart journal,* **27**(21), pp. 2588-2605.

LAURENT, S., COCKCROFT, J., VAN BORTEL, L., BOUTOUYRIE, P., GIANNATTASIO, C., HAYOZ, D., PANNIER, B., VLACHOPOULOS, C., WILKINSON, I., STRUIJKER-BOUDIER, H. and ON BEHALF OF THE EUROPEAN NETWORK FOR NON INVASIVE INVESTIGATION OF LARGE ARTERIES, 2007. Abridged version of the expert consensus document on arterial stiffness. *Artery Research,* **1**(1), pp. 2-12.

LEAROYD, B.M. and TAYLOR, M.G., 1966. Alterations with age in the viscoelastic properties of human arterial walls. *Circulation research,* **18**(3), pp. 278-292.

LI, Y., BORLOTTI, A., PARKER, K.H. and KHIR, A.W., 2011. Variation of wave speed determined by the PU-loop with proximity to a reflection site, *Proceedings of the Annual International Conference of the IEEE Engineering in Medicine and Biology Society, EMBS* 2011, pp. 199-202.

LI, Y. and KHIR, A.W., 2011. Experimental validation of non-invasive and fluid density independent methods for the determination of local wave speed and arrival time of reflected wave. *Journal of Biomechanics,* **44**(7), pp. 1393-1399.

LI, Y., 2012. *Propagation and reflection of pulse waves in flexible tubes and relation to wall properties,* PhD Thesis Brunel University.

LI, Y., WANG, J., DOLAN, E., GAO, P., GUO, H., NAWROT, T., STANTON, A.V., ZHU, D., O'BRIEN, E. and STAESSEN, J.A., 2006. Ambulatory Arterial Stiffness Index Derived From 24-Hour Ambulatory Blood Pressure Monitoring. *Hypertension,* **47**(3), pp. 359-364.

LIGHTHILL, J., 1978. *Waves in fluids.* Cambridge: Cambridge University Press.

LIU, Z.R., TING, C.T., ZHU, S.X. and YIN, F.C., 1989. Aortic compliance in human hypertension. *Hypertension,* **14**(2), pp. 129-136.

LIU, Z., BRIN, K.P. and YIN, F.C., 1986. Estimation of total arterial compliance: an improved method and evaluation of current methods. *American Journal of Physiology - Heart and Circulatory Physiology,* **251**(3), pp. H588-H600.

MACRAE, J.M., SUN, Y.-., ISAAC, D.L., DOBSON, G.M., CHENG, C.-., LITTLE, W.C., PARKER, K.H. and TYBERG, J.V., 1997. Wave-intensity analysis: A new approach to left ventricular filling dynamics. *Heart and vessels,* **12**(2), pp. 53-59.

MANISTY, C., MAYET, J., TAPP, R.J., PARKER, K.H., SEVER, P., POULTER, N.H., THOM, S.A.M. and HUGHES, A.D., 2010. Wave Reflection Predicts Cardiovascular Events in Hypertensive Individuals Independent of Blood Pressure and

Other Cardiovascular Risk Factors. An ASCOT (Anglo-Scandinavian Cardiac Outcome Trial) Substudy. *Journal of the American College of Cardiology,* **56**(1), pp. 24-30.

MANISTY, C.H., ZAMBANINI, A., PARKER, K.H., DAVIES, J.E., FRANCIS, D.P., MAYET, J., MCG THOM, S.A. and HUGHES, A.D., 2009. Differences in the magnitude of wave reflection account for differential effects of amlodipine- versus atenolol-based regimens on central blood pressure: An anglo-scandinavian cardiac outcome trial substudy. *Hypertension,* **54**(4), pp. 724-730.

MATTHYS, K.S., ALASTRUEY, J., PEIRÓ, J., KHIR, A.W., SEGERS, P., VERDONCK, P.R., PARKER, K.H. and SHERWIN, S.J., 2007. Pulse wave propagation in a model human arterial network: Assessment of 1-D numerical simulations against in vitro measurements. *Journal of Biomechanics,* **40**(15), pp. 3476-3486.

MCDONALD, D., 1955. The relation of the pulsatile pressure to flow in the arteries. *Journal of Physiology,* **127**, pp. 533-552.

MEAUME, S., RUDNICHI, A., LYNCH, A., BUSSY, C., SEBBAN, C., BENETOS, A. and SAFAR, M.E., 2001. Aortic pulse wave velocity as a marker of cardiovascular disease in subjects over 70 years old. *Journal of hypertension,* **19**(5), pp. 871-877.

MEINDERS, J.M. and HOEKS, A.P.G., 2004. Simultaneous assessment of diameter and pressure waveforms in the carotid artery. *Ultrasound in Medicine and Biology,* **30**(2), pp. 147-154.

METAFRATZI, Z.M., EFREMIDIS, S.C., SKOPELITOU, A.S. and DE ROOS, A., 2002. The Clinical Significance of Aortic Compliance and Its Assessment with Magnetic Resonance Imaging. *Journal of Cardiovascular Magnetic Resonance,* **4**(4), pp. 481-491.

MILNOR, W.R. and BERTRAM, C.D., 1978. The relation between arterial viscoelasticity and wave propagation in the canine femoral artery in vivo. *Circulation research,* **43**(6), pp. 870-879.

MILNOR, W.R. and NICHOLS, W.W., 1975. A new method of measuring propagation coefficients and characteristic impedance in blood vessels. *Circulation research,* **36**(5), pp. 631-639.

MITCHELL, G.F., 2009. Clinical achievements of impedance analysis. *Medical and Biological Engineering and Computing,* **47**(2), pp. 153-163.

MITCHELL, G.F., HWANG, S.-, VASAN, R.S., LARSON, M.G., PENCINA, M.J., HAMBURG, N.M., VITA, J.A., LEVY, D. and BENJAMIN, E.J., 2010. Arterial stiffness and cardiovascular events: The framingham heart study. *Circulation,* **121**(4), pp. 505-511.

MITCHELL, G.F., PARISE, H., BENJAMIN, E.J., LARSON, M.G., KEYES, M.J., VITA, J.A., VASAN, R.S. and LEVY, D., 2004. Changes in arterial stiffness and wave

reflection with advancing age in healthy men and women: The Framingham Heart Study. *Hypertension,* **43**(6), pp. 1239-1245.

MOENS, AI., 1879. Der erste Wellengipfel in dem absteigenden Schenkel der Pulscurve. *Pflüger, Archiv für die Gesammte Physiologie des Menschen und der Thiere,* **20**(1), pp. 517-533.

MOHIUDDIN, M.W., LAINE, G.A. and QUICK, C.M., 2007. Increase in pulse wavelength causes the systemic arterial tree to degenerate into a classical windkessel. *American Journal of Physiology - Heart and Circulatory Physiology,* **293**(2), pp. H1164-H1171.

MOHIUDDIN, M.W., RIHANI, R.J., LAINE, G.A. and QUICK, C.M., 2012. Increasing pulse wave velocity in a realistic cardiovascular model does not increase pulse pressure with age. *American Journal of Physiology - Heart and Circulatory Physiology,* **303**(1), pp. H116-H125.

MYNARD, J.P., PENNY, D.J., DAVIDSON, M.R. and SMOLICH, J.J., 2012. The reservoir-wave paradigm introduces error into arterial wave analysis: A computer modelling and in-vivo study. *Journal of hypertension,* **30**(4), pp734-743.

NEWMAN, D.L., BOWDEN, L.R., GOSLING, R.G. and WILLE, S.D., 1972. Impedance of aortic bifurcation grafts. *Journal of Cardiovascular Surgery,* **13**(2), pp. 175-180.

NEWTON, I., 1687. *Principia Mathematica.*

NICHOLS, W.W., CONTI, C.R., WALKER, W.E. and MILNOR, W.R., 1977. Input impedance of the systemic circulation in man. *Circulation research,* **40**(5), pp. 451-458.

NIKI, K., SUGAWARA, M., CHANG, D., HARADA, A., OKADA, T., SAKAI, R., UCHIDA, K., TANAKA, R. and MUMFORD, C.E., 2002. A new noninvasive measurement system for wave intensity: Evaluation of carotid arterial wave intensity and reproducibility. *Heart and vessels,* **17**(1), pp. 12-21.

OCHI, H., SHIMADA, T., IKUMA, I., MORIOKA, S. and MORIYAMA, K., 1991. Effect of a decrease in aortic compliance on the isovolumic relaxation period of the left ventricle in man. *American Journal of Noninvasive Cardiology,* **5**(3), pp. 149-154.

OHTE, N., NARITA, H., SUGAWARA, M., NIKI, K., OKADA, T., HARADA, A., HAYANO, J. and KIMURA, G., 2003. Clinical usefulness of carotid arterial wave intensity in assessing left ventricular systolic and early diastolic performance. *Heart and vessels,* **18**(3), pp. 107-111.

O'ROURKE, M.F., 2002. From theory into practice: Arterial haemodynamics in clinical hypertension. *Journal of hypertension,* **20**(10), pp. 1901-1915.

O'ROURKE, M.F., 1982. Vascular impedance in studies of arterial and cardiac function. *Physiological Reviews,* **62**(2), pp. 570-623.

O'ROURKE, M.F. and NICHOLS, W.W., 2005. Aortic diameter, aortic stiffness, and wave reflection increase with age and isolated systolic hypertension. *Hypertension,* **45**(4 SUPPL.), pp. 652-658.

O'ROURKE, M.F., STAESSEN, J.A., VLACHOPOULOS, C., DUPREZ, D. and PLANTE, G.E., 2002. Clinical applications of arterial stiffness; definitions and reference values. *American Journal of Hypertension,* **15**(5), pp. 426-444.

O'ROURKE, M.F. and TAYLOR, M.G., 1967. Input impedance of the systemic circulation. *Circulation research,* **20**(4), pp. 365-380.

PAGE, C.M., 2010. *Evidence of left ventricular wall movement actively decelerating aortic blood flow,* PhD Thesis Brunel University.

PAPAGEORGIOU, G.L., JONES, B.N., REDDING, V.J. and HUDSON, N., 1990. The area ratio of normal arterial junctions and its implications in pulse wave reflections. *Cardiovascular research,* **24**(6), pp. 478-484.

PAPAIOANNOU, T.G., PROTOGEROU, A.D., STAMATELOPOULOS, K.S., VAVURANAKIS, M. and STEFANADIS, C., 2009. Non-invasive methods and techniques for central blood pressure estimation: Procedures, validation, reproducibility and limitations. *Current pharmaceutical design,* **15**(3), pp. 245-253.

PARKER, K.H., 2009. An introduction to wave intensity analysis. *Medical and Biological Engineering and Computing,* **47**(2), pp. 175-188.

PARKER, K.H., ALASTRUEY, J. and STAN, G.B., 2012. Arterial reservoir-excess pressure and ventricular work. *Medical and Biological Engineering and Computing,* 50, pp. 419-424.

PARKER, K.H. and JONES, C.J.H., 1990. Forward and backward running waves in the arteries: Analysis using the method of characteristics. *Journal of Biomechanical Engineering,* **112**(3), pp. 322-326.

PARKER, K.H., JONES, C.J.H., DAWSON, J.R. and GIBSON, D.G., 1988. What stops the flow of blood from the heart? *Heart and vessels,* **4**(4), pp. 241-245.

PEDLEY TJ, 1980. *The fluid mechanics of large blood vessels.* Cambridge: Cambridge: C.U.P.

PENNY, D.J., MYNARD, J.P. and SMOLICH, J.J., 2008. Aortic wave intensity analysis of ventricular-vascular interaction during incremental dobutamine infusion in adult sheep. *American Journal of Physiology - Heart and Circulatory Physiology,* **294**(1), pp. H481-H489.

PERMUTT S and RILEY R.S., 1963. Hemodynamics of collapsible vessels with tone: the vascular waterfall. *Journal of Applied Physiology,* **18**(5), pp. 924-932.

POISEUILLE, J., 1846. *Recherches experimentales sur le mouvement des liquides dans les tubes de tres-petits diametres.* Memoires presentes par divers savanta a l'Acad Sci de l'Institut de France.

RABBEN, S.I., BJÆRUM, S., SØRHUS, V. and TORP, H., 2002. Ultrasound-based vessel wall tracking: An auto-correlation technique with RF center frequency estimation. *Ultrasound in Medicine and Biology,* **28**(4), pp. 507-517.

RABBEN, S.I., STERGIOPULOS, N., HELLEVIK, L.R., SMISETH, O.A., SLØRDAHL, S., URHEIM, S. and ANGELSEN, B., 2004. An ultrasound-based method for determining pulse wave velocity in superficial arteries. *Journal of Biomechanics,* **37**(10), pp. 1615-1622.

RAMSEY, M.W. and SUGAWARA, M., 1997. Arterial wave intensity and ventriculoarterial interaction. *Heart and vessels,* **12**(SUPPL. 12), pp. 128-134.

RENEMAN, R.S. and HOEKS, A.P., 1996. Diameter and compliance in the human carotid artery: variations with age and sex. *Ultrasound in medicine & biology,* **22**(2), pp. 271-272.

RIEMANN B., 1860. *Gesammelte mathematische Werke und wissenschaftlicher Nachlass.* Liepzig: BG Teubner.

RIETZSCHEL, E.R., DE BUYZERE, M.L., BEKAERT, S., SEGERS, P., DE BACQUER, D., COOMAN, L., VAN DAMME, P., CASSIMAN, P., LANGLOIS, M., VAN OOSTVELDT, P., VERDONCK, P., DE BACKER, G. and GILLEBERT, T.C., 2007. Rationale, design, methods and baseline characteristics of the Asklepios Study. *European Journal of Cardiovascular Prevention and Rehabilitation,* **14**(2), pp. 179-191.

RUBIN, M.R., MAURER, M.S., MCMAHON, D.J., BILEZIKIAN, J.P. and SILVERBERG, S.J., 2005. Arterial stiffness in mild primary hyperparathyroidism. *Journal of Clinical Endocrinology and Metabolism,* **90**(6), pp. 3326-3330.

SAFAR, M., 1990. Ageing and its effects on the cardiovascular system. *Drugs,* **39**(SUPPL. 1), pp. 1-8.

SAGAWA, K., LIE, R.K. and SCHAEFER, J., 1990. Translation of Otto frank's paper "Die Grundform des arteriellen Pulses" Zeitschrift für Biologie 37: 483–526 (1899). *Journal of Molecular and Cellular Cardiology,* **22**(3), pp. 253-254.

SAMAR, R.E. and COLEMAN, T.G., 1978. Measurement of mean circulatory filling pressure and vascular capacitance in the rat. *American Journal of Physiology - Heart and Circulatory Physiology,* **234**(1), pp. H94-H100.

SCHIPKE, J.D., HEUSCH, G., SANII, A.P., GAMS, E. and WINTER, J., 2003. Static filling pressure in patients during induced ventricular fibrillation. *American Journal of Physiology - Heart and Circulatory Physiology,* **285**(6), pp. H2510-H2515.

SCHRAM, M.T., HENRY, R.M.A., VAN DIJK, R.A.J.M., KOSTENSE, P.J., DEKKER, J.M., NIJPELS, G., HEINE, R.J., BOUTER, L.M., WESTERHOF, N. and STEHOUWER, C.D.A., 2004. Increased Central Artery Stiffness in Impaired Glucose Metabolism and Type 2 Diabetes: The Hoorn Study. *Hypertension,* **43**(2 I), pp. 176-181.

SEGERS P, DUBOIS F, DE WACHTER D and VERDONCK P, 1998. Role and Relevancy of a Cardiovascular Simulator. *Cardiovascular Engineering,* **3**(1), pp. 48-56.

SEGERS, P., MYNARD, J., TAELMAN, L., VERMEERSCH, S. and SWILLENS, A., 2012. Wave reflection: Myth or reality? *Artery Research,* **6**(1), pp. 7-11.

SEGERS, P., RIETZSCHEL, E., HEIREMAN, S., DE BUYZERE, M., GILLEBERT, T., VERDONCK, P. and VAN BORTEL, L., 2005. Carotid tonometry versus synthesized aorta pressure waves for the estimation of central systolic blood pressure and augmentation index. *American journal of hypertension : journal of the American Society of Hypertension.,* **18**(9 Pt 1), pp. 1168-1173.

SMOLICH, J.J., MYNARD, J.P. and PENNY, D.J., 2010. Wave intensity analysis of right ventricular and pulmonary vascular contributions to higher pulmonary than aortic blood pressure in fetal lambs. *American Journal of Physiology - Heart and Circulatory Physiology*, **299**(3), pp. H890-H897.

SRIDHARAN, S., BURROWES, L., BOUWMEESTER, J., WANG, J., SHRIVE, N. and TYBERG JV, 2012. Classical electrical and hydraulic Windkessel models validate physiological calculations of Windkessel (reservoir) pressure. *Canadian Journal of Physiology and Pharmacology*, **90**(5), pp. 579-585.

STARLING EH., 1897. Some points in the pathology of heart disease. *Lancet*, **1**, pp. 652–655.

STERGIOPULOS, N., WESTERHOF, B.E. and WESTERHOF, N., 1999. Total arterial inertance as the fourth element of the windkessel model. *American Journal of Physiology - Heart and Circulatory Physiology*, **276**(1 45-1), pp. H81-H88.

STERGIOPULOS, N., YOUNG, D.F. and ROGGE, T.R., 1992. Computer simulation of arterial flow with applications to arterial and aortic stenoses. *Journal of Biomechanics,* **25**(12), pp. 1477-1488.

SUGAWARA, M., NIKI, K., FURUHATA, H., OHNISHI, S. and SUZUKI, S., 2000. Relationship between the pressure and diameter of the carotid artery in humans. *Heart and vessels*, **15**(1), pp. 49-51.

SUGAWARA, M., NIKI, K., OHTE, N., OKADA, T. and HARADA, A., 2009. Clinical usefulness of wave intensity analysis. *Medical and Biological Engineering and Computing*, **47**(2), pp. 197-206.

SUN, Y.H., ANDERSON, T.J., PARKER, K.H. and TYBERG, J.V., 2000. Wave-intensity analysis: A new approach to coronary hemodynamics. *Journal of applied physiology,* **89**(4), pp. 1636-1644.

SWALEN, M.J.P. and KHIR, A.W., 2009. Resolving the time lag between pressure and flow for the determination of local wave speed in elastic tubes and arteries. *Journal of Biomechanics,* **42**(10), pp. 1574-1577.

SYLVESTER, J.T., GILBERT, R.D., TRAYSTMAN, R.J. and PERMUTT, S., 1981. Effects of hypoxia on the closing pressure of the canine systemic arterial circulation. *Circulation research,* **49**(4), pp. 980-987.

TANAKA, M., SUGAWARA, M., NIKI, K., IZUMI, T., TARUI, I., KODERA, H., OKADA, T. and HARADA, A., 2009. Comparison of two ultrasonic methods of one-point measurement of pulse wave velocity - Where to set the echo-tracking positions, in the adventitia or intima? *World Congress on Medical Physics and Biomedical Engineering: Image Processing, Biosignal Processing, Modelling and Simulation, Biomechanics,* 7 September 2009 through 12 September 2009 2009, pp. 518-520.

TAYLOR, M.G., 1966. Wave transmission through an assembly of randomly branching elastic tubes. *Biophysical journal,* **6**(6), pp. 697-716.

TORTORA, G. and GRABOWSKI, R., 1993. *Principles of anatomy and Physiology* 7 edn. New York: Harper Collins.

TYBERG, J.V., DAVIES, J.E., WANG, Z., WHITELAW, W.A., FLEWITT, J.A., SHRIVE, N.G., FRANCIS, D.P., HUGHES, A.D., PARKER, K.H. and WANG, J.-., 2009. Wave intensity analysis and the development of the reservoir-wave approach. *Medical and Biological Engineering and Computing,* **47**(2), pp. 221-232.

VAN DEN BOS, G.C., WESTERHOF, N., ELZINGA, G. and SIPKEMA, P., 1976. Reflection in the systemic arterial system: effects of aortic and carotid occlusion. *Cardiovascular research,* **10**(5), pp. 565-573.

VAN POPELE, N.M., GROBBEE, D.E., BOTS, M.L., ASMAR, R., TOPOUCHIAN, J., RENEMAN, R.S., HOEKS, A.P.G., VAN DER KUIP, D.A.M., HOFMAN, A. and WITTEMAN, J.C.M., 2001. Association between arterial stiffness and atherosclerosis: The Rotterdam study. *Stroke,* **32**(2), pp. 454-460.

VERMEERSCH, S.J., RIETZSCHEL, E.R., BUYZERE, M.L., BORTEL, L.M., GILLEBERT, T.C., VERDONCK, P.R. and SEGERS, P., 2009. The reservoir pressure concept: The 3-element windkessel model revisited? Application to the Asklepios population study. *Journal of Engineering Mathematics,* **64**(4), pp. 417-428.

VERMEERSCH, S.J., RIETZSCHEL, E.R., DE BUYZERE, M.L., DE BACQUER, D., DE BACKER, G., VAN BORTEL, L.M., GILLEBERT, T.C., VERDONCK, P.R. and SEGERS, P., 2008. Age and gender related patterns in carotid-femoral PWV and carotid and femoral stiffness in a large healthy, middle-aged population. *Journal of hypertension,* **26**(7), pp. 1411-1419.

VERSPRILLE, A., JANSEN, J., DROP, A. and HULSMANN AR, 1985. Mean systemic filling pressure as a characteristic pressure for venous return. *Pflügers Archiv,* **405**(3), pp. 226-233.

VLACHOPOULOS, C., AZNAOURIDIS, K. and STEFANADIS, C., 2010. Prediction of Cardiovascular Events and All-Cause Mortality With Arterial Stiffness. A Systematic Review and Meta-Analysis. *Journal of the American College of Cardiology,* **55**(13), pp. 1318-1327.

WANG J.J., FLEWITT, J.A., SHRIVE, N.G., PARKER, K.H. and TYBERG, J.V., 2006. Systemic venous circulation. Waves propagating on a windkessel: Relation of arterial and venous windkessels to systemic vascular resistance. *American Journal of Physiology - Heart and Circulatory Physiology,* **290**(1), pp. H154-H162.

WANG, J.J., O'BRIEN, A.B., SHRIVE, N.G., PARKER, K.H. and TYBERG, J.V., 2003. Time-domain representation of ventricular-arterial coupling as a windkessel and wave system. *American Journal of Physiology - Heart and Circulatory Physiology,* **284**(4 53-4), pp. H1358-H1368.

WANG, J.J., SHRIVE, N.G., PARKER, K.H., HUGHES, A.D. and TYBERG, J.V., 2011. Wave propagation and reflection in the canine aorta: Analysis using a reservoir-wave approach. *Canadian Journal of Cardiology,* **27**(3), pp. 389.e1-389.e10.

WATANABE, H., OHTSUKA, S., KAKIHANA, M. and SUGISHITA, Y., 1993. Coronary circulation in dogs with an experimental decrease in aortic compliance. *Journal of the American College of Cardiology,* **21**(6), pp. 1497-1506.

WEBER, E. and WEBER, W., 1825. *Wellenlehre auf Experimente gegrundet, oder uber die Wellen tropbarer Flussigkeiten mit Andwendung auf die Schall- und Lichtwellen.* Leipzig: Fleischer.

WESTERHOF, N., BOSMAN, F., DE VRIES, C.J. and NOORDERGRAAF, A., 1969. Analog studies of the human systemic arterial tree. *Journal of Biomechanics,* **2**(2), pp. 121-134,IN1,135-136,IN3,137-138,IN5,139-143.

WESTERHOF, N., ELZINGA, G. and SIPKEMA, P., 1971. An artificial arterial system for pumping hearts. *Journal of applied physiology,* **31**(5), pp. 776-781.

WESTERHOF, N., ELZINGA, G. and VAN DEN BOS, G.C., 1973. Influence of central and peripheral changes on the hydraulic input impedance of the systemic arterial tree. *Medical and Biological Engineering,* **11**(6), pp. 710-723.

WESTERHOF, N., LANKHAAR, J.-. and WESTERHOF, B.E., 2009. The arterial windkessel. *Medical and Biological Engineering and Computing,* **47**(2), pp. 131-141.

WESTERHOF, N., SIPKEMA, P., VAN DEN BOS, G.C. and ELZINGA, G., 1972. Forward and backward waves in the arterial system. *Cardiovascular research,* **6**(6), pp. 648-656.

WOMERSLEY, J.R., 1955. Method for the calculation of velocity, rate of flow and viscous drag in arteries when the pressure gradient is known. *The Journal of physiology*, **127**(3), pp. 553-563.

World Health Organisation, Cardiovascular diseases. Online fact sheet. http://www.who.int/mediacentre/factsheets/fs317/en/index.html. 2012.

YAMAMOTO, J., TRIPPODO, N.C., ISHISE, S. and FROHLICH, E.D., 1980. Total vascular pressure-volume relationship in the conscious rat. *American Journal of Physiology - Heart and Circulatory Physiology*, **238**(6), pp. H823-H828.

YOUNG, T., 1809. The Croonian Lecture: On the Functions of the Heart and Arteries. *Philosophical Transactions of the Royal Society of London*, **99**, pp. 1-31.

ZAMBANINI, A., CUNNINGHAM, S.L., PARKER, K.H., KHIR, A.W., THOM, S.A.M. and HUGHES, A.D., 2005. Wave-energy patterns in carotid, brachial, and radial arteries: A noninvasive approach using wave-intensity analysis. *American Journal of Physiology - Heart and Circulatory Physiology*, **289**(1), pp. H270-H276.

ZAMBANINI, A., KHIR, A.W., BYRD, S.M., PARKER, K.H., THOM, S.A.M. and HUGHES, A.D., 2002. Wave intensity analysis: A novel non-invasive method for determining arterial wave transmission. *Computers in Cardiology*, pp. 717-720.

List of Publications

Publications related to this thesis are underlined.

PEER-REVIEWED JOURNAL PUBLICATIONS

1. **A. Borlotti**, A.W. Khir, E.R. Rietzschel, M.L. De Buyzere, S. Vermeersch, and P. Segers. Non-invasive determination of local pulse wave velocity and wave intensity: changes with age and gender in the carotid and femoral arteries of healthy human. Journal of Applied Physiology 113:5, 727-735, 2012.
2. **A. Borlotti** and A. Khir. Wave speed and intensity in the canine aorta: analysis with and without the windkessel model. Engineering in Medicine and Biology Society,EMBC, 2011 Annual International Conference of the IEEE, 219-222.
3. Y. Li, **A. Borlotti**, K. Parker and A. Khir. Variation of wave speed determined by the PU-loop with proximity to a reflection site. Engineering in Medicine and Biology Society,EMBC, 2011 Annual International Conference of the IEEE, 199-202.
4. **A. Borlotti**, S. Vermeersch, E. Rietzschel, P. Segers and A. Khir. A comparison between local wave speed in the carotid and femoral arteries of healthy humans: Application of a new method. Engineering in Medicine and Biology Society (EMBC), 2010 Annual International Conference of the IEEE, 2857-2860.
5. Y. Li, **A. Borlotti**, S. Hickson, C. McEniery, I. Wilkinson and A. Khir Using magnetic resonance imaging measurement for the determination of the local wave speed and arrival time of reflected waves in human ascending aorta. Engineering in Medicine and Biology Society (EMBC), 2010 Annual International Conference of the IEEE, 5153-5156.
6. F. Clavica, J. Alastruey, **A. Borlotti**, S. J. Sherwin, A. W. Khir. One-dimensional computational model of pulse wave propagation in the human bronchial tree. Engineering in Medicine and Biology Society (EMBC), 2010 Annual International Conference of the IEEE, 2473-2476.

CONFERENCE PROCEEDINGS

1. **A. Borlotti** and A.W. Khir. Pulse wave velocity and wave intensity in the carotid artery of healthy human: Windkessel and Windkessel-less analysis, Artery Meeting 2012, Vienna.
2. **A. Borlotti**, Y. Li and A.W. Khir. Experimental comparison of different methods for the determination of local wave speed, Bioengineering Conference 6^{th}-7^{th} September, Oxford **(oral presentation)**.
3. **A. Borlotti** and A.W. Khir. Windkessel and Windkesselless models of wave propagation, 34th Annual International Conference of the IEEE EMBS Conference 28th August-1st September 2012, San Diego.
4. **A. Borlotti**, S. Vermeersch, E. Rietzschel, P. Segers and A. Khir. Determination of carotid and femoral wave speed and distensibility in a healthy population using a new non-invasive technique, Artery Meeting 2011, Paris.
5. **A. Borlotti**, S. Vermeersch, E. Rietzschel, P. Segers and A. Khir. Diameter and velocity based technique for the determination of local wave speed and intensity in the carotid artery of healthy human, Physiological Fluid Mechanics Conference, 2011, London.
6. G. Casagrande, **A. Borlotti**, D. Carugo, R. Fumero and M. L. Costantino, Physical simulator of fluid and mass transfer during dialysis, GNB Congress 2010, 8-10 July, Turin, Italy, 2010.
7. G. Casagrande, **A. Borlotti**, D. Carugo, R. Fumero and M. L. Costantino, Two-pool physical simulator of the inter-compartmental mass transfer during dialysis, ASAIO Conference 2010, 27-29 May, Baltimore, Maryland, USA, 2010.